University of Technology, Sydney

Faculty of Science

A STUDY OF THIN-FOIL ROLLING AND THE DEVELOPMENT OF AN Al-Fe-Mn-Si LIGHT GAUGE FOIL ALLOY

Part 1

Course: N054 Doctorate in Science – (by Thesis)

Author: Matthew Mansell

Supervisor: Dr. Greg Heness

2007

UNIVERSITY OF TECHNOLOGY
LIBRARY
SYDNEY

CERTIFICATE OF AUTHORSHIP/ORIGINALITY

I certify that the work presented in this thesis has not previously been submitted for a degree nor has it been submitted as part of requirements for a degree except as fully acknowledged within the text.

I also certify that the thesis has been written by me. Any help that I have received in my research work and the preparation of the thesis itself has been acknowledged. In addition, I certify that all information sources and literature used are indicated in the thesis.

Signature of Candidate

Production Note:
Signature removed prior to publication.

14th December 2006.

ACKNOWLEDGMENTS

I would like to thank the following people who have assisted in the production of this thesis:

IAS, in particular Tony Santino for assistance on modelling of thin film foils.

ALCOA AUSTRALIA ROLLED PRODUCTS for their support on this project.

Dr Greg Heness, who's assistance was essential in completing this thesis, and his support in upgrading from a masters to a doctorate in Applied Science.

Milt Milner, Rob Sanders Jr, Mike Ringle, Tom Rouns and other members of ATC for there assistance in analysing the microstructure.

Jennifer Russell, Paul Munro and members of the Department of Physics – UTS for their assistance with surface topography.

My wife Fiona, children Tamika and Jai - Your support and patience over the years has kept me going when I wanted to stop, and I dedicate this to you.

CONTENTS

LIST OF FIGURES

LIST OF TABLES

ABSTRACT

There has been a trend in recent years to produce thinner but stronger thin-foil aluminium alloys at higher production velocities. This thesis discusses and examines product quality, rolling parameters, thermal treatment, web handling and alloy development in the context of the production of thin-foil aluminium products. The information is to be included in the ALCOA metallurgical database

Web failures are categorised and investigated over the life of the project. A short definition is provided followed by remedies to reduce or avoid re-occurrences. The effect of boundary lubrication between the metal and roll surfaces on web failure is summarized by the Mansell curve. The Mansell curve expresses rolling lubrication as a function of film strength and film thickness, and will be useful in determining rolling lubricant composition and temperature.

Optimal settings based on current rolling practices are determined for unwind tension/stress, lubricant viscosity, load and rewind tension/stress to achieve a consistent desired mill speed. The parameters are determined using existing rolling theory and are essential in maintaining production volume with decreasing gauge.

The improved stability of the process provides the foundation for trials on a new unique high strength alloy, AA8150 and accompanying process, developed and registered by the author. Alloy 8150 utilises a unique combination of high cold reduction, solid solution strengthening, constituent and dispersion strengthening to produce a fine grained structure with high strength and formability characteristics.

The wrought aluminium alloy 8150 contains iron, manganese and silicon at greater than 20% from the eutectic composition. High cold reduction with no intermediate thermal treatment results in highly misorientated random alignments in the deformation zone that surround large constituent particles, $Al_{12}(FeMn)_3Si$ and $(FeMn)Al_6$, making them effective recrystallisation nuclei sites. The $Al_{12}(FeMn)_3Si$ and $Al_{12}(MnFe)_3Si$ dispersoids/precipitates that occur during thermo-mechanical processing reduce the energy of the high angle boundaries, 'pinning' the boundary causing a new boundary to be formed as it curves around the particle, enhancing the nucleation of recrystallisation sites.

CHAPTER 1 INTRODUCTION

1.1. World Growth - Export Overflow

Aluminium foil is generally characterised as an aluminium product rolled to a thickness of less than 200 microns (Europe) or 0.006 inches (USA). Various combinations of alloy, temper, gauge and width cater to several markets ranging from packaging and automotive applications to construction and communication. Common alloys include 1145, 1200, 3003, 3004, 5050, 7072, 8006 and 8011[1].

Since the turn of the century, Europe has been the birthplace to some of the most innovative and well-regarded foil manufacturing companies in the industry. There are some 40-plus companies rolling foil, utilising nearly 200 foil mills and representing almost 40% of the world's population of mills. Collectively they form the European Aluminium Foil Association (EAFA). An excellent overview of European foil plants by country is provided by Hall[2].

Steady growth over the past 30 years in the packaging and construction industries has resulted in an increased demand for aluminium[3]. In the European foil market, (specifically Germany, France and the UK) the percentage of total aluminium to the packaging market increased from 12% in 1970 to 21% in 1995.[4] A slump in domestic growth between 1991 and 1996 resulted in many EAFA countries re-focusing on export markets including Australia, and investigating future growth areas such as communications and the automotive industry.

As an example, in 1997 the EAFA reported that foil production in the European Union, as well as the Czech Republic, Hungary and Turkey, increased by 11.3% to 597,000 metric tonnes. Internal consumption rose by 10.6% with exports to non-EAFA-member countries rising by 15.2%[5]. In Germany, the total foil production in 1994 showed an increase of 9.2%. This was primarily due to exports, with domestic growth contributing only 2%[6]. By 1997, over 70% of Germany's foil turnover was achieved abroad[7]. Since 1997, there has been a 15% increase in total foil deliveries to the EAFA regions, Figure 1.1[8].

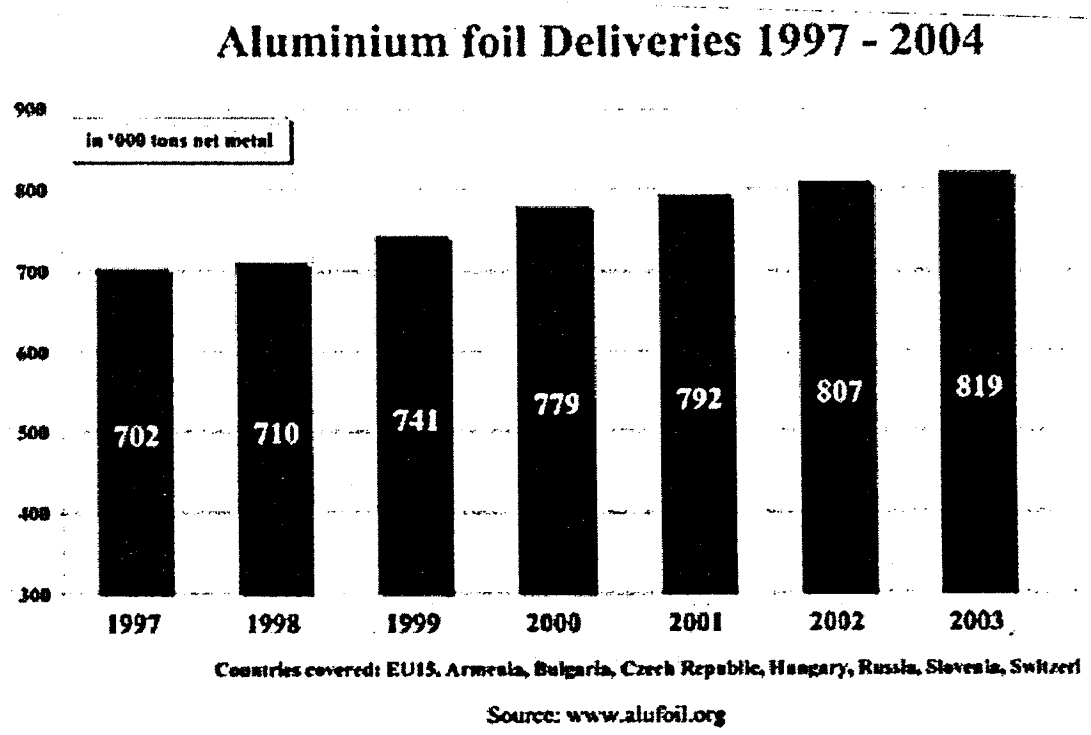

Figure 1.1. Aluminium foil deliveries 1997-2004 to the EAFA

Until 1990 in China, there was little domestic development of household and industrial foil with the majority of production in China for cigarette packaging. Locally made 2-high foil rolling mills at over 100 foil manufacturing plants reported a total under-utilised capacity of 150,000 tonnes per year,[9] as shown by China's production capacity only reaching in excess of 100,000 tonnes in 1996[10]. From 1993, 4-high mills have been imported from several countries such as the USA, Germany and the UK, however domestic development is still in its infancy.

United States foil shipments (including export shipments) have shown a similar growth rate to Europe. Table 1.1 shows the annual rate of growth from 1988 to 1998 was 3.6%. The slight dip in 1989 – 1990 is most likely due to economic recession[11].

Year	Domestic	Export	Total
1988	961	34	995
1989	917	30	947
1990	903	33	936
1991	899	53	952
1992	925	59	985
1993	951	70	1021
1994	1060	81	1141
1995	1099	74	1173
1996	1163	82	1245
1997	1180	82	1262
1998	1223	75	1298

Table 1.1. **US aluminium foil shipments (including imports)**[10]
Note all figures are in millions of pounds

1.2. Aluminium Foil: Innovations and Outlooks

The continuing demand for high quality foil products with decreased uniform gauges and increased widths to meet new applications have resulted in several new developments in the key process areas such as mechanical flexibility, accurate on-line process management and powerful rapid process control.

These developments extend to material quality, productivity and yield. Other areas of importance namely ease of maintenance, safety, energy consumption and environmental effects challenge existing rolling concepts and are becoming influential in recent mill design and development. Advanced technology is being applied at plants across the industry, whether using the ingot casting route or the continuous thin-slab and sheet casting routes[12,13,14].

These changes are not only limited to the process, but also the metallurgical aspects of foil production. Traditionally, aluminium foil has been manufactured from a very pure material, however new alloys with controlled iron, silicon, magnesium and manganese content have been developed making it possible to produce stronger, more isotropic materials that are more suitable for creating products with complex shapes. Control of the composition leads to a reduction of minor elements (<0.05%) such as 'heavy' metals. This has the effect of promoting technological and environmental impact advantages for the end product[15].

Casting

Aluminium is traditionally produced via an ingot rolling route (up to 1300mm thick and more than 2800mm wide) or using continuous casting technology such as that developed by Hunter in the 1950's[16]. Recent developments in thin gauge casting technology have allowed aluminium foil to be produced in a more efficient and cost effective manner and with a lower initial capital base i.e. avoids the need for a 'hotline structure' comprising of scalper, pre-heating furnaces, hot rolling mills and associated storage areas.

A study in 1997 indicated that the share of continuous casters in the global aluminium flat rolled product output was 16-17%[17], with much effort being directed at expanding the range of products that can be competitively made by strip casting.

Continuous casting lines are capable of producing aluminium strip down to 2mm thickness and widths approaching 2000mm[18]. A joint venture between Hunter and Norandal to develop a wide caster capable of producing 1.2mm strip for aluminium foil may eventually remove the need for cold rolling mills. Davy currently manufactures a four-high aluminium strip caster producing strip as thin as 1.0mm and as wide as 1.8m[19,20].

Reynolds Aluminium were working on a 'Continuous Drag Caster', which has a production rate some 600 – 800% faster than conventional twin roll casters at gauges of 1.1mm and less, however with the take-over by ALCOA, further development has been suspended[21].

Strip casting has a much higher solidification rate than Direct-Chill (DC) casting. Consequently, the intermetallic particle size distribution is different with cast strip displaying a far greater abundance of smaller particles. The cast strip also contains larger amounts of elements in solid solution and since no heating to rolling temperatures are necessary the elements in solid solution stay in solution. These differences explain why standard compositions for DC-cast foil are not always optimal for use in strip cast foil[22].

While there is great enthusiasm for strip casting, it has become evident that continuously cast strip cannot match the quality of strip produced by conventional hot rolling; especially for hard alloys and products that specify high surface or mechanical requirements. It is difficult to cast alloys with more than 3% magnesium, any heat-treatable alloys, or strip that requires a decorative streak-free surface after bright anodising.

Continuous cast strip has limitations for products requiring extensive forming due to surface texture anomalies known as "orange-peel". Another negative of continuous casting is the requirement of filtration systems to deliver metal with excellent micro-cleanliness over extended campaigns. This has lead to further improvements in deep-bed filtering systems of molten casting metal.

Rolling

Modern aluminium foil rolling mills are designed to roll super-wide and extra-light foils at high speeds. The speed range of these mills goes up to 2500m/min, with strip widths of 2400mm and gauges of less than 6 microns. Specially designed mechanical, electrical and electronic components, automatic foil threading and feeding, digital mill control, flatness and gauge control systems,[23,24] reliable roll coolant circulation and filtration systems,[25] fume exhaust cleaning and rolling oil recovery as well as foil separating and doubling systems[26,27] are necessary to successfully run these high-tech foil mills[28].

While considerable investment has been made in downstream cold rolling and foil rolling in recent years, residual difficulties can often be traced back through the process to the hot mill. As a result, the hot rolling process is receiving increasingly more attention as a means of gaining competitive advantage in the areas of material quality and plant productivity. A recent example of mill modernisation is a project by Mannesmann Demag to improve the hot rolling process through both new hot mills and the equally important areas of existing hot mill and hot line modernisation[29].

1.3. Foil in Australia – Thesis Justification

The Australian domestic market for aluminium foil is a mixture of light gauge foil (generally less than 10μm), household foil (10 – 20μm), semi-rigid foil (15-50μm) and heavy gauge foil including finstock (40 – 200μm). From 1980 to 1988, consumption increased from 12,500 tonnes to 18,000 tonnes.[30] In the late 1990's until mid 2000's, the market has fluctuated with a recent drop in demand largely attributed to product substitution, the decline in international travel and hot meals no longer served domestically, and down-gauging of products.[31]

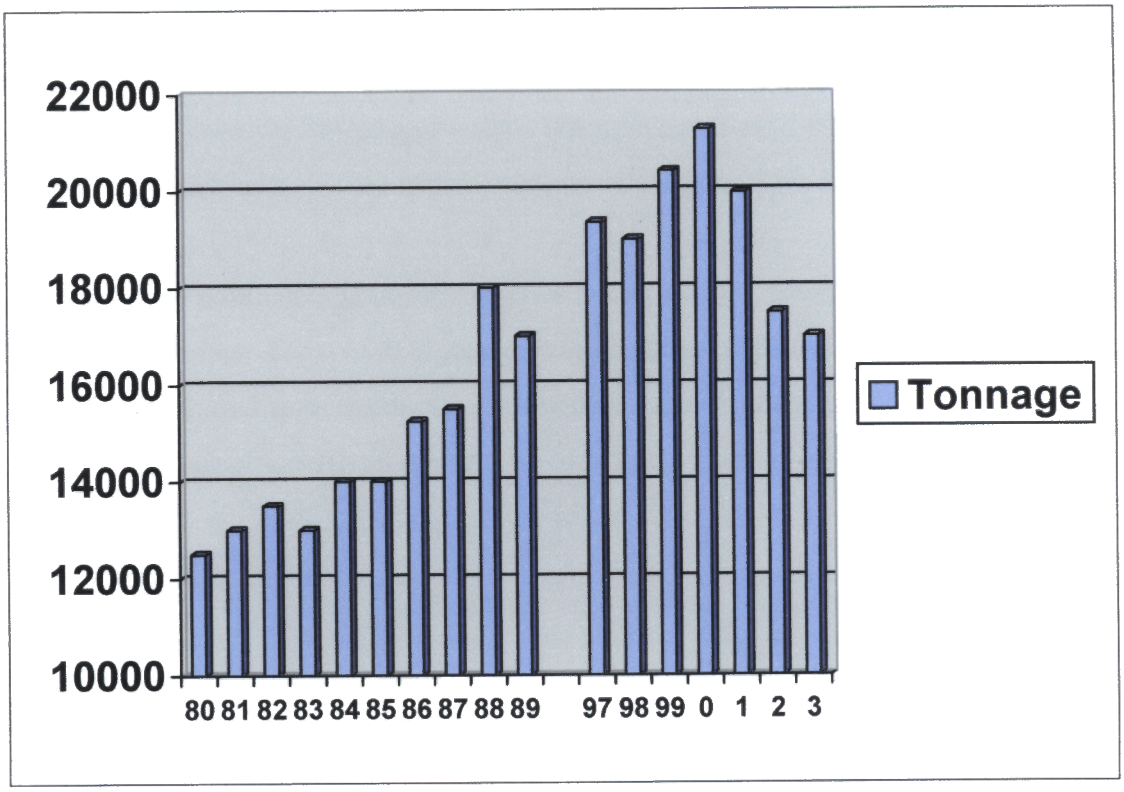

Figure 1.2. Foil domestic market 1980 - 89, 1997 - 2003

Increased export overflow from members of the European Aluminium Foil Association (EAFA) and Asian countries such as Korea in combination with reduced Australian import tariff rates has lead to several overseas companies pursuing sales in the local Australian market. The principal advantage local suppliers have over imported products is shorter lead times resulting in improved delivery performance, and local on-call technical support.

The Australian heavy gauge foil market (greater than 40 microns) is comprised largely of generic products such as heavy gauge packaging and finstock, with price being a significant factor in determining sales success. With the withdrawal of CAPRAL from the foil rolling market (they plan to slit and distribute locally), ALCOA AUSTRALIA ROLLED PRODUCTS (AARP) has become the only local manufacturer of foil products.

Insulation, light-gauge packaging and household foil (less than 20 microns) are at the niche end of the foil market. Light gauge foil is domestically produced at a final gauge of 6.35 microns at widths up to 1422mm while household foil is manufactured at gauges between 10 to 15 microns. Alloy compositions have moved towards higher-strength iron-rich alloys such as 8011, 8079 and 8021, especially tailored for thin-strip roll casting. These will reduce the number of cold rolling passes such that 0.6mm foil stock will be cold rolled in one to two passes from 1-2mm cast gauge[32].

The ability to produce high strength alloys at low gauges drives the domestic market to produce thinner foils with higher strengths using a higher iron alloy, while not compromising quality or production throughput. This thesis will examine and discuss the rolling concepts involved to produce light gauge foil. In addition, developmental work looking at high iron-manganese alloys for thin film foil rolling will be investigated.

The thesis is divided into five sections:

- Chapter 1 is an introduction to the foil industry in Australia. It is also includes the thesis justification.
- Chapters 2 to 5 are a literature review of several areas related to foil production; thin-film modelling, boundary lubrication, web handling, annealing characteristics and alloy appraisal. Specific issues pertaining to aluminium rolling defects and creasing will also be discussed. The Aluminium Foil Industry is relatively young and guarded, only a limited amount of technical information on matters such as alloy development, modelling, lubrication and annealing have been published.

- Chapters 6 and 7 catalogues web failure in thin film foil over a 5 year period, as well as optimisation of closed gap strip velocities to improve throughput. The benchmark and optimisation chapters consist of an experimental procedure, results, discussion, and conclusion sections. The chapter structure has been designed to aid in future referencing at other ALCOA locations.
- Chapters 8 to 11 investigate the surface properties and metallurgical structure of aluminium alloy 8150, the effect of the alloy composition on mechanical properties and annealing characteristics. The chapters describe the experimental design, the results, discussion, conclusion and overall summary of the findings.
- The appendices are an integral part of the thesis, containing an expanded summary of alloy properties and testing procedures. There is also a large section dedicated to recovery and recrystallisation.

LITERATURE SURVEY

CHAPTER 2 ALUMINIUM AND ITS ALLOYS

Chapter 2 provides information on aluminium and its alloys used in the light gauge foil industry for use within ALCOA on its database. A brief discussion on aluminium the metal including casting, 1xxx series alloys and their evolution into the 8xxx series is included. Further discussion on recrystallisation and recovery is provided in Appendix 13. Recrystallisation and recovery is critical in understanding the strengthening mechanisms of alloy 8150.

The formation of surface oxides is discussed in relation to stickiness of a thermally processed coil. A comparison of surface oxide composition and thickness is to be made between alloy 1145 and alloy 8150 in Chapters 8-10.

2.1. Introduction

Sir Humphrey Davy first proposed the suggestion of a 'new' metal (now known as aluminium) sometime between 1808–1812. In 1854, Henri Sainte-Claire Deville commenced the first small-scale production of 97+% aluminium via sodium reduction, with full-scale production commencing in 1857. The now familiar Hall-Heroult reduction process replaced this costly process in the late 1880's[33].

The metallurgical properties of aluminium can be enhanced by thermal treatments and alloy additions. In 1907, Wilm performed the first conscious "aluminium alloy" trials to improve hardness, however it was not until the early 1920's that this phenomena was understood. Further alloy development in combination with two World Wars helped promote the use of aluminium across industries from avionics to structural engineering[16].

Aluminium production and consumption increased by approximately 8% per year from the end of World War 2 until the mid-1970's, slowing down to around 5% in subsequent years. The recent growth in primary aluminium consumption by market segment from 1970 to 1995 is shown in Figure 2.1.

From 1970 to 1995, primary aluminium production doubled, with secondary aluminium production increasing from 25.7% to 27.2% of total consumption. Due to increased energy costs, the high cost of constructing a smelter coupled with the growing emphasis on recycleability, this trend is expected to continue. Figure 2.2 compares primary to secondary aluminium production in the western world from 1970 to 1995.

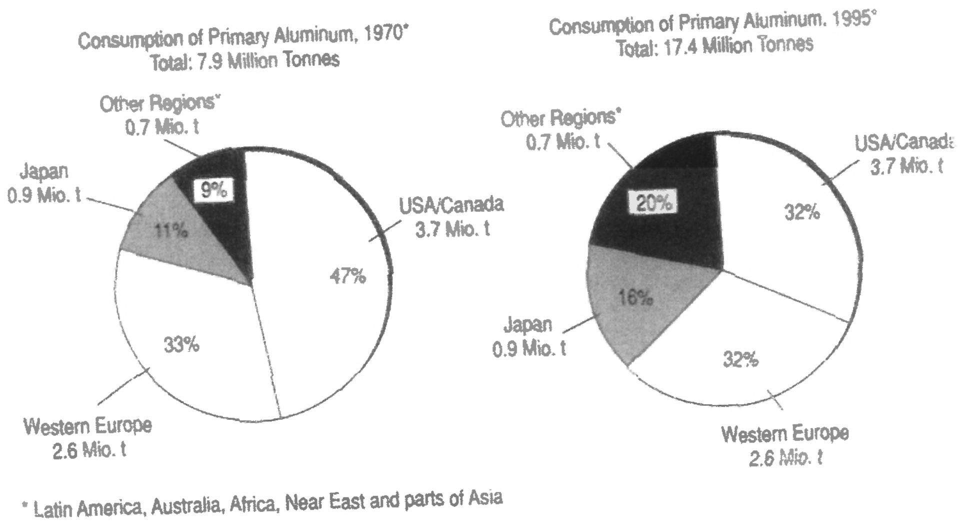

Figure 2.1. Primary aluminium production by region[33].

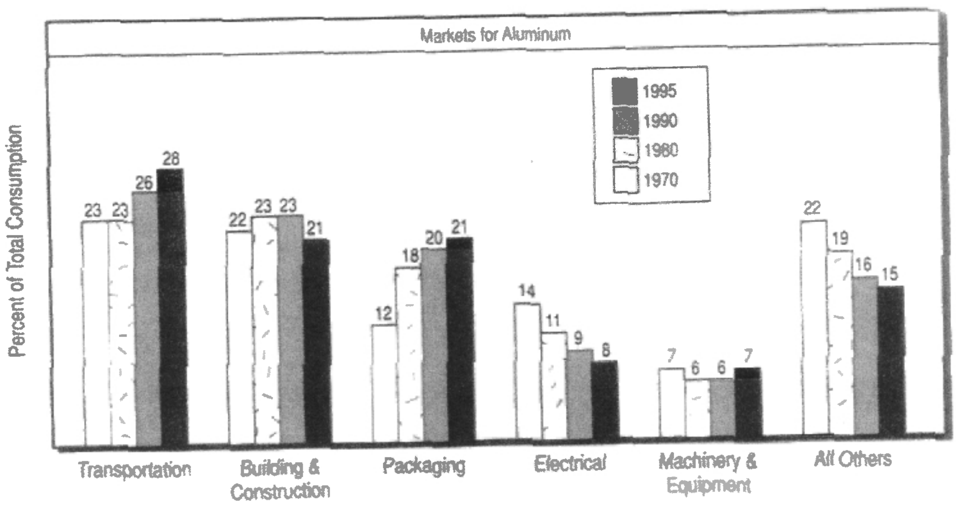

Figure 2.2. Recent growth of aluminium production in the western world[33].

2.2. Aluminium Designations

Aluminium alloys are classified into two major categories: cast compositions and wrought compositions. Approximately 85% of the aluminium produced worldwide is for wrought products - rolled plate (>6mm thickness), sheet (0.15 – 6mm), foil (<0.200mm), extrusions, forgings and wire[34]. The explosion of new alloys based on various alloying elements has resulted in the categorisation via an alloy designation system for the most beneficial alloys.

Initially individual firms developed their own alloy identification systems, with countries having their own specifications and standards. This inconsistency resulted in confusion and numerous complications, encouraging a concerted international effort to adopt a unified system of alloy and temper designations. The result was a requirement for individual countries to draft national specifications that met international agreed limits for materials having the same designation. The Aluminium Association (AA) system is the most widely recognised.

The AA system comprises of four digit combinations that are used to produce a list of wrought composition families. The *1xxx* series refers to purity aluminium (>99%) with the second digit representing modifications to these impurity limits, while the third and fourth digits represent the minimum aluminium content[35]. For other families, the first digit represents the major addition, i.e. *2xxx* denotes copper; the second digit is a sequential number assigned to indicate modifications to the original alloy, and with the third and fourth digits having no specific meaning[36]. The major alloying elements, designations, end uses and intermetallic phases for the wrought aluminium alloy families are listed in Table 2.1.

The temper designation system for aluminium and aluminium alloys covers all product forms except ingot, Figure 2.3. The system is based on the sequences of mechanical or thermal treatments (or both) used to produce various tempers. The conditions used during a heat treatment to produce a given temper in one alloy (eg: time, temperature and quenching rate) may differ for those employed to produce the same temper in another alloy.

1xxx	Controlled unalloyed (pure) composition; electrical, chemical and packaging industries, light gauge foil;	$FeAl_3$, Fe_3SiAl_{12}
2xxx	Copper is the principal alloying element, though other alloying elements, notably magnesium maybe specified; aircraft industries;	$CuAl_2$, Mg_2Si
3xxx	Manganese is the principal alloying element; general purpose, canstock and architectural applications;	$(Fe,Mn)_3$, $SiAl_{12}$, Mg_2Si
4xxx	Silicon is the principal alloying element; welding rods and brazing sheet;	Si
5xxx	Magnesium is the principal alloying element; Boat hulls, gangplanks, products exposed to marine environment;	Mg_2Al_3, Mg_2Si
6xxx	Magnesium and silicon are the principal alloying elements; architectural extrusions;	Mg_2Si
7xxx	Zinc is the principal alloying element, but other elements such as copper, magnesium, chromium and zirconium may be specified;	Al_7Cu_2Fe, $CuMgAl_{12}$, $(Mg,Al,Cu)Zn_2$, $Al_2Zn_3Mg_3$
8xxx	Alloys including iron, tin and some lithium compositions, characterising miscellaneous compositions.	
9xxx	Reserved for future use	

Table 2.1. Designation system and precipitates for aluminium[35,36]

The basic temper designations are, Figure 2.3:

F, as Fabricated: For product shaped by cold working, hot working or casting processes in which no special control over thermal conditions or strain hardening is employed. For wrought products, there are no mechanical property limits.

O, Annealed: Wrought products that are annealed to obtain the lowest-strength temper.

H, Strain Hardened: Wrought products that have been strain hardened without supplementary thermal treatments resulting in a reduction in strength.

W, Solution: An unstable temper applicable for alloys with strength changes at room temperature over time after solution heat treatment.

T, Solution: A temper applied to alloys that become stable within a few weeks of solution heat treatment or artificial aging.

Wrought products that are strengthened by strain hardening have a nomenclature consisting of an H followed by 2 or more digits.

H1X: Products strained-hardened to achieve desired strength without supplementary thermal treatments.

H2X: Products that are strained-hardened to more than desired final amount, then partially annealed to reduce the strength at the desired level.

H3X: Applies only to alloys that gradually age-soften at room temperature such as Al-Mg alloys. Strain hardened products whose mechanical properties are stabilised by a low-temperature thermal treatment or heat induced during fabrication. This does not apply to light gauge foil alloys.

The 'X' corresponds to the degree of strain-hardening remaining after rolling and/or partially annealing; is does not directly correspond to the cold-reduction experienced by the metal (except for H1X tempers). Examples include:

H18 An ultimate tensile strength (UTS) achieved by equivalent cold-reduction of 75% after fully annealing.

H14 Applies to a material strengthened to one-half UTS level of H18.

H19 Applies to a material with UTS of 2.0 ksi (14Mpa) greater than that of H18.

H26 Applies to a material strengthened to three-quarters UTS level of H18 by cold-rolling and partial annealing.

H34 Applies to a material strengthened to one-half UTS level of H18 but achieved by stabilising after cold-rolling.

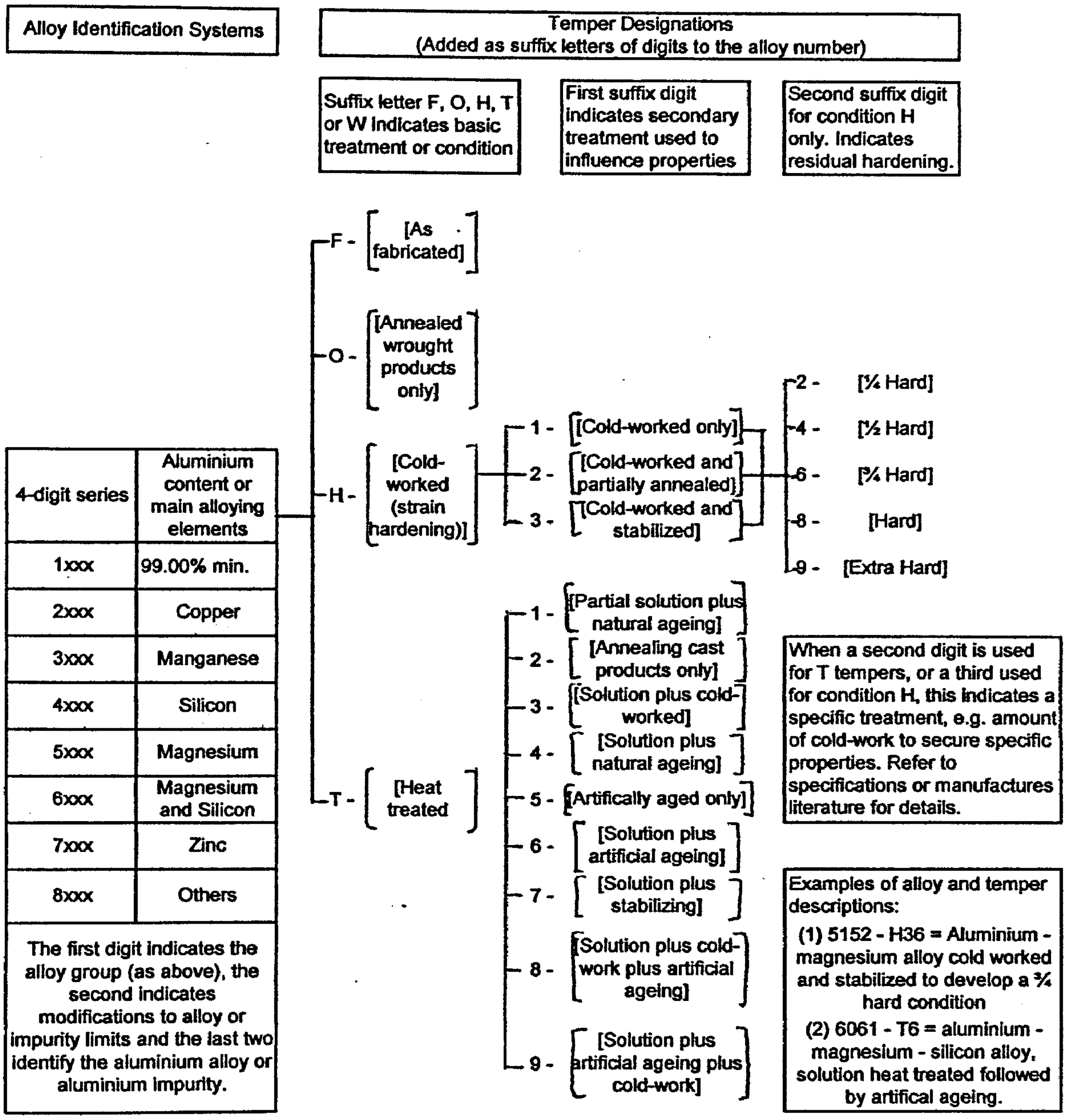

Figure 2.3. Temper designations

2.3. Foil Alloys

A solid metal is an effective barrier to light, water vapour, oxygen and other gasses that constitute aromas and odours. Consequently, a metal foil is an excellent product for the preservation of food or other goods. Aluminium offers barrier properties as well as good corrosion resistance, non-toxicity, the ability to be rolled to thin gauges and other product-specific attributes such as low spring-back properties for confectionery.

Foil has traditionally been rolled from primary aluminium (99.7+% purity) or low addition alloy stocks such as 1145 and 1235. With the advent of casting technology and consumer trends towards higher-strength lower-gauge product, many high iron and silicon alloys have been successfully introduced to the market place. If the silicon content is increased as in AA8011 or AA8111, the mechanical strength increases significantly over traditional alloys. For even greater improvements in strength, with minimal loss in ductility, the iron content is increased as in AA8079 for DC casting; in the case of strip casting, iron and manganese additions are made to produce AA8xxx alloys, Figure 2.4.

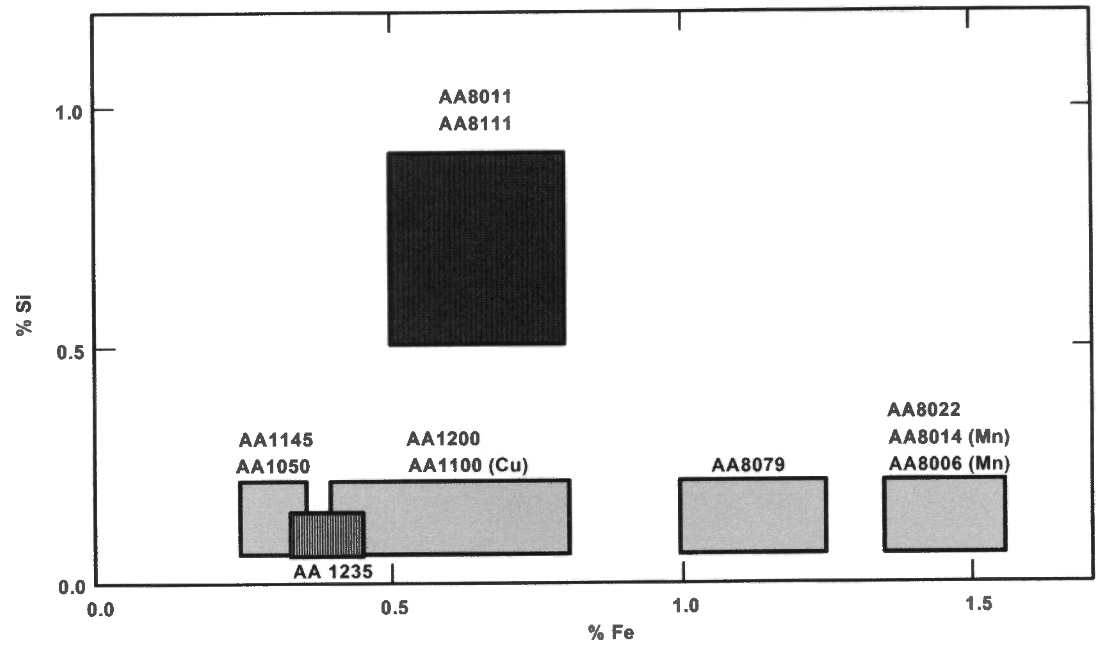

Figure 2.4. **Typical concentration of iron and silicon in foil alloys Al-Fe(Mn)-Si (1xxx, 8xxx), Al-Fe-Mn (8xxx)[37].**

Alloy development in terms of composition, casting and processing equipment is secretive in nature with several patents outstanding. Information on foil alloys tends to focus on purity, 1xxx series aluminium alloys and commercially sold production equipment. Monteiro gives a broad description of aluminium alloys used in foil production[38].

2.3.1. Aluminium – The Metal

Aluminium is a single isotope metal that contains 13 protons and 14 neutrons in its nucleus, giving it the atomic number 13 and a mass number 27. The electrons are distributed with the following arrangement:

$$\boxed{(1s)^2, (2s)^2, (3s)^6, (3p)^1}$$

The two electrons in the (3s) sphere explain the existence of monovalent aluminium, however in the solid lattice or molten state, hybridisation allows the three valency electrons to behave identically. The atoms in solid aluminium are arranged in a three-dimensional face-centred-cubic lattice type arrangement. A summary of the atomic and nuclear properties of aluminium is given in Table 2.2.

Property	Value	Source
Atomic Number	13	
Atomic Weight	26.9901	
Atomic Radius @ 25°C	1.42885Å	
Isotopes	None	
Valency	3	
Ionic radius Al^{+3}	0.57Å 0.50Å	Goldschmidt Pauling
Ionisation Potential Work Function (eV)	42	
Neutron Absorption Cross-section		
Reaction δab Scattering δ	230±5 1.4±0.1	

Table 2.2. Atomic and nuclear properties[16]

Primary aluminium is produced in a variety of grades ranging from 99% to greater than 99.999%. Three different types, corresponding to three different production methods, can be distinguished:

1. Commercially pure Aluminium comes from the reduction of alumina (Al_2O_3) in an electrolytic cell and accounts for the bulk of commercial production. It ranges in purity from 99% to 99.9%, with most of the impurities coming from either batch variation or multi-sourced raw materials;
2. Refined Aluminium is produced by electro-refining commercially pure aluminium in a three-layer cell. Its purity ranges from 99.9% to 99.99+%;
3. Zone-refined aluminium - With the correct starting material and technique, low yields with less than 1ppm impurities are produced.

Secondary aluminium is produced by re-melting fabrication scrap to produce an alloy that is usually less pure than the corresponding primary because of unavoidable contamination with other materials.

There is a large volume of published work on commercially pure aluminium and its alloys available for discussion and interpretation. A comprehensive study by Mondolfo[39] reviews a large volume of literature on the structure and properties of aluminium and its alloys. A summary of the physical properties of pure aluminium is given in Appendix 1[16].

2.3.2. 1xxx Alloys

Improvements in refining and smelting technology have led to a wide variety of lxxx alloys ranging in composition from 99.0 to 99.99% aluminium. Alloys refined to greater than 99.99% aluminium are very expensive to produce, and are used only in specialised applications. Most physical properties are changed by the addition of one or more alloying components; the major elements being categorised by the alloy designation system. The rates of change for each incremental addition are specific for each element and depend, in many cases drastically, on whether a solid solution or a second phase is formed.

Accompanying the deliberate additions of alloying elements to primary aluminium, impurities to the order of parts-per-million may have highly significant effects. The impurity interactions may be quite complex and can be highly beneficial or highly detrimental depending on the elements involved and the properties required. The main impurities are normally iron and silicon, with other elements (unless designated in quantities of less than 0.05 wt%) totalling 0.15 wt% and controlled to obtain microstructures or properties for specific end uses. The more important physical properties and the influence of purity are shown in Table 2.3.

Property	**Purity**				
	99.999%	99.99%	99.8%	99.5%	99.0%
Melting Pt °C		660.2			657.0
Boiling pt, °C		(2480)			
Latent heat of fusion, cal/g		94.6			93.0
Specific heat at 100°C, cal/g		.2226			.2297
Density at 20°C, g/cm^3	2.7	2.7	2.7	2.71	2.71
Electrical resistivity μΩ-cm at 20°C	2.63	2.68	2.74	2.80	2.87
Temp coefficient of resistivity		0.0042	0.0042	0.0041	0.0040
Coeff. of thermal expansion x 10^6 (20°C – 100°C)		23.86	23.5	23.5	23.5
Thermal Conductivity c.g.s. units at 100°C		0.57	0.56	0.55	0.54
Reflectivity (total)		90%	89%	86%	
Mod. Of Elasticity lb/in^2 x10^{-6}		9.9			10.0
Tensile strength, tons/in^2	2.25	3.8	4.4	5.2	5.8
Brinell hardness P/D^2 = 5	11	15	19	21	22

Table 2.3. Effect of purity on the properties of 1xxx alloys[16]

2.3.2.1. The Effect of Individual Additions for Foil Alloys[40]

Foil alloys require high purity levels to aid in achieving optimum properties for specific applications. Some elements, such as iron and silicon, are inherent in the production of aluminium but improve alloy properties when controlled. However other introduced elements including lead and beryllium can have a detrimental influence on an alloy, both in terms of mechanical properties and toxicity. A table describing individual effects of elemental additions to aluminium foil alloys is given in Appendix 2.

Non-metallic Inclusions:

Non-metallic inclusions are usually generated during the casting process and include dirt, dust and broken refractory fragments. These particles become embedded in the metal matrix, resulting in foil porosity and processing issues. Elimination of non-metallic inclusions is one of the more developed processes in aluminium production, with several melt filtration techniques routinely used in standard cast shop operations[40].

Alloying Elements:

Small additions of alloying elements (iron, silicon and manganese) are of little concern in standard foil production, having a positive effect up to a specified limit. Of more importance is the relative composition ratio for the various alloying elements. With all alloying elements in proportion by composition, the possibility of forming coarse intermetallic phases is minimised. Special care may be required when dealing with the iron/silicon ratio.

Alkaline and Alkaline Earth Metals:

Alkaline metals (mainly lithium, sodium and potassium) and metals of the alkaline earths (beryllium, magnesium and calcium) are known to have a strong influence on the properties of the surface aluminium oxide film. Strong surface segregation leads to massive enrichment of impurity elements at the oxide surface or at the interface between the oxide film and the base metal, Figure 2.5.[40]

This can result in deficiencies in adhesion strength, lacquerability and corrosion resistance. Modelling the process, the rate-determining step is the diffusion of impurity atoms to the surface. In light gauge foils, the surface coverage is such that with extended annealing times, the trace elements segregate to the two foil surfaces. Experimental observations point to grain boundary diffusion as the important mechanism for surface segregation. As limitations will be stricter for newly developed, extremely fine-grained foil, techniques for the effective control of alkaline and alkaline earth metals are critical.

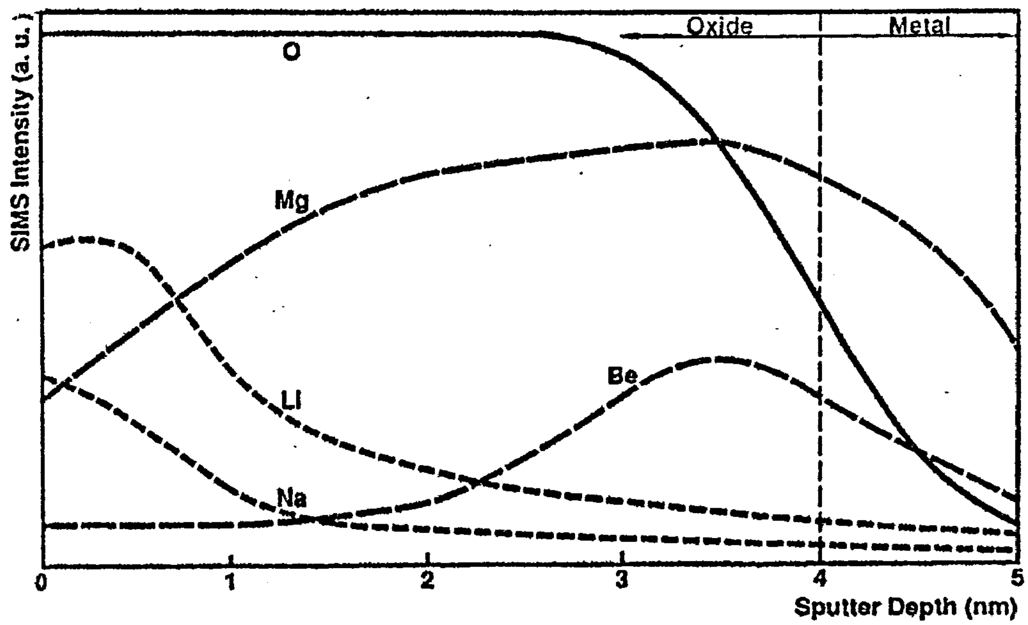

Figure 2.5. Segregation effects in a 1xxx series alloy[40]

Transition Metals:

Increased levels of transition elements can have both a beneficial and detrimental effect on the properties of aluminium foil as given in Table 2.4.; for example iron and manganese as discussed in Chapter 2.3.2.3 – 2.3.2.4, and 2.3.3. However other elements, while not directly affecting the mechanical properties of the aluminium foil, can influence recovery and recrystallisation kinetics. Small additions of titanium, vanadium, chromium and zirconium have a noticeable effect on recrystallisation, resulting in improved thermal stability of the foil materials, but significantly coarsening recrystallised grain size.

	As-rolled			260°C / 10 min		
	UTS (MPa)	YS (MPa)	E (%)	UTS (MPa)	YS (MPa)	E (%)
AA 1050	160	145	3.3	85	45	32
+0.05% Cr	165	150	3.4	100	75	21
+0.05% Ti	160	145	3.4	100	70	35
+0.05% Zr	160	150	3.1	135	130	4

Table 2.4. Effect of small additions of chromium, titanium, zirconium on the properties of AA1050 100 micron foil

Trace elements like cobalt and nickel have low solubility in aluminium and are expected to substitute for iron atoms in the primary intermetallic phases, having little impact on the final foil characteristics. Copper and zinc, at relatively low additions (<0.1%) have relatively no effect on the material characteristics in 1xxx alloys used in light gauge foil rolling. However the presence of copper or zinc can have a negative impact on the corrosion behaviour of the material due to changes in the electrochemical potential of the aluminium matrix.[40]

Other Elements:

Increased levels of silicon will have minimal influence on aluminium foil alloys. The same is true for small germanium contaminations. Elements including lead, tin, gallium and indium segregate to the grain boundaries reducing the corrosion resistance of recrystallised foil materials. As much light gauge foil comes into direct and indirect contact with food, specific limits on elements known or suspected to have an influence on the health of the consumer of the packaged food are imposed. For example low limits exist for lead, arsenic, mercury, cadmium and beryllium.

A tentative summary of the metallurgical effects of individual impurity elements on aluminium foil quality is given in Table 2.5.

Element	Effect	Critical Limits
Li, Na, K,..... Be, Mg,......	Detrimental	100 ppm (lower – as specific)
Ti, V, Cr, Zr, ...	Positive or negative	0.01 – 0.05%
Mn Fe Co, Ni Cu, Ag Zn	Positive Positive Indifferent Positive / indifferent Indifferent	0.05 – 0.1% 0.5 – 1.0% 0.05% 0.1 – 0.3% 0.1 – 0.3%
Si, Ge Sn, Pb	Indifferent Negative	0.2 – 1.0% 0.01 – 0.05%

Table 2.5. Impurity summary[40]

2.3.2.2. Casting of Aluminium Alloys

The treatment of molten aluminium typically involves alloying, fluxing, degassing and inclusion removal processes. There are essentially four ways to remove inclusions from molten aluminium, each with varying levels of efficiency, Table 2.6.;

- Sedimentation, or settling in the furnace for about 30-60 minutes
- Flotation via furnace fluxing or rotors (comprehensively investigated by Szekely[41] and Simensen[42])
- Cake-type filtration via ceramic foam filters
- Deep bed filtration via a bed filter or rigid media tube filter.

Type	Efficiency	Smallest Particle Removed (μm)
Sedimentation	50-80%	90
Furnace Fluxing	30-90%	~40
Rotors	60-70%	
Ceramic Foam Filters	~85%	20-40
Deep-bed Filtration	90-95%	2-10

Table 2.6. Filtration efficiency

The settling out of inclusions such as titanium boride (TiB_2) clusters or the flotation rate of the alkali chlorides is governed by a combination of particle size and particle density. The effect of settling time on inclusions can be estimated by plotting inclusion concentration versus time, which indicates a point of diminished returns is reached after about one hour[43]. Settling is most effective for large heavy inclusions and is approximated under stagnant melt conditions according to Stoke's Law, equation 2.1:

$$\boxed{V = 2\,g\,R^2\,\Delta\,d\,/\,9\,\mu} \qquad (2.1)$$

V is terminal velocity, μ is viscosity in poise, g is gravity, Δd the density difference and R the particle radius.

The basic principles and benefits of the filtration of aluminium alloys as a supplement to furnace treatments have been long understood, particularly in relation to foil. There are some general rules governing the efficiency of all filtration systems:

- At high filtration speed, efficiencies decrease or fall over time.
- Dense particles are invariably removed more effectively than light particles.
- Large particles are invariably removed more effectively than small particles.
- No filter is completely reliable and all are subject to inclusion release upon start-up and under steady-state melt flow conditions. Reliability of the filter increases with increasing particle density and with decreasing filtration speed.

Impurities present in the melt in solid, liquid or gaseous form are known to influence mechanical properties, surface finish and web break frequency at lower gauges. Therefore it is economically and technologically advantageous to reduce the level of inclusions by filtration[44,45]. A list of potential impurities is given in Table 2.7.

Classification	Type	Form	Dimensions (μm)	Potential Source(s)
Oxides	Al_2O_3	Particles, Skins	0.2 – 30 10 – 5000	Melting, alloying, metal transfer turbulence
	MgO	Particles, Skins	0.1 – 5 10 – 5000	Melting, alloying, metal transfer turbulence
	$MgAl_2O_4$	Particles, Skins	0.1 – 5 10 – 5000	Melting, alloying, metal transfer turbulence
	SiO_2	Particles	0.5 – 5	Melting, alloying, metal transfer turbulence
Non – Oxide	Salts Chlorides Fluorides	Particles	0.1 – 5	Filter and metal handling system release,
	Carbides Al_4C SiC	 Particles Particles	0.5 – 25	Refractory deg. Potroom metal, ref/metal reactions
	Nitrides AlN	Particles Skins	10 – 50	Mould gas mixture
	Borides TiB_2 AlB_2	Particles - Clusters Skins	 1 - 30 0.1 - 3	Grain refiner, inadequate resonance time, filter release

Table 2.7. Inclusions in aluminium[46]

It is recognised that two filtration modes may operate[47]:

i. Cake Filtration – The formation of a 'cake' of large particles that attach to the inlet filter wall, growing during filtration by intercepting more particles. Generally the melt flow rate decreases during this process as a consequence of the cake resistance.

ii. Depth Filtration – The particles are trapped throughout the interior wall surface of the filter. The most accepted hypothesis of aluminium deep filtration states that fluid drags small inclusions at low concentrations towards the filter wall where they may attach. For larger particles, the inertia favours their interception with the filter walls.

Note that surface and depth straining filtration modes are inactive in molten aluminium systems as the inclusions present in liquid aluminium are much smaller than the pores of the filter media most commonly used[48].

Rigid media tube filters employ cake-mode filtration, where the inclusions are captured at the incoming surface of the filter. The first inclusions trapped are larger than the filter pore size. As more inclusions are caught, smaller particles can be captured, Figure 2.6. However the increase in cake build-up results in an exponential pressure drop with time across the filter. The failure mode is frequently termed "blinding failure".

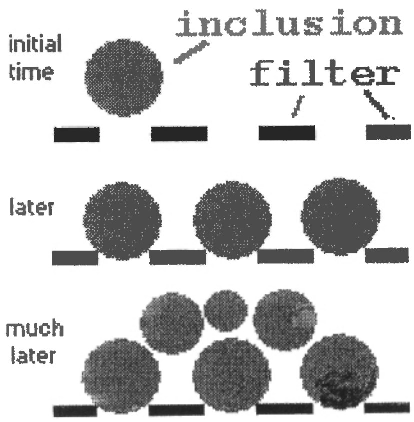

Figure 2.6. Cake-mode filtration

Both deep bed and ceramic filters make use of depth-mode filtration. The inclusions are captured throughout the thickness of the filter, and are always smaller than the openings in the filter, Figure 2.7. The filter works by employing a combination of mechanical entrapment in the pores, surface attraction van der Waals forces and sedimentation to capture particles. Unlike cake-mode filtration, the pressure drop across the filter is linear with time.

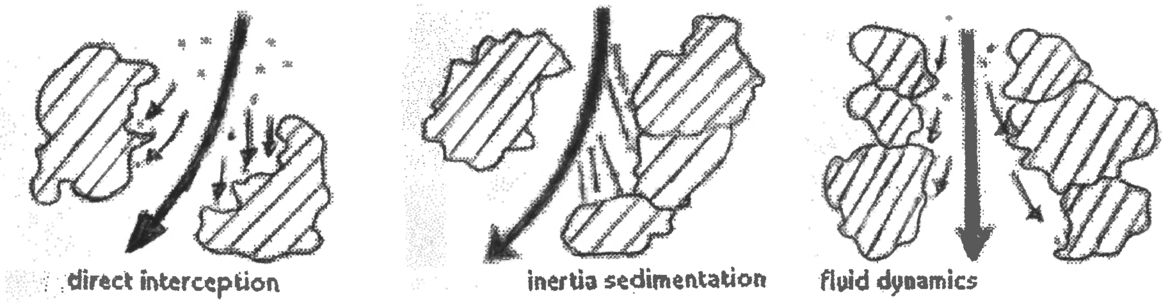

Figure 2.7. Depth-mode filtration

It is not immediately obvious that ceramic foam filters employ depth-mode rather than cake-mode filtration. The evidence for depth-mode filtration is that[47,48]:

- Inclusions are found throughout the thickness of spent filters;
- The captured inclusions are usually much smaller than pore openings;
- The metallostatic head across the filter to maintain a constant flow rate increases linearly with time;
- A cake is almost never found on the filter surface.

Filters in common use today can be categorised as:

- Packed Bed Filters or "PBF";
- Rigid media or tube filters or "RMF";
- Ceramic Foam or "CFF".

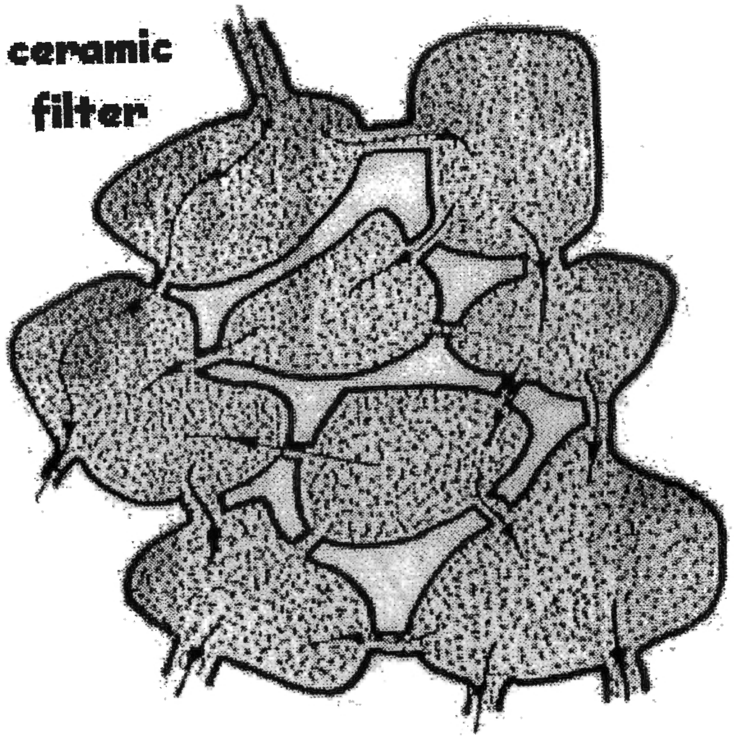

Figure 2.8. Section of a CFF

The open cell structure of a ceramic foam filter can be viewed as the opposite or negative of a cemented rigid media filter, Figure 2.8. In the foam filter, inclusions (dark dots) are trapped in the hollows whereas in the rigid media filters, inclusions are trapped in the intersections, Figure 2.9.

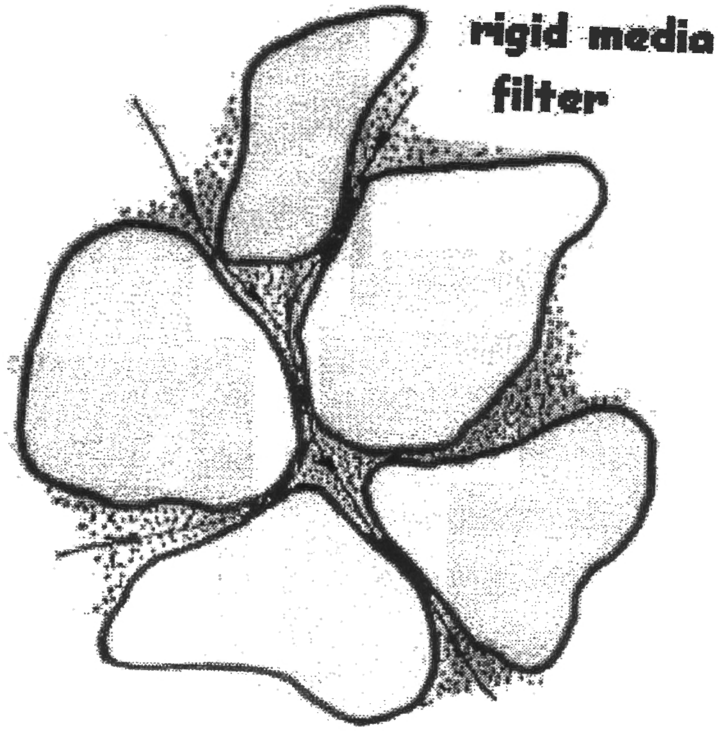

Figure 2.9. **Filter section of a RMF**

Traditionally liquid aluminium filtration employed the use of ceramic foam filters (CFF). The large acceptance of CFF's is based on their structural properties that allow a low fluid flow resistance and high filtration efficiency at a relatively low cost. In recent years there has been a move away from rigid, coherent filtering media towards loose mass separate particles such as deep-bed filtration (DBF) as the market for metal with high cleanliness increases.

Deep bed filtration consists of packed bed of refractory particles through which molten metal flows. The inclusions deposit onto the filter media through diffusion, direct interception, gravity, and/or surface forces. The primary mode of transport of inclusions smaller than 30μm to the grain surface of the filter medium is due to flow dynamics, while surface forces are responsible for the retention of the inclusion. For inclusions greater than 30μm, mechanical entrapment has been observed as the filtering mechanism.

Each has its own advantages and disadvantages as summarised in Table 2.8.

	Advantage	Disadvantage
Ceramic Foam Filter	• New filter for every cast • Very low capital cost • Visual check of filter integrity at start and end of each cast • Flexible for all alloy changes • Less potential for catastrophic inclusion releases • Sealing almost a non-issue	• Moderate filtration efficiency • Labour required for bowl clean-up and set-up for each cast • Potential for unstable operation
Bed Filter	• Excellent efficiency • No attention other than skimming and heaters required between bed changes • Long life – used for many casts	• Large metal volume • Large flushes for alloy change • Inclusions accumulated over many casts gives potential for large inclusion releases • Safety issues around box changes • High capital cost
Rigid Media Filter	• Media has high strength allowing it to be fabricated in semi-complex shapes • Large filtration area in a given volume (eg tube bank) • Excellent filtration efficiency • Used for many casts	• High capital cost • Large metal volume • Large flushes for alloy change • Potential to run with compromised seals/tubes without knowing it • Potential for large inclusion releases

Table 2.8. Advantages/disadvantages of filtration types

When looking at the important process variables that affect filtration efficiency, mathematical modelling is a useful tool in optimising filter design. During molten metal filtration, the rate of inclusion entrapment per unit packing volume $\left(\frac{\partial \sigma}{\partial \tau}\right)$ is a function of the initial inclusion concentration in the melt.

$$\boxed{\frac{\partial \sigma}{\partial \tau} = KC} \qquad (2.2)$$

where K is the kinetic parameter, C the inclusion concentration in the melt and τ is the characteristic time. In general K is a function of σ, the concentration of entrapped inclusions, as well as the melt physical properties, melt flow rate and inclusion shape and size. Hence K can be expressed as:

$$\boxed{K = K_0\left(1 - \frac{\sigma}{\sigma_m}\right)} \qquad (2.3)$$

By setting the appropriate conditions it is possible to determine the outlet concentration as a function of time. Assuming that the filter bed has only been exposed to a few residence times, then $\left(\frac{\sigma}{\sigma_m}\right) \rightarrow 0$, and the partial differential equation simplifies to:

$$\boxed{\frac{C_0}{C_i} = \exp-\left(\frac{K_0 Z}{U_m}\right)} \qquad (2.4)$$

where Z is the distance to the filter entrance, U_m the melt approach velocity, and C_i is the inlet concentration.

At the exit of the filter this equation reduces to:

$$\boxed{\frac{C_0}{C_i} = \exp-\left(\frac{K_0 L}{U_m}\right)} \qquad (2.5)$$

where C_o is the outlet concentration and L is the height of the filter bed.

Experiments can be designed to measure C_i, C_o, U_m and L, and thus K_o. Rearranging equation (2.5) gives:

$$\boxed{\frac{1}{U_m} = \frac{1}{K_o L}\ln\left(\frac{C_i}{C_o}\right)} \qquad (2.6)$$

If K_o is not a function of melt velocity, U_m, then a plot of $1/U_m$ versus $\ln(C_i/C_o)$ will yield a straight line with a slope of $1/K_oL$ passing through the origin. However if the assumption that Ko is independent of the melt velocity cannot be made, the dependence of Ko on Um can be expressed as a first order approximation linear function such as:

$$\boxed{K_o = K_o' + K_o'' U_m} \qquad (2.7)$$

and when combined with equation (2.5) gives:

$$\boxed{\frac{1}{U_m} = \frac{1}{K_o' L}\ln\left(\frac{C_i}{C_o}\right) + \left(-\frac{K_o''}{K_o'}\right)} \qquad (2.8)$$

The above suggests that a plot of $1/U_m$ versus $\ln(C_i/C_o)$ will also give a straight line with an intercept of value $\left(-\frac{K_o''}{K_o'}\right)$ and a slope of $\left(\frac{1}{K_o' L}\right)$.

From equation (2.8), the capture kinetics are a function of two terms: the first an intrinsic bed constant, attributable to the characteristics of the filter bed, i.e. filter media size and type, bed porosity and tortuosity, flow geometry, etc.; while the second is a variable which modulates the effect of melt velocity.

The fundamental parameter which characterizes the performance of a filter is the kinetic parameter K, which is a function of the magnitude of the coefficient K_o and the relative bed retention, $\left(\frac{\sigma}{\sigma_m}\right)$ as shown in equation (2.3). The coefficient K_o is a function of the melt velocity through the filter, U_m, the inclusion size, d_i, the filter grain size, d_g, and the melt system.

A summary of each of the salient points for the four particle removal techniques is given in Table 2.9[49]:

Sedimentation:	Gravity driven sedimentation in aluminium can be effective for inclusions>90μm
Flotation:	Most single stage back mix sparging devices cannot remove inclusions <30-40μm.
Cake Mode Filtration:	The specific cake resistance increases with filtration pressure and subsequently results in improved capture efficiency in constant rate filtration Filtration pressure change is an exponential function of time in constant rate filtration.
Deep Bed Filtration:	Deep bed filters can also exhibit cake mode behaviour, depending on operating conditions Optimising high-media surface-area effects make deep bed filters particularly effective at removing dilute inclusion concentrations of a size <20μm. Maintaining the integrity of the refractory wall downstream of the filter is extremely important.

Table 2.9. Filtration summary

2.3.2.3. Phases and Microstructure in lxxx Alloys

Second phase particles play a major role in determining recrystallisation behaviour, finishing characteristics, and mechanical properties of non heat-treatable alloys. The microstructure of the alloy depends on both the phases produced during casting and also on the modifications they undergo during preheating. The phases and microstructure depend on the thermodynamics of the system, but they are also quite sensitive to kinetic factors because of the many possible metastable equilibria.

The relevant phase reactions in the lxxx alloys are those of the Al-Fe-Si system. The Al-Fe equilibrium phase diagram shows that the solid solubility of iron is very low, less than 0.05%. Since the iron content of most alloys is significantly above this amount for 1xxx alloys, iron-bearing phases are expected to form at grain and cell boundaries by a eutectic reaction during solidification.

For alloys with low manganese contents and an iron/silicon ratio of greater than one, the Al-Fe equilibrium diagram predicts that the iron in aluminium-based alloys will be present in the form of an Al_3Fe constituent. However in most commercial solidification processes such as Direct Chill (DC) or roll casting of lxxx alloys, the transformation to the equilibrium phases is quite slow and any of up to 6 metastable iron-bearing phases such as Al_6Fe or Al_mFe can occur instead, even in the absence of silicon[50]. Iron-bearing phases form during solidification and are called constituents:

Al_3Fe is the stable equilibrium binary Al-Fe intermetallic phase in aluminium-rich alloys and forms only at freezing rates less than 1°C/sec. Thus is typically found only in the centre of commercial aluminium ingots. The binary Al-Mn system does not have a structural analogue to Al_3Fe.

Al_6Fe is a metastable phase formed at freezing rates between 1-10°C/sec. It is often seen in the outer few centimetres of commercial aluminium ingots. Al_6Mn is an equilibrium phase in the Al-Mn binary system and between the two binary endpoints, manganese and iron substitute freely for each other. X-ray diffraction can differentiate between Al_6Fe, $Al_6(Fe,Mn)$, $Al_6(Mn,Fe)$ and Al_6Mn.

Al_mFe is a metastable phase typically formed at freezing rates greater than 10°C/sec and probably contains about 1% Si. The relative stability of Al_6-type phases and Al_mFe is strongly influenced by impurities.

$Al_{12}Fe_3Si$ (αAl-Fe-Si) is an equilibrium ternary phase that can form during several stages of processing: during solidification as a constituent, during preheat by transformation of a metastable constituent, or during preheat as a dispersoid. The Manganese-bearing variant of this phase, $Al_{12}(Fe,Mn)_3Si$, is especially prone to form as a dispersoid.

$Al_9Fe_2Si_2$ is another ternary equilibrium phase that forms at higher silicon contents than does $Al_{12}Fe_3Si$.

Phase	Vol. % in a 0.2% Fe alloy	Wt% Si required to form phase
Al_3Fe	0.35%	None
Al_6Fe	0.61%	None
$Al_{12}Fe_3Si$	0.47%	0.034
$Al_9Fe_2Si_2$	0.57%	0.10

Table 2.10. Phases present in 1xxx series alloys

Of course silicon is never completely absent. When silicon is present, the possible number of metastable phases that may be found in the lxxx alloy sheet increases to more than a dozen. High-temperature thermal treatments transform the Al_6Fe or Al_mFe to the stable Al_3Fe phase, which occupies approximately half the volume of the Al_6Fe phase.

Fe-bearing phases and structural streaking:

The segregation of iron-bearing constituents according to freezing rate leads to "fir tree" structure in 1xxx, 3xxx and 5xxx ingot. There is a well-defined boundary between regions of the ingot that contain mostly Al_mFe and regions that contain mostly Al_6Fe. The scalped surface is primarily Al_mFe but can also contain pockets of Al_6Fe. The Al_6Fe-bearing regions cannot be seen on the as-rolled surface however, etching and anodising highlights these areas. This leads to structural streaking.

Changing the relative stability of the Al_6Fe-type phases and the Al_mFe phase can control structural streaking. Small chromium additions stabilise Al_mFe and make it impossible to find Al_6Fe phases on the scalped surface. Chromium additions as little as 0.02% extends the range of freezing rates for Al_mFe down to about 1°C/sec, effectively eliminating Al_6Fe formation. On the other hand, magnesium tends to favour the formation of Al_6Fe-type phases. At a given iron content, each iron-bearing phase will occupy a different volume in the microstructure.

Preheating:

Preheating typically involves the transformation of Al-Fe phases to ternary phases like $Al_{12}Fe_3Si$. High temperatures and low silicon contents favour the formation of Al_3Fe. By looking at the relative amounts of Al_6/Al_m, $Al_{12}Fe_3Si$ and Al_3Fe, the preheat of an alloy received can be determined. An investigation into the effect of pre-heat time and temperature on the primary particle size in 99.45% purity aluminium cast block showed that while the effect of temperature was inclusive, soak times greater than 50 hours for temperatures greater than 460°C resulted in detectable primary particle size growth[51].

Recovery and Recrystallisation:

Recovery in lxxx-HlX sheet is thermally activated, making it both time and temperature dependent. Recovery will typically begin immediately upon heating to temperatures above that at which the rolling deformation was performed. However, recovery can take place at room temperature for long-term exposures (>10 years) of 1100-H18 sheet[52]. Figure 2.10 illustrates the changes in mechanical properties that occur upon heating of alloy 1100-H19 sheet to progressively higher temperatures. Strength is lost through the initial annihilation of free dislocations and later through the growth of the subgrain structure. During recovery, a minimum in the tensile elongation is typically observed in the 180-240°C temperature range.

A rapid drop in strength and increase in ductility accompany the onset of recrystallisation as strain-free high angle grain boundaries are formed. The concepts of particle-stimulated nucleation (PSN) and Zener Drag describe the recrystallisation behaviour of cold-rolled lxxx sheet quite adequately[53,54,55]. The reduction in grain size with increasing iron content can be explained by an increase in the volume fraction of critical-sized iron-bearing particles which can act to nucleate recrystallised grains[56,57].

The deleterious effect of silicon on final grain size is caused by precipitation of silicon from solid solution prior to or during the annealing operation. The fine silicon particles impede early stages of recrystallisation within deformation zones and lead to a reduction in the number of deformation zones that can be effective nuclei for new grains[58].

The effect of cold reduction on grain size is also consistent with PSN as the increased intensity of the deformation zones adjacent to particles at higher cold reductions serves to activate additional particles of smaller sizes as nucleation sites for recrystallisation.

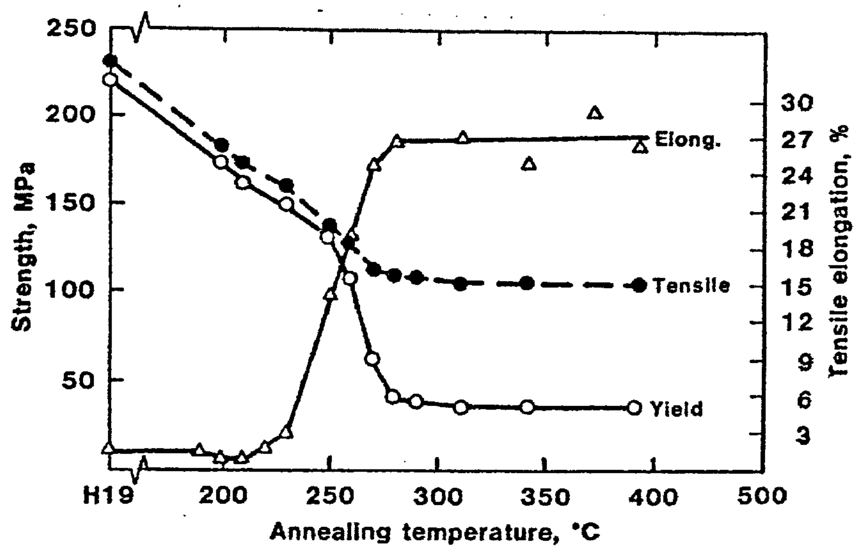

Figure 2.10. **Isochronal annealing curve for alloy 1100-H19**

The presence of iron in solid solution can affect the onset of recrystallisation. The effect is most noticeable in high-purity alloys[59], but can also be observed in commercial-purity alloys. The retardation of recrystallisation by iron in solution is caused by precipitation of fine Al-Fe particles during annealing. The specifications for 1145, currently the principle alloy produced in Australia for thin-foil product, are given in Appendix 3.

2.3.2.4. Strengthening Mechanisms in Foil Alloys

The mechanical properties of light gauge foil are difficult to measure due to the very low final product gauge, usually in the order of 5 to 20 microns. One of the more successful means of measuring foil strength and ductility employs a bladder to 'burst' through a clamped circular sample of foil and measuring the force in kPa required to inflate the bladder until it bursts through the foil sample. This test is referred to as the Burst or Mullens Test, Appendix 7.

Burst strength is strongly dependent on alloy composition and process conditions and can be estimated from foil tensile properties using the below formula[60]. Typical burst strength of foil alloys at various gauges is shown in Figure 2.11.

$$\boxed{\text{Burst Strength} = \text{constant x thickness x (UTS x elongation at fracture)}^{1/2}} \quad (2.9)$$

Metals deform plastically via the movement of dislocations through a lattice. The dislocations are able to move by mechanisms known as glide, cross slip and climb[61,39]. To achieve mechanical strengthening, the dislocations are hindered by various methods. In non-heat treatable alloys, strengthening occurs by grain and substructure refinement, strain hardening, dispersion strengthening and solid solution strengthening[35]. Other less common means include crystal structure and microstructure anisotropy[39].

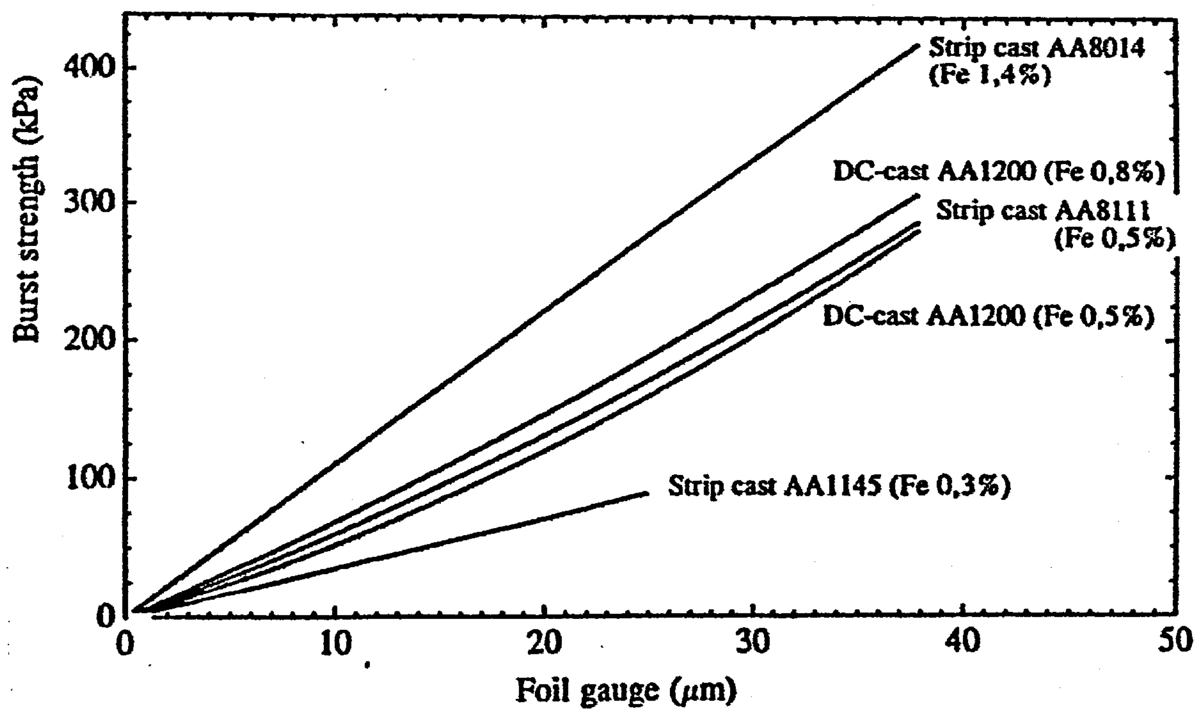

Figure 2.11. Typical burst strengths

Grain Size:

Grain size has a strong influence on both elongation and tensile strength of foil products. If the grain size is larger than 10 to 20% of the foil thickness the foil properties are reduced. However when applied to 6.3μm foil, the large boundary size increases the yield strength to the order of 200 MPa and ductility is very low. Hence a compromise between grain size, strength and ductility is required.

Aluminium's high stacking fault energy and cellular substructure promote some strengthening. Strength is related to grain size by a Hall-Petch equation, (2.10). Decreasing grain size increases the strength of the metal.

$$\boxed{\sigma_y = \sigma_o + kd^{-m}} \qquad (2.10)$$

σ_y =yield stress, σ_o = frictional stress, k = constant, d = cell size, m = variable exponent.

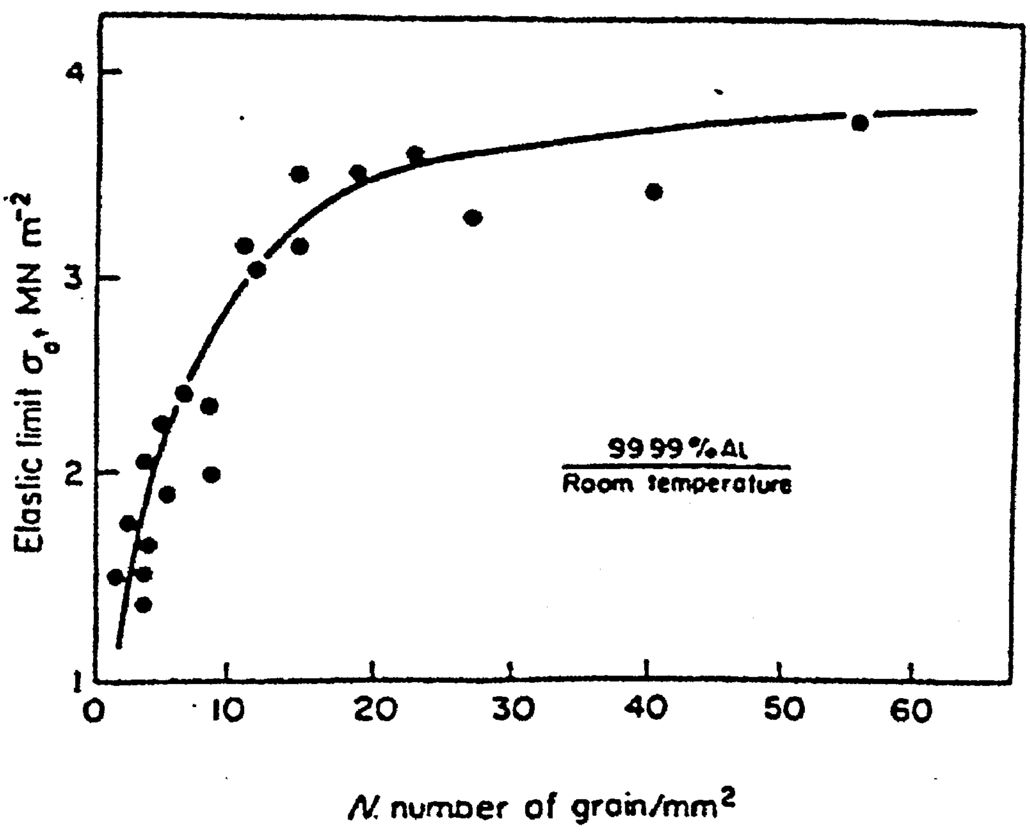

Figure 2.12. **Variation of yield strength with grain size**[62]

Grain size is strongly affected by composition, with elements such as copper, iron, magnesium and manganese decreasing grain size. The most effective inoculant is titanium boride, which promotes a fine grain structure by promoting nucleation sites within the molten metal.

Strain Hardening:

Strain hardening occurs in most working and forming operations and is the main method for strengthening heavy gauge non-heat-treatable alloys. In lxxx alloys where strength levels are very low (14-28 MPa fully annealed) strain hardening is accomplished through rolling of sheet materials at below recovery temperature. During rolling, the dislocation density increases when dislocation multiplication occurs faster than annihilation by dynamic recovery. Cold deformation is particularly effective in strengthening as recovery processes are thermally activated and are hence generally inhibited.

The increase in dislocation density causes the dislocations to interfere with each other and hinder the others movement, causing a rise in yield strength[39]. This is also referred to as work hardening. Its behaviour is modified by temperature and strain rate, with low temperatures producing more pronounced strain hardening, while at mildly elevated temperatures, the balance between work hardening rate, dynamic recovery and recrystallisation is very complex.

The influence of microstructure on strain hardening of H1X lxxx series alloys has been demonstrated in a three phase trial to vary the calculated constituent volume fraction as shown in Figure 2.13[63,64]. Increased constituent content increased strength by about 7 MPa per volume percent for both the H1X and annealed ("O") tempers. Thus increasing constituent volume yielded no additional benefits in subsequent strain-hardening during rolling.

Preheating conditions were also varied in order to produce either the Al_3Fe phase or the Al_6Fe phase. The Al_3Fe H1X material retained higher strength after rolling due to the larger amount of iron retained in solution. The constituent/yield strength dependence was similar in magnitude regardless of the type of constituent present, namely Al_6Fe or Al_3Fe.

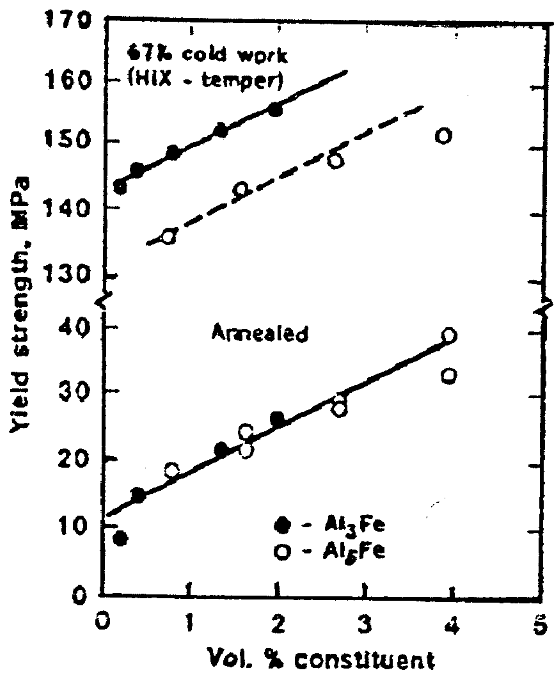

Figure 2.13. **Volume fraction in 1xxx alloys**

Dispersion Hardening:

Dispersion hardening occurs because of the ability of non-deformable incoherent precipitates to interface with glide dislocations[65]. The alloy strength is independent of mechanical properties of the particle, but strongly dependent on particle size and dispersion[66]. The hardening effect is greatest when particles are by-passed, not just cut, with strength increasing as particle size and spacing decreases. They also restrict grain growth during annealing, optimising grain size.

Dislocations by-pass particles via the Orowan-mechanism, shown in Figure 2.14[67]. An Orowan or prismatic loop is generated around a precipitate on passing, inducing mean stresses in the matrix and effectively shortening the precipitate spacing, with particle strengthening proportional to spacing:

$$\boxed{\tau \propto Gb/l} \qquad (2.11)$$

where τ is the shear stress, G is the matrix shear modulus, b is the Burgers vector, and l is the interparticle spacing.

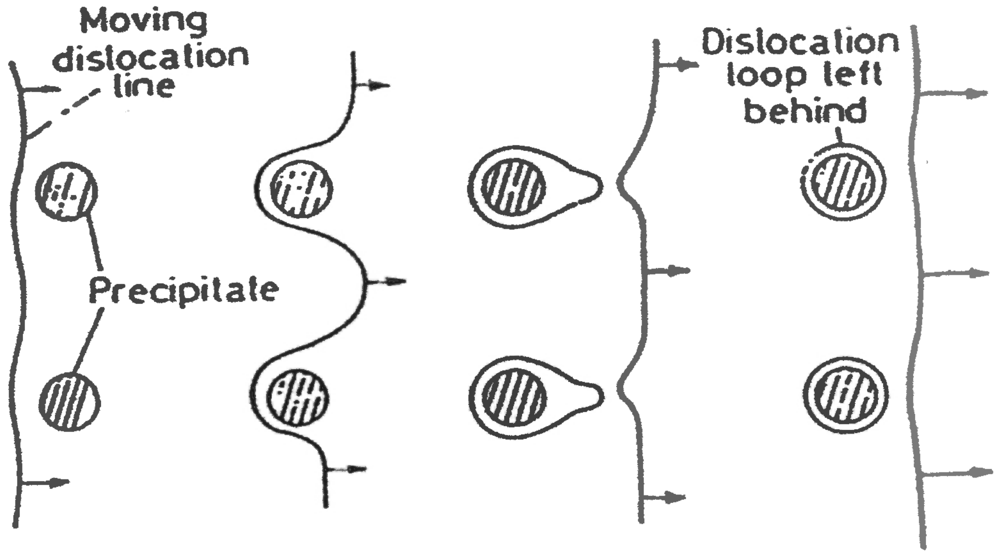

Figure 2.14. **Schematic representation of Orowan looping[67].**

In the second part of three phase trial, the H1X alloys were cold-rolled an additional 90% without an anneal (H19)[64]. The lower-iron alloys strengthened more than the high-iron alloys. The strength increase (delta = YS_{H19} -YS_{H1X}) after 90% cold reduction in the iron alloy series varied with the mean interparticle spacing of the constituent. The lattice strain actually decreased with increasing iron content, indicating that the additional volume fraction of iron-bearing constituents promotes particle induced dynamic recovery for rolling to very high strains. This interpretation is reasonable since the cold rolling of the Al-Fe alloys promotes the accumulation of dislocations in cellular structures, as shown in Figure 2.15.

Figure 2.15. **Cell dislocation cellular Structures**

Solid Solution:

The principal of solid solution strengthening is the diffusion of atoms to positions of distortion in the matrix around dislocations hindering dislocation movement[39]. Interstitially dissolved elements have a far greater strengthening effect than substitutionally dissolved elements. On an atomic basis manganese is the most effective strengthener; however manganese has a maximum solubility of only 0.2-0.3 weight percent. Magnesium is very affective on a weight basis due to its high solubility in aluminium and is the main solid solution strengthening element in 5*xxx* alloys.

Solutes can enhance strain hardening by[68]:

i) Increasing the rate of dislocation multiplication;

ii) Reducing the rate of recovery;

iii) Decreasing the dislocation mobility; or

iv) Precipitation during deformation.

High purity aluminium has very low strength, and early workers reported that solute elements invariably increase the strength of a solid solution[69]. In the third phase of the trial, silicon was varied from 0.05% to 0.60% with a 0.27% iron base. The higher strength with increased silicon in solid solution is a typical solute atom strengthening effect in that the silicon atoms impede dynamic recovery during rolling and promote strain hardening through dislocation multiplication.

Figures 2.16 – 2.18 show the effect of some alloy additions on mechanical strength upon addition to high purity aluminium. Work by Stumpf found that these ternary alloys enhance the strengthening effect when in combination with the combined solid solution strengthening effect of magnesium, copper, silicon and zinc. This combined increase is greater than predicted by the sum of the individual components indicating a synergistic effect[70].

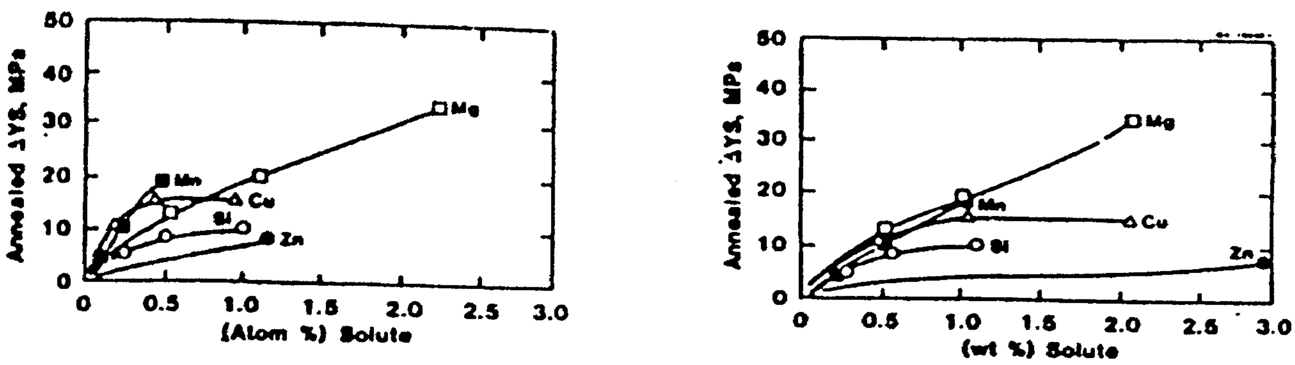

(a) (b)

Figure 2.16. **Effects of alloy additions on aging in aluminium, (a) atomic %; (b) weight %**

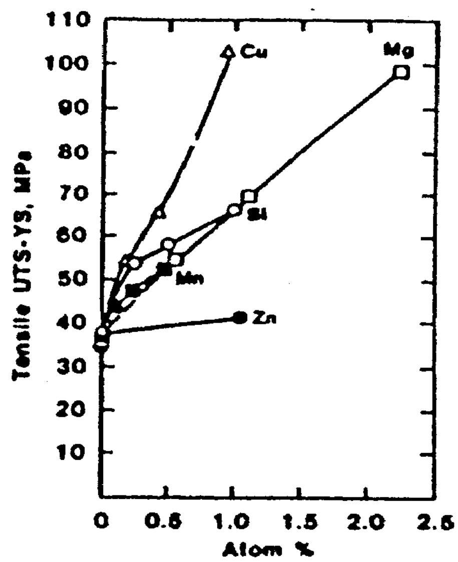

Figure 2.17. **Effects of alloy additions on UTS in aluminium**

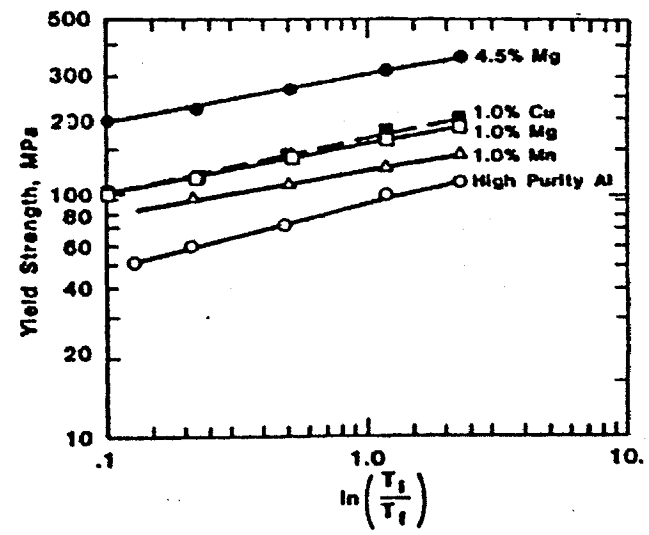

Figure 2.18. **Effects of alloy additions on yield strength in aluminium**

2.3.2.5. Annealing of 1xxx Alloys

The tensile strength of aluminium and its 1xxx series alloys increases as cold reduction percentages increase as shown in Figure 2.19 for an 1145 equivalent alloy. The increase in strength is accompanied by a decrease in ductility. When a cold worked sample is annealed the strength is reduced, slowly at first as static recovery occurs, increasing as true recrystallisation sets in until a steady state microstructure characteristic of annealed metal is reached. This is shown in Figure 2.20 where the relationship between temperature and time is characterized.

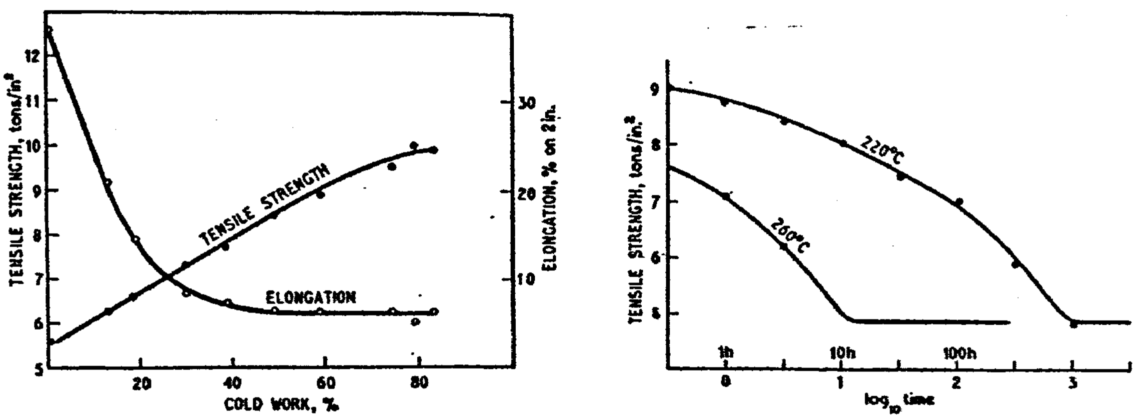

Figures 2.19 - 2.20. Cold work and time/temperature factors for 1XXX alloy

Figure 2.20 indicates that the recrystallisation process takes time to complete and at higher temperatures requires less soaking time. However the percentage cold work also affects time. A small amount of cold work can require high recrystallisation temperatures, often producing coarse grained structures. As the percentage cold work increases, the recrystallisation temperature decreases, rapidly at first, before slowing until a flat maximum is reach at 80%. Similarly, grain size decreases until 80% cold work is achieved.

By altering annealing time and temperature in conjunction with the amount of cold work on recrystallised grains and purity levels, desired strength/ductility combinations can be achieved for various applications.

Typical mechanical properties for the various tempers, known as partial anneals, and purities are given below in Table 2.11.[16]

Purity (%)	Temper	0.1% Proof Stress (MPa)	Tensile Strength (MPa)	Elongation (%)	Brinell Hardness
99.99	O		52.4		15
	½ H		72.8		22
	H		96.5		30
99.8	O		60.7	50	19
	½ H		91.0	17	31
	H		122.7	11	38
99.5	O		71.7	47	21
	½ H	85.5	99.3	13	33
	H	107.6	129.6	10	40
99.2	O	27.6	80.0	43	22
	¼ H	80.0	93.8	20	31
	½ H	93.8	107.6	12	35
	¾ H	104.8	121.3	11	38
	H	121.3	142.0	10	42

Table 2.11. Typical mechanical properties for various tempers and purities.

2.3.2.6. Surface Oxide Studies

During the heat-treatment of 1xxx series thin-foil aluminium alloys, an aluminium oxide layer forms at the metal surface. The oxide layer is initially amorphous, becoming increasingly crystalline as time and temperature increase[71,72,73,74]. At room temperature, the surface oxide exists as a natural amorphous γ-Al_2O_3, which grows by outward diffusion of metal ions as temperature increases[75]. At temperatures below 350°C oxide growth follows inverse logarithmic laws, reaching a limiting thickness of 2.5nm at room temperature to 5nm at 350°C. There is usually some oxide enrichment of alkali and alkali earth metals.

The temperature at which the oxide begins to crystallize lies between 300°C and 425°C[76-77], which is generally above that used in thin-foil heat treatment practices however well within the ranges used for heavy gauge foil practices (40-200μm). While the oxide crystallization temperature and hence the oxide thickness is not agreed in literature, there is general agreement that the kinetics of oxide growth change when temperatures reach 350°C and again at 450°C[78].

At temperatures between 350°C and 450°C, oxide growth follows a parabolic law, possibly due to either a change in the morphology of the oxide or a change to the rate control by simple diffusion of metal through the oxide film. For temperatures above 450°C, the kinetics of oxidation become complex, with oxide growth up to 57nm have been reported for samples exposed to 640°C for long periods of time[79].

During the thermal heat treatment of aluminium alloys, surface enrichment of select elements is noted to modify the chemical properties of the oxide film and influence many properties of aluminium products. There has been considerable research into surface enrichment in surface aluminium oxides, and it is generally agreed that alkali (Li) and alkaline (Mg) earth metals, present at even ppm level impurities, migrate to the oxide surface during heat treatment of commercial aluminium alloys[72,80]. This reduces surface adhesion, lacquerability and corrosion resistance.

At temperatures as low as 260°C, impurities such as magnesium, lithium and sodium are enriched in the oxide surface of aluminium foils. At temperatures greater than 340°C, almost all the available magnesium in the order of 50ppm has been completely oxidised. This is independent of residual surface lubricants such as rolling oils[80].

While alkali and alkaline earth metal have similar effects, lithium and sodium are enriched in a very thin (approx. 1nm) layer at the intermediate oxide/air phase boundary, while thermal enrichment of magnesium leads to a concentration maximum near the amorphous oxide/metal interface. Surface enrichment factors are generally around 5000 for lithium and 1000 for magnesium[81].

The magnesium enrichment at the oxide surface may have a deleterious effect on surface properties such as heat-seal adherence in foils[82], and an enhanced susceptibility of surface corrosion in the presence of humidity resulting in interfacial reactions and delamination problems in the case of lacquered foil[83]. There will also be an overall decrease in surface corrosion resistance as alkali and alkaline earth metal cations incorporated in the oxide layer shorten the incubation period for aluminium hydroxide nucleation and accelerate its growth rate[84]. Magnesium oxides have also been reported to create welding difficulties[85].

During heat-treatment, magnesium migrates to the oxide surface where it is oxidised to form MgO 'islands'. Further heat-treatment grows and joins the 'islands' to form a continuous magnesium layer over the Al_2O_3. This is demonstrated by the Lea and Ball model for the growth of oxide film on Al-Mg alloys during heat-treatment, Figure 2.21.

Surface studies indicate that surface contamination on commercial samples of aluminium foil is due to adsorbed hydrocarbons with some carbonate and organic carboxylic. The source of the carbon compound residues is believed to derive from the oxidation of the degraded fatty acid additive anions contained in the original rolling lubricant.

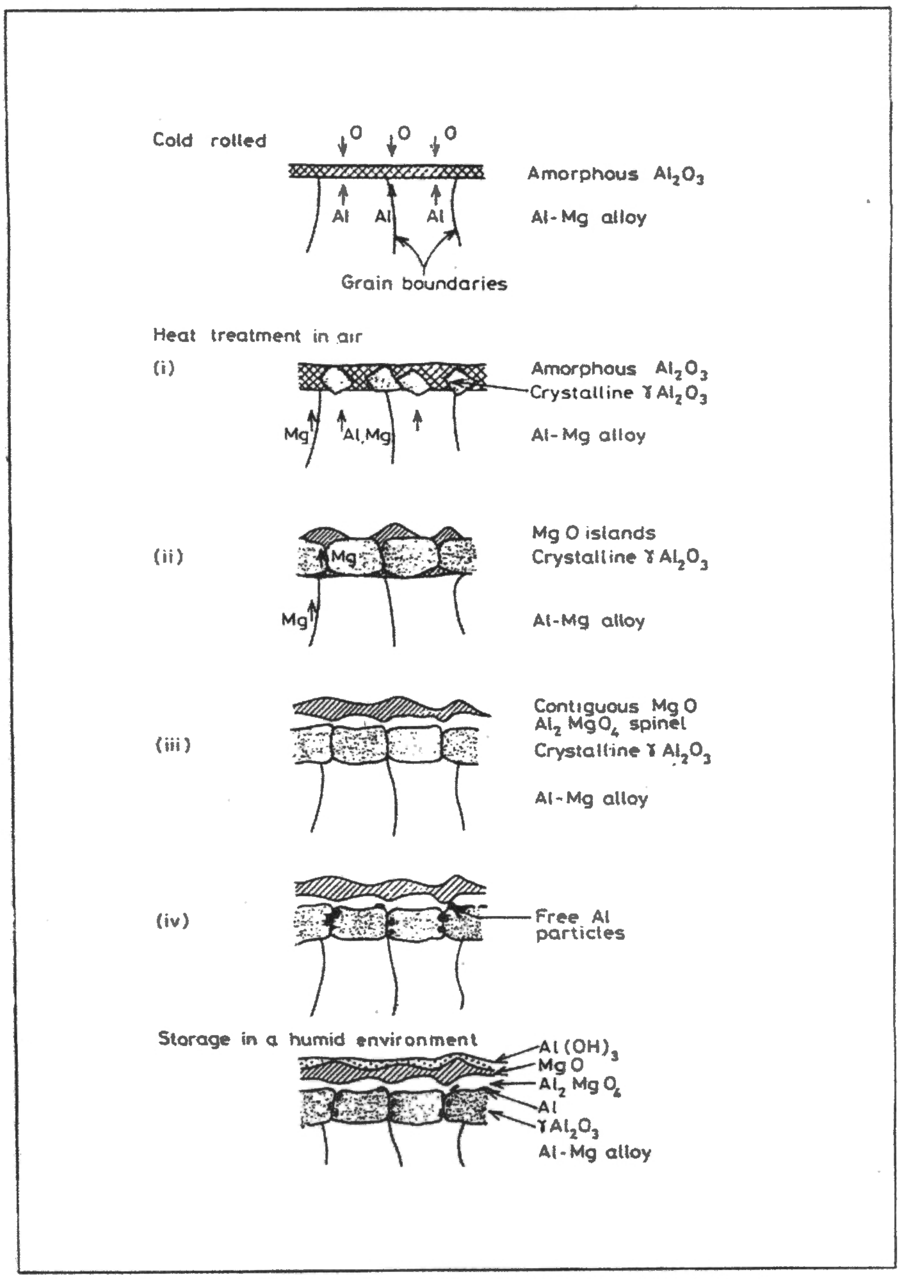

Figure 2.21. **Schematic Model of Oxide Film Growth for Al-Mg Alloys[72].**

Williams[78] examined the influence of carbonaceous surface contamination and surface oxides on thin-foil alloy 1145 aluminium foil unwind characteristics. The investigation incorporated SEM examination, SIMS analysis of the surface composition and XPS analysis (including ion etching) of the oxide and oxide thickness.

The surface oxides of 1145 alloy were observed to be featureless Al_2O_3 with similar morphology, structure and composition for free-unwinding and sticky coils. Depth profiling at the surface found the oxygen levels to have a consistent and gradual decrease indicating the oxide layer is coherent and continuous - (Figures 2.22 – 2.25). Magnesium was present at the surface, along with sodium, calcium and potassium from the rolling oil or rolled in material.

It was found that at least 60% of the original rolling lubricant remains on the strip following annealing in an oxidised and polymerised form that induces stickiness. XPS and static SIMS surface analysis of the carbonaceous surface contamination found that the residue is mainly composed of straight chain aliphatic hydrocarbons slightly polymerised to a molecular weight between 1350 and 4000, along with some alkoxygroups, ketones, carboxylic acids and carbonates. The carbonaceous residue layer was found to be less than 0.3nm thick as carbon levels dipped after one minute of ion etching.

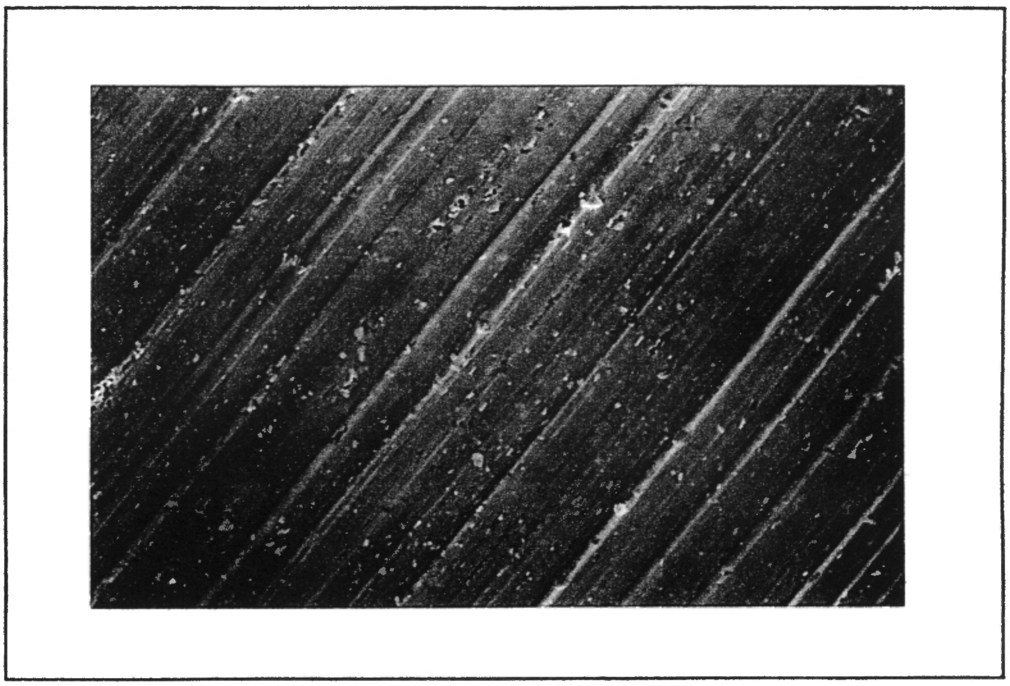

Figure 2.22. **SEM photos of foil surfaces 500x – bright side**[78]

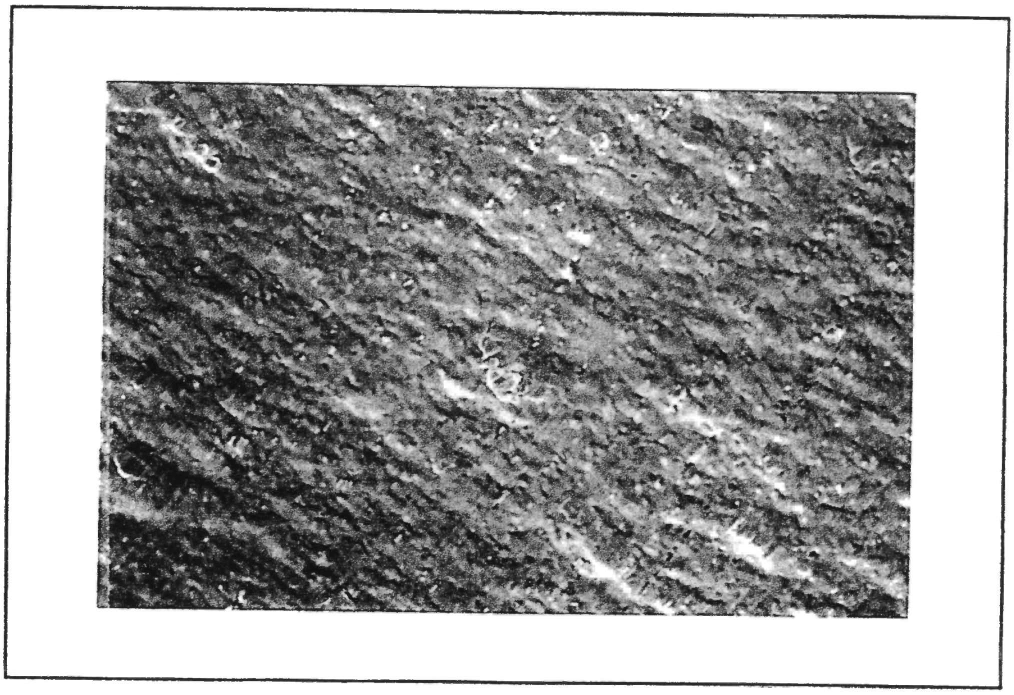

Figure 2.23. **SEM photos of foil surfaces 500x - matte side**[78]

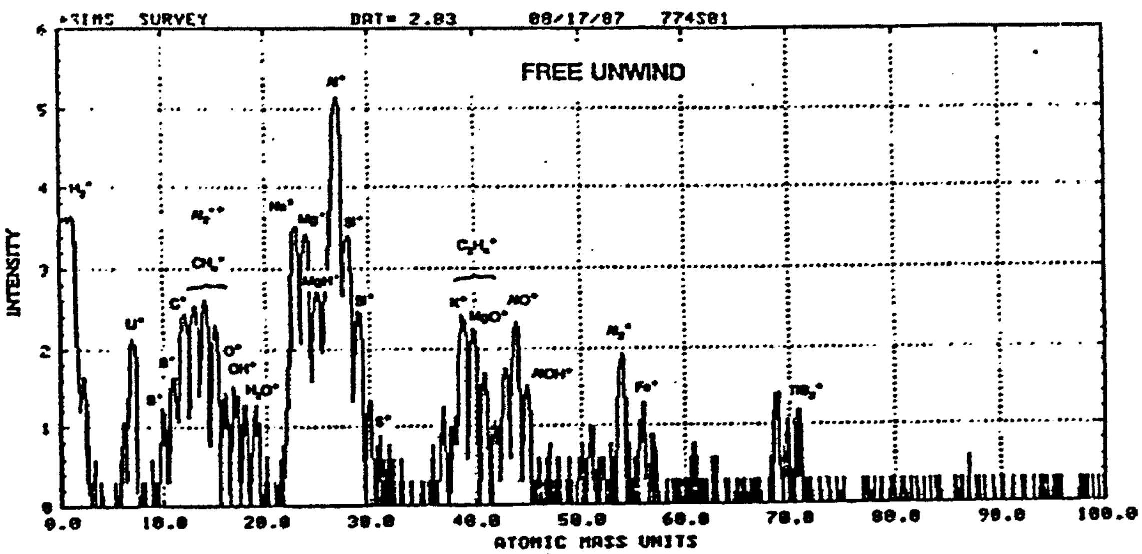

Figure 2.24. Secondary ion mass spectroscopy of matte foil surface for 1145 alloy - free unwind[78]

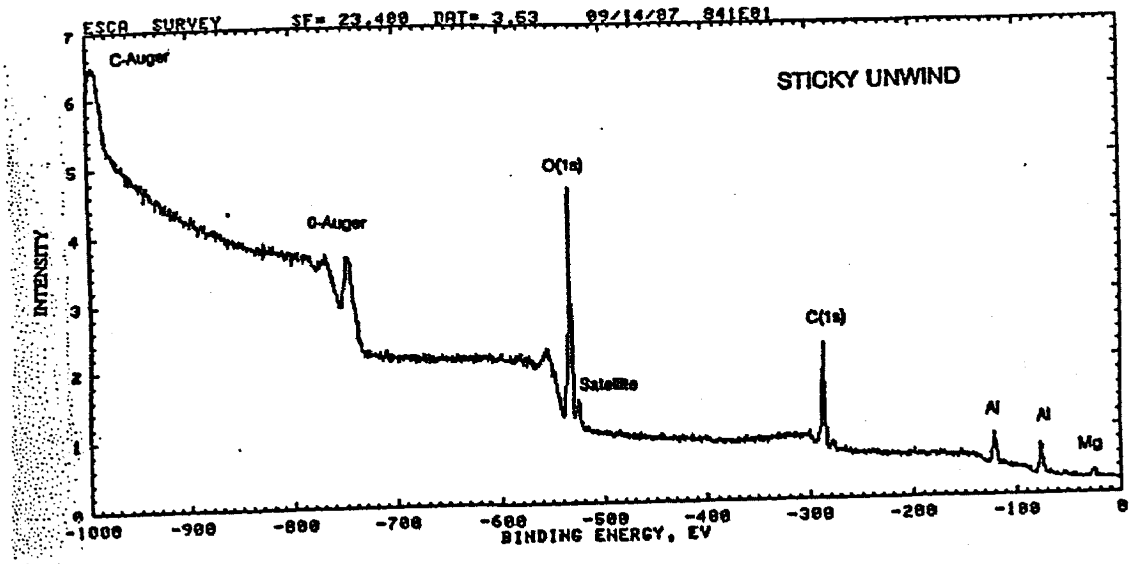

Figure 2.25. X-ray photoelectron spectroscopy of matte foil surface for 1145 alloy – sticky unwind[78]

2.3.3. 8XXX Alloys

Since the first alloy additions in the early 1900's, inventors have blended strong, high melting metals such as iron and nickel with aluminium in an attempt to produce a light, strong alloy. In recent years, there have been several alloys developed to give higher strength without significant loss of ductility by increased additions of silicon, iron and manganese. For light gauge foils, increased strength allows foil to be processed with less risk of a web break. From a customer standpoint, it enables lower gauges without decreases in strength or ductility to be employed for various applications.

The properties of an aluminium alloy are determined by its microstructure. The best combination of properties is achieved by controlling the grain size and hence composition. If iron is the only addition, $FeAl_6$ is formed during rapid cooling as a coupled eutectic that upon working and annealing transforms into finely dispersed $FeAl_3$. In the presence of manganese the $(FeMn)Al_6$ compound is formed, and with silicon present as an impurity (most in solution), small amounts of Fe_2SiAl_8 or $(FeMn)_3SiAl_{15}$ may form. In all cases these constituents are present as very fine dispersions, which can be used in combination with various annealing temperatures to control strength and ductility (particularly for Al-FeMn alloys)[86].

Al-Fe Alloys:

Iron reduces the grain size, with the reduction limited during crystallization from the melt but appreciable in recrystallisation as $FeAl_3$ particles tend to pin dislocations and thus hinder grain growth. The formability of aluminium-iron alloys such as 8079 depend mainly on size and distribution of intermetallic particles; coarse crystals of $FeAl_3$ tend to crack and produce notches that reduce formability and fatigue resistance; finely dispersed $FeAl_6$ does not have the same effect. In wrought alloys, iron is more evenly dispersed, with the change in properties shown in Table 2.13.

	Al 99.99%		Al+1%Fe		Al+1.7%Fe		Al+2.5%Fe	Al+10%Fe
	O	H	O	H	O	H	O	O
UTS (MPa)	45	130	110	160	120	190	110	100
YS (MPa)	24	120	-	-	80	170	-	-
%E	49	6	38.3	12.6	30	7.5	24	5
H_v(MPa)	140	320	-	-	300	440	-	350

Table 2.12. Mechanical properties of aluminium-iron alloys

Interpretation of the data in Table 2.12 indicates that the best compromise between Iron additions and metallurgical/mechanical properties occurs between 1.0 - 1.7% iron due to eutectic formation. The increased iron content improves mechanical strength through solid solution hardening for both annealed and temper product at a similar rate, implying no work hardening benefits.

The eutectic solid solubility of iron in aluminium is between 0.03% - 0.05% at eutectic temperature, decreasing to less than 0.00% at 700 Kelvin (K). Any residual iron is usually designated as $FeAl_3$ (40.7% iron), however some analyses have reported Fe_2Al_7, Fe_4Al_{13} or Fe_6Al_{19}. The $FeAl_3$ compound forms directly from the liquid at 1420K, with the eutectic within the range 1.7-2.2% iron, Figure 2.26. The metastable compound $FeAl_6$ is found in rapidly chilled alloys, and is isomorphous with $MnAl_6$. Formation of $FeAl_6$ instead of $FeAl_3$ is probably a nucleation phenomenon as $FeAl_3$ is nucleated at lower undercooling (<8K) while $FeAl_6$ has a higher undercooling (>10K).

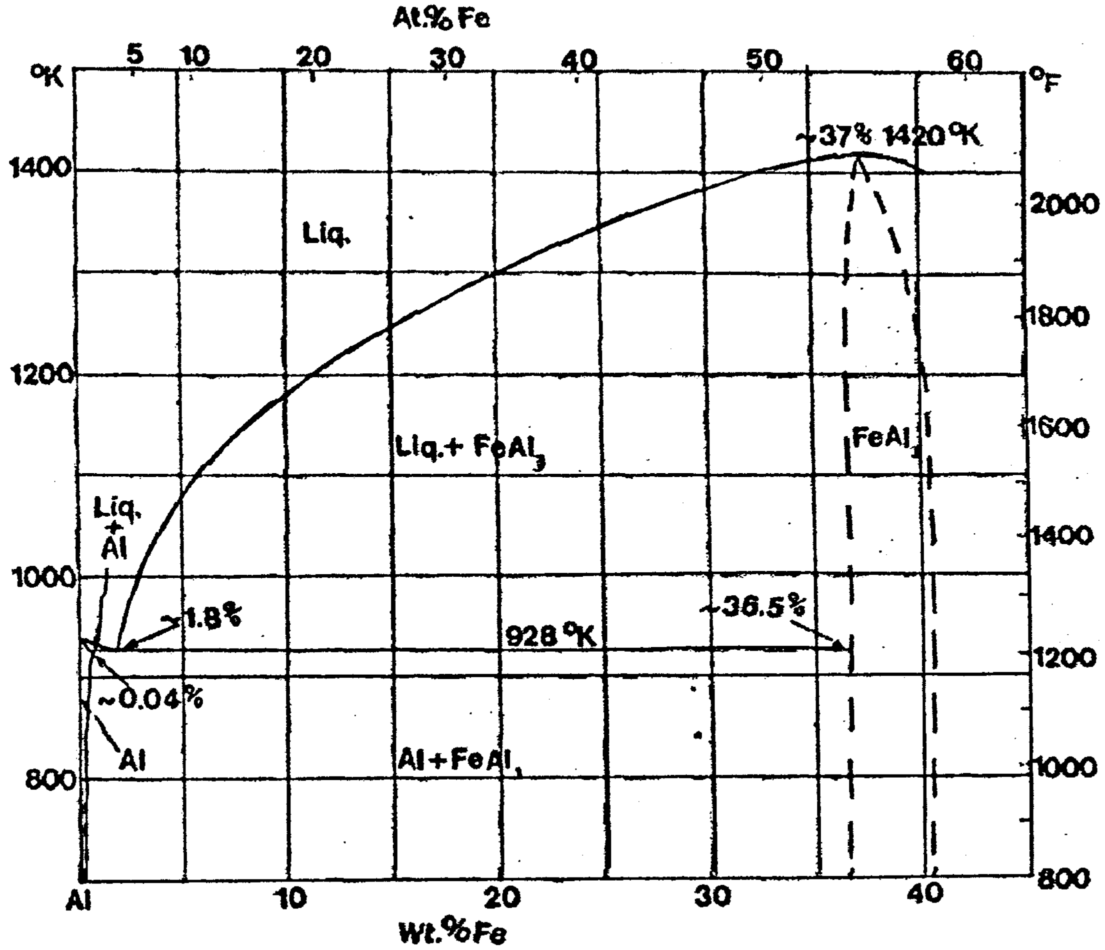

Figure 2.26. **Aluminium - iron phase diagram**[39]

Al-Fe-Si Alloys:

Alloys with significant additions of iron and silicon (for example 8011) have been used for many years as a principal alloy for strip cast aluminium product due to its grain refining characteristics. It is well known that iron and silicon affect the mechanical properties of aluminium alloys as they can transform or precipitate easily with heat treatment at temperatures between 473K to 873K, Figure 2.27. In foil stock production, homogenising or hot rolling at temperatures between 673K to 773K promotes iron and silicon precipitation resulting in mild work hardening and subsequent lower softening temperatures[87].

Less than 0.2% silicon dissolves in $FeAl_3$, the solubility of iron in silicon is negligible. The fields of existence of the ternary phases in the solid state are mostly outside their range of primary crystallization, and completion of peritectic reactions is necessary for equilibrium to be established. For this reason most commercial alloys are not in equilibrium and it is not uncommon to find alloys in which $FeAl_6$, $FeAl_3$, Fe_2SiAl_8, $FeSiAl_5$ and $FeSiAl_4$ may coexist with one another and with silicon.

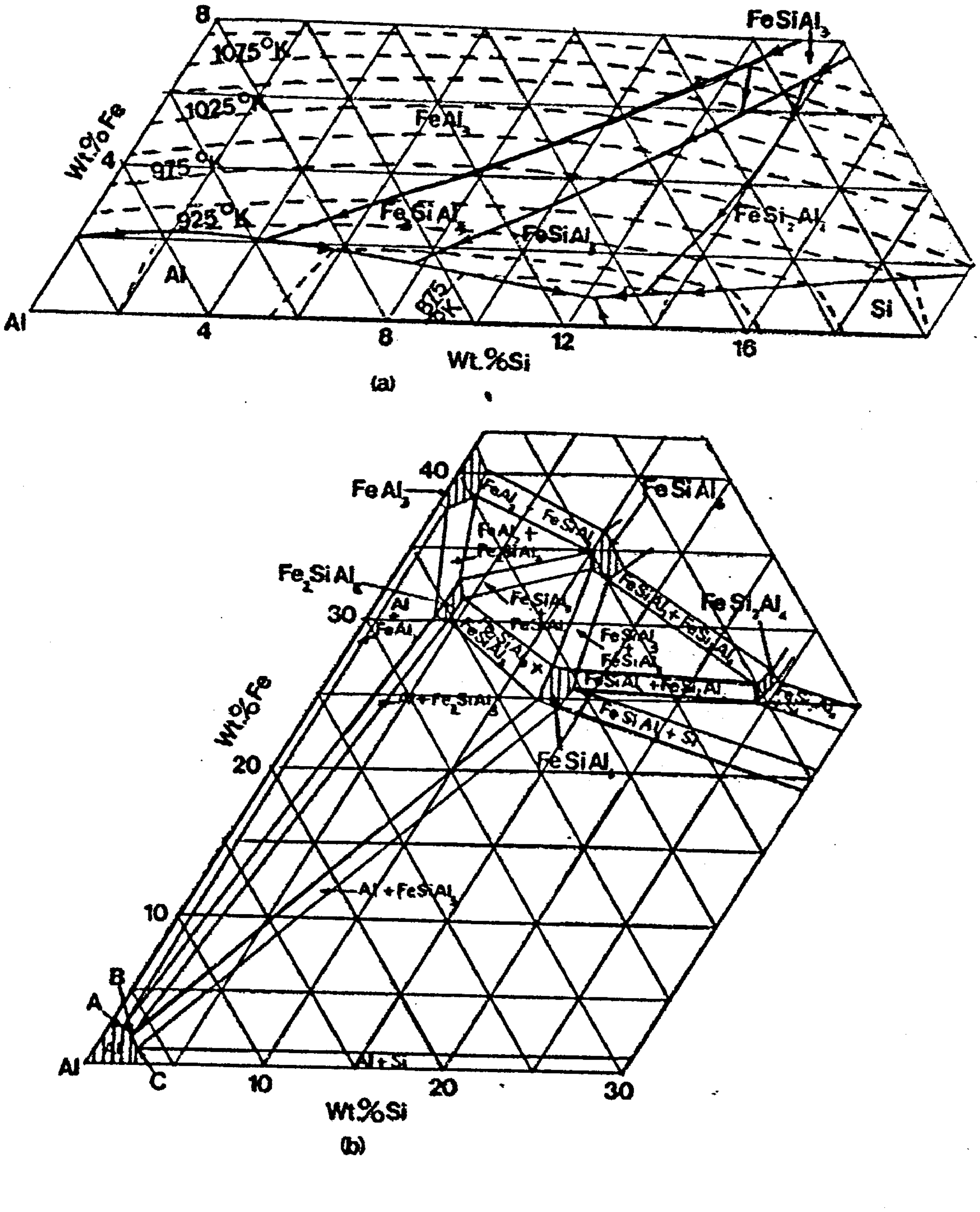

Figure 2.27. **Aluminium – iron – silicon phase diagram**[39]

Al-Fe-Mn-Si Alloys:

The development of alloys such as 8006[88], 8014 and 8022 that combine the effect of iron, manganese and silicon have enabled low-gauge high-strength applications to be explored, Figure 2.28. The as-cast alloys generally contain 5-20% by volume unaligned intermetallic rods with an average diameter of 0.1 – 1.5 microns, preferably between 0.1 – 0.8 microns, and are essentially free of primary intermetallic particles. During cold working, the rods are dispersed through the metal matrix with the aspect ratio of the rods after deformation between 1:1 to 5:1 and evenly distributed. If the volume fraction is less than 5%, the mechanical properties become too low, if greater than 20%, ductility and toughness decrease.

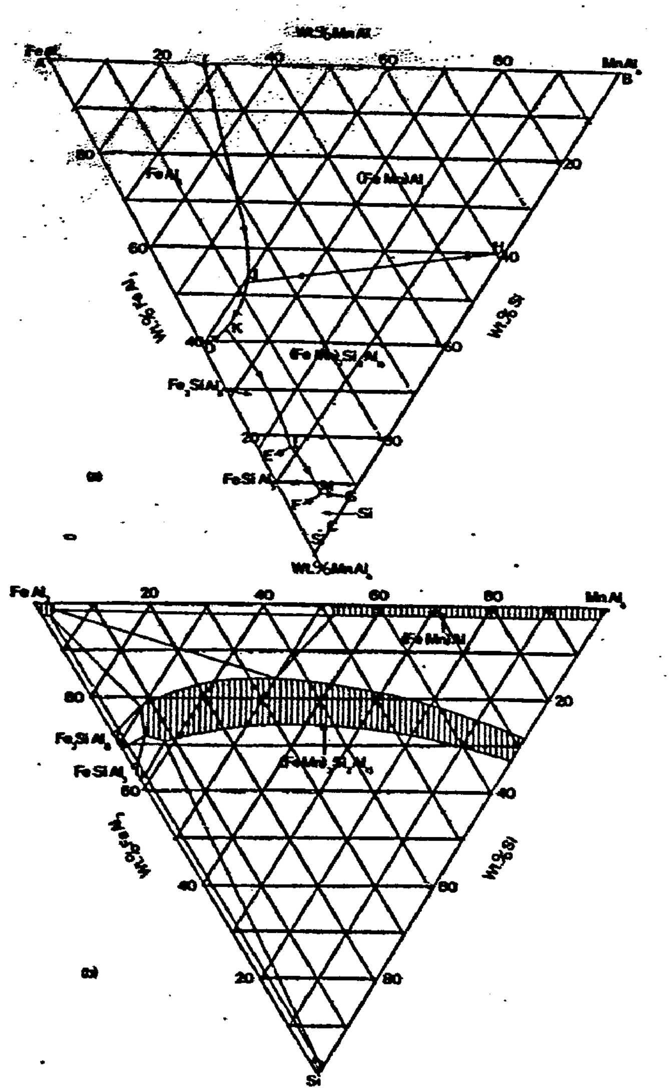

Figure 2.28. **Aluminium – iron – manganese - silicon phase diagram[39]**

CHAPTER 3 ROLLING THEORY

Modelling of closed gap rolling is a relatively new discipline, with little published information until the early 1990's. In the context of this thesis it is important to determine what parameters to manipulate to increase rolling speeds. The information is to be included in an ALCOA database dedicated to foil products.

3.1. Introduction

There are several processing methods that employ permanent plastic deformation to achieve a desired dimensional and metallurgical structure. One method, the practice of flat rolling, aims to reduce the thickness of a metal slab or strip by passing it through a pair of driven rolls under load at nominal or elevated temperature. Flat rolling has many technological areas and associated rolling models as shown in Figure 3.1. Of these, only roll gap theory will be discussed at any great length as it is the model most relevant to thin foil rolling. Flatness and profile, thermal analysis, material properties and roll stack deflection are related to casting, hot rolling and open gap processes as many downstream properties are determined by up-stream processing.

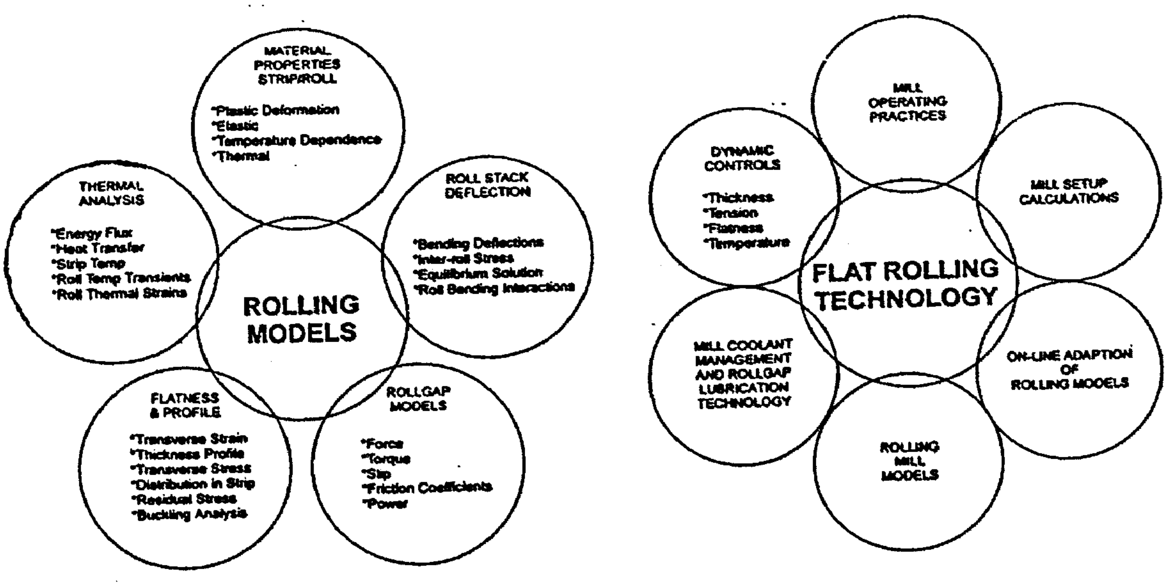

Figure 3.1. **Major areas associated with flat rolling technology**

Rolling gap theory is concerned with the solution(s) of equations describing the deformation phenomena occurring in the roll gap to predict roll force, roll torque and the forward slip ratio. The control of strip centre-line thickness requires knowledge of the relationship between changes in force and strip exit thickness. This relationship is satisfactorily explained for a majority of cold-rolling processes, however in cases where roll deformation becomes significant when compared to the metal strip thickness, the relationship is not as well understood.

A considerable volume of published literature exists on the topic of strip rolling theory, with the mathematical modelling contribution explored by Domanti and McElwain[89]. The principal avenues of research are as follows:

Applied Mechanics:
Force equilibrium equations and plasticity yield criteria are solved analytically to produce a differential equation that can be integrated for the vertical pressure distribution. Both circular and non-circular arcs of contact can be considered and sticking or slipping contact may occur.

Fluid Mechanics:
The deforming strip is regarded as a viscous fluid in a converging channel.

Hydrodynamic Lubrication Model:
Avoids the assumption of a priori surface shear relationship by utilising a liquid film interface between the strip and the roll. Orowan's equations are normally assumed with circular and non-circular arc roll deformations able to be considered.

Slip Line Field Solutions:
Take into account large degrees of non-homogeneous deformation.

Heuristic Geometrical Approach:
Uses priori knowledge of the form of a pressure distribution to derive simplified model equations.

Finite Element Models:
Constitutive equations in two dimensions with approximate friction models to represent the shear stress between the strip and the roll.

The most appropriate model is dependant on the degree of homogeneous compression or the degree of flattening of the rolls. Figure 3.2 represents a range of gauges and illustrates where a more sophisticated rolling theory can be applied. The Oworan Model represents classical analysis for circular-arc situations, while the Formula Based Rollgap Model is a simplified model with adjustable constants for automotive applications. An introduction to the fundamentals of open-gap rolling by Wusatowski provides a fundamental explanation of the Orowan Model[90].

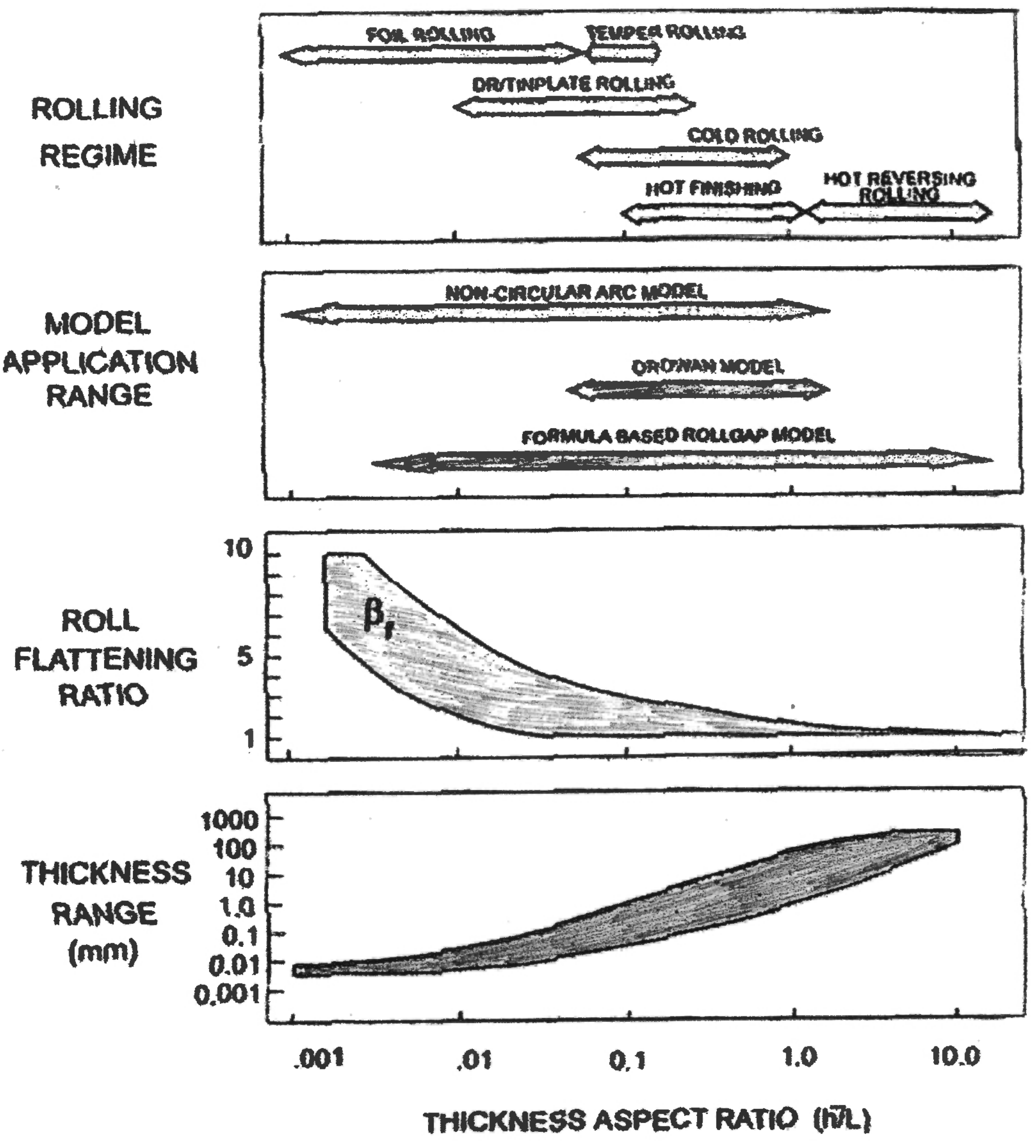

Figure 3.2. Rolling regimes for different mill types

3.2. Circular Arc Rolling Model (Orowan's Model)

Although developed over 50 years ago, the "slab" model remains a fundamental component of many rolling theories to obtain a satisfactory method of calculating roll pressure and torque from geometrical and physical data of the rolls and rolled material[91]. Equations describing the horizontal face equilibrium of a small element of the strip in the plastic region (Figure 3.3) are combined with a suitable yield criterion to yield a first-order differential equation for the roll pressure through the roll gap.

Orowan's model is based on the following assumptions:

1. The deformation could be represented as a plane strain, i.e. no transverse strains.
2. The arc of contact is circular although its radius may change, modelled by Hitchcock's formulae[92].

$$\boxed{\frac{1}{R}-\frac{1}{R'}=\frac{cP}{L^2}} \tag{3.1}$$

R = radius, L = length of arc, c = elastic constant, P = force

3. Coulomb friction with the possibility of sticking.
4. The material is incompressible.
5. Non-parallel compression plates approximate the stress distribution through the strip thickness.

Using these assumptions, a number of important and useful geometrical and kinematic relationships can be derived. Examining the roll gap geometry, Figure 3.4, with an exaggerated angle of contact φ_m, an arbitrary point through the roll gap may be located in terms of angle φ or the coordinate x, both measured from the exit plane. Generally the angle of contact φ_m is small (less than 7 degrees), and therefore the length L of the arc of contact is equal to $R'\varphi_m$.

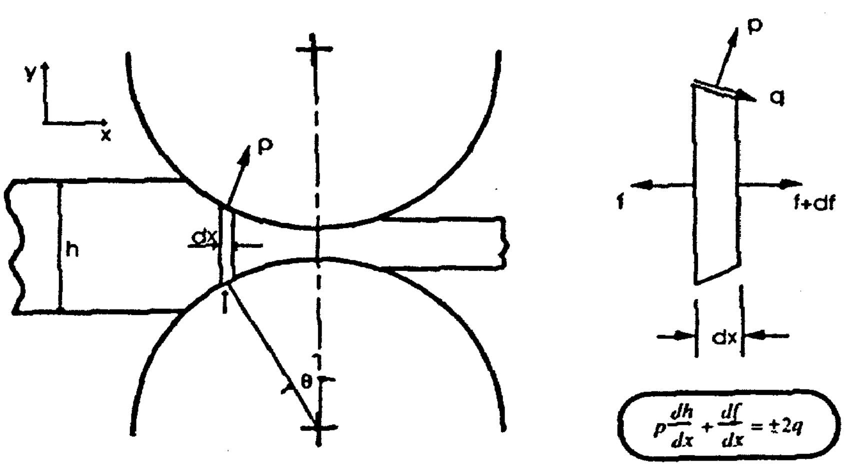

Figure 3.3. Slab-based rolling model

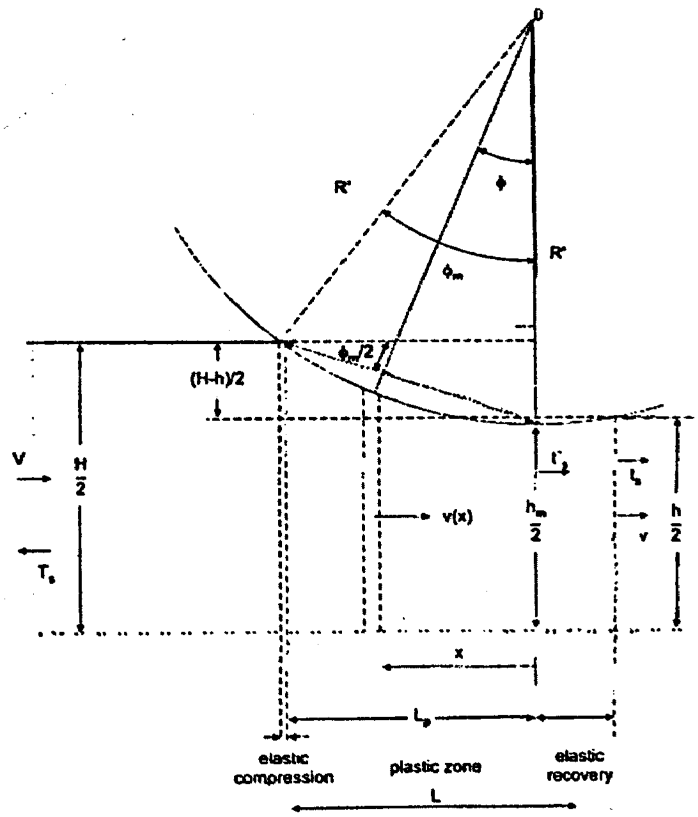

Figure 3.4. Roll gap geometry

The nomenclature used in the below models is based on Figure 3.4.

Length of Contact Arc L:

$$\boxed{\text{Tan}\ (\varphi_m/2) = \frac{\frac{1}{2}(H-h)}{L_p}} \tag{3.2}$$

If L_p is assumed equal to the chord length, and tan $\left(\frac{\varphi_m}{2}\right)$ is approximated by $\left(\frac{\varphi_m}{2}\right)$, the well-known result for the length of the arc of contact may be derived:

$$\boxed{L_p = \sqrt{R'(H-h)} = \sqrt{R'\delta}} \tag{3.3}$$

where the draft δ is defined as the change in thickness for the pass. Note that this includes the length of the plastic deformation zone L_p, and ignores the elastic zone length L_e.

Mass Flow Relationship:

For homogeneous, steady speed rolling, the mass of material passing any given point in the roll gap per unit time is constant (M). That is:

$$\boxed{M = W\rho h(x)v(x) = W\rho HV = w\rho hv} \tag{3.4}$$

Assuming that the density and width is constant this gives the useful special result for cold rolling:

$$\boxed{VH = v(x)h(x) = vh} \tag{3.5}$$

Thickness Variation Through the Roll gap:

Since the arc is similar, the thickness $h(\varphi)$ at any given point is represented by:

$$\boxed{h(\varphi) = h + 2R\ (1\text{-}\cos\varphi)} \tag{3.6}$$

Replacing (1-cosφ) by the approximation $\varphi^2/2$ leads to:

$$\boxed{h(\varphi) = h + 2R'\,\varphi^2} \tag{3.7}$$

and expressing φ in terms of x $(=R'\varphi)$

$$\boxed{h(x) = h + (H-h)\,x^{*2}} \tag{3.8}$$

Velocity Variation Through the Roll gap:

The strip accelerates through the roll gap from an initial entry velocity of V to the exit velocity v. Combining the mass flow and thickness variation equations derived previously leads to the result:

$$\boxed{v(\varphi) = \frac{vh}{\left[h + 2R'(1-\cos\varphi)\right]}} \quad (3.9)$$

or in terms of x^*:

$$\boxed{v(x^*) = \left[\frac{v}{1+\left(H/h - 1\right)x^{*2}}\right]} \quad (3.10)$$

Forward Slip Ratio:

The forward slip ratio f may be derived from the preceding equation by substituting V_p for $v(\varphi)$ and the neutral angle φ_N for φ:

$$\boxed{Vp = \frac{vh}{\left[h + 2R'(1-\cos\varphi_N)\right]}} \quad (3.11)$$

or in terms of f,

$$\boxed{f = \frac{v}{V_p} = 1 + \frac{2R'(1-\cos\varphi_N)}{h}} \quad (3.12)$$

A more useful form of this equation is in terms of the neutral point coordinate, x_N^*,

$$\boxed{f = \frac{v}{V_p} = 1 + x_N^{*2}\frac{H-h}{h}} \quad (3.13)$$

Deformed Roll Radius:

When the change in strip thickness is significantly larger than the radial roll surface deflection, it is reasonable to assume a circular arc of contact. Hot rolling and cold rolling of sheet products meet this requirement. Foil rolling, temper rolling and double cold reduction of tinplate may not.

The classical work on this topic is contained in an ASME report by Hitchcock (1935)[92] who showed that the typical pressure distributions in rolling tend to maintain an approximately circular arc of contact whose change in curvature is given by:

$$\boxed{\frac{1}{R}-\frac{1}{R'}=\frac{cP}{L^2}} \quad (3.14)$$

where c is an elastic constant $\boxed{\frac{16(1-\upsilon^2)}{\pi E}}$. For the case where L is replaced by the expression ($L_p + L_e$) this becomes,

$$\boxed{R' = R\left[1+\frac{R'cP}{\left(L_p+L_e\right)^2}\right]} \quad (3.15)$$

$$\boxed{R' = R\left[1+\frac{cP}{\left(\sqrt{H-h_m}+\sqrt{h-h_m}\right)^2}\right]} \quad (3.16)$$

If elastic recovery effects are ignored, then the more familiar form is achieved;

$$\boxed{R' = R\left[1+\frac{cP}{\delta}\right]} \quad (3.17)$$

This equation is not recommended for any cold rolling calculations as elastic effects can be significant. For a more detailed background on the concepts of rolling, the textbooks by Roberts are recommended.

Due to the lack of computing power to manually calculate the pressure distributions and rolling forces, numerous simplifications were made to cater for specific rolling classes. With the advent of the computer, simplifications were no longer required due to improved solution times, allowing the introduction of asymptotic techniques to approximate solutions of governing equations, and increased sophistication of numerical models, in particular models solved by the finite element method

3.2.1. Asymptotic Techniques

The asymptotic technique applies suitable scaling of the parameters of interest in differential equations with the magnitude of the resulting terms examined. By including only the terms of greatest importance, an approximate or 'leading-order' solution can often be obtained. The advantage of the asymptotic approach is that they in general provide simpler analytical approximations while allowing the relative importance of parameters to be assessed.

Leading-order approximations differ from the inhomogeneous Orowan model by generating non-linear shear stress distributions through the strip thickness, and predicting variations in yield stresses through the thickness of the strip as a result of variations in the degree of work hardening[93,94].

3.2.2. Finite Element Methods

Progress in developing finite element models of flat sheet rolling has progressed at a rapid rate over the past 25 years. Finite element models have the following distinctions:

a) The models are considered to be two or three-dimensional. If constraints to either displacement or velocity in one of the three dimensions are used to simplify a three-dimensional analysis, the model is referred to as 'quasi three-dimensional'.

b) A strip material model; The major ones include viscoplastic, rigid plastic, elastoviscoplastic and elastic-plastic.

c) A roll model; Rigid or elastic body.

d) The model formulation is generally considered Eulerian (steady-state), Lagrangian (non-steady-state), or a hybrid of the two.

The earliest approach in the mid to late 1970's was based on viscoplastic and elastoviscoplastic material models where once the yield stress is exceeded, the strain rate is proportional to stress. These Eulerian-based approaches solve for the velocity and stress fields and iterate to obtain a free surface. In general, viscoplastic and elastoviscoplastic models are more representative of hot rolling situations where strain rate effects are more dominate[95].

The rigid-plastic finite element analysis of strip rolling was developed in the early 1980's. The rigid-plastic material model differs from the viscoplastic model as, in general, the solution is not time dependant. Both Eulerian and Lagrangian formulations were used with a range of material and friction models[96,97]. By the mid 1980's, elastic-plastic analysis of rolling using two-dimensional models became more popular[98]. A number of three-dimensional analyses resulted in an extension of the application of elastic-plastic modelling in two-dimensions during the mid-late 1980's until the early 1990's[99].

Three-dimensional analysis began using quasi three-dimensional models because of the limitations on the number of nodes and the number of degrees of freedom that could be solved in a realistic time frame on the available computers in the early 1980's[100]. The limited width-depth ratio that could be tackled during this time meant that the models were not suitable for three-dimensional modelling of flat strip rolling.

The three-dimensional analysis of the rolling of flat material where the strip width-thickness ratio may exceed 1000 has precluded the use of the finite element approach owing to the high computational requirement. However in cold-rolling simulations when rolling thinner strips, the increase in the length of contact as a result of roll deformation can cause significant increases in the roll load[101].

3.3. Non-Circular Arc Rolling Model[102]

Rolling theories based on a deformed circular arc predict a rapid increase in rolling load as rolling exit gauge decreases. As the roll radius to deformed roll radius ratio approaches zero, the roll load moves towards a second order dependence on the friction hill parameter $f(\lambda)$. Consequently, the larger rolling loads produced larger roll deformations resulting in a flattening of the work rolls as shown by Larke and Orowan[103]. Further reduction of the strip is no longer possible introducing the concept of a limiting reduction. They concluded that the Hitchcock method cannot be used except when roll flattening represents a small correction only.

Researchers in the 1950's and 1960's used improved roll deformation models to consider issues including minimum thickness, maximum reduction and the condition for the onset of yield[104,105,106]. However these approaches were plagued by numerical convergence problems when applied to thinner materials, often predicting indentations in the roll surface or oscillating roll pressure distributions.

The convergence difficulties remained unresolved until Fleck and Johnson developed a model for foil rolling which assumed the existence of up to five regions within the roll gap, Figure 3.5[107]. The first two regions relate to elastic compression followed by plastic reduction at the roll gap entry. This is followed by a region of contained plastic flow where no reduction occurs and the roll surfaces become flat and parallel. The last two regions are an area of plastic reduction followed by an elastic recovery region.

The shear stresses at the roll surface in the central region can be predicted by Coulomb friction, reducing the rate of pressure rise in the flattened region, consequently avoiding the roll indentation phenomenon characterised in earlier models. Further development work in 1992 included a more realistic roll deformation model employing influence functions rather than a simpler scalar model, however required solution times were two orders of magnitude longer than before[108]. Gratacos investigated the modelling of cold rolling and temper rolling using a finite element approach reporting results similar to those of Fleck[109].

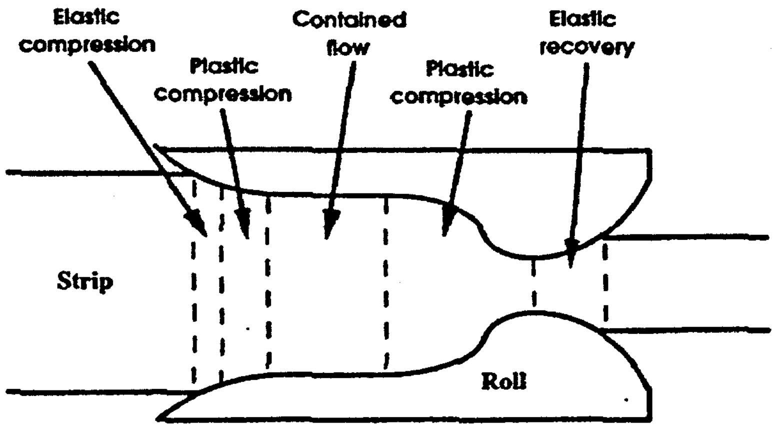

Figure 3.5. Typical roll gap profile as predicted by the Fleck and Johnson model

The non-circular arc roll gap model assumes plane strain compression and consists of the following components:

- Model for the roll pressure in the plastic regions
- Model for the roll pressure in the elastic regions
- Model for the roll deformation
- Yield stress Model
- Temperature Model
- Initialisation and convergence algorithm

3.3.1. Roll Pressure in the Plastic Region

For non-circular arc models, the angular position of the element does not define the roll surface angle. Here the differential equation for the horizontal force will contain two angles θ, the angle from the vertical roll centreline, and ϕ the angle of the roll surface to the horizontal. The differential equation for the horizontal force for slipping, $t_f(\theta)$ is:

$$\boxed{\frac{dt_f(\theta)}{d\theta} = -2R(\theta)\cos(\theta)s(\theta)(\tan(\phi) \pm \mu)} \qquad (3.18)$$

And for sticking, (when $2\mu s > k$):

$$\boxed{\frac{dt_f(\theta)}{d\theta} = -2R(\theta)\cos(\theta)\left(s(\theta)\tan(\phi) \pm \frac{k}{2}\right)} \tag{3.19}$$

where R is the roll radius, μ the coefficient of friction and $s(\theta)$ is the normal roll pressure that is given by:

$$\boxed{s(\theta) = \frac{\left(\frac{t_f(\theta)}{h(\theta)}\right) + kw}{\left[1 \pm \mu\left(\frac{1}{\phi} - \frac{1}{\tan\phi}\right)\right]}} \tag{3.20}$$

where k represents the yield stress and w the inhomogeneity function.

3.3.2. Roll Pressure in the Elastic Region

A model for the entry and elastic zone pressure distributions can be derived from the vertical and horizontal equilibrium equations with the assumption that $\boxed{\frac{\partial \tau_{xy}}{\partial y}}$ is negligible, which yields differential equations for the tension force $t_f(\theta)$ and the vertical stress $p(\theta)$:

$$\boxed{\frac{dt_f(\theta)}{dx} = \frac{2(\tan\theta \mp \mu)p(\theta)}{(1 + \mu\tan\theta)}} \tag{3.21}$$

$$\boxed{\frac{dp(\theta)}{dx} = \left(\frac{E}{1-\nu^2}\right)\frac{d\varepsilon_y}{dx} - \frac{2\nu(\tan\theta \mp \mu)p(\theta)}{h(\theta)(1-\nu)(1+\mu\tan\theta)}} \tag{3.22}$$

The above differential equations are integrated numerically from the entrance contact point until the commencement of yield. In the exit region this is from the contact point to the point of minimum strip thickness. The difference between the calculated stresses and those required by the yield criterion is used to correct the minimum strip height in subsequent iterations.

3.3.3. Roll Deformation Model

Once the pressure profile is obtained, an updated roll pressure is determined using the Jortner influence function[110]. Note that the influence function decays very slowly once the angle exceeds 0.05 rad.

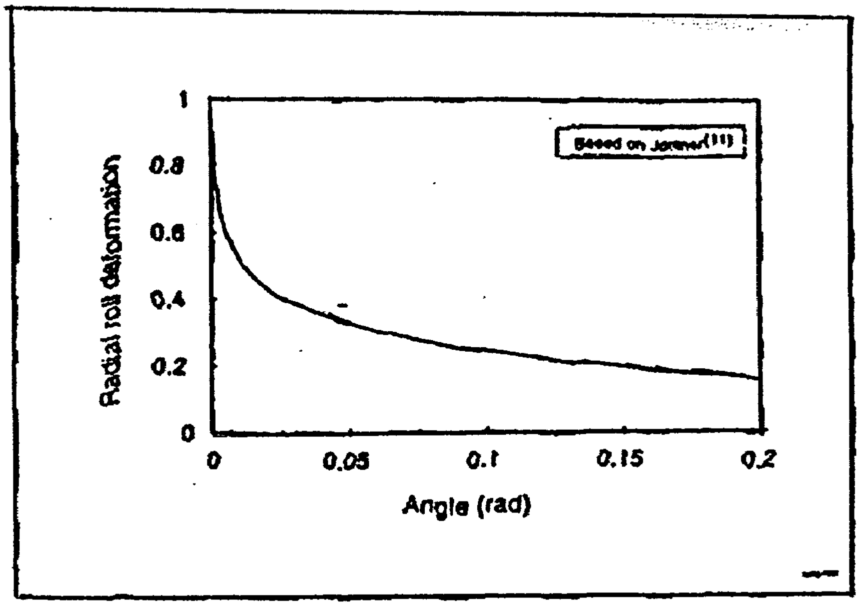

Figure 3.6. Jortner influence function normalised to have unit maximum

The roll radial deformation $\Delta R(\theta)$ is given as:

$$\boxed{\Delta R(\theta) = \frac{R}{\pi E}\int_{\theta_{entry}}^{\theta_{exit}} u(\theta - \theta')s(\theta')d\theta'} \tag{3.23}$$

Where the influence function $u(\theta)$, $|\theta| > \alpha$ is

$$\boxed{u(\theta) = (1-\nu-2\nu^2)\frac{\pi}{2}\cos(\theta).\mathrm{sgn}(\sin\theta)) + (1-\nu^2)\sin(\theta).\log_e\left(\tan^2\left(\frac{\theta}{2}\right)\right)\Bigg]_{\zeta=\theta-\alpha}^{\zeta=\theta+\alpha}} \tag{3.24}$$

And θ is the angle between the centreline of the sector over which the uniform pressure is applied and the point of influence, and α is the half angle of the sector over which the pressure is applied.

If the angle θ is less than α then a singularity is encountered in the analysis. The influence function may then be determined as:

$$\boxed{u(\theta) = \bar{u}(\theta) - \frac{1}{\pi}(1 - \nu - 2\nu^2)} \qquad (3.25)$$

where $\bar{u}(\theta)$ is the value obtained from the above equation

Under the assumption that friction force is related to roll pressure by the Coulomb friction law, an iteration of roll pressure and roll profile distributions could result in an instability as the roll profile flattens out. This results in a rapid increase in roll pressure, causing an indentation in the roll, implying an increase in strip thickness[111].

Fleck and Johnson proposed that in the roll gap, flat parallel regions exists where no further reduction occurs and the shear or frictional stress at the roll/strip interface assumes a value below that predicted by the Coulomb friction law. This assumption makes it no longer possible to predict the roll pressure by the plasticity equations in the constrained plastic flow region. The roll pressure solution can be obtained by inverting the roll pressure relationship defined by the roll deformation influence functions.

In discrete form, the roll deformation at node i may be expressed as:

$$\boxed{\Delta R(i) = \frac{R}{\pi E_R}\sum_{j=0}^{j=n} s(j)U_d(abs(i-j)+1)} \qquad (3.26)$$

where $\boxed{U_d(|i-j|+1) = u(2*(|i-j|+1)*\alpha)}$

s(j) is the roll pressure at node j and E_R is Young's modulus for the roll.

For a node k in the flattened region,

$$\boxed{\sum_{j=j_1}^{j_2} u^*(i,k)s(j) = \frac{\pi E_R}{R}(\Delta R(i) - \Delta R(k)) - \sum_{1}^{j_1-1} u^*(i,k)s(j0 - \sum_{j_2+1}^{n} u^*(i,k)s(j)} \quad (3.27)$$

Where $u^*(i,k)=U_d(|i-j|+1)-U_d(|k-j|+1)$ and j_1 represents the first node in the flattened region and j_2 is the final node in the flattened region. As the terms ΔR_k, for $k=j_1 \ldots j_2$, may be determined form the assumption that the roll is flat, it is possible to invert the above set of equations and solve for s(k) for $k=j_1 \ldots j_2$. Having thus determined the roll pressure profile $s(\theta)$, the value of the roll frictional forces may be obtained directly form the horizontal equilibrium equation.

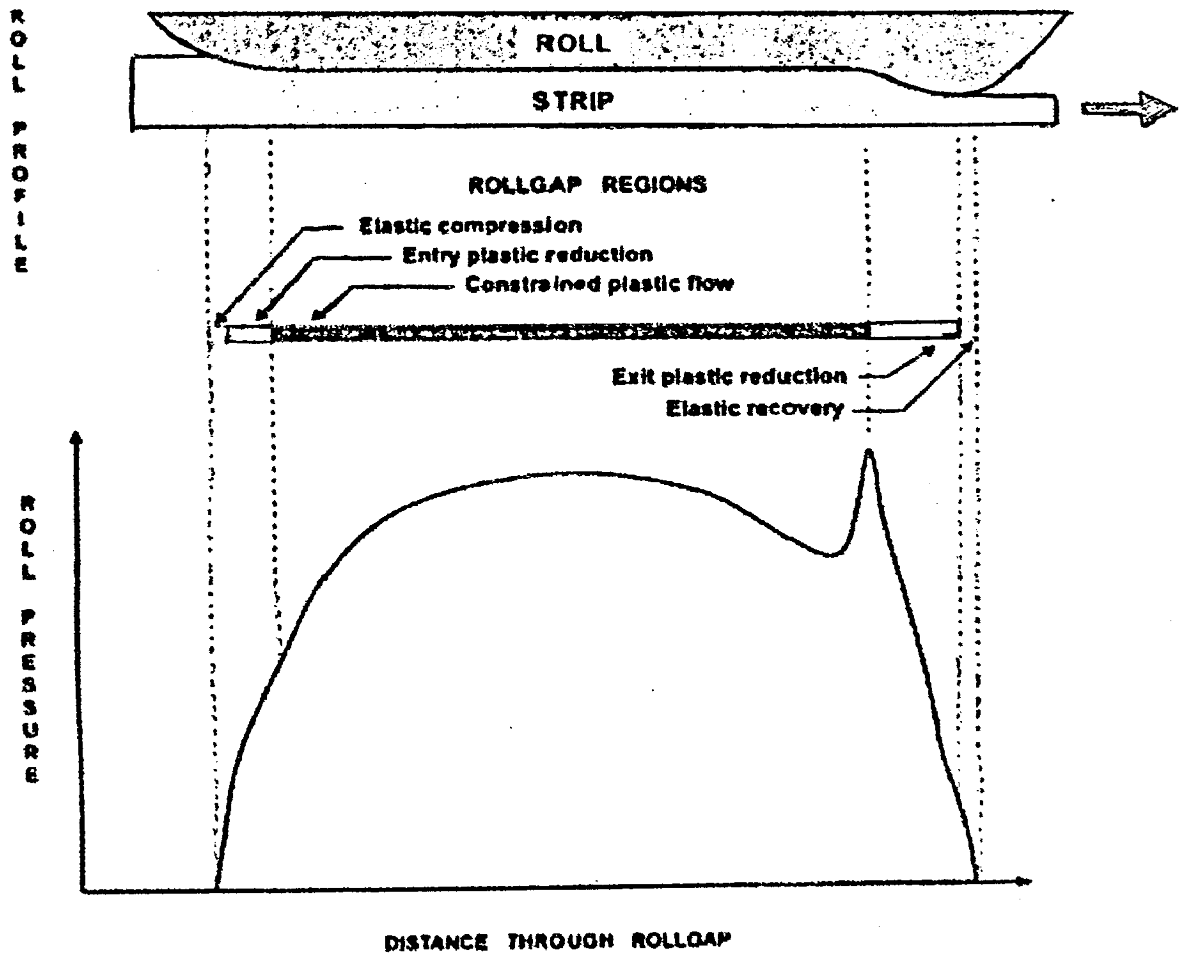

Figure 3.7. **Pressure spike from roll flattening**

A graphical representation of the solution where significant roll flattening occurs reveals a pressure spike at the end of the region of the constrained plastic flow which corresponds to the neutral point in conventional rolling theory, Figure 3.7. Upstream of this point the material is assumed to slip backwards relative to the roll, causing the pressure to increase. On the exit side of this point, the sign of the relative slip is reversed and, as in conventional rolling theory, the resulting change in direction of the frictional force causes the roll pressure to fall rapidly.

3.3.4. Yield Stress Model

The plane strain rate yield stress, $k(\varepsilon\dot{\varepsilon}\Theta)$, of a cold rolled material will typically depend on the degree of cold working from the annealed state $\in$, the strain rate $\dot{\varepsilon}$ and temperature Θ. This relationship is often modelled as the sum of separate components such that:

$$\boxed{k(\varepsilon,\dot{\varepsilon},\Theta) = k(\varepsilon,0,\Theta_0) + \Delta k_{\dot{\varepsilon}} + \Delta k_{\Theta}.} \tag{3.28}$$

The terms $\Delta k_{\dot{\varepsilon}}$ and Δk_{Θ}. represent strain rate and temperature effects respectively and $k(\varepsilon,0,\Theta_0)$ corresponds to the room temperature uni-axial compression test result that would typically be measured at a low strain rate.

3.3.5. Temperature Model

The heat flow per unit strip volume governing the strip temperature arises from three main sources:

1. Deformation energy E_r, assumed to be uniformly distributed throughout the strip
2. Frictional energy E_f due to the relative sliding at the roll/strip interface and
3. Conduction between the strip and the roll E_c.

The change in average strip temperature Θ through the roll gap may be expressed as:

$$\boxed{\Theta(x^*) = \Theta(l) + \frac{E_S(x^*)}{\rho_S C_S}} \qquad (3.29)$$

where $E_S(x^*)$ is the cumulative energy into the strip at any point whose dimensionless coordinate x^* is measured from the exit plane and ρS and CS are the strip density and specific heat respectively.

The net strip energy for the complete roll gap length E_S is related to the proportion of deformation energy converted to heat energy β_1, and the proportion of frictional energy flowing into the roll β_2.

$$\boxed{E_S = \beta_1 E_r + (1-\beta_2)E_f - E_c} \qquad (3.30)$$

The balance of the energy E_{RW} flows into the work rolls:

$$\boxed{E_{RW} = E_c + \beta_2 E_f} \qquad (3.31)$$

For the case of homogeneous deformation, the specific energy terms E_r and E_f may be written as:

$$\boxed{E_r = \int_h^H \frac{k(\varepsilon,\dot{\varepsilon},\Theta)}{h'}dh'} \text{ and } \boxed{E_f = \frac{2\mu}{Lh}\int_0^1 \left|\frac{\Delta v(x')}{v}\right| s(x')dx'} \qquad (3.32)$$

where $\Delta v(x)$ is the relative speed difference between the strip and roll and v is the strip exit velocity.

The calculation of E_c requires a different approach where h^* is a dimensionless thickness, α_s is the strip thermal diffusivity, Θ_R is the initial roll surface temperature at the roll gap entry and τ_g is the strip transit time in the roll gap. If h^* is greater than one, then the strip and roll can be modelled as the contact of two semi-infinite solids for a short time τ_g.

$$\boxed{E_C = \frac{4\rho_S C_S \beta_2(\overline{\Theta} - \Theta_R)}{h^* \sqrt{\pi}}} \qquad (3.33)$$

where:

$$\boxed{h^* = \frac{h}{4\sqrt{\alpha_s \tau_g}}} \quad \boxed{\overline{\Theta} = \frac{1}{3}\Theta(1) + \frac{2}{3}\Theta(0)} \quad \boxed{\beta_2 = \frac{1}{\left[1 + \sqrt{\frac{\rho_s C_s k_c}{\rho_R C_R k_R}}\right]}} \qquad (3.34)$$

Further terms can be added to reflect the influence of scale layers or trapped lubricant films[112]. Typically the condition for h* to equal unity corresponds to 0.4mm, suggesting that the approximation may be no longer appropriate for thin strip rolling. For values of h* much less than unity, the thermal strip inertia has a diminished significance and the strip temperature tends to follow the roll surface temperature. In these cases, a majority of the generated energy (E_r+E_f) will flow into the roll. The strip and roll may be considered as a thermally insulated infinite body with a time dependent heat flow applied at this surface. The solution to this classic problem for the roll/strip interface temperature as a function of time t is:

$$\boxed{\Theta(t) = \frac{E_{RW} h v}{k_R L}\sqrt{\frac{\alpha_R \tau_g}{\pi}}} \qquad (3.35)$$

that may be combined with an energy balance to yield the strip temperature at the roll gap surface through the roll gap.

3.3.6. Initialisation and Convergence Algorithm

For cases where flattening is moderate, a variable number of nodes in the two regions of plastic reduction at the roll gap are maintained by increasing the total number of nodes as the roll flattens, improving computational speed. In general, the use of sixty nodes in the two regions of plastic reduction would result in a maximum error of 5%.

In cases of extreme roll flattening, the use of an approximate solution to the pressure distribution in the flat region has been found to produce satisfactory solutions

3.4. Particle Break-Up Modelling

3.4.1. Introduction - Particle Effects on Recrystallisation

During slab-to-sheet rolling, intermetallic particles fracture as a function of matrix flow stress, as opposed to fracture by compressive forces resulting from the rolls crushing the particles. As the plasticity of the matrix decreases with temperature, the flow stresses increase leading to fracture, drawing apart of the particle fragments. Fracture is assumed to occur at internal weaker flaws near the centre of the particle where tensile forces are the greatest resulting in the formation of two new equal sized particles.

Many commercial alloys contain both large and small particles. Particles in metallic matrices are usually divided into groups based on size and distribution. Coarse particles are defined as having a diameter greater than 1μm, fine particles less than 1μm. Dispersion is based on the nearest-neighbour particle centre-to-centre distance[113].

Many researchers including Humphreys,[114] Hansen and Bay,[115] and Doherty and Martin[116] have reviewed the effect of second phase particles on primary recrystallisation, often termed Particle Stimulated Nucleation (PSN). The key conclusions were:

i) Acceleration of recrystallisation occurs when large particles are present. The deformation zone around the large particle has a higher stored energy and greater mis-orientations than in the matrix. Higher particle density results in smaller recrystallised grain sizes.

ii) Retardation of recrystallisation occurs in the presence of fine particles where the mean spacing is of the order of the sub-grain size. Fine dispersions retard sub-grain coarsening inhibiting nucleation.

iii) Nucleation originates in the deformation zone, but not always at the particle/matrix interface. Nucleation occurs by a rapid polygonisation process involving sub-boundary migration.

Particles barely affect the growth of recrystallised grains, suggesting that retardation of recrystallisation is largely a consequence of the inhibition of nucleation, implying further that particles affect the final grain size that is determined by the nucleation rate.

Fine dispersions will tend to pin grain growth, reducing the driving for recrystallisation, whilst large particles stimulate nucleation. In AA5083, particles larger than one μm are effective as nuclei with finer dispersoids inhibiting the growth of new grains[117]. There are many factors that affect particle role in primary nucleation. The major factors are outlined below:

a) The Deformed State

Particle size has been shown to affect the sites at which nucleation occurs. Alloys with particles less than 0.1μm have a much lower rate of recrystallisation nucleation than single phase alloys. Humphreys believed that this was due to more homogenous slip in alloys leading to fewer sites for nucleation[118]. Large particles stimulate recrystallisation nucleation, with lattice rotations believed to be the nucleation mechanism[119].

Particles that deform with the matrix have been shown to affect recrystallisation behaviour via non-homogenous slip. In non-deformable particles, Ashby demonstrated that geometrically necessary dislocations are generated at the particles[120]. Distribution of dislocations is a function of particle size and strain as shown in Figure 3.8.[121] The white circles indicate no PSN, with the black dots showing PSN. The two criteria for growth beyond the nucleus into the deformation zone are that sufficient misorientation must occur in the deformation zone and the driving force for nucleation must be sufficient for the nucleus to grow.

Deformation temperature has been shown to affect the formation of the deformation zone and growth of the nucleus beyond the particle. Humphreys and Kalu showed that a critical strain rate is required for particle stimulation to occur and that this is dependent on temperature with dislocations able to climb around particles without forming deformation zones.[122]

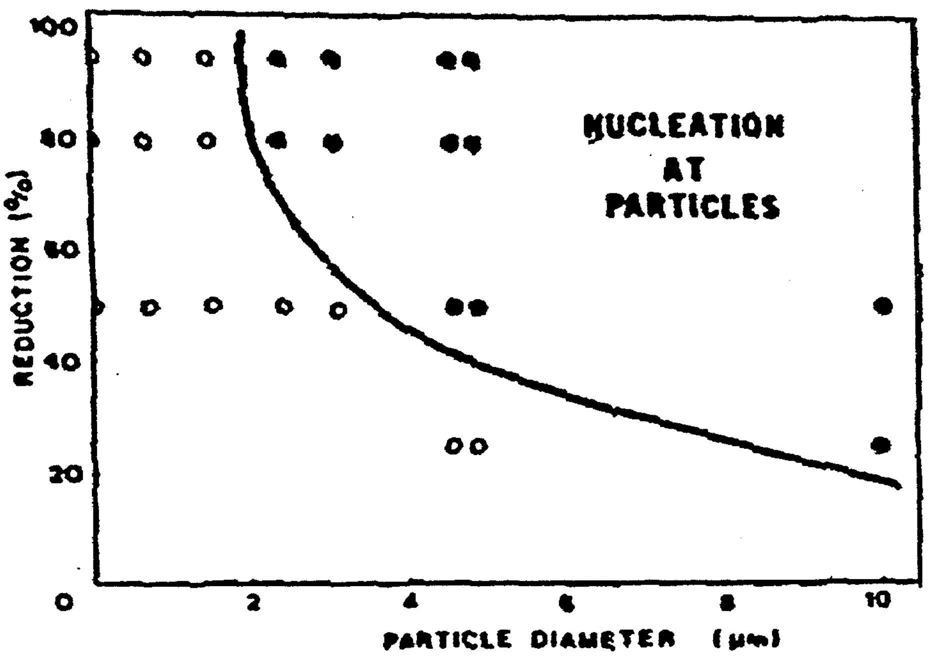

Figure 3.8. **Conditions of strain and particle size for which PSN occurs in an aluminium silicon alloy.**

b) Particle Distributions

A recent study in the distribution of critically sized particles in an aluminium matrix showed that nucleation is preferred at sites of particle clustering.[123] Large particles with small spacings inhibit recrystallisation by particle pinning effects. A retarding force referred to as Zener drag arises from the reduction in interface energy that occurs when a particle is situated at a boundary[124].

3.4.2. Particle Break-up Theory

In developing a break-up model for slab-to-sheet rolling, three distribution theories are utilised:

a) The log-normal distribution, which has been thoroughly examined in literature.

b) The Brittle Fracture Theory as suggested by Wallin et al;[125] and Jayatilaka and Trustrum,[126] which gives a better description of the large size tail of distributions.

c) The Comminution Theory, which employs a logarithmic size range and represents the size distributions by a vector of the relative frequencies in each range or bin.

Thickness estimates normally refer to a specific width, a frequently measured parameter in image analysis systems. The parameter (P) is derived from the perimeter of the particle and the area (A) from the area of a particle, assuming the particle is rectangular:

$$\boxed{Specific\_Width = P\frac{1+\sqrt{1-\frac{16*A}{P^2}}}{4}} \tag{3.36}$$

Conventional quantitative description of particle shape is limited once roundness is examined. Once the value of roundness exceeds $\pi/4$, the expression for specific width includes a negative square root:

$$\boxed{roundness \equiv \frac{4\pi A}{P^2} \leq 1} \tag{3.37}$$

$$\boxed{\text{i.e. } \frac{A}{P^2} \leq \frac{\pi}{4}} \tag{3.38}$$

Work by Ren found a majority of the particles in AA9033 and AA9215 were elliptical and Tibballs has used an ellipse with the same area and perimeter as the particle to describe thickness[127,128]. By evaluating the elliptical integral for the perimeter of an ellipse for varying aspect ratios, the equivalent elliptical aspect ratio 'a' is then used to determine equivalent length (l) and equivalent width (w)[129]:

$$\boxed{a \approx \frac{1+\frac{1}{3}\sqrt{1-R}}{1-\sqrt{1-R}}} \tag{3.39}$$

$$\boxed{l = \sqrt{\frac{4aA}{\pi}}} \tag{3.40}$$

$$\boxed{w = \sqrt{\frac{4A}{\pi a}}} \tag{3.41}$$

In order to describe the distributions of width and length for a given sample, a log-binomial distribution is appropriate. This is due to length being greater than width by definition and length distribution being truncated for lower sizes by the limitations of pixel size. This information allows the mean and median (and their respective standard deviations) to be determined for the equivalent elliptical length and width of the particles using equations (3.40) and (3.41).

Major factors ignored in the model include the change in particle properties during rolling and the rotation of elongated particles into alignment with the rolling direction. Both factors are expected to change the parameters of the selection matrix.

3.4.2.1. Log-Normal Distribution[130]

The size and distribution of second-phase intermetallic particles in aluminium alloys govern many important properties such as second-phase strengthening and the volume fraction of randomly orientated grains for recrystallisation nucleation. Cold rolling operations can fracture larger particles, with matrix flow stresses drawing them apart. The size distribution of particles after cold rolling prior to recovery defines the potential number of grains with random orientation.

Particle size distributions are characterised by evaluating parameters of standard distributions. Three apply to the particular analysis shown in Figure 3.9. They are:

i) Cross-section area, A

ii) Perimeter of rectangular equivalent to particle, P

iii) Roundness, R, a size-independent ratio of area to perimeter squared.

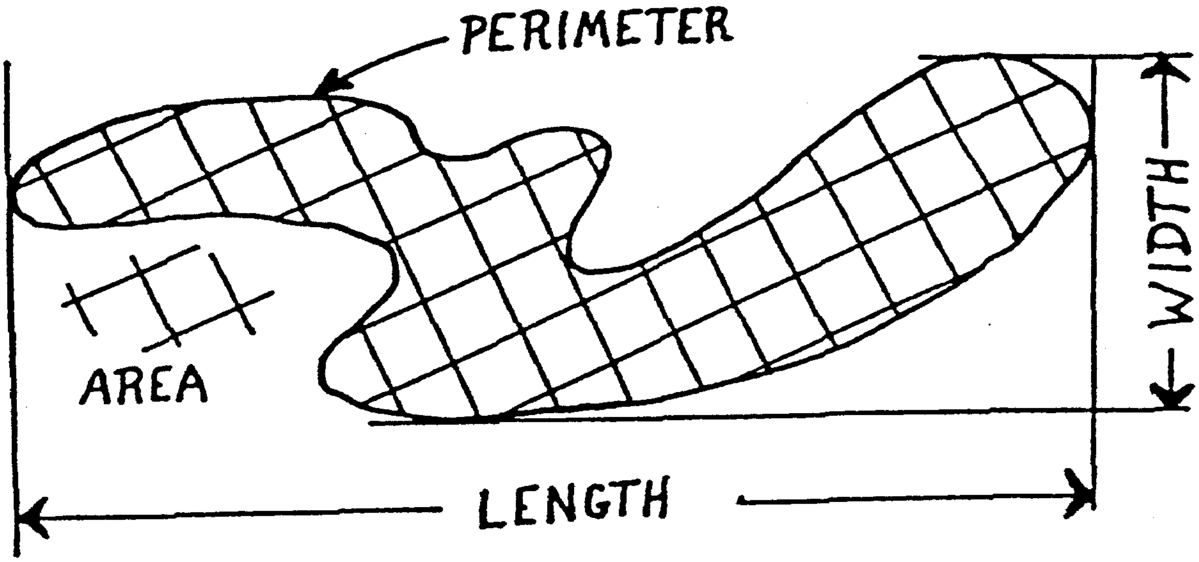

Figure 3.9. **Particle dimensions**[131]

When size and shape data are taken together, a joint distribution is used based on a log-binomial distribution that fits parameters to particle length and width values. The log-binomial distribution, Z is given by:

$$\boxed{\begin{aligned} Z = NL_2(\ln(x),\ln(y))d\ln(x)dy = \frac{Nd\ln(x)d\ln(y)}{2\pi\ln(\sigma_x)\ln(\sigma_y)\sqrt{1-\rho^2}}.\exp\{-\frac{1}{2(1-\rho^2)} \\ [(\frac{\ln(x)-\ln((<x>)}{\ln(\sigma_x)})^2 + (\frac{\ln(y)-\ln(<y>)}{\ln(\sigma_y)})^2 \\ -2\rho\frac{\ln(x)-\ln(<x>)}{\ln(\sigma_x)}\frac{\ln(y)-\ln(<y>)}{\ln(\sigma_y)}]\} \end{aligned}} \quad (3.42)$$

On assigning length l to x and width w to y and introducing the parameters $a1 - a6$, the Jacobian required for the least squares analysis can be derived if the derivatives {dZ/dai} are known:

a1 =N	
a2 =ln(<l>)	
a3 =ln(<w>)	(3.43)
a4 =ln(σl)	
a5 =ln(σw)	
a6 =ρ,	

Once the parameters *a1* ..*a6* have been estimated from the particle frequency histogram, other parameters describing the distribution may be derived.

3.4.2.2. Fracture of Brittle Particles Theory

Wallin et al[126] described the fracture of brittle intermetallic particles in a ductile matrix at hot rolling temperatures using fracture probability. The theory builds on a statistical approach to brittle fracture that justifies the use of the Weibull function to describe fracture probabilities. The approach is extended to include both length and width of each particle.

Large flaws leading to fracture occur with a frequency described by the size distribution function. It is these flaws that control the strength of the material.

$$\boxed{f(s)=\frac{c^{\upsilon-1}}{(\upsilon-2)!}s^{-\upsilon}e^{-\frac{c}{s}}} \qquad (3.44)$$

s describes the size of the flaw, c/s is the most frequent size of the flaw and υ describes the rate at which f(s) decays for larger flaws.

Integrating with respect to applied stress σ, the probability of failure of a single flaw is unity when K_{IC} for the particle equals the critical stress intensity factor for the matrix.

$$\boxed{f(s)\sim s^{-\upsilon}F(\sigma)\approx\frac{1}{\upsilon!}\left(\frac{\sigma^2\pi c}{K_{IC}^2}\right)^{\upsilon-1}\left[1-\frac{\sigma^2\pi c}{K_{IC}^2}\frac{\upsilon-1}{\upsilon+1}\right]} \qquad (3.45)$$

The probability of failure of the intermetallic material Pf is that of the weakest link:

$$\boxed{Pf = 1\text{- } Probability\ of\ surviving\ N\ flaws = 1\text{-}[1\text{-}F(\sigma)]^N} \tag{3.46}$$

$$\boxed{\approx 1 - exp[-NF(\sigma)]} \tag{3.47}$$

Since N is proportional to the volume V of material, and $F(\sigma) \approx \sigma^2$, this relates directly to the Weibull probability distribution for fracture under applied stress that has long been employed to describe brittle fracture where the number of flaws is sufficient to allow a statistical approach:

$$\boxed{P(\sigma) = 1 - \exp[-V(\frac{\sigma}{\sigma_0})^m]} \tag{3.48}$$

The Weibull modulus is then equitable with the flaw size distribution, and the normalisation factor:

$$\boxed{\sigma_0 \approx K_{IC}\sqrt{\frac{(\frac{1}{2}m+1)!}{\pi c}}} \tag{3.49}$$

Wallin applied this equation to the Weibull distribution of individual intermetallic particles, relating the volume V to the size of the particle, and the stress on the particle to the load exerted on it by flow stresses in the matrix σ_{flow}:

$$\boxed{\sigma = 2k\frac{l}{h} = \frac{2\sigma_{flow}}{M}a} \tag{3.50}$$

The variables are length of the particle l, thickness h, aspect ratio a, the averaged Schmid factor M and matrix shear stress k.

3.4.2.3. Comminution Theory.

Two vectors (f_0, f_1) containing mass fractions of particle sizes before and after ore-beneficiation process are related by two matrices. Based on standard sieve mesh sizes, each matrix forms discrete distributions of particle sizes within geometric classifications. Selection matrix 'S' describes the probability of particle breakage during processing and breakage matrix 'B' describes the distribution of fragment sizes resulting from the fracture of particles of each size class:

$$\boxed{f_1 = BSf_o + (1 - S)f_o} \tag{3.51}$$

The first term is the fractured component and the second the unfractured component. There are a number of breakage matrix functions used during mineral processing but none adequately model the mechanisms that occur during rolling operations.

The choice of the breakage function should reflect the observation that the tensile strength is the greatest in the centre of the particle resulting in two fragments approximately half the original length but equal in width. Rearranging equation (3.51) to give the selection probability:

$$\boxed{S_{ij} = \frac{\sum_i (I - B)^{-1}_{ji} (f_0 - f_1)_i}{f_{0j}}} \tag{3.52}$$

The element $B_{jl,ik}$ of the breakage matrix is then significantly non-zero only for $j = I$-1 and I-1 and $l = k$ or k-1.

3.4.2.4. Model Development

The model uses a combination of a log-binomial distribution to store shape and size data efficiently, and an extended vector representation (which enables size and shape data to be included) to perform calculations. In determining the parameters of the break-up model, a breakage function B must first be chosen. The B is a measure of the size distributions of fragments when a particle fractures and the choice should reflect the observation that the tensile stress are greatest in the centre of the particle.

To calculate the ideal particle strength, σ_o the average particle strength, σ_p is multiplied by two and divided by the Schmid factor. To obtain a selection function, $\sigma_o = 2\sigma_p/M$ is substituted into equation (3.48), where the Schmid parameter M accounts for particle orientation. The Schmid parameter is an orientation factor based on the crystallography of the matrix. For particles well aligned with the shear forces the Schmid factor approaches 2, but for particles badly aligned with the shear forces the Schmid factor approaches 4.

Normalising the frequency functions f and F to particle volume (μm^3), utilizing the discrete representation of particle size l_i and aspect ratio w_k, and noting $V=(l_i \times w_k)^{3/2}$ and $a=l_i/w_k$, a selection matrix element can be written:

$$\boxed{S_{ik,ik} = 1 - \exp[-(l_i w_k)^{\frac{3}{2}} (\frac{\sigma_{flow} l_i}{\sigma_p w_k})^m]} \tag{3.53}$$

To estimate values of m and hence σ_p, a line on the right of the length versus width scatter diagram is used. The line can be parameterised as:

$$\boxed{\begin{array}{l} \log(w) = \beta + \alpha \log(l) \\ where \\ m = \dfrac{3(\alpha + 1)}{2(\alpha - 1)} \end{array}} \tag{3.54}$$

The Weibull parameter m, which controls the relative importance of length and thickness of particles in the fracture mechanism can be determined from the scattergrams. Work by Jayatilaka and Trustrum[132] and Wallin et al.[126] has found the value of m for bulk glass to be 3.4, for ceramic oxide particles in copper to be 5.4, for spheroidised particles in steel to be 3.5, and for rod shaped particles in aluminium to be 1.5.

To estimate m, a line to the right of the scattergrams is drawn and the slope α, determined and substituted into equation (3.54). The value of m is assumed to remain constant for all passes at all temperatures examined[133].

The Weibull modulus is used to evaluate the relative importance of particle volume $(w \times l)^{3/2}$ in determining the selection function as described by equation (3.53).

$$\boxed{S_{ik,\,ik} = 1 - \exp[-(\frac{\sigma_{flow}\, l_i}{\sigma_p\, w_k} \times (l_i w_k)^{\frac{3}{2}})^m]} \qquad (3.55)$$

The average particle strength is a measure of the force required to fracture a randomly orientated particle and is determined by equation (3.13). This can be interpreted as the ultimate tensile strength (U.T.S.) of the particle as they are assumed to break by brittle fracture. The measurement is highly dependant on the orientation of the particle to the matrix shear applied.

To assess the validity of the assumption that the particles fracture along their weakest planes and not by crushing, the hardness is related to the U.T.S. by equation (3.56)[134].

$$\boxed{3 \times H_v = U.T.S.} \qquad (3.56)$$

As an example, particles of Al_3Fe have an average hardness of 400-450 H_v.

CHAPTER 4 ROLLING LUBRICATION – TRIBOLOGY

Rolling lubrication for thin foil rolling and its effects on annealing (batch or flash) have not been well documented with few references available. The effect of rolling lubricants on surface properties and defects as a function of rolling, slitting and subsequent thermal treatments is examined in Chapter 8 to 10 under surface studies.

4.1. Functions of Lubrication

Rolling was first applied to the cold working of lead and gold in the 15th century[135] and narrow strips of coinage in the 16th century[136]. However it was not until the rolling of sheet, particularly aluminium that the importance and subsequent development of lubricants and lubricating systems occurred. Light mineral oils with small additives such as lanolin were adequate for the low speed employed in the first half of the 20th century. However more powerful drives permitted increased production rates, heavier reductions and higher speeds, all of which impose severe conditions on the lubricant.

One of the most important but least understood characteristics of tribology is the lubrication interaction between the rolls and the metal. Lubricants are often thought of as agents for reducing friction and wear. However in practice they must fulfil a number of additional criteria, often resulting in a compromise being struck:

1. Controlled friction – low friction reduces force and power requirements, resulting in more homogenous deformation and preventing metal-to-metal contact, while optimising the reduction capacity through a low viscosity load carrying film.

2. Thermal insulation – provide thermal insulation and cooling to the strip and the rolls while controlling the thermal camber of the work rolls.

3. Controlled stability – it should be stable (or if changes occur be beneficial or harmless) and unaffected by time, temperature, oxidation, bacteriological attack, and contamination, non-abrasive, and amenable to replenishment. Any residual by-product should be harmless, not interfere with finishing operations, accumulate in recesses, or cause metallurgical or chemical changes in the product on annealing or storage.

4. Control of metal pickup – limits the amount of roll-wear and wear debris. If the continuity of the parting lubricant film is locally lost, the residual lubricant should wash away any pickup or debris.

5. Protection of old and new surfaces – the lubricant should have a wetting and spreading characteristic that permits it to follow the extension of the metal surface to produce a uniform foil surface finish suited to its subsequent applications (in conjunction with initial roughness and process conditions).

6. Adaptability to working conditions – the lubricant must be able to perform its functions at the pressures, temperatures and relative sliding velocities prevailing from the process. It should not be corrosive to the product or rolls and on annealing promote adhesion and unwind characteristics.

7. Durable rapid response – must exert its influence in the short time available during the actual metalworking process. Must be able to withstand repeated or continual encounters.

8. Cost – a more costly lubricant may be able to be justified in terms of energy savings, processing steps, surface preparation, lubricant removal, and disposal.

9. Application, removal and disposal – the lubricant will have long shelf life, be easy to apply (and remove) in a controlled manner in an environmentally acceptable manner or be treated for returning to the process.

10. Handling and safety – as the rolling lubricant may come into contact with food and individuals, it must comply with public health regulations such as: Non-toxic controlled emissions, high flash point to reduce fire risks, good ageing properties so as to not become acidic, no evidence of brown staining during annealing.

11. Integrated approach – the basic philosophy of the rolling fluid composition is to match the fluid and all service requirements on a particular mill i.e. the use of the same blend pack for three separate functions on a pack mill: Rolling, between pack lubricant or matting fluid, all mill components powered by hydraulics.

4.2. Fundamentals in Metalworking

The basic laws of friction were first recognized by Leonardo da Vinci in 1508, however it was not until the late 18th century that Coulomb developed a theory postulating that friction was due to both surface roughness and adhesion. The principles of hydrodynamic theory of lubrication were developed over a number of years in the late 19th and early 20th centuries; boundary lubrication in the 1930's and dry and lubrication friction theories in the 1940's.

Friction is defined as "the resisting force tangential to the common boundary between two bodies when, under the action of an external force, one body moves or tends to move relative to the surface of the other"[137]. The coefficient of friction - f - indicates the efficiency of sliding or rolling and the energy requirements and is a ratio of the frictional force F, divided by the load, L;

$$\boxed{f = \frac{F}{L}} \qquad (4.1)$$

The basic laws of friction for rolling friction are:

- The friction force inversely varies with load;
- The rolling friction force is inversely proportional to the diameter of the rolling element;
- The rolling friction force is lower for smooth surfaces than for rough surfaces;
- Static friction is significantly greater than kinetic friction;
- If rolling elements exhibit significant contact deformation hysteresis, rolling friction is increased.

When discussing flat rolling of aluminium sheet, friction at the roll bite is dependent on film thickness and to a lesser extent, film strength and shear strength of a particular rolling lubricant. The Wilson-Walowitz equation, Figure 4.1, can be used to estimate film thickness in open gap rolling and gives a good representation of the relative effects of several variables, shown in Table 4.1[138].

Symbol	Definition	Parameter change	Film thickness change
H	Viscosity at Inlet Temperature	↑	↑
N	Roll Velocity	↑	↑
S	Inlet Sheet Surface Speed	↑	↑
A	Pressure Viscosity Coefficient	↑	↑
Y	Material Yield Strength	↑	↓
T	Sheet Tension	↑	↑
R	Work Roll Radius	↑	↑
$H_1 - H_2$	Reduction	↑	↓
Fl	Lube Film Thickness		

Table 4.1. Wilson - Walowitz variables

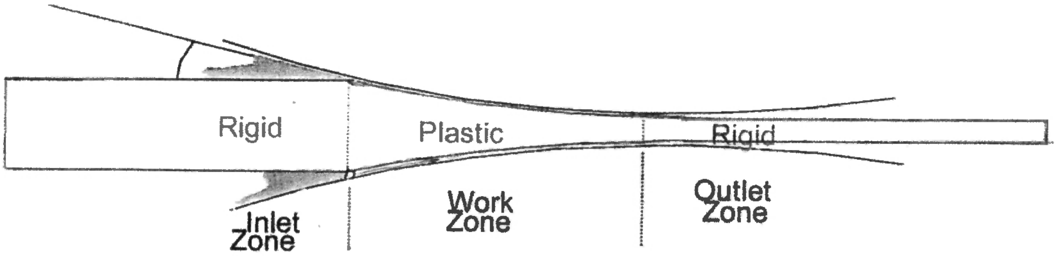

Film thickness is a function of inlet zone conditions and not work zone conditions.

$$\text{Film Thickness} = \left(\frac{3na(v+S)}{1-\exp(-a(Y-T))} \right) \left(\frac{R}{H1-H2} \right)^{1/2}$$

R = Roll Radius
H1-H2 = Reduction
n = Temperature viscosity coeff
a = Pressure viscosity coeff
v = viscosity
S = Surface Speed
Y = Yeild Strength
T = Tension

Figure 4.1. Wilson – Walowitz equation

The believed effect of increasing several additional rolling parameters on film strength and thickness is shown in Table 4.2[138]. The relative effects of the below parameters have not been confirmed via systematic experimentation.

Additional Variables Increased	Film Strength	Film Thickness
Coolant Temperature	-	↓
Metal Temperature	-	↓
Acid Concentration	↑↑	↑
Alcohol Concentration	↑	↑
Ester Concentration	↑	↑
Mat Fluid Temperature	-	-
Mat Fluid Amount	-	-
Roll Roughness	-	↑
Heavy Oil	↑	↑
Roll Force	-	↓

Table 4.2. Addition film parameters

4.2.1. Lubrication Regimes

There are several regimes of lubrication mechanisms that show that lubricant film thickness and the coefficient of friction respond to several variables. These can be conveniently summarized with the help of the Stribeck curve. The Stribeck curve, Figure 4.2, shows the variation of the co-efficient of friction as a function of dynamic fluid viscosity μ, rotating speed N, and load pressure P.

Boundary lubrication occurs under conditions of low speeds, low viscosity and high load resulting in a high and constant friction. Insufficient lubrication at the roll bite results in discrete fractures in the lubrication film between the roll and the strip. Consequently, metal-to-metal contact occurs with friction dependent on the physical properties of the surface films formed by the lubrication on the metal surface as well as the environmental and operational conditions. Under conditions of boundary lubrication, there is a greater chance of energy loss through the deformation of the surfaces.

At optimum combinations of speed and viscosity and load, friction is at a minimum. Increased speed shears the viscous fluid thereby increasing friction. This is referred to as hydrodynamic lubrication. It arises from excessive film thickness 'flooding' the roll bite such that the viscosity of the fluid or fluid friction becomes the primary factor that determines the level of friction.

In any practical rolling application, some sliding or slippage occurs. When the friction force has two components, rolling and slippage, elastohydrodynamic lubrication (EHD) or plastohydrodynamic lubrication (PHD) is said to occur. For non-metalworking situations, hydrodynamic and EHD lubrication covers much of the $\eta v/p$ range, and the boundary and EHD regimes merge through a relatively small zone of mixed-film lubrication.

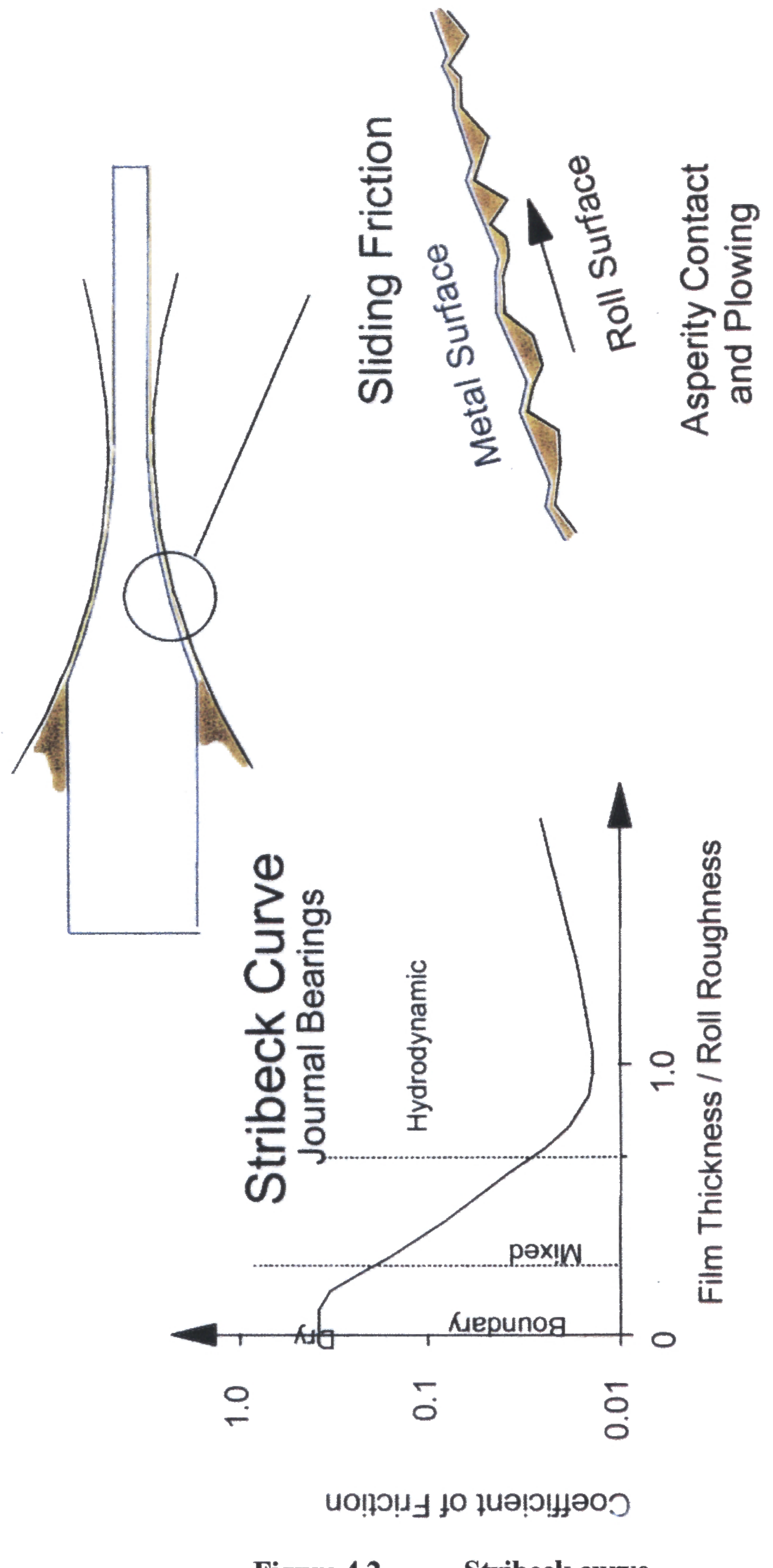

Figure 4.2. **Stribeck curve**

In most metal deformation processes conducted with a liquid lubricant, film thickness is insufficient to provide a complete separation of surfaces. This situation has been described as quasihydrodynamic or thin-film lubrication, but the physical reality is best expressed by the term "mixed-film lubrication". This term embodies the essence of a vast body of observations, according to which asperities are in boundary or micro-PHD/EHD contact whereas the troughs (valleys) are filled with a liquid, Figure 4.2.

Schey has rationalized a regime of lubrication mechanisms for metalworking with the aid of a modified Stribeck diagram, Figure 4.3. Due allowance is made for the plastic deformation of the workpiece[139]. As a three-dimensional diagram would be required for changes in interface pressure, the modified Stribeck curve is shown at the point where the coefficient of friction is minimised.

At low viscosity and/or speed, hydrodynamic effects are discouraged. The entrapped film thickness is insufficient to generate hydrodynamic pockets and only boundary lubricant films separate the surfaces. If weak junctions are formed, smearing may occur due to lubricant breakdown. As viscosity-speed increase, the entrapped film thickness increases forming some hydrodynamic pockets resulting in a mixed-film regime and a rapid decrease in the coefficient of friction.

Once the entire surface is covered with a hydrodynamic film, the minimum co-efficient of friction is reached resulting in a roughened surface. A further increase in viscosity or speed increases the drag in the hydrodynamic film causing a slight increase in friction. The increase may be cancelled due to a drop in viscosity resulting from heating at higher rates of shear, Figure 4.3. For more detailed information on lubrication regimes, "Tribology in Metalworking – Friction, lubricant and wear" by Schey is recommended[139].

Increasing interface pressure reduces the entrained film thickness. As increased pressure is often a consequence of heavier deformation and thus larger surface extension, the lubrication mechanism shifts towards boundary. Thus increasing pressure has the opposite effect of increasing viscosity-speed and the coefficient of friction usually increases. At very light pressures, contact is established over asperity tips only and the fluid present moves freely around and does not share in supporting the load.

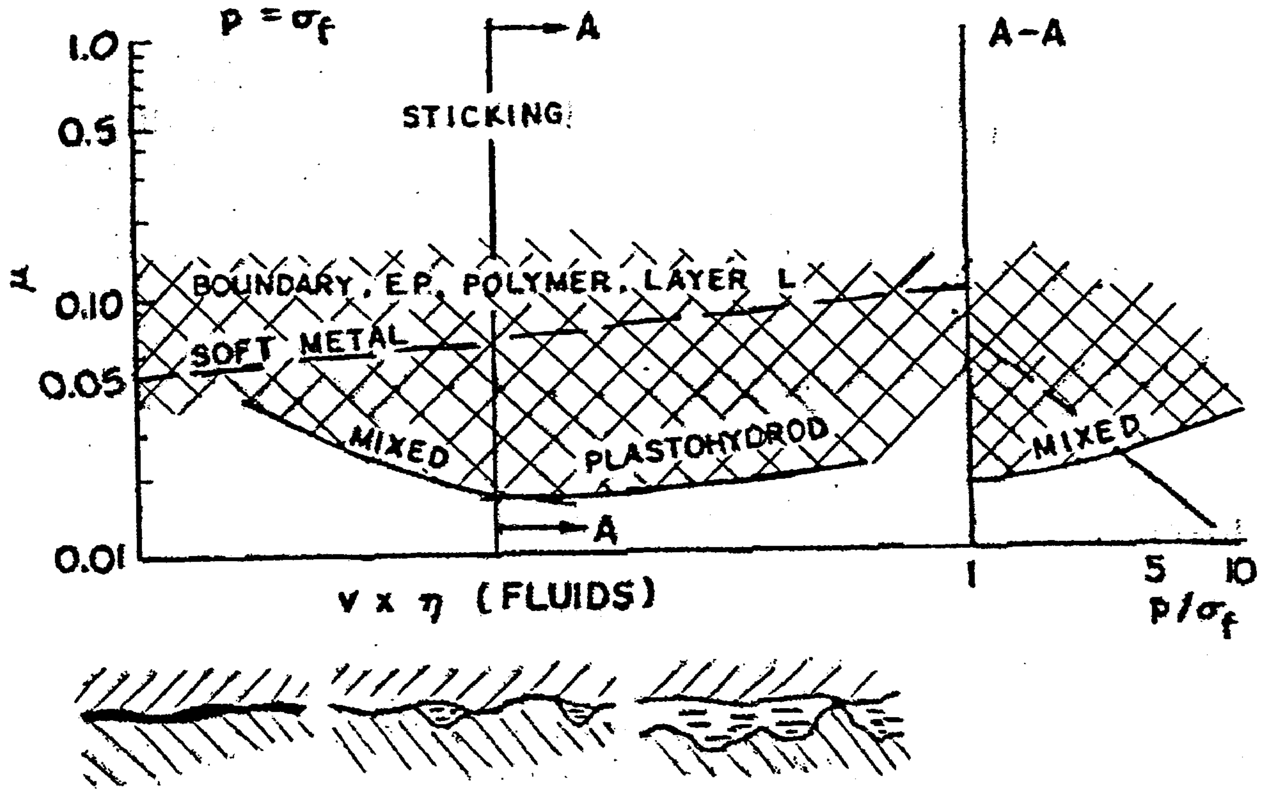

Figure 4.3. Modified Stribeck diagram

4.3. Rolling Lubricants

4.3.1. Base Oils

Rolling lubricants are generally low viscosity mineral or synthetic petrochemical base oils with low levels of surface-active additives to promote film strength. The development of rolling fluid additions is a relatively new and secretive area of research and published information is scarce, however in recent years some papers evaluating several lubricating systems have been published[140,141,142]. The requirements of the base oil are best summarized by Guminski and Willis[143]:

1. During application, the flash point should be as low as deemed safe,

2. The boiling range should not extend more than 90°C, preferably less than 60°C. To reduce staining the boiling range should start a low temperature consistent with the desired flash point,

3. The bromine number should be <1 and preferably <0.6 to avoid brown staining. The bromine number indicates the degree of unsaturation.

4. The total sulphur content should be less than 0.08%, preferably less than 0.06% to reduce brown staining,

5. The acidity of a fresh sample should be negligible and should not increase on ageing for 24 hours at 110°C in the presence of aluminium drillings to >0.025 mg KOH/g. Increased acidity of the rolling lubricant promotes white staining,

6. Aromatics and naphthenes should be below 35%, as they promote brown staining and deteriorate the ageing properties of the base oil,

Hydrocarbons of widely ranging viscosities from solvent like liquids to semisolid waxes are used in large quantities as the viscous agents required for the establishment of plastohydrodynamic or mixed film lubrication. Their lubricating properties and stain properties can be closely controlled through control of their chain length structure and purity.

Natural oils and fats are valuable lubricants on account of their viscosity, favourable pressure-viscosity exponents and early solidification. Derivatives obtained from their processing are important lubricant additives. Soaps formed by reaction with a metal are valued for their favourable rheology.

Metalworking oils contain 10 to 70 carbon atoms per molecule. As chain length increases, viscosity, flashpoint, fire-point and boiling-point increase. Viscosity increases with pressure and decreases with temperature. Temperature dependence is best represented by the semi-empirical Walther relationship as shown in Figure 4.4.

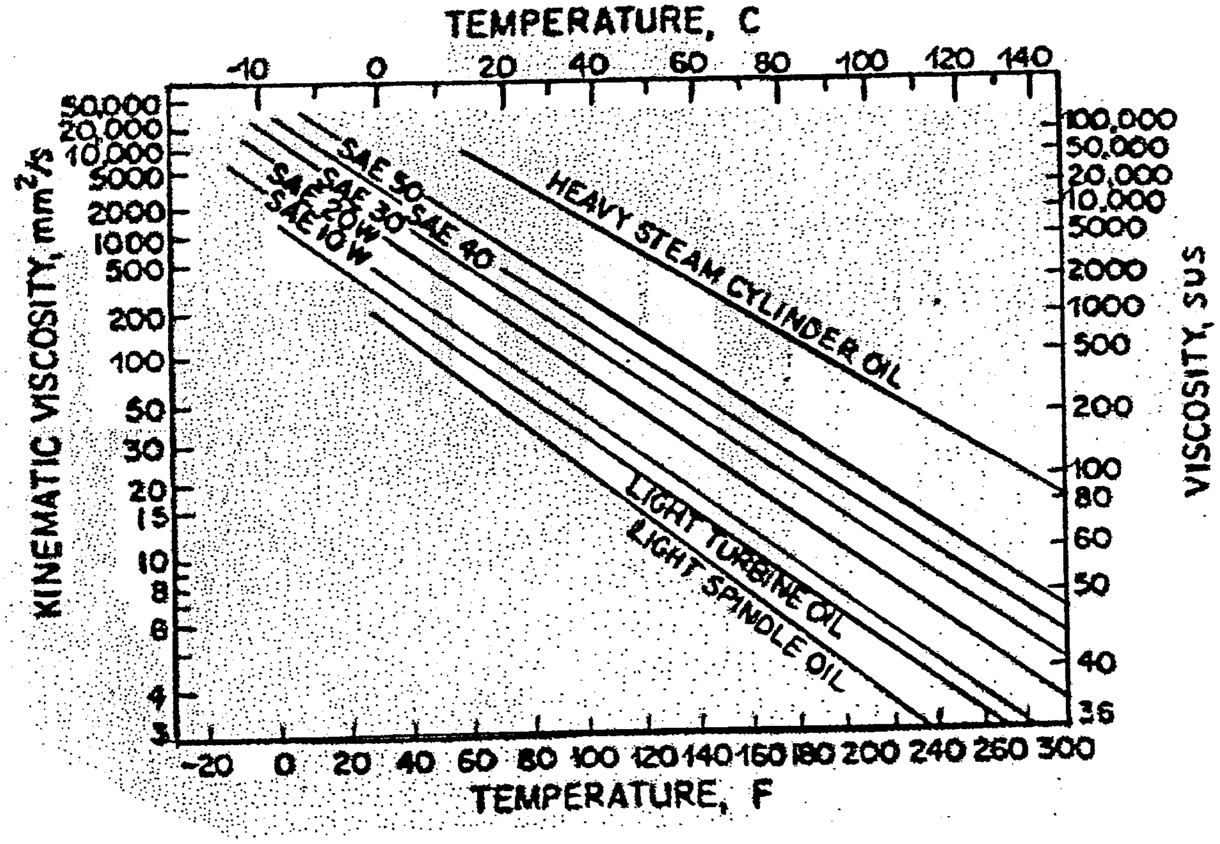

Figure 4.4. **Variation of viscosity with temperature for mineral oils**

Straight chain saturated hydrocarbons (paraffin) within the range C_{12} to C_{14} have been found to be the most suitable for base oils as they have a high lubricating efficiency and produce a good surface finish[144,143]. For a given weight, straight-chain saturated hydrocarbons have relatively low densities and viscosities, but lose less of their viscosity with increasing temperature; they are also less compressible and have lower pressure-viscosity exponents. Thus their viscosity increases with pressure less rapidly, but they solidify at lower pressures.

Highly paraffinic oils are not desired on the grounds of staining. It is inconclusive whether more refined oils stain less, but it is more important that the oil should be narrow cut to reduce the distillation boiling range. Oily residues on worked metal surfaces undergo distillation during annealing possibly leading to brown stains. For a given temperature, staining intensity increases with chain length, therefore narrow-cut oils are preferred when staining is a problem.

A lubricant can function only if properly applied and maintained. Maintenance and control of recirculating systems are of particular importance. Spent lubricants must finally be disposed of in an ecologically acceptable manner.

4.3.2. Lubricant Additions

Few substances fulfil all the requirements of a metalworking lubricant. The predominance of the mixed-film lubricant mechanism demands that boundary and EP lubricants be added to substances possessing only viscous properties, thus most metalworking lubricants are compounded with one or more additives. Mineral oils are invariably compounded and even natural fats, waxes and soaps benefit from additions of free fatty acids, EP agents, or layer-lattice compounds. Greases, composite structures of oil and thickener are valued for their ability to form films even under conditions that are not favourable for hydrodynamic lubrication.

To promote shear strength, pressure absorption capacity and improved viscosity-temperature behaviour, commercial additive packages composed of alcohol, fatty acid and esters are added to the base oil, preferentially adsorbing to the metal surface providing excellent film strength. Additive concentrations are generally between 0.5% to 5% and must meet the same flash point, staining and acidity criteria as the base oil[145].

For boundary additives, as little as 0.1% fatty acid reduces friction in the working of aluminium, with no further improvement noted above 1%. Fatty esters, oils or soap additions are needed in larger quantities in the order of 1% to 10%. Brown staining imposes a limitation on additive chain length and composition. They are edible, and thus can be used on food packaging products. The have the general form RCOOH or carboxylic acids. Viscosity increases with chain length. Their value as lubricants relies on both viscosity and boundary activity. Higher melting point and thus higher transition temperature of long chain acids are generally better boundary lubricants. Unsaturation does reduce oxidative stability, allow polymerisation and promote staining, but there is no evidence on whether it improves boundary lubricity. Fatty alcohols of the general structure RCH_2OH are derived mostly from saturated acids or esters.

The aim of EP additives is to provide protection in the temperature range encountered over asperities as shown in Figure 4.5 for the mixed film lubrication regime in the sliding of iron. EP additives are mandatory when boundary additives would be totally ineffective or would breakdown at the higher temperature developed in the process.

Hydraulic fluids, oil mist and tramp oils can pollute the rolling lubrication package resulting in excessive oil residue levels. High residue levels leave an organic by-product after the volatile components are removed under heat, promoting stickiness. This is further compounded with high levels of residue lubricant lengthening the annealing cycle. Excessive coolant can also result in wrap slippage or telescoping when handling eccentric coils.

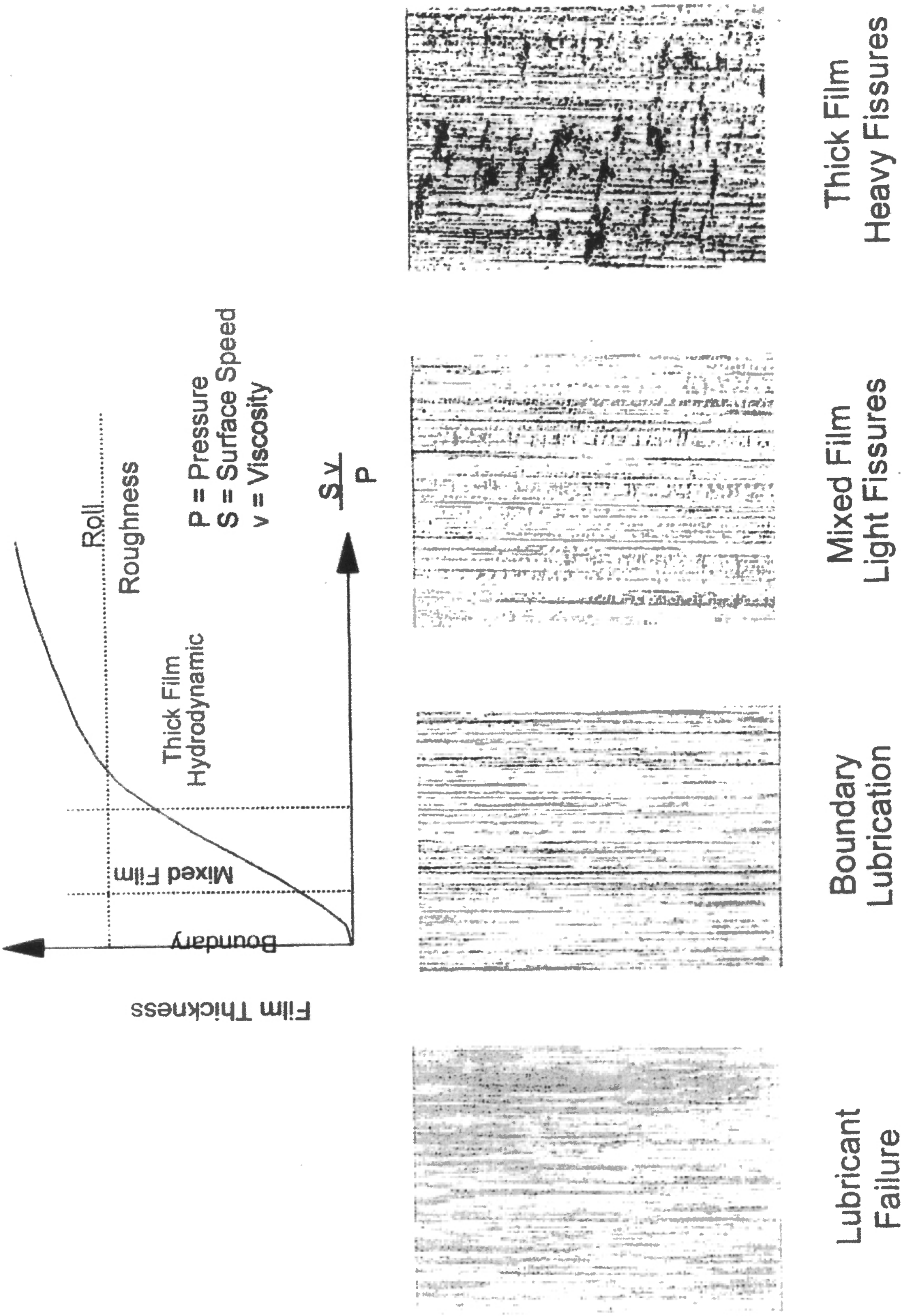

Figure 4.5. **Schematic illustration of the mode of action of a compound oil-based lubricant.**

4.4. Batch versus Flash Annealing of Foil Alloys

Foil product is annealed by one of two means; batch annealing – a slow, lower temperature anneal in a box-type furnace; or flash annealing – a much faster, higher temperature anneal in a continuous annealing furnace. Figures 4.6 and 4.7 illustrate the effect of the two annealing processes on work hardening and softening of foil alloys between 210μm to 17μm thick[146]. Flash annealing produces fine crystallised grains resulting in improved strength during foil processing.

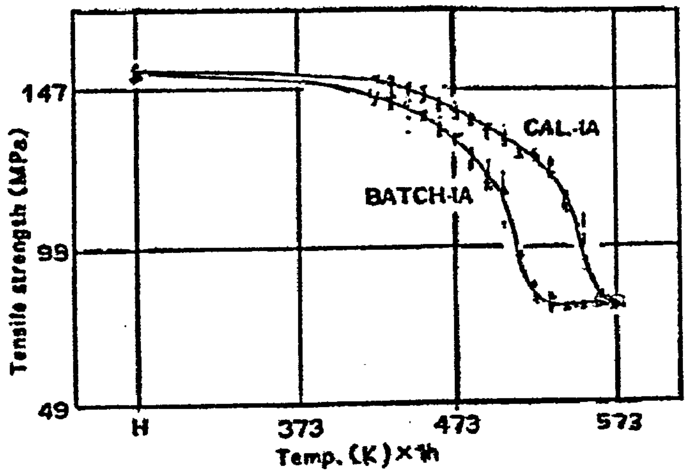

Figure 4.6. **Tensile strength versus temperature for flash annealing**

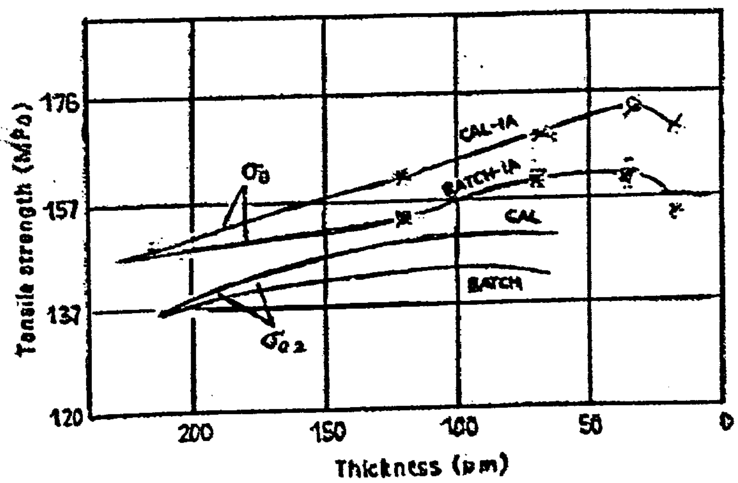

Figure 4.7. **Tensile strength versus thickness for flash annealing**

When the number of grains within a thickness is below five, the elongation significantly decreases; hence it is favourable to make the grains smaller in final annealed foil[147]. While the annealing mode has little effect on grain size at the intermediate anneal stage, during the final annealing stage it is pronounced. This is due to the batch annealing process promoting iron and silicon precipitation.

However, when industrial productivity considerations are taken into account, it is unsuitable to apply continuous annealing to large foil coils, hence final annealed foil is batch annealed. Therefore the grain size of final annealed foil does not depend on the equipment for intermediate annealing; rather it tends to depend on foil thickness and annealing temperature. Furthermore, during final annealing, coils can be kept between 543K to 573K for several days to remove the remaining residual lubrication oil.

During final annealing, soluble silicon precipitates onto the sub-boundaries and the elongation drops. For this reason it is difficult to produce high strength foils by partial annealing of pure aluminium[148]. This has lead to the development of high iron alloys, such as 8079, which exhibit high strength, large elongation and fine grains, as well as work softening after heavy cold deformation. The softening observed in heavily deformed Al-Fe alloys is believed to be due to dynamic recovery, however, static recovery after deformation might play an equally important roll, Figure 4.8[149,150].

In the manufacturing process for 8079, flash annealing is utilised only to obtain uniform and fine grain structures in hot rolled strip that may have irregular microstructure because the annealing is not sufficient to control precipitation of iron for work softening properties. The grain size of final annealed foil is very fine (about 10μm) and higher toughness in bending or bulging is obtained, Figure 4.9. Recently, there has been some developmental work into substituting a part of the iron by manganese (for example 8014) for light gauge foils, but as yet this is not widely used[151].

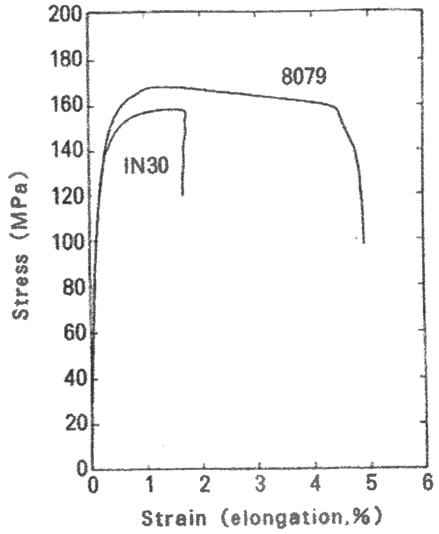

Figure 4.8. **Softening in aluminium - iron alloys, 8079 and IN30.**

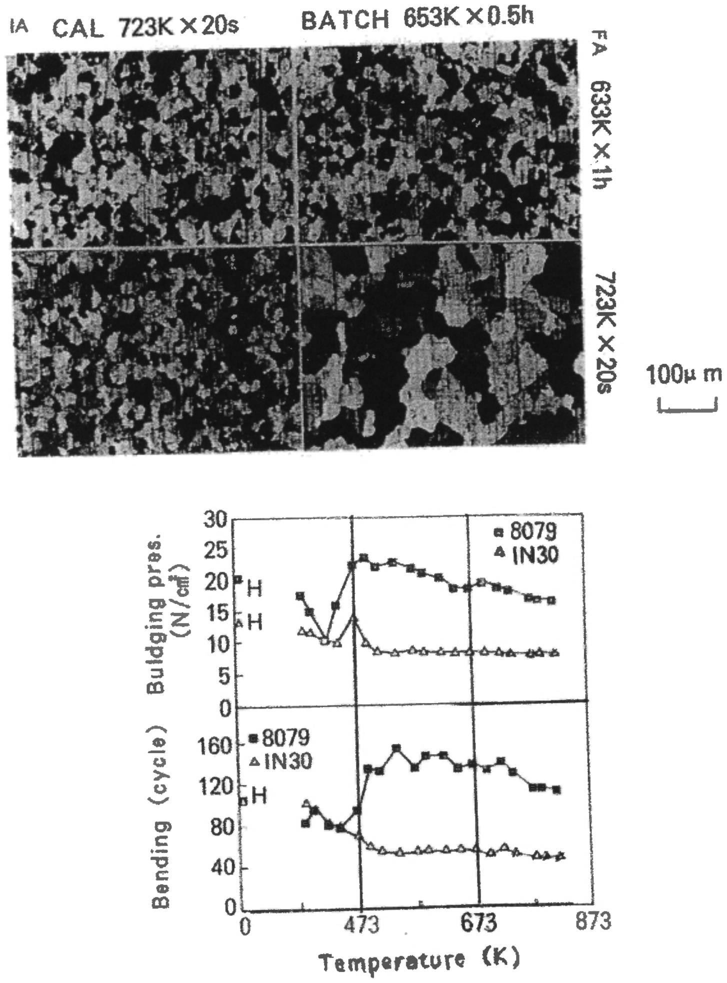

Figure 4.9. **Grain size effect on bending and burst strength for 8079 and IN30.**

4.5. General Adhesion Principles - Stickiness

Stickiness can be described as the adhesion between aluminium foil wraps in a coil post final annealing. It can occur uniformly across the strip, or at discrete locations within a coil, and promotes localised yielding leading to creasing on unwind, or in some cases tears in the foil leading to web failure.

The four basic theories of adhesion proposed in literature are the adsorption theory, the diffusion theory, the electrostatic theory and the mechanical theory and these have been thoroughly reviewed by Wake[152] and are summarised below:

i. The adsorption theory assumes that adhesive macromolecules physically adsorb onto the substrate and are held by various forces. The principal attractive force is believed to be dispersion forces such as Van der Waal's forces. Molecular interactions such as covalent bonding are believed to be secondary to dispersion forces. Surface wetting and chemical interactions are also believed to play a part in the adsorption process, and can be used to explain the abnormally high strength bonds occasionally found.

ii. Diffusion bonding is usually used to explain the adhesion of the same or similar polymers such as contact ceramics and heat-sealing thermoplastics. Long chain molecules are assumed to diffuse across the interface effectively eliminating the interface. For 'contact' bonds, chemical interactions are used to explain the adhesion.

iii. Electrostatic forces are generated when two dissimilar materials are brought in contact resulting in a charge at the surface interface. Electrostatic attraction is usually accompanied by dispersion forces and is used to explain bonding processes such as the photostatic process and metallised films.

iv. Mechanical adhesion is where mechanical interlocking or keying of the adhesive forms the bond. Adhesive flows into and around asperities or pores of the substrate forming an interlock bond. In the case of textiles or fibrous substrates chemical influence are also used to explain bonding.

Stickiness is not a well understood phenomena associated with annealing. There are two hypotheses put forward in literature to explain the mechanisms of stickiness resulting from annealing. One involves the oxidation and subsequent polymerisation of rolling oil contaminant and additives, the second pertains to the oxidation of aluminium surfaces. Published literature is neither comprehensive nor does it supply fully supported details of the possible causes of stickiness.

Historically, the basic rules for achieving dry, flat and free-winding foil are[153]:

- Slow controlled heating
- The lowest possible treatment temperature
- Optimum ventilation
- Long annealing times
- Controlled cooling

It is suggested that foil rolled bright on both sides has a tendency to develop stickiness; however this has only been supported through empirical observations.

A comprehensive report by Hofling and Baur[154] reported that:

1. Stickiness increased with annealing temperature
2. Stickiness increased with annealing time
3. High heating rates reduce stickiness
4. Inert gas anneals result in less stickiness.

However Hofling and Baur[154] were unable to categorize the contribution to stickiness of water vapour in the furnace atmosphere and subsequent reactions with the aluminium to form surface oxides. Work by Strohmeier[155] found that the presence of Ammonium Fluoborate during annealing of aluminium foil did not offer any significant protection against hydroxide formation in wet environments when compared to typical Aluminium foil behaviour.

Based on analysis of reaction products using gas chromatography, Hofling and Baur speculated that oxidation rather than evaporation was the predominate mechanism for removal of rolling oil during degreasing annealing[154]. Dean and Hauser expanded on this, stating that unsuitable residual surface oil (load bearing additives or extraneous lubricating oils)" will polymerise into higher molecular weight compounds that act as adhesives and that control of both rolling oil composition and annealing practices are necessary to avoid stickiness of the residues left on the foil[156]. This is represented as an idealized temperature/time diagram as shown in Figure 4.10.

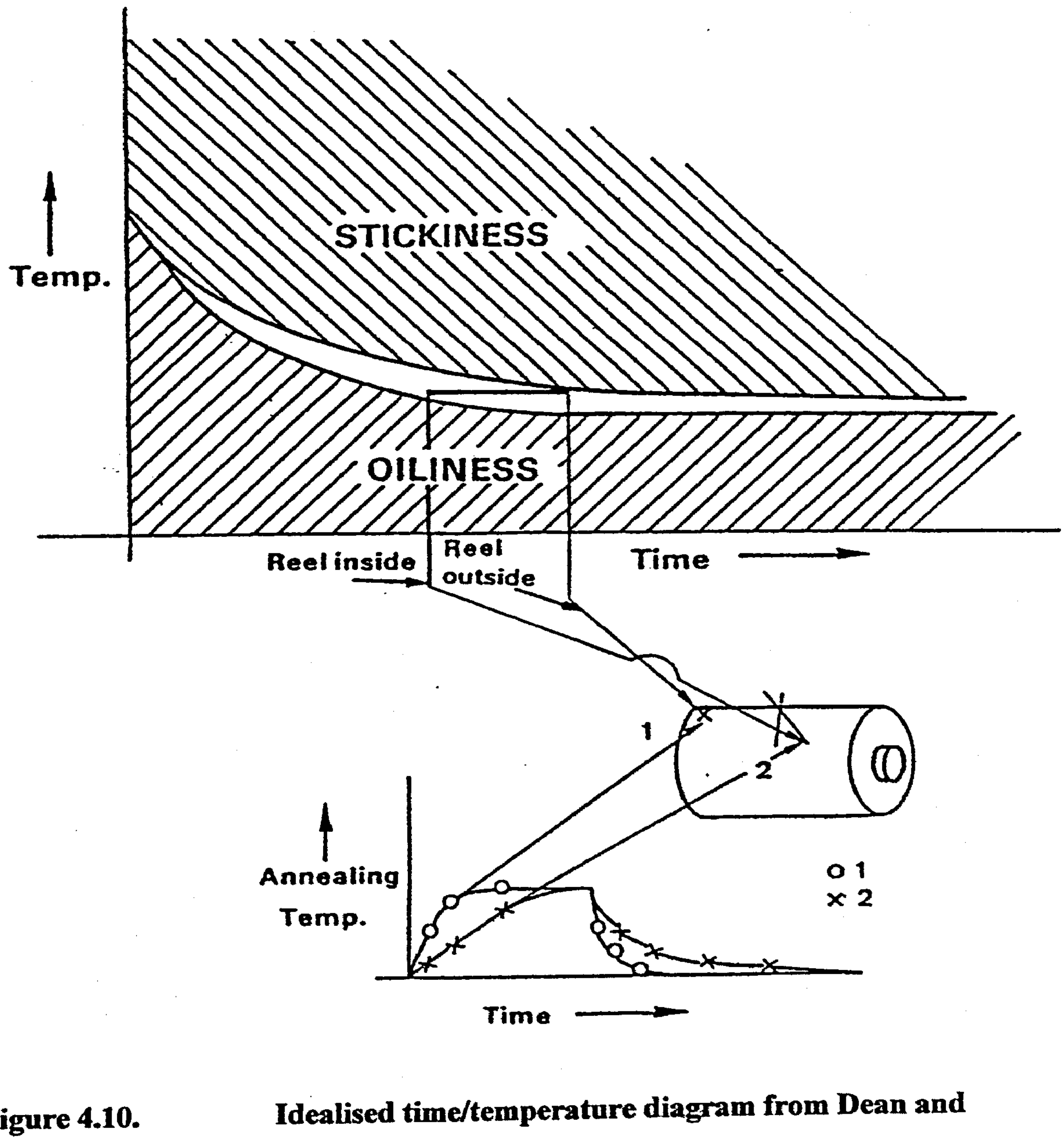

Figure 4.10. **Idealised time/temperature diagram from Dean and Hauser[156].**

Williams work went further to say that residual lubricant oxidation and polymerisation poses a mechanism for stickiness[78]. Her conclusions were as follows:

1. Approximately 60% of original lubricant remains following annealing, but the composition of residue does not include any original rolling oil components.
2. Annealing residue is most likely a straight chain aliphatic hydrocarbon with some oxidized functional groups.
3. Lubricant oxidation is the principal means of oil removal, with the subsequent polymerisation mechanism causing stickiness/wetness issues.
4. High heating rates reduce stickiness as it decreases the production of oxidized and acidic products available for further reaction during soak.
5. Higher temperatures/times promote stickiness by accelerating the polymerisation reaction. Rewind tensions and humidity have a strong influence on coil stickiness.

The overall mechanism for stickiness and wettability is complex and hence difficult to represent schematically. A simple representation of stickiness as a function of time, temperature, rewind humidity, tension and heating rate based on William's work is presented in Figure 4.11[78].

There has been some speculation that surface oxidation of aluminium is a potential mechanism for stickiness. Aluminium oxides are amorphous structures between 1.4 to 2.5nm thick at room temperature becoming more crystalline as time and temperature increase[157]. Annealing temperatures below 350°C result in inversely logarithmic growth until a limiting thickness between 2.8 to 5.0nm is reached[158,159]. At temperatures between 350°C to 450°C oxides follow parabolic growth laws, reaching between 5 to 6nm[160]. At temperatures in excess of 450°c growth laws become complex with oxide thickness known to exceed 50nm[161]. Work by Williams[78] showed that aluminium surface oxide thicknesses were lower on foil samples exhibiting unwind stickiness. This demonstrated that aluminium surface oxides did not improve welding or interlocking of oxide surfaces, discounting it as a source of stickiness.

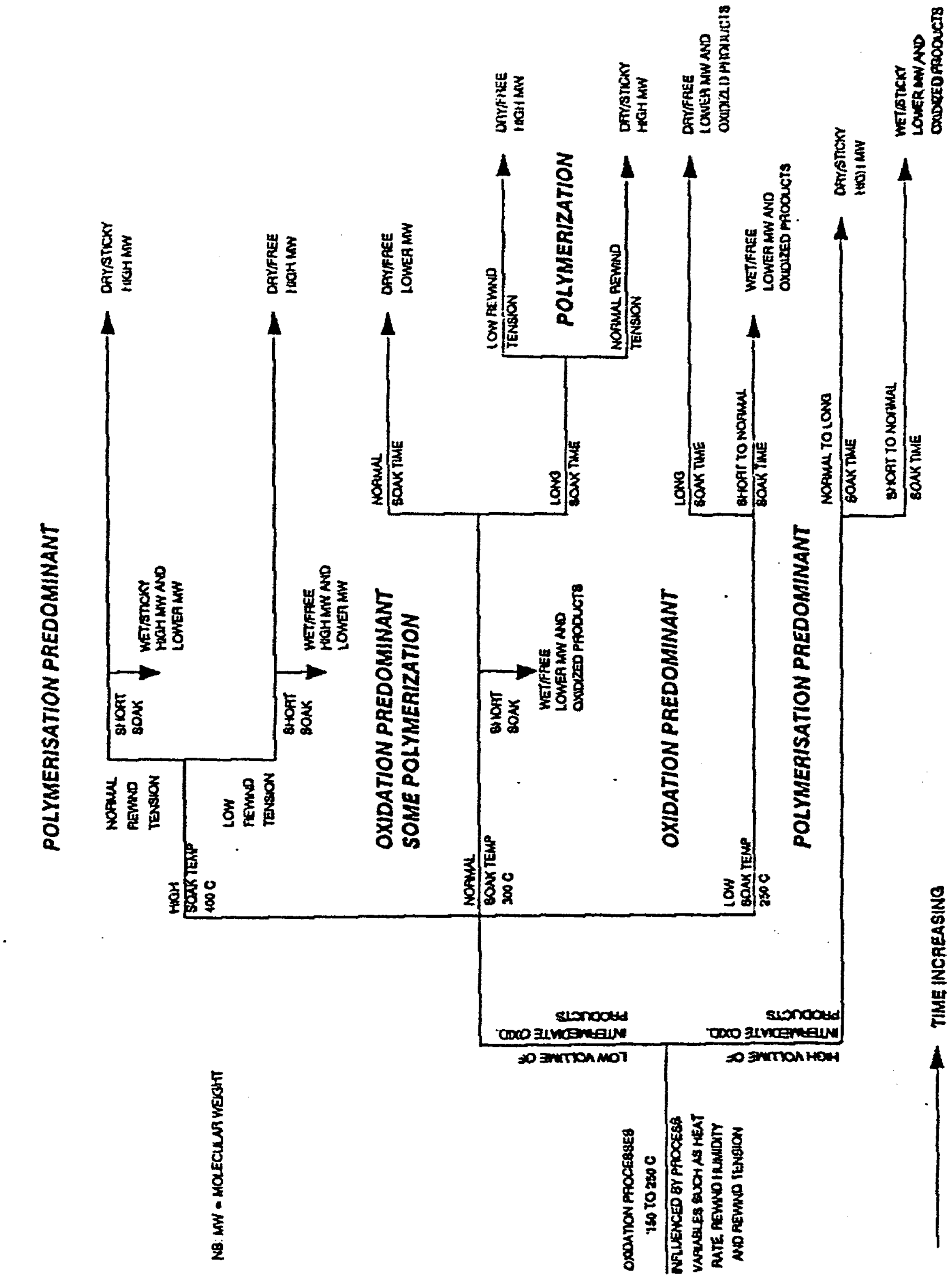

Figure 4.11. **Schematic for the development of coil stickiness and wettability**

CHAPTER 5 WEB HANDLING

Web handling theory looks at the process of unwinding a strip of thin flexible material or "web" under tension at the beginning of a process, transporting it through a process line, and rewinding the web under tension at the end of a process. Web handling processes can contribute to shape or tracking defects, and is a factor in determining annealing cycles which in turn affects surface properties. Chapters 8 to 10 aim to collate and expand on current published knowledge in the area of defects and mechanical influences.

A correctly wound coil:

- Will not unravel during transportation and handling
- Will have a reasonably straight side-wall with no damaged or bent wraps
- Has a circular mandrel that fits on a customer mandrel
- Has no internal defects caused by the winding process such as variable wrap densities and scratches

5.1. Introduction

Tracking a strip through the line involves both lateral and longitudinal dynamics and control, with web handling and winding problems resulting in line problems, excessive downtime, quality defects and ultimately scrap product[162]. Up until the late 1980's, little attention was paid to the development of web handling theory, with a rudimentary understanding that tension should not exceed 14 MPa during unwind and rewind operations[163].

There are many factors that influence coil winding operations. These include:

- Traction between the wraps
  - Surface roughness
    - Incoming roughness
    - Coating type
    - Thickness
  - Entrained Air
    - Ironing roll
    - Process speed
  - Wrap angle, web perpendicular to rolls
  - Lubricant thickness and viscosity
- Winding tension
  - Nominal tension (excessive, loose)
  - Tension upsets or losses
  - Taper tension schemes
- Web Shape
  - Metal thickness profile
  - Metal camber
- Tracking Disturbances
  - Equipment/roller misalignment
  - Roller geometry (taper, concavity)
  - Aerodynamic or thermal disturbances
- Influence of mandrel and core or spool
- Handling methods

Process lines can be divided into many different zones, each with their own tension and tension control systems, but still dependant on each other. A disturbance that occurs in a given zone will transfer across a bridle into an adjacent zone or zones. During the rolling and finishing operations of light-gauge foil, high and low tension zones in the strip can result in compressive and tensile stresses. Compressive lateral stresses can gather as fine ripples parallel to the processing direction while tension buckling in the high-tension zone may produce a coarser ripple.

5.2. Metal Dimensions

The incoming dimensions of the web prior to processing are critical to the tracking behaviour of the web.

Camber is a term used to describe the lateral curvature in the web. During processing, segments of the web are deformed to varying degrees resulting in a build-up of residual stresses. Once a critical stress S_{CR} (or tension T_{CR}) is achieved, longitudinal length differences of adjacent strands across the width of a web result in an uneven surface. This is often termed *'poor flatness'* with long centre strands resulting in centre buckles and long edge strands producing edge waves, Figure 5.1.

$$S_{CR} = \frac{EeW}{L^2} \qquad\qquad T_{CR} = \frac{EteW^2}{L^2} \tag{5.1}$$

where L = length (in.), W = width (in.), e = offset (in.), E = modulus (psi), t = thickness (in.), T_{cr} = critical tension (lbs), S_{cr} = critical stress (psi)

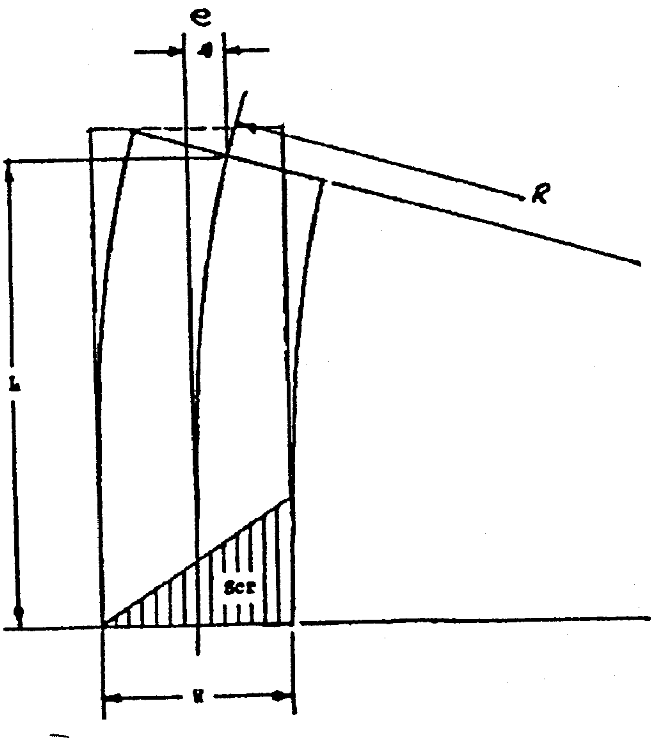

- L = length (in.)
- W = width (in.)
- e = offset (in.)
- E = Modulus (psi)
- t = thickness (in.)
- T_{cr} = critical tension (lbs)
- S_{cr} = critical stress (psi)

Figure 5.1. **Web camber**

The variation in lateral thickness across a sheet or web has an effect on the stress distribution. The amount that the centre of the sheet is thicker than the edges is referred to as *Profile* or *Metal % centre*. The amount one side of the sheet is thicker than the other is termed *Wedge* or *Metal % sideset*. The effects of wedge and profile are more pronounced at lower gauges, with negative profiles resulting in creasing of foil product. High thickness at the edge can trap more air in the coil and cause winding problems such as starring.

Thicker at the centre	Stress concentration in the centre	High-tension collapse.
Thicker at the edges	Traps more air in the coil	Increased risk of clockspring and sag collapse.
Uniform thickness	Slightly thicker in centre due to hotmill metal profile	Good wall – "Crown Pulley Effect"

Table 5.1. Effect of thickness

The wedge and profile targets vary by product and location, Figure 5.2. As a guide, the profile should be in the range of 0.1 to 0.5%, with a wedge of less than 0.8%. A micrometer can be used to measure hot rolled profile gauge and substituted into the standard equations (5.2):

$$\%P = \frac{e-\bar{e}}{\bar{e}} \qquad \%W = \frac{e_1 - e_2}{e} \qquad e = \frac{e_1 + e_2}{2} \qquad (5.2)$$

e = thickness at the centre; e_1 and e_2 = thickness 10mm from the edge

P = Profile, W = Wedge

$$\%P = \frac{e - e}{e} x\,100 \qquad with\ e = \frac{e_1 + e_2}{2}$$

Figure 5.2. Wedge and profile measurements

5.3. Traction

5.3.1. Air Entrapment

During processing, the web aims to position itself perpendicular to the rotational axis of each roll it approaches to enable maximum web traction (Normal Entry Theory), entrapping air between a web and roll. The amount of web traction is determined by the surface characteristics of the web and roll i.e. surface roughness and condition, and the wrap angle of the web on the roll in combination with tension.

Air entrapped between the web and the roll during rewinding is determined by roll diameter, web tension and web speed, Figure 5.3. The entrained air layer is greater with high web speed, larger roll diameters or low tension. When the air layer reaches a critical thickness, physical contact between the web and the roller surface is lost; tension between zones is reduced with idler rolls not turning and driven rolls not contacting and hence driving the strip.

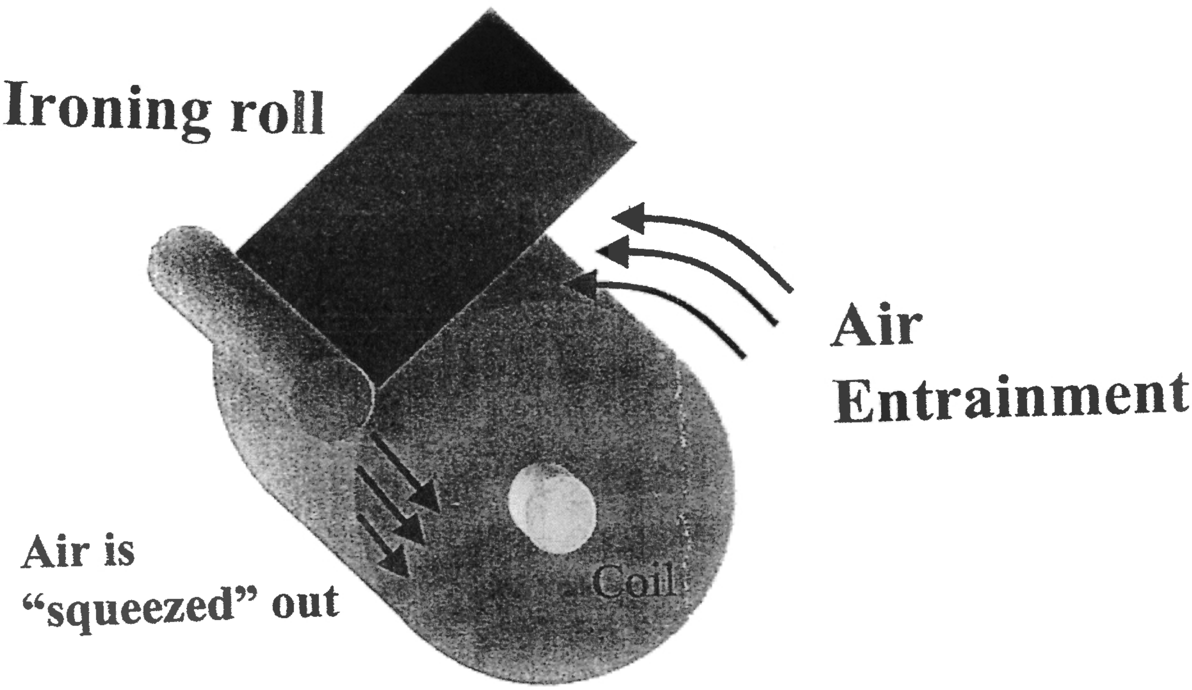

Figure 5.3. Ironing roll

Ironing rolls minimize the air film thickness within the coil. Only a small amount of pressure is required. The amount of air entrained in a coil without an ironing roll is described by the Knox-Sweeney equation:

$$h_0 = 0.643R\left(12\mu V / T\right)^{2/3} \qquad (5.3)$$

h_0 = the thickness of the air layer, R = coil radius, V = the sheet speed, T = sheet tension in pounds / linear inch, μ = viscosity of air.

5.3.2. Lubricant

The coefficient of friction (COF) or η, simply put, is a measure of traction between wraps of a wound coil during processing and is used to determine the tendency for coils to collapse, telescope, or clockspring.

COF is proportional to the "real" area of contact between wraps. With no lubrication, a smooth web surface has a higher COF than rough surface due to the greater initial area of contact. As lube thickness increases, surface voids are filled increasing the real contact area, resulting in rougher web surfaces have more traction and smoother web surfaces. Hence in production environments, rougher web surfaces are less prone to COF collapses than for smooth web surfaces with equivalent levels of residual surface lubrication, Figure 5.4.

Roll misalignment in mill or finishing equipment can result in a change of web direction inducing shear stresses[164]. The shear stresses result in the formation of undulating waves in the direction that cannot support compressive stress causing the web to slide over the rolls as traction is inadequate[165]. Modifications to the roll camber have reverse effects, with crowned rolls supporting stable tracking but can cause wrinkling of thin sheet while dished rolls spread the sheet but cause unstable tracking.

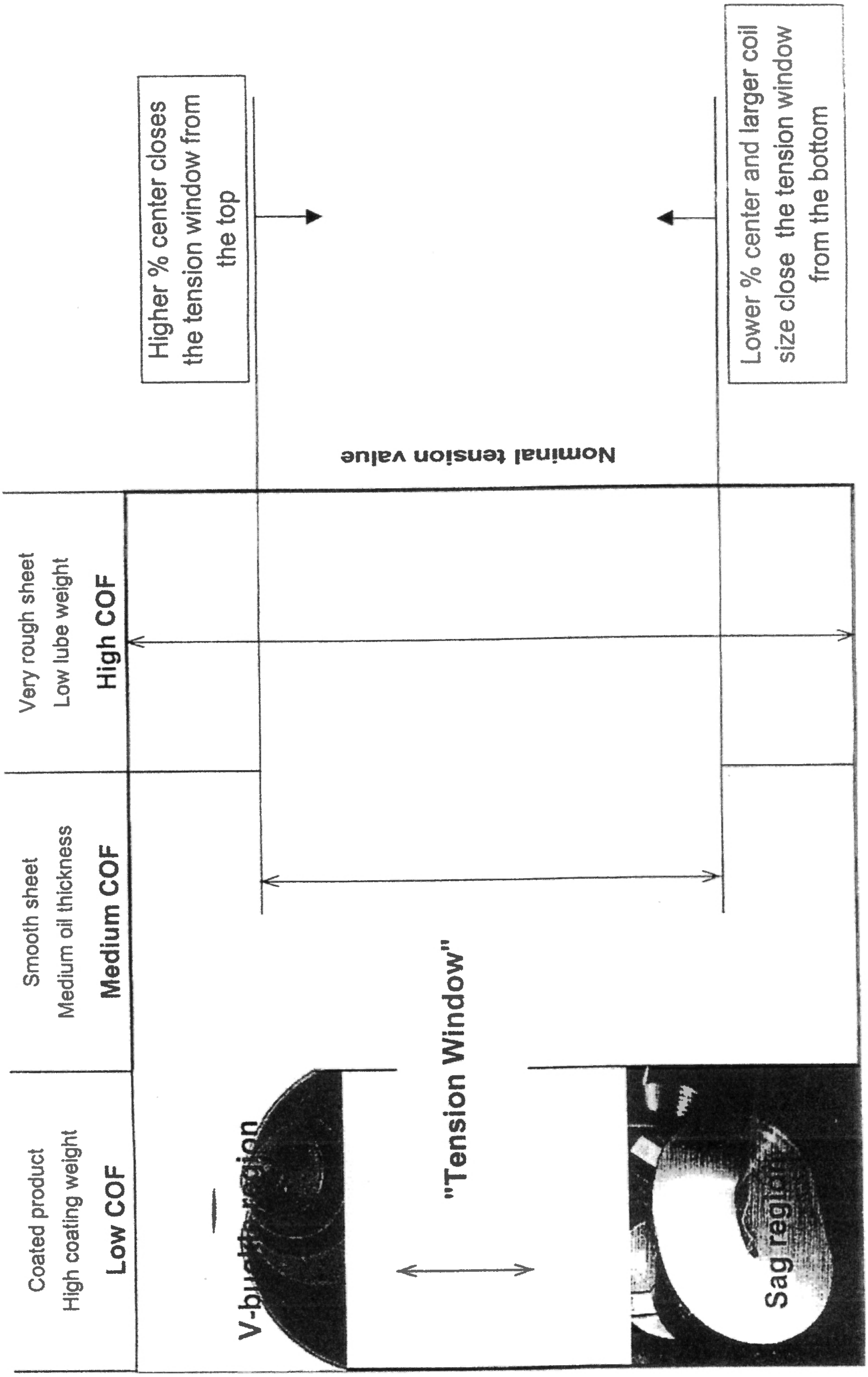

Figure 5.4. COF collapse

5.4. Tension

Tension is the single most important parameter in winding. It provides normal force to the roll to give traction to driven and idler rolls, minimising slippage, reducing or eliminating buckles due to cross web strain variation (such as drive system instabilities, core out-of-roundness, rolls not cylindrical, bent shafts, inadequate roll balance, process influences such as web flutter, shock), providing radial stress between layers of a wound roll and influencing air entrapment.

Optimum tension depends on product characteristics and other winding factors. Taper tension must be used on some products to avoid clock springing, particularly foil. Tension is a force that tends to stretch or elongate, expressed as either units of force (newtons) or units of stress (Pascals). An unevenly unwound coil can result in either excessive or loose wind tension. Excessive tension may telescope or distort the wound coil while insufficient tension may lead to coil sag.

Fundamental web equation: Tension stress = t = W/A = $\frac{Ewh}{L}\int_0^t (V_{out} - V_{in})$

$$\text{E = Young's modulus, w = web width, h = web thickness, V = velocity, A = cross-sectional area, W = tension force} \quad (5.4)$$

Web tension can be calculated using a load-cell to directly measure the load imparted on a pass-line fault or can be indirectly measured with a calculation based on the reel drive operating parameters (armature current, voltage, angular velocity) of a tension actuator, Figure 5.5.

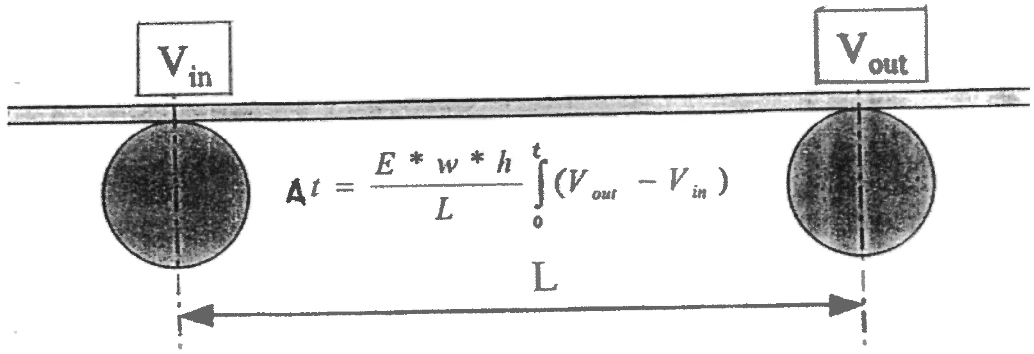

Figure 5.5. Web tension

5.4.1. Torque Capacity

During processing, the rotary force or "motor torque" must be transmitted from the mandrel through the core and through every wrap in the coil to the sheet at the outer diameter. If any part breaks down, you have the "slip clutch effect", i.e. slippage as layers cannot transmit torque.

To prevent slippage, the torque capacity of the coil must exceed the torque input from the motor, Figure 5.6. The torque capacity is dependent on surface area, traction (measured as the co-efficient of friction) and radial pressure. The inner diameter of the coil has the least surface area along with potentially low radial stress and is the area where slippage is most likely to occur. In foil rolling, the co-efficient of friction during rolling approaches zero, however the slippage effect is minimised by the thin gauge of the material and clockspring rarely occurs.

$$\text{Torque Capacity} = R \times 2\pi R \times W \times F_R \times \mu \qquad (5.5)$$

F_R = radial pressure, R = Radius, W = sheet width, μ = coefficient of friction

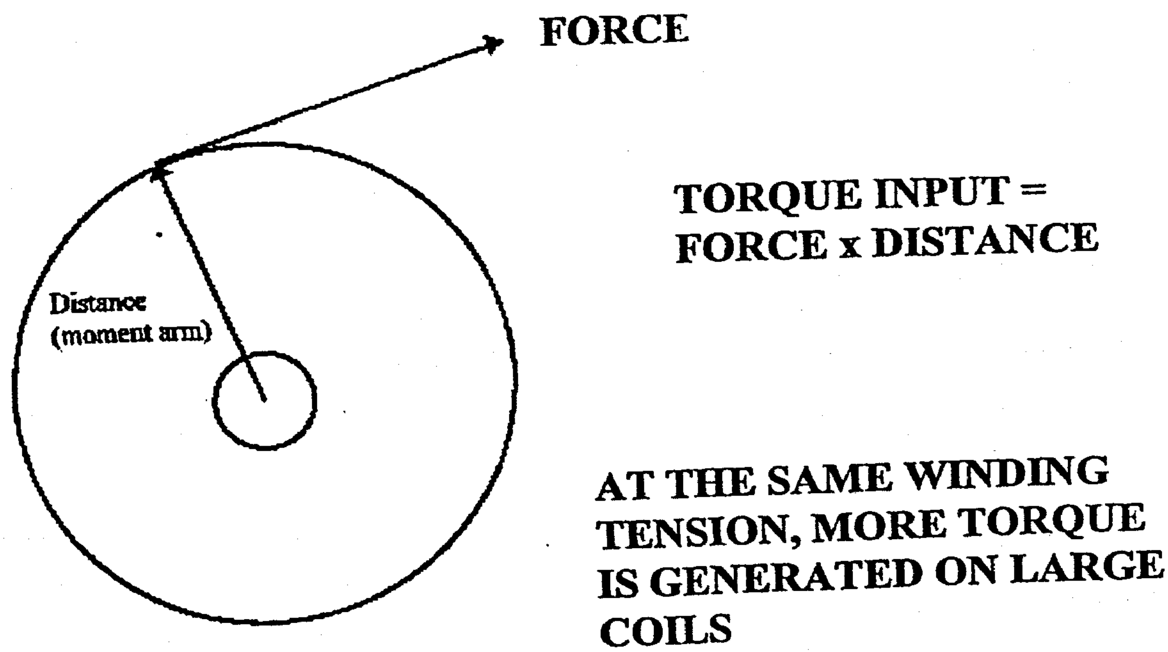

Figure 5.6. **Torque capacity**

At heavier gauges, inner diameter slippage or clockspring can result in friction scratches and out-of-round inner diameters making it hard to load onto mandrels for further passes, Figure 5.7. The most common causes are:

1. Low tension at the beginning of a coil – results in lower radial stress, making the ID more likely to slip.

2. A very low coefficient of friction (COF) – Certain coating and wax combinations give the sheet a low COF. This factor reduces the torque capacity of the entire coil and the ID in particular

3. Ironing roll not in contact at the ID – i.e. more entrained air

CLOCKSPRINGING

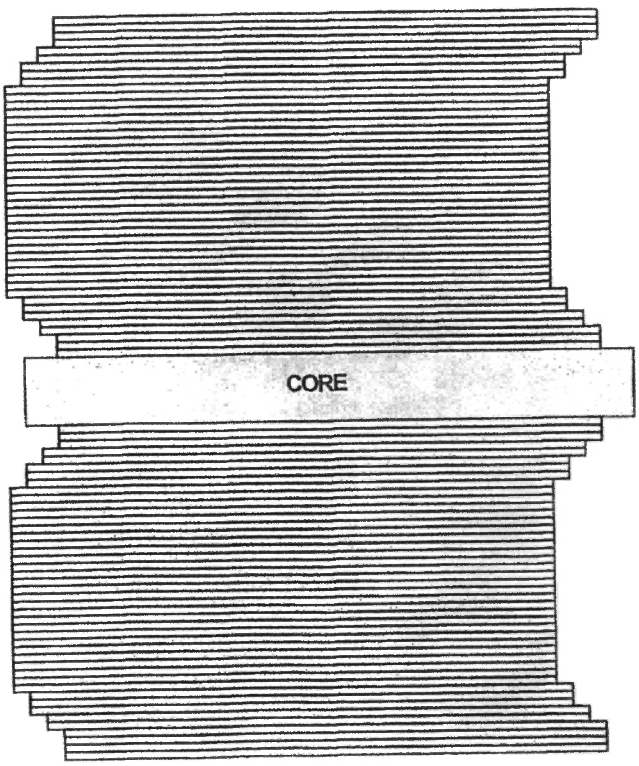

- **Mechanism:**
  - Torque capacity at ID was exceeded - interlayer slippage caused "cinching" of the ID.
- **Possible causes:**
  - Low tension at ID
  - Heavy lubricant at ID
  - Sheet surface too smooth
  - Tension increasing as coil is wound
  - Edge buildup trapping air at ID
- **Potential solutions:**
  - Implement tapered tension
  - Increase sheet roughness
  - Provide a better thickness profile
  - Lower lubricant thickness at ID

Figure 5.7. Clockspring schematic

5.4.2. Torque Calculations

Winders are used to un-wrap and re-wrap webs to and from coils, and to regulate the unwinding and line tension in the entry and exit sections of a system. Armature voltage and current along with motor efficiency are used to measure torque while delivered mandrel torque is calculated using the gearbox ratio and efficiency (motor and equipment losses must be included in the calculation). Torque is converted to tension based on the coil diameter.

Rolls are used to support, transport and manipulate the web. Some are designed to impart a tension change in the web while others are intended only for support or guidance. Anytime a web passes over a roll, a change in tension will occur.

Tension changes are caused by:

1. Sliding friction between the web and roll (if the roll is not turning)
2. If the roll is turning (i.e. no macro-slip), roll bearing friction and windage (drag) must be overcome.
3. If the speed is changed the roll inertia must also change (roll mass must be accelerated)
4. If the roll is driven, the torque imparted to the roll will be transmitted to the web.

The maximum tension that can be imparted to a roll without macro-slippage is represented by the Capstan equation, Figure 5.8. This can be used to calculate the minimum wrap angle to prevent slippage between a roll and the web.

$$\frac{t_2}{t_1} \leq e^{\mu\theta} \text{ or } \theta \geq \frac{1}{\mu}\ln\left(\frac{t_2}{t_1}\right) \quad \text{as a general rule of thumb, } t_2/t_1 = 2 \quad (5.6)$$

μ = web to roll coefficient of friction, θ = wrap angle in radians

Rolls generate web tension changes. At steady-state velocity, downward tension increases when passing over an idler roll (bearing drag). A driven roll in regeneration mode increases downweb tension and a driven roll in motoring mode generates a decrease in downweb tension

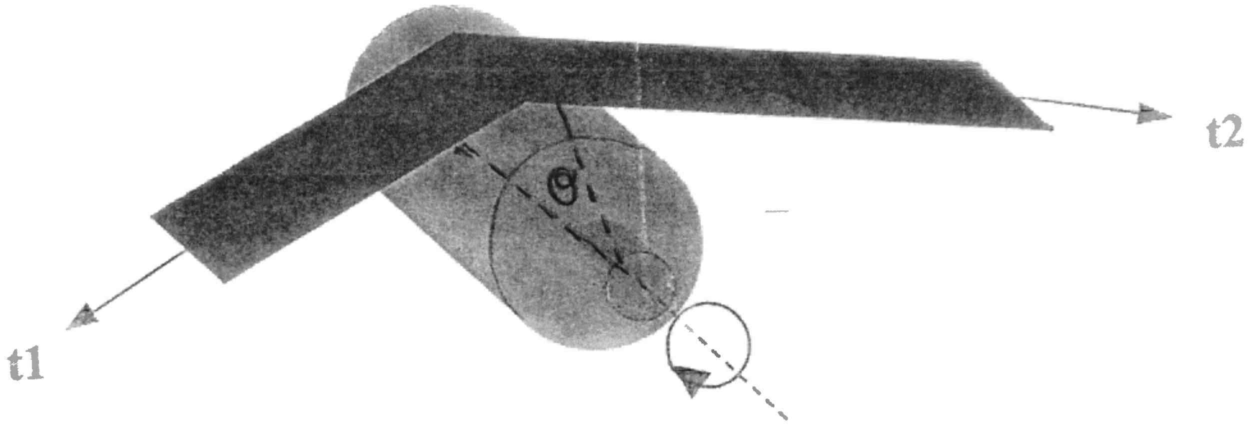

$$\text{Capstan Eqn: } \frac{t_2}{t_1} \leq e^{\mu\theta} \text{ or } \theta \geq \frac{1}{\mu} \ln\left(\frac{t_2}{t_1}\right)$$

Figure 5.8. Torque calculations using the Capstan equation

5.4.3. Inertial effects (acceleration / deceleration)

In practice, not only does the web change velocity constantly but all elements connected to the web must also change velocity. The inertial mass associated with acceleration and deceleration can have a significant effect on the web tension stress, hence the inertia of the entire winder system must be taken into account. During acceleration, system inertia must be accelerated consuming part of the motor power; during deceleration, system inertia must be decelerated so additional power is released to the winder system, Figures 5.9 - 10.

Since the torque required during acceleration and deceleration is significant and changes with coil diameter, an inertia compensation system is used to dynamically calculate inertia and to compensate the drive control system.

When the line speed changes, the inertial mass of the various rolls in the line must be accelerated or decelerated. It the rolls are driven, the inertial load can be estimated and compensated in the same way winders are compensated. If the roll is not driven, roll acceleration torque is delivered to/from the roll via the web. In this instance little can be done to eliminate tension changes as the web passes over the roll. During acceleration, down-web tension versus steady-state will increase; during deceleration, down-web tension versus steady state will decrease.

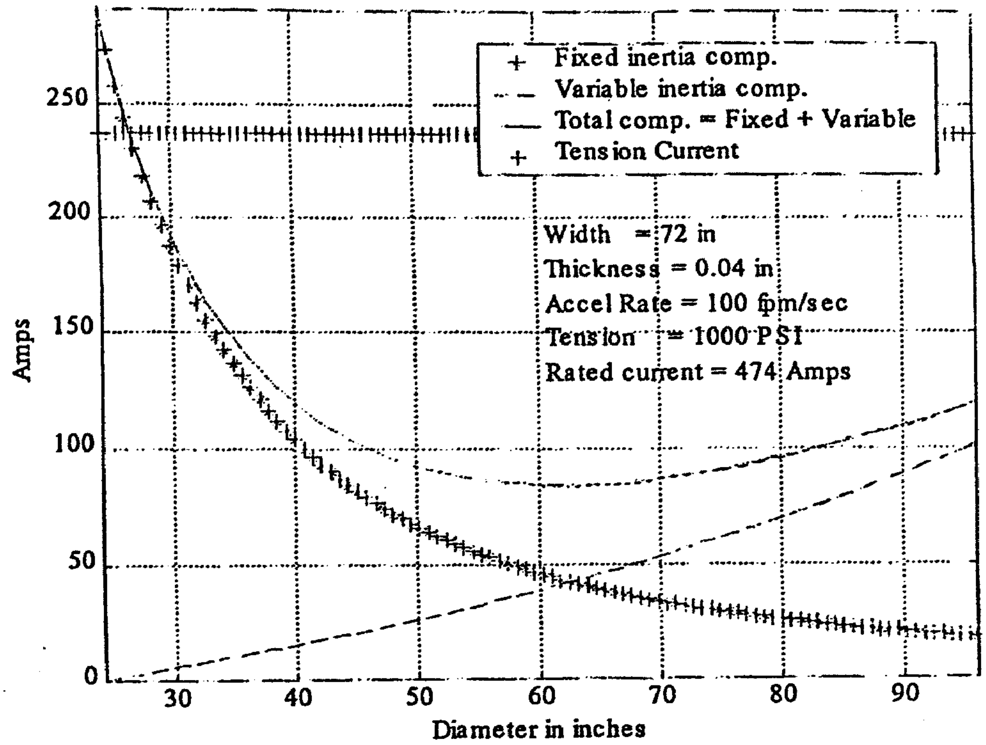

Figure 5.9. **Inertial effects – acceleration**

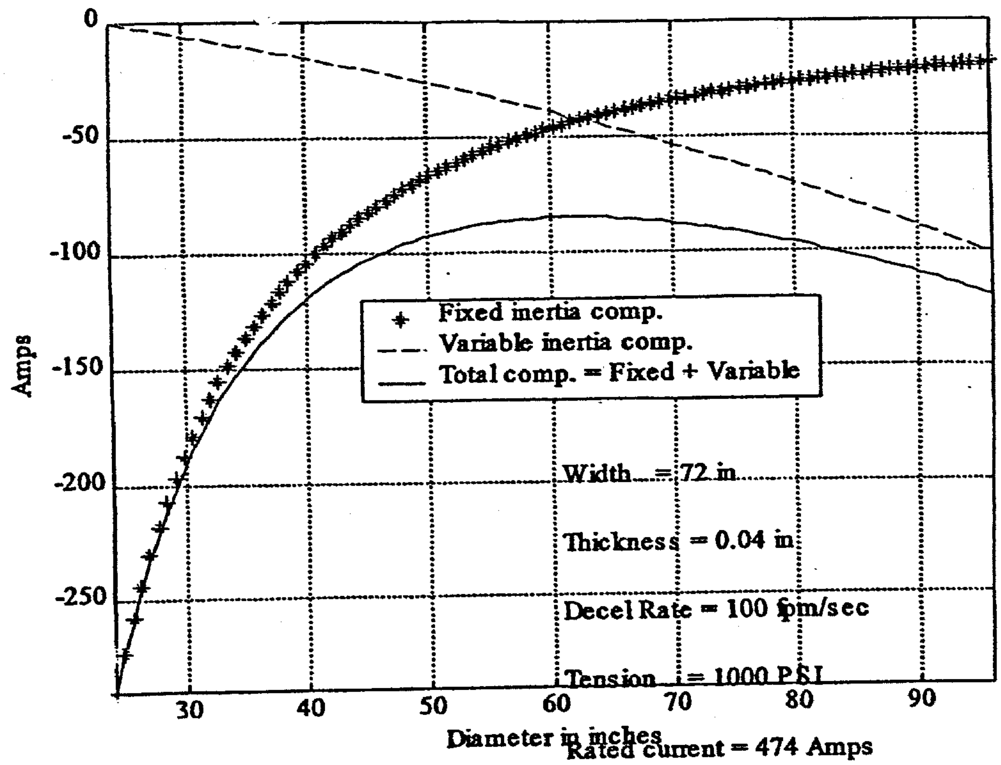

Figure 5.10. **Inertial effects – deceleration**

5.5. Wrinkles / Creasing

A crease is defined as a line or fold that results from ridges and groves (ripples) in aluminium foil strip coming into contact with one or more rolls. *Styner* showed that when a web ripple pass between a set of rolls, the ripples are effectively ironed and hard folded, emerging as creases in the foil[162]. For ripples passing over cylindrical rolls, *Friedrich* confirmed that ripples in foil are capable of collapsing to form a crease in the foil[166]. Creases run in the direction of rolling and may contain a shear component giving slight sideways displacement. Creasing may be fine or course, vary in position across the web, and vary in length from 3mm to hundreds of metres. This defect has also been called a "zipper" due to its zipper like appearance, Figure 5.11. Refer to Chapter 6.1.2, Figures 'm' and 'n' for actual images of zipper-like defects.

The most common sources of wrinkles are:

- Misaligned rolls with short spans
- Roll geometry problems (out-of-round, too much crown, nip pressure, raised or depressed zones on driven and idler rolls)
- Tension disturbances (too little tension – smoothing out lost; too much – excessive traction)
- Sheet problems (buckle, wave, camber, sheet misaligned at splice)

Wrinkles result from compressive forces such as bending and friction in the cross-web direction overcoming the web strength. While bending forces try to straighten the sheet, friction forces trying to hold in the wrinkle. The forces are dependant on the tractional engagement of the web with the roll i.e. web thickness, tension and roll radius for bend; tension, width, wrap angle and roll roughness for friction.

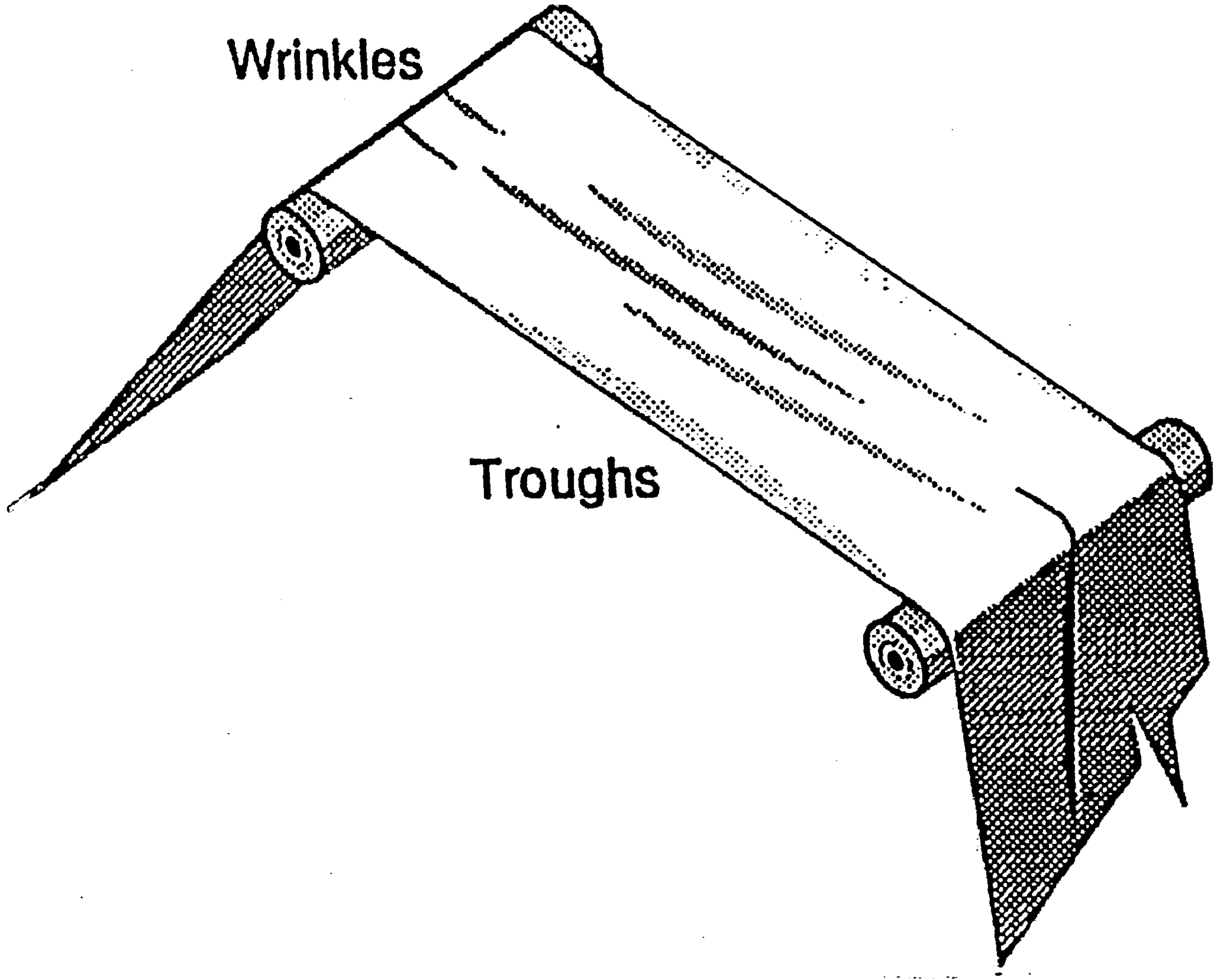

Figure 5.11. **Wrinkles on light film web**

To reduce the incidence of wrinkles, the wrap angle, surface roughness or tension are decreased, reducing traction. Increasing the roller diameter or speed has a similar effect. The tendency of the web to buckle is related to the cube of the thickness i.e. small changes in thickness increase the probability of wrinkles.

$$\boxed{\begin{array}{l} P_{CR} \propto EI \\ I = \dfrac{wt^3}{12} \\ P_{CR} \propto t^3 \end{array}} \tag{5.7}$$

5.5.1. Non-Uniform Strip Elongation

5.5.1.1. Shape

A major contributor to non-uniform strip elongation in foil rolling is the variation in thickness across the width of a strip due to generic profile errors or localised thermal and mechanical shape defects. The thickness variations instigate compressive lateral stresses in which aluminium foil may buckle and ripple in the rolling direction in any zone. The stress distributions across rectangular sheets are illustrated for the four principal shape defects[167], Figure 5.12.

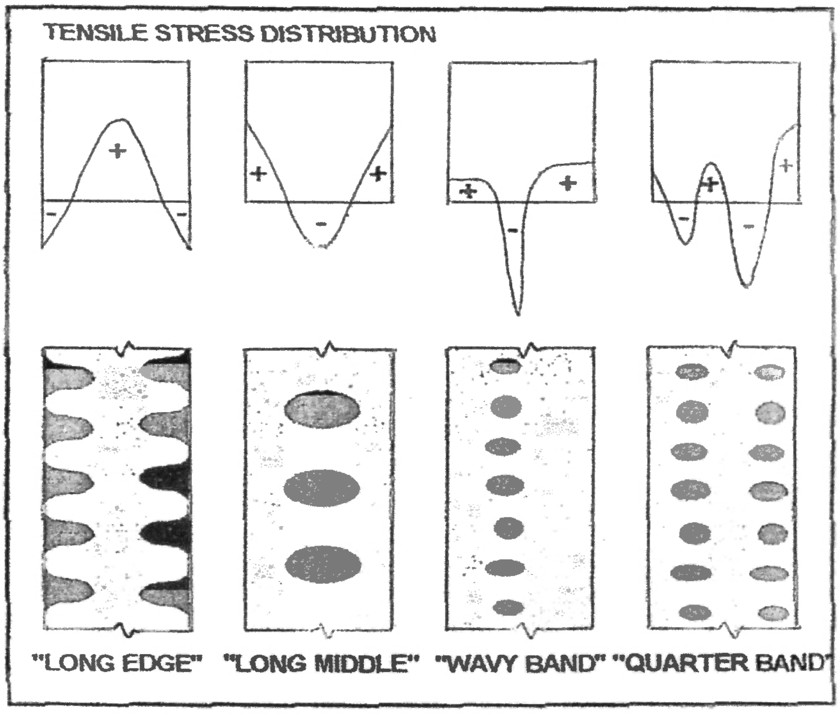

Figure 5.12. Stress distribution

The critical compressive stress to achieve web rippling is calculated via[168]:

$$\sigma_{cr} = k\pi^2 E / 12(1 - v^2) \times (t/b)^2 \qquad (5.8)$$

E = modulus of elasticity in compression, t = thickness of the foil, b = width of the foil, a = length of the foil, v = Poisson's ratio, k = constant; f(side support, b/a, web shape)

Several thin membrane models have been developed which indicate that elastic buckling or rippling is dependant on the relative intensity of lateral compression to axial stretching, among a number of other factors[169,170,171]. This is supported by Segedin et al. when investigating the effects of non-uniform applied stresses on a rectangular plate[172].

5.5.1.2. Tension Buckling

If differences in tension are not sufficient to initiate non-uniform elongation, tension buckling can occur when compressive lateral tensile stresses at any point within a sheet reach a critical level relative to the size of the area were they are found[173]. This was successfully applied to buckling or rippling of flexible fabric sheets when the external forces were not uniformly distributed over the edges[174]. Regions outside the buckled zones were relatively stress-free.

Work by several researchers established the following expression for critical axial strain under which a sheet buckles:

$$\boxed{\varepsilon_c^2 \geq (B/YWL)} \qquad (5.9)$$

where if the length to width ratio (WL) is kept constant, larger sheets will buckle first. In addition, more flexible web lowers the bending stiffness to in-plane modulus (B/Y) reducing the critical strain level.

5.5.1.3. Ripple Collapse Producing Creasing

Non-uniform strip elongation, tension buckling and roller mis-alignment are the three principal modes of machine directional web rippling. When the web ripples interact with nip or cylindrical rolls, depending on several variables, creasing can occur. For ripples that are rolled between nip or work rolls, the rips are ironed and hard-folded resulting in a crease or zipper defect.

The interaction between ripple and cylindrical rollers is more complex. Work by Freidrich and Styner indicated that foil ripples collapse to form a crease as they encounter cylindrical rollers that provide out-of-plane guiding[175,162]. Once the lateral stress is reached, an unstable ripple will collapse on itself to produce a crease in the foil. This lateral stress can be expressed as a function of web rigidity for ripple stability:

$$\text{Web Rigidity} = \frac{Eh^3}{12(1-\gamma^2)} \tag{5.10}$$

E is Young's modulus, h is web thickness and γ is Poisson's ratio.

Geometric parameters appear to have more influence on lateral stress and hence ripple stability than material parameters. Two useful ratios, ripple-height ratio and ripple-aspect ratio, can be used to quantify the geometric parameters:

- The ripple-height ratio is obtained by dividing the roller diameter by the height of the deformed ripple. For ratios less than 10, the lateral stress increases exponentially increasing the likelihood of crease formation.
- The ripple-aspect ratio is obtained by dividing ripple height by ripple width. In general, ripples with a ripple-aspect greater than 0.64 will collapse.
- Wrap angle; as the wrap angle increases, stress response increases.
- At low-to-moderate tension, ripple stress is primarily a result of deformation. At higher tensions, ripple stress is a function of applied tension.
- Ripple stability is a function of both Young's Modulus and foil thickness.
- Poisson's ratio has little effect on the lateral stress due to the unconstrained region in the vicinity of the ripple that is free to deform in the lateral direction.

If the friction coefficient between the web and the roll is low enough, the web may be stable at lower web rigidity values because the web tends to flatten out due to web slippage.

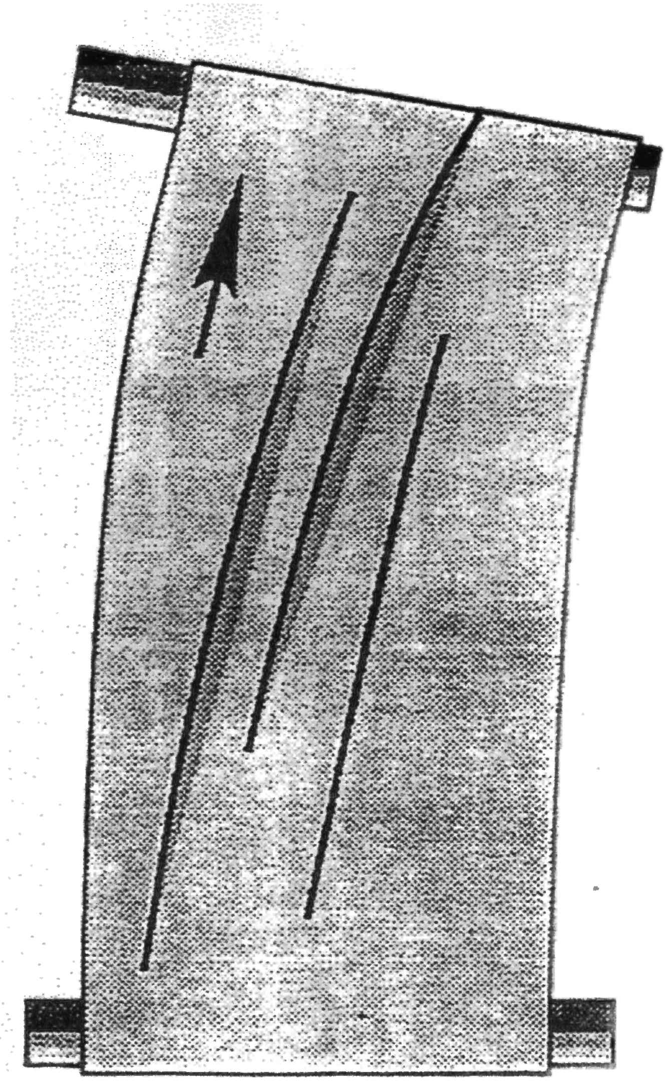

Figure 5.13. **Web rigidity**

5.5.2. Shape Issues

A crease is defined as a line or fold that result from ripples in aluminium foil strip coming into contact with one or a set of rolls. There are several causes of ripples, with non-uniform strip elongation a major contributor in foil rolling. Non-uniform elongation results from variations in thickness across the width of a strip due to generic profile errors or localized thermal and mechanical shape defects. The thickness variations instigate compressive lateral stresses and can result in one of five principal shape defects:

a. Wavy Edges

The strip is thinner at the edges resulting in wavy edges, Figure 5.14. There are several causes including:

- Excessive reduction resulting in excessive roll deflection.
- Thermal camber issues due to too much coolant, incorrect spray arrangement / adjustment on cold rolls.
- Mechanical camber issues, excessive negative camber.

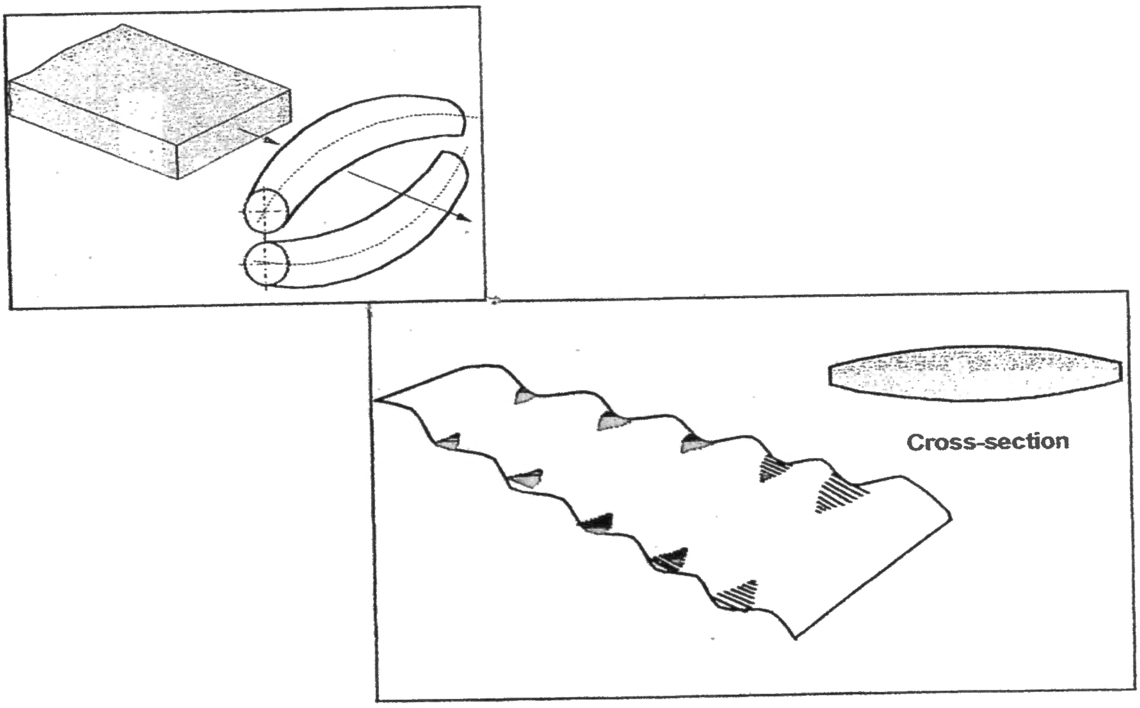

Figure 5.14. Wavy edges

If only one side is wavy, the principle causes include:

- Rolls out of balance / alignment.
- Thermal strain on the roll due to poor cooling control.
- Poor incoming profile.

b. Centre Buckles

The strip is thinner at the middle, resulting in buckles in the centre of the coil, Figure 5.15. This may be due to:

- Insufficient reduction.
- Too much thermal camber – rolls overheat, insufficient coolant, incorrect spray arrangement or adjustment.
- Mechanical camber issues – excessive positive camber.

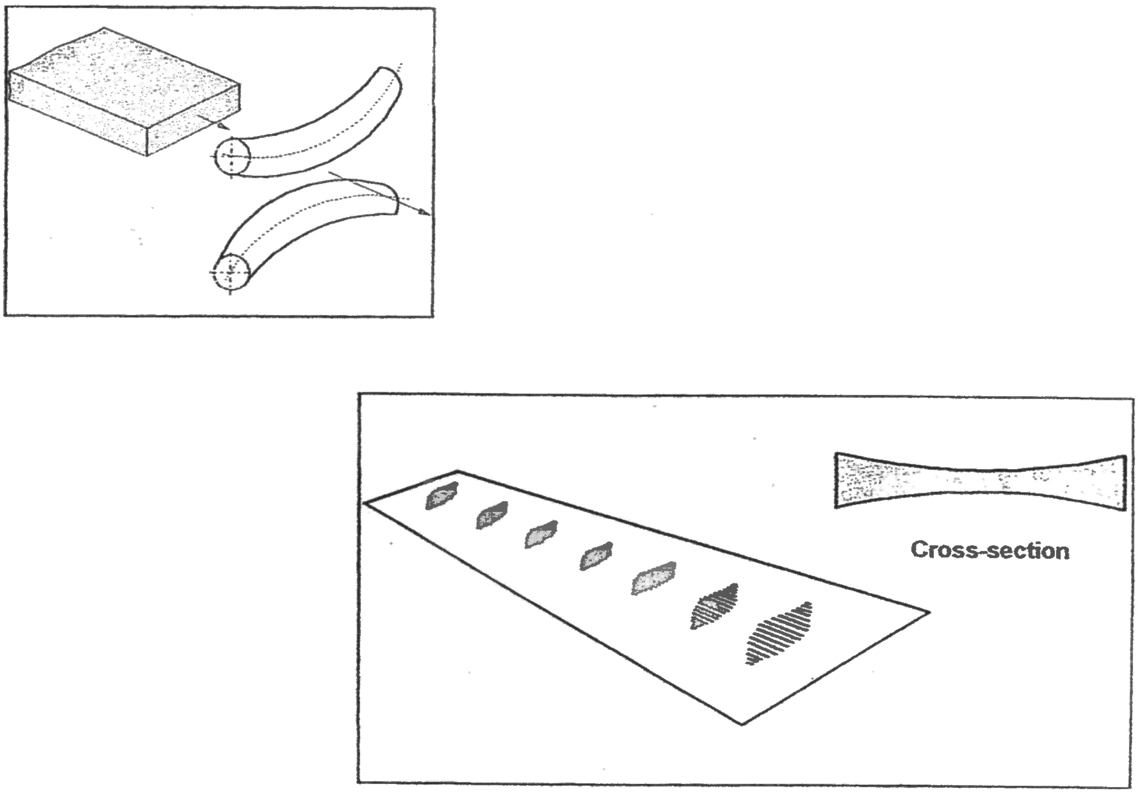

Figure 5.15. **Centre buckles**

c. *Quarter Buckle*

Two wavy bands appear about a quarter width in from the edge, Figure 5.16. This may be due to:

- A cumulative effect of positive camber produced by the rams and deflection produced by the strip. Excessive friction may exacerbate the problem and it is more prevalent in wide strip.

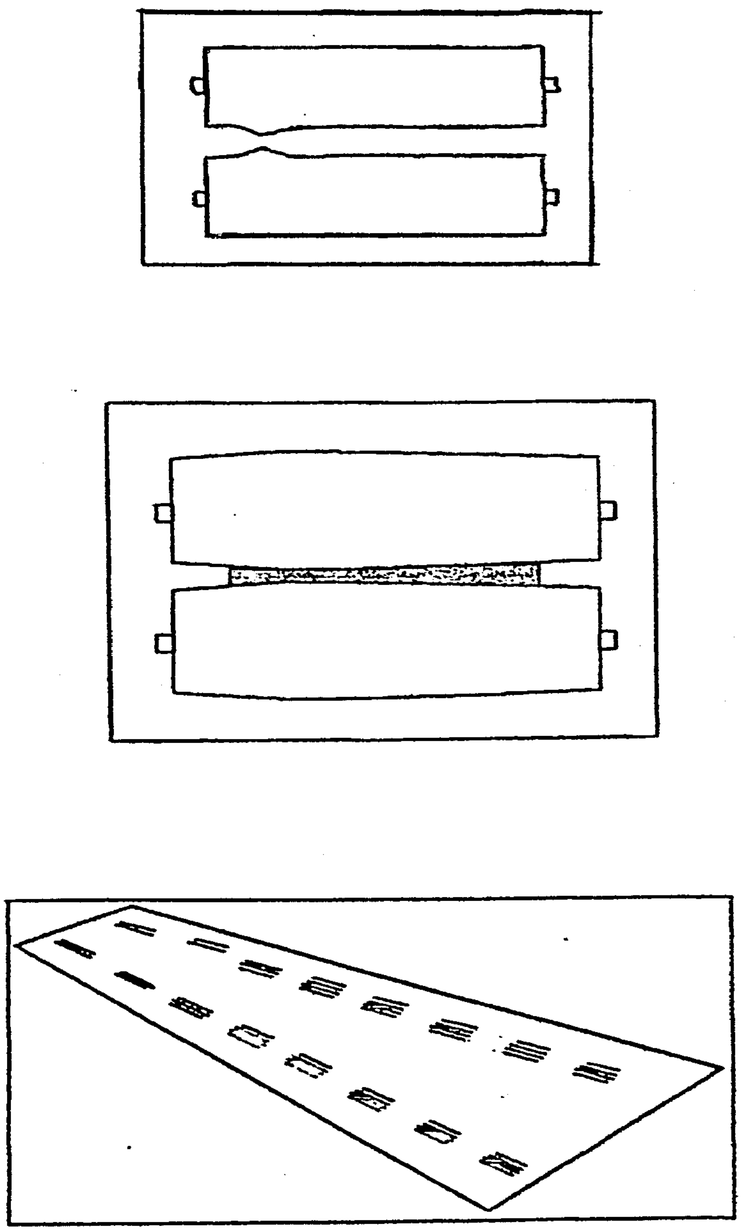

Figure 5.16. **Quarter buckle**

d. Hot Spots

A narrow band at any position across the strip due to:

- Roll wear.
- Localised thermal camber resulting from a cooling or lubrication breakdown which in turn causes excessive localised friction.

Thermal camber issues can also be attributed to changes in strip width, narrow to wide, Figure 5.17.

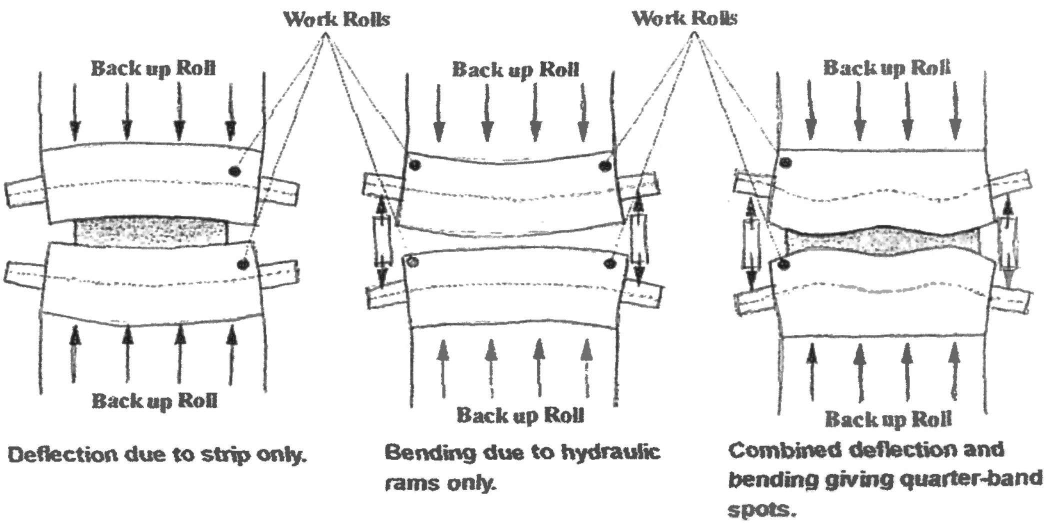

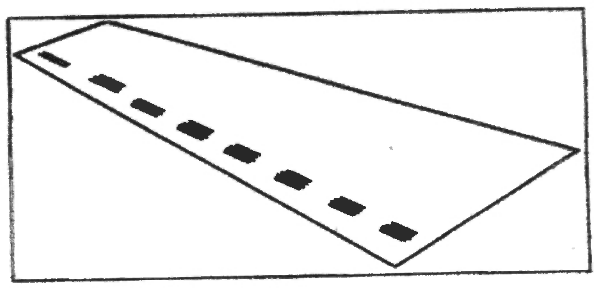

Figure 5.17. **Hot spots**

e. *Hot Buckling*

Hot buckling is a result of roll crown (shape) leading to non-uniform tension, Figure 5.18. Sagged strip portions contact the roller and the subsequent friction results in expansion heat buckles. The hot buckling critical tension decreases with greater roller crown and wider, thinner, hotter strips, and increases as the roller central flat portion is extended. For each strip width, there exists a maximum crown that presents no hot buckling problems.

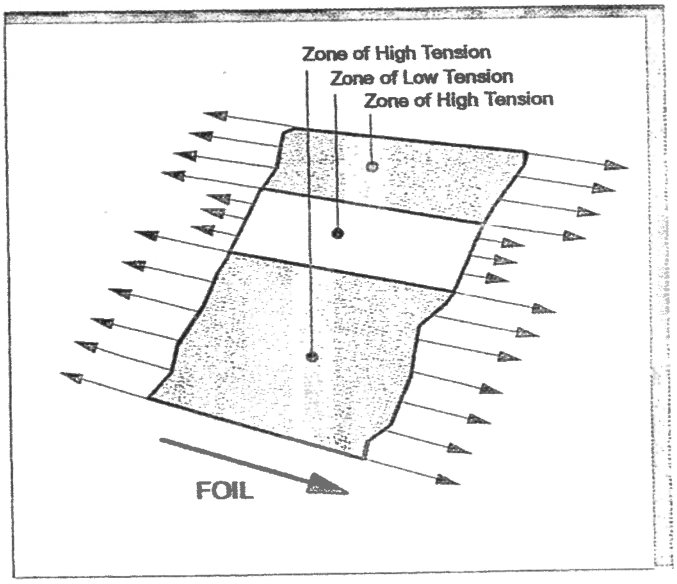

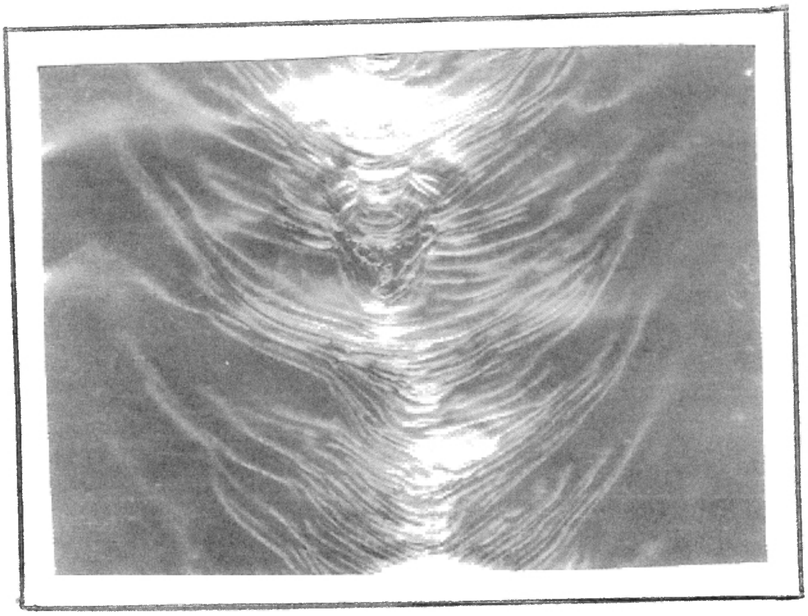

Figure 5.18. **Hot buckling**

5.5.3. Reducing Creasing through Mechanical Means

Over long spans, ripples can attain a 'critical' ripple aspect ratio and subsequent ripple development as a result of non-uniform web elongation, tension buckling and roll misalignment. There are several mechanical methods that can be employed to counter and even eliminate both foil-stock and machine induced directional ripples[162].

Pinch rolls:

This requires uniform pressure side to side, uniform roll hardness, uniform material properties or pinch roll bending may cause the sheet to pull in from the edges which is inherently unstable.

Idler Rolls:

The foil span can be reduced with the introduction of idler rolls, smooth surfaced aluminium or steel free-spinning rolls that rotate under the action of web contact maintaining tension at high speeds with minimum distortion, Figure 5.19.

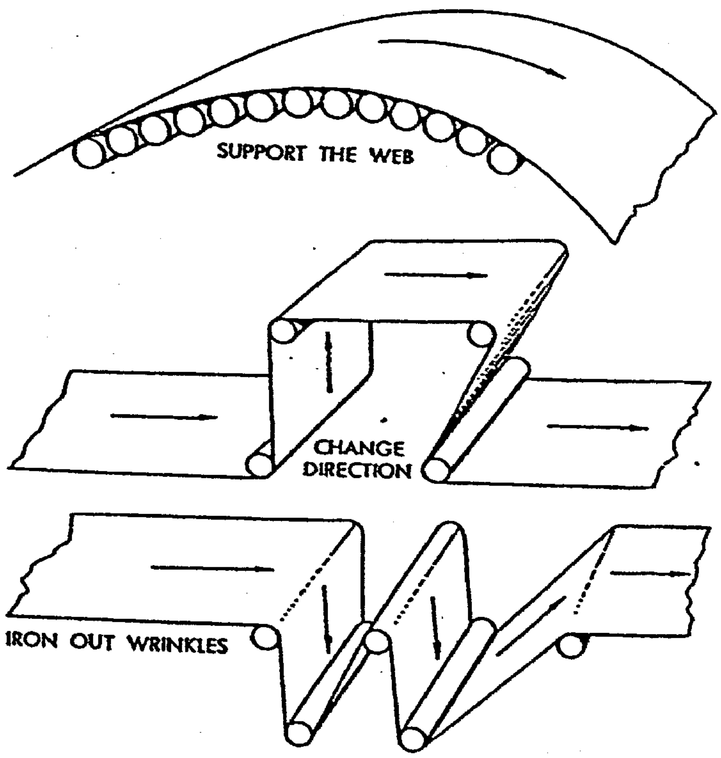

Figure 5.19. **Idler rolls**

The three basic functions of an idler roll are to:

1. Support the web of the material.
2. Change the direction in which the web travels.
3. Prevent / reduce ripples via a levelling action.

Spreader Rolls:
Spreader rolls are specialised idler rolls that, when appropriate tensions are used, are very effective in 'ironing out' incoming feed ripples by reducing the span length and limiting the amount of free travel. The principal variants are the Herringbone or Chevron roll, and the Curved roll.

Herringbone Rolls are generally positioned in regions of aggressive ripple formation such as immediately after an unwind coil, Figure 5.20. The roll surface is a corrugated 'V' pattern of wide, shallow square grooves with rounded corners, spreading the web toward the edge of the roll

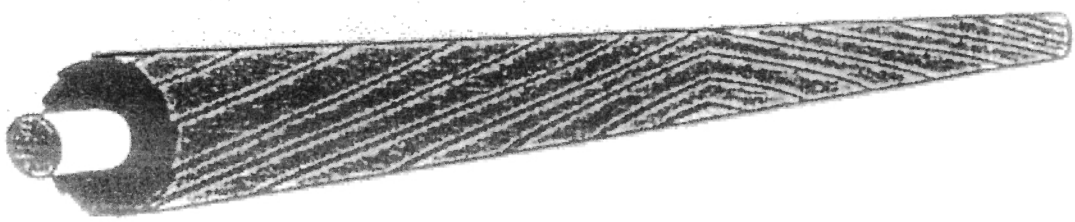

Figure 5.20. **Herringbone roll**

A Curved or 'Bow-shaped' roll is designed to increase the available surface contact area, resulting in a taut web across the strip. The roll should be positioned near or at a ripple formation point, with the bow apex angled slightly into the web in the direction of the metal flow. The two types of roll are the fixed bow and adjustable bow, Figure 5.21.

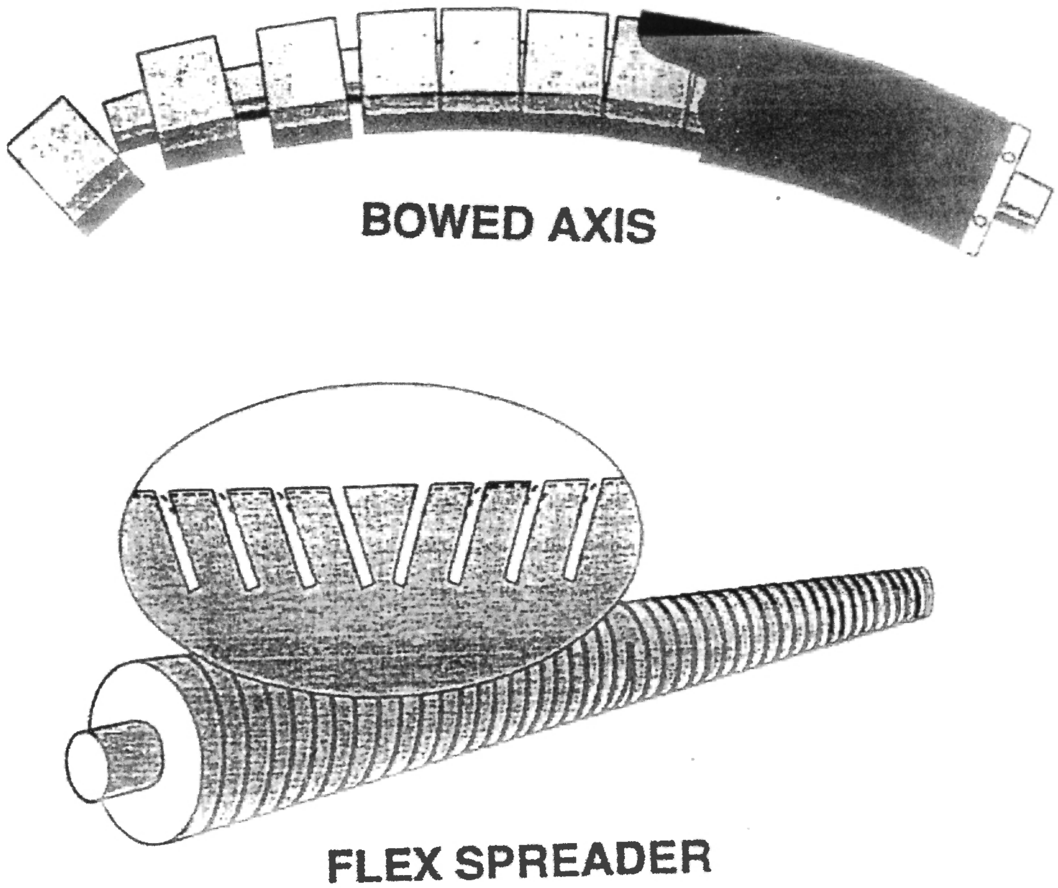

Figure 5.21. **Curved roll**

Ironing Roll Camber – Crown:

During finishing operations, creasing can occur during the rewind separation phase of the light-gauge foil process. Decreasing separating speed will reduce creasing however reduced throughput capacity of the slitter will be unacceptable. Work on the ironing roll camber has shown that a slightly negative/positive camber reduces the occurrence of creasing without decreasing separating speed. Crowned rolls will behave like curved rolled but with a lower magnitude.

BENCHMARKING AND OPTIMISATION

The following information relates to an examination and characterisation of web failures as well as specific analysis of problems encountered over the life of the project.

- Chapter 6.1 provides a broad description of defects that occurred intermittently over the past years. A short definition is provided followed by remedies to reduce or avoid re-occurrences as determined during the thesis.

- Chapter 6.2 documents specific issues that arose during the course of the project, and are examined in more detail. The effect of boundary lubrication on web failure for foils is summarized by the Mansell curve.

- Chapter 7 provides an assessment of mill productivity focusing on steady-state mill velocity. Optimal settings based on current rolling practices are recommended for unwind tension/stress, lubricant viscosity, load and rewind tension/stress to achieve the desired mill speed. The factors were chosen based on ease of adjustment and monitoring over a short time period and are known not to significantly influence the slitting and annealing characteristics.

CHAPTER 6 WEB FAILURE

One of the fundamental aspects of thin-foil foil rolling is the control and prevention of web failures during processing, in particular during the final-single pass and pack/doubling-pass. High web failures or break-rates, affect the mill asset utilisation with regards to steady-state running of the mill as well as the operating personnel psyche.

Before any work on alloy development or down-gauging is to commence, a thorough understanding of web failure mechanisms and the subsequent reaction is instigated and appropriate changes to process operations implemented. There is a common unfounded perception that increased rolling velocity results in increased web failure.

This chapter is included to incorporate a good understanding of the many web failure issues that occur during the production of thin foil product. A high incidence of web failures reduces the drive for increased line speed or equipment utilisation as increased rolling speeds are thought to contribute to increased web failure (discussed in Chapter 7). Without low web failure rates and high production rates, further work on alloy development focusing on surface studies and improved mechanical properties is futile (Chapters 8 - 10) as poor mill throughput offsets any financial gain.

Due to the high number of pictorials, the following pages dedicated to miscellaneous web failures have been divided into two columns, with descriptive information on the left and accompanying photos on the right.

6.1. Miscellaneous Web Failures

In the production of light gauge foil, web failures on both the single and back passes are key factors that can reduce mill throughput to unacceptable levels. There is a reason for every break on a mill and the ensuing paragraphs categorise some of the defects experienced during rolling, and list causes. This does not extend to include web failures due to machine related issues such as loss of tension or gauge spikes.

The defects are categorised using the following criteria:

- Casting Defects – occurring during casting of the billet / ingot
- Rolling Defects – occur during wrought fabrication
- Handling and Storage Damage – occurs between processing stages or at the end of the process

6.1.1. Casting Defects[176]

Casting defects are generally a result of either inferior casting practices or inadequate control over casting variables. Inclusions are non-metallic particles that are unintentionally included during casting, or are pressed into the alloy during deformation. The presence of inclusions in aluminium alloy products can result in a wide variety of problems for customers. The brittle particles can lead to pinholes in foil, breakage during wire drawing, tear-offs during can manufacture, ultrasonic indications in thick plate, or surface defects in sheet or extruded products.

Much of the extraneous particulate matter in aluminium alloys originates from grain refiner additions. Hence grain refining is not recommended for light gauge alloys; however despite this they are used in many Asian countries in thin-film foil alloys. Particles of Al_2O_3 tend to be comparatively small and well distributed, originating from more than one source such as casting refractories and pickup. They are difficult to eliminate using conventional metal filtration methods as discussed in Chapter 2.3.2.2.

Grain refiner problems:

Grain refiners are used to assist in the solidification of molten metal during casting, particularly for wrought applications. They can also be used to promote recrystallisation during the annealing process of a finished product. The most common grain refining elements are titanium and titanium-boride.

Extensive work by Gray and Fricke[177] found that TiB_2 is the most frequent refiner inclusion and was often associated with $TiAl_3$. For this reason, grain refiner additions have been removed from foil block rolled at Yennora.

Grain refiner particles (TiB_2) are capable of agglomerating, often appearing as a dark string of hard particles in wrought alloys within a cross-section of sheet material (a). There is little doubt that grain refiners can be dirty as tramp elements and colour coding paint used to code the grain refiner addition have been in the vicinity of defects.

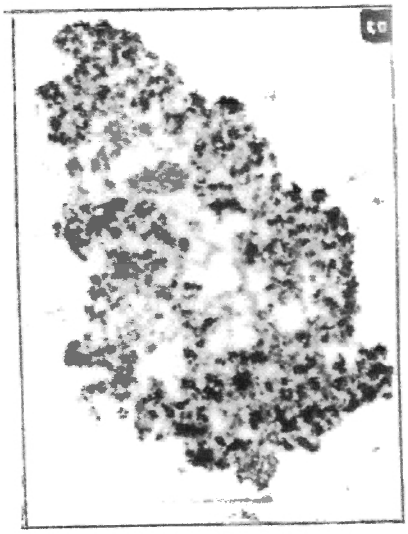

(a)

Aluminium oxide:

Aluminium oxides are a multiphase system, commonly used in casting-areas as a refractory or abrasive, and are usually found as particulate inclusions (b). Surface oxidation at the surface of liquid aluminium (and to a lesser extend solid aluminium) can give rise to a less frequent chemical form of Al_2O_3.

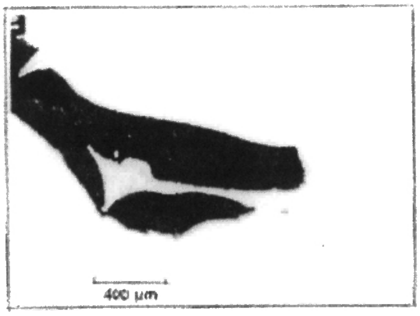

(b)

Unless sufficient scalp depth is obtained, the oxide can be rolled into the surface of wrought products resulting in a film-like or flake-like form within the metal (c). They can also result from downstream roll pick-up.

(c)

Aluminium oxide particles are often associated with stringers, the most common being TiB_2 from grain refiner additions (d). There are two ways for the two materials to be found together.

In one case, oxide particles are apparently present in the grain refiner and its incomplete dispersion leaves oxides and titanium-bearing particles in one area. In the second form of association, dross films floating in liquid aluminium tend to sweep up undissolved titanium particles and depositing them on very thin Al_2O_3 films. Supporting this hypothesis is the fact that normal intermetallics can sometimes be found on the films.

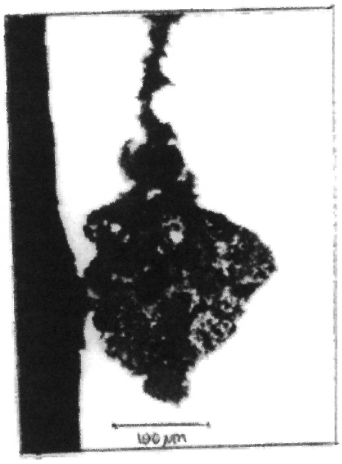

(d)

Aluminium intermetallics:

Abnormally large constituent particles, although not strictly inclusion-type defects as they contain normal alloying elements, are not wanted because of their size (e).
The abnormal constituents are usually iron-bearing and may be found when casting temperatures have fallen too low and large crystals nucleate in the melt.

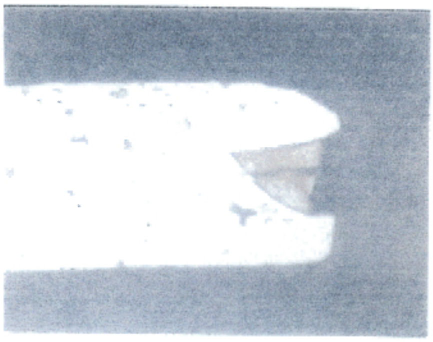

(e)

Al-Si-O:

Al-Si-O_2 particles from refractory blankets used by some ingot plants may occasionally be observed as inclusions. The particles are distinctive in their spherical appearance but may often by fractured be rolling or forming operations.

These particles may sometimes be reported as spinels since SiO_2 may react during thermal treatments with magnesium in the alloy.

6.1.2. Rolling Defects

Holes/Voids:

Holes are voids in rolled product greater than 0.2mm as per European Standard EN 546-4 for foil. The causes include metallic and non-metallic inclusions, hard particles in the rolling lubricant or from the environment, and rolled-in and rolled-over scratches from prior rolling passes (f). To reduce the risk, metal and rolling oil cleanliness is critical, as well as avoiding heavy scratches and marks.

(f)

Herringbone:

Herringbone is a result of localized lubrication breakdown at the mill bite giving rise to a repeated pattern of chevrons or 'herringbone', predominately at the edge of the coil (g). It can occur during all cold and foil rolling stages of processing. It is dependant on a number of factors including coolant viscosity, coolant composition, surface finish and shape of the incoming metal, load and roll grind.

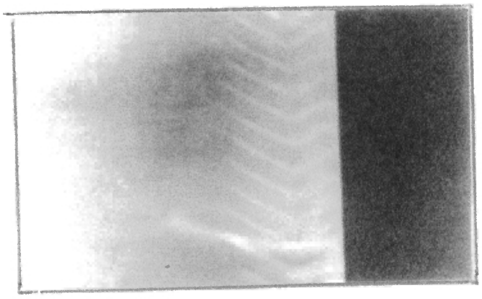

(g)

Edge cracks:

Edge cracks are fractures along the edge of the aluminium strip, sometimes only fractions of a millimetre long (h). They are generally a result of poor slit edge quality from upstream processing, but are accentuated by tight edges.

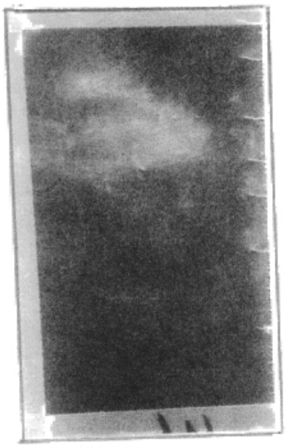

(h)

Chatter Marks:

Chatter marks are regular corrugations perpendicular to the rolling direction and are usually accompanied by a loud high-pitched resonance called roll chatter. It generally occurs during acceleration or deceleration of mill speed for short period of time, and can result in strip-breaks as gauge decreases (i).

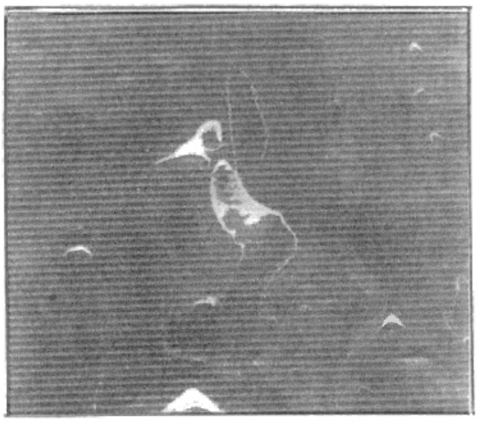

(i)

There are several causes including mechanical vibration of the rolls, lubrication breakdown at the roll bite, and incorrect rolling parameters (load tension, speed).

Slivers:

Slivers are slender fragments of 'blistered' aluminium that are partially removed from the strip due to poor cast quality, or improper rolling practices (j). They generally occur during hot rolling, and can be attributed to insufficient lubrication during rolling, localized mechanical damage to the work rolls or the block, coarse scalping and even friction scratches.

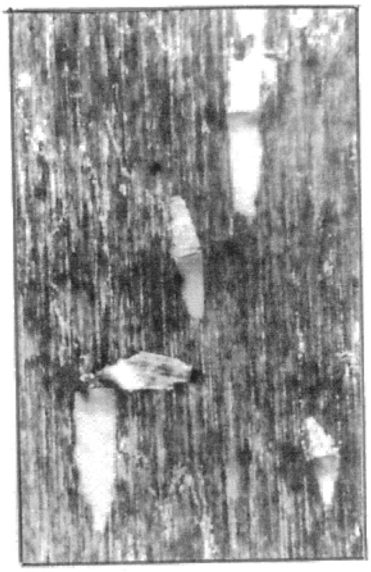

(j)

Rolled in Dirt:

Rolled in dirt results from contaminates such as oil, grease and dirt from the factory environment being embedded in the aluminium surface during the rolling process. It appears as dark speckles or streaks on the aluminium surface and can occur during hot, cold and foil rolling (k).

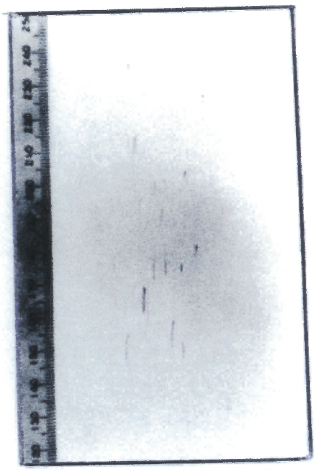

(k)

Rolled-in-metal:

Appears as an extraneous piece of metal embedded in the rolled product surface, usually elongated in the rolling direction (l). As the number of reduction passes increase, the defect can result in laminations. Sources of rolled-in-metal include detached slivers, edge trim, thermocouple and scratch brush wires.

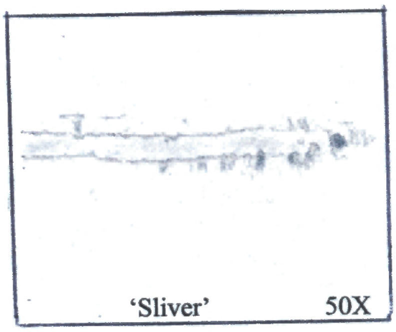

(l)

Splits:

Splits are longitudinal wrinkles that collapse at the entry bite and are rolled in (m). A split or crease can be as short as 300mm or extend for many meters prior to breaking. They are generally located near the centre, but can wander from side to side. The exact cause of splits is not fully established, however it is related to incoming shape (profile) from upstream processing, uneven coolant application or incorrect unwind tension.

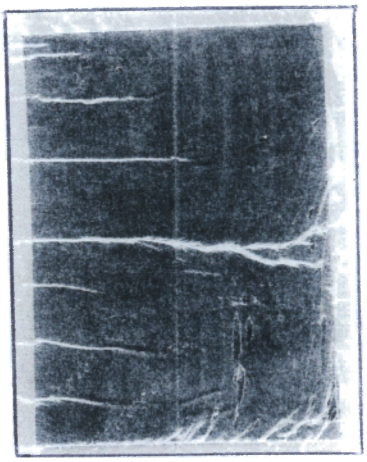

(m)

Tension cuts:

Tension cuts are angular splits in the metal, starting toward the centre and finishing near the edge (n). The cause is related to excessive heat generation coupled with bad incoming shape resulting in a crease that folds over and splits. This defect can be reduced by an increase in unwind tension

(n)

Line of holes:

A line of holes is an indication of a scratch on the aluminium surface during the processing of a coil (o). The scratches are mechanical in nature, vary in length from a few millimetres to several metres and occur while the metal is being processed under tension.

Holes are an indicator of a minor upstream failure such as a seized roll or mechanical contact. The only way to prevent these types of defect is through regular maintenance checks and good housekeeping.

Scratches can also be a result of inadequate coolant filtration; however these defects tend to occur in more than one position.

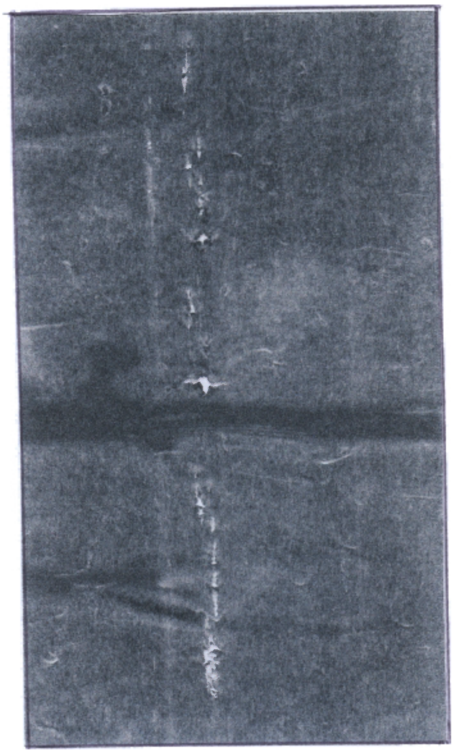

(o)

Broken Matte:

Broken matte is an appearance of bright speckles dispersed throughout the dull textured surface (p). During pack rolling, where two adjacent metal web layers are passed through a set of rolls under load, a fluid boundary or matte between the strips is required to prevent the two metal surfaces touching and welding together.

(p)

If the matte fluid application is insufficient, on separation the weld is 'broken' resulting in a shiny surface. The cause is related to the friction between the foil strips. Factors that induce broken matte include inadequate and uneven lubrication; low roughness on previous pass; different thickness between both foil strips; different roughness, diameter in both work rolls and different coiling/decoiling tensions.

Streaky Matte:

Streaky matte results from minute differences in matte surface topography as a result of insufficient matte fluid during doubling, or flatness problems in a localized region of the strip resulting in a long shiny streak on the matte side of the strip (q). This is controlled by ensuring adequate lubrication between the strips.

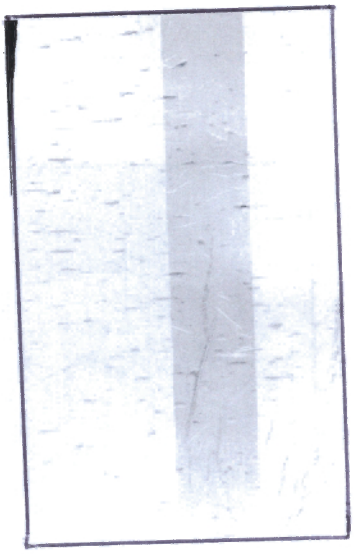

(q)

Roll holes:

A roll hole is a repeated hole with a specific pitch that occurs in the same position across the strip (r). The pitch length will indicate which mill roll is the source of the defect. The source of the hole is either a damaged work roll due to a foreign body passing between the rolls while under pressure or a marking on the bridle or ironing rolls.

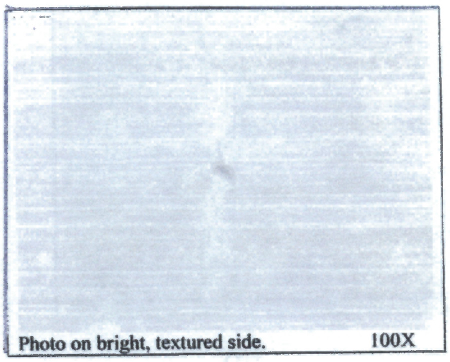
Photo on bright, textured side. 100X

(r)

Grain Streaking:

Non-uniform surface appearance parallel to roll direction on matte-side, and on the bright-side if severe (s). They are caused by coarse elongated grains formed during the casting process, but can be eliminated by adequate reductions and fine, uniform grain size after last thermal.

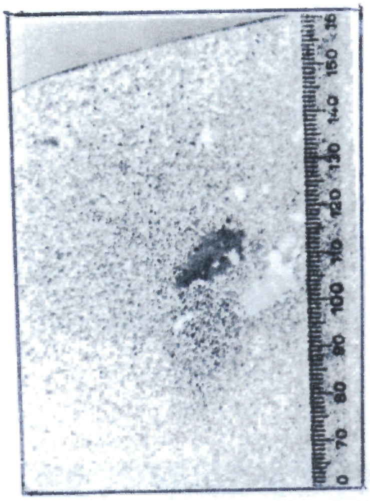

(s)

Laminations:

Laminations are believed to develop during hot rolling and are related to deformation through the roll bite (t). Small cracks at the surface parallel to the rolling direction break-up during foil rolling, taking on an appearance similar to that of a succession of tightly packed edge cracks.

(t)

Dross:

Dross is a casting chlorine based impurity that is processed down to foil gauge. The defect appearance is similar to a sliver, however is usually associated with a ring of deformed metal surrounding it (u).

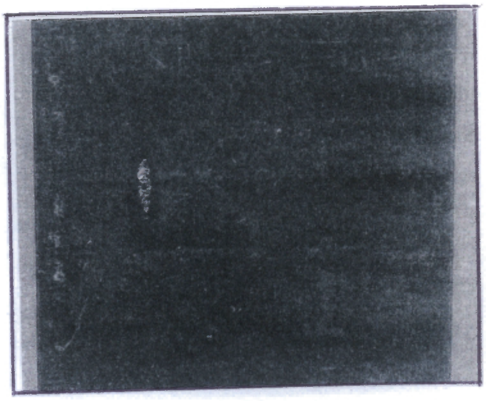

(u)

Mill lines:

Mill lines are straight lines parallel to the rolling direction. They are generally a result of going from narrow to wide product after an extended campaign without doing a roll change (v). While these lines will not cause a strip break at low gauge, they are visually undesirable.

(v)

Waterstain:

Water stain is surface oxidation that results from strip contact with water, and is promoted by elevated temperatures and pressures. Local oxidation occurs resulting in a hard, brittle region surrounding the aluminium matrix (w).

The most common source for water stain is compressed air associated with shape control and coolant carry-over. Another source is water ingress from rain is drawn into the coil via capillary action at the edges. To rectify, store the coil away from doors, have a compressed air dew point of less than 5°C, install water filters as close to the end use as practically possible.

(w)

6.1.3. Handling or Storage Defects

Telescoping:

Telescoping appears when a set of successive wraps or coil windings slip laterally, usually in the inner portion of the coil (y). Telescope can occur from low coil tension, wedge metal profile, unbalanced workrolls or a cold-mill start-up, and is prompted by excessive oil carry-over or incorrect rewind start.

(y)

Handling Scratches:

Handling scratches are random scratches on the aluminium that can vary in size, form and direction. They are generally caused by abrasive contact during transportation or when struck by a moving object.

Short, longitudinal scratches parallel to the rolling direction are often termed friction scratches (z). They are generally a result of relative movement between adjacent wraps, and if rolled over can result in slivers.

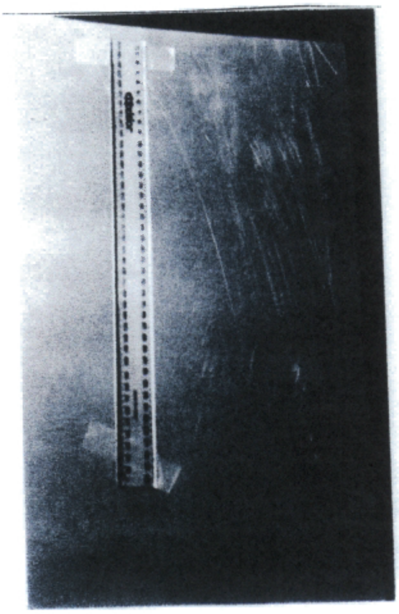

(z)

A gouge is a gross form of a scratch, and usually requires a large amount of force to occur.

Stepouts:

Stepouts, like telescoping, are a result of successive wraps slipping laterally relative to the body of the coil (aa). Stepouts are sharp, distinct slippages, as opposed to smooth gradual lateral wrap oscillations.

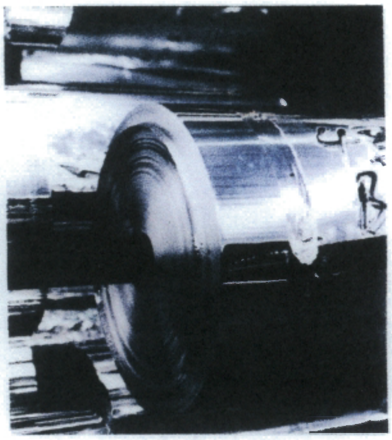

(aa)

Bridging:

Bridged coils can be identified by an easily identifiable ^ - shaped defect or groove at the coil wall. Bridging can result from either coil miss-handling such as a dropped coil (ab) or incorrect rolling tensions.

An increase in localized recoil tension occurs during processing. This can be due to ironing roll vibrations, non-concentric, non-parallel cores or bad incoming shape. As coil build-up and rewind speed increase, bridging is more likely to occur.

(ab)

6.2. Other Influences on Web Failure

6.2.1. Effects of Boundary Lubrication on Web Failure

Tribology (rolling lubrication in this context) and its influence on thin foil rolling is not well understood. Product quality and flat rolling efficiency are known to be considerably influenced by the friction in the deformation zone. A description of the fundamental concepts behind the application of rolling lubricants is given in Chapter 4. When industrial applications where lubricants are used, the friction conditions are a combination of hydrodynamic and boundary friction i.e. a mixed lubrication regime. As rolling speeds increase, additional lubricant is transported into the deformation zone shifting the friction condition towards hydraulic lubrication, reducing the total friction force.

Three independent mechanisms are responsible for entrainment of lubricant into the roll gap[178]:

1. Contact between the lubricant and the metal surface boundary layers drags the lubricant into the deformation zone. This includes both physical adsorption and adhesion of chemical reaction products.
2. Lubricant is carried into the deformation zone in the asperity valleys of the surfaces.
3. A speed dependence of the lubricant entrainment due to the hydrodynamic effects in the inlet zone. If the supply of lubricant is sufficient to induce a hydrodynamical pressure build-up, the strip will deform plastically drawing the extra lubricant into the deformation zone. The equilibrium of fluid flow into the inlet zone can be expressed in a simplified manner by the Reynolds differential equation:

$$\boxed{h_{S0} = \frac{3\eta}{\alpha} \times \frac{V_0 + V_u}{1.15k_{f0} - \sigma_0}} \qquad (6.1)$$

where h_{S0} is the entrained film thickness, η the dynamic viscosity, α the opening angle of the inlet wedge, V_0 the incoming velocity, V_u the circumferential velocity of the rolls, k_{f0} the yield stress of the web, and σ_0 the back tension.

Work by Oskar, Rasp and Draese[178] found that changes in friction could be demonstrated with the rolling parameters, thickness reduction and forward slip as well as with the surfaces of rolled sheets. They found that the influence of roll speed and oil viscosity on friction behaviour is largely significant for annealed product, and much smaller for strain hardened material at lower velocity. Little has been documented on these phenomena, with no graphical representation of the effect of film thickness to film strength for thin foil foils. A graphical representation will aid in determining rolling lubrication temperatures and compositions to optimise rolling velocities without compromising surface quality.

As roll speeds increase, thickness reductions become almost independent of speed, particularly for low viscosity lubricants. However sample thickness was independent of roll speed when no lubricant is used. The forward slip of strain hardened material strongly decreases with roll speed if high viscous oils are used, whereas for softer material the forward slip is generally between 0-4%.

The thickness reduction and the forward slip clearly show how the friction condition in the roll gap improves when roll speed or lubricant viscosity is increased. The increasing reduction at constant roll force as well as the reduction in forward slip, demonstrates the rising hydro-dynamical part of friction in the mixed lubrication regime.

6.2.1.1. Experimental

There are many factors that can affect rolling lubricant viscosity, and some of these are listed in Appendix 4, but this is by no means exhaustive[179]. Of these, rolling lubrication temperature was a parameter that can be easily measured and controlled. Over a period of approximately five weeks, the rolling temperature was varied between target parameters of 35°C and 60°C. It was found very quickly that temperatures above 42°C promoted herringbone, a common known defect discussed in Chapter 6.1.2.

At temperatures below 42°C, the surface appears shiny with no visible fissures on the surface of the foil and herringbone is minimal, Figure 6.1. However at rolling lubrications temperatures below 38°C, a series of transverse fissures parallel to the rolling direction appeared on 6.5μm micron foil ultimately leading to web failure, Figure 6.2. The nature of the transverse fissures resulted in the defect being referred to as "ladders".

Accompanying the fissure was a visually noticeable decrease in overall metal brightness. Several attempts were made to quantify this using a reflectometer but were unsuccessful. Closer examination of the web surface in the vicinity of the defect showed similar surface fissures in the area bordering the cracks, albeit on a smaller scale, Figure 6.3. Note that the fissures immediately adjacent to the cracks effectively disappear. This is believed to be due to the reduced web stress in the vicinity of the formed crack.

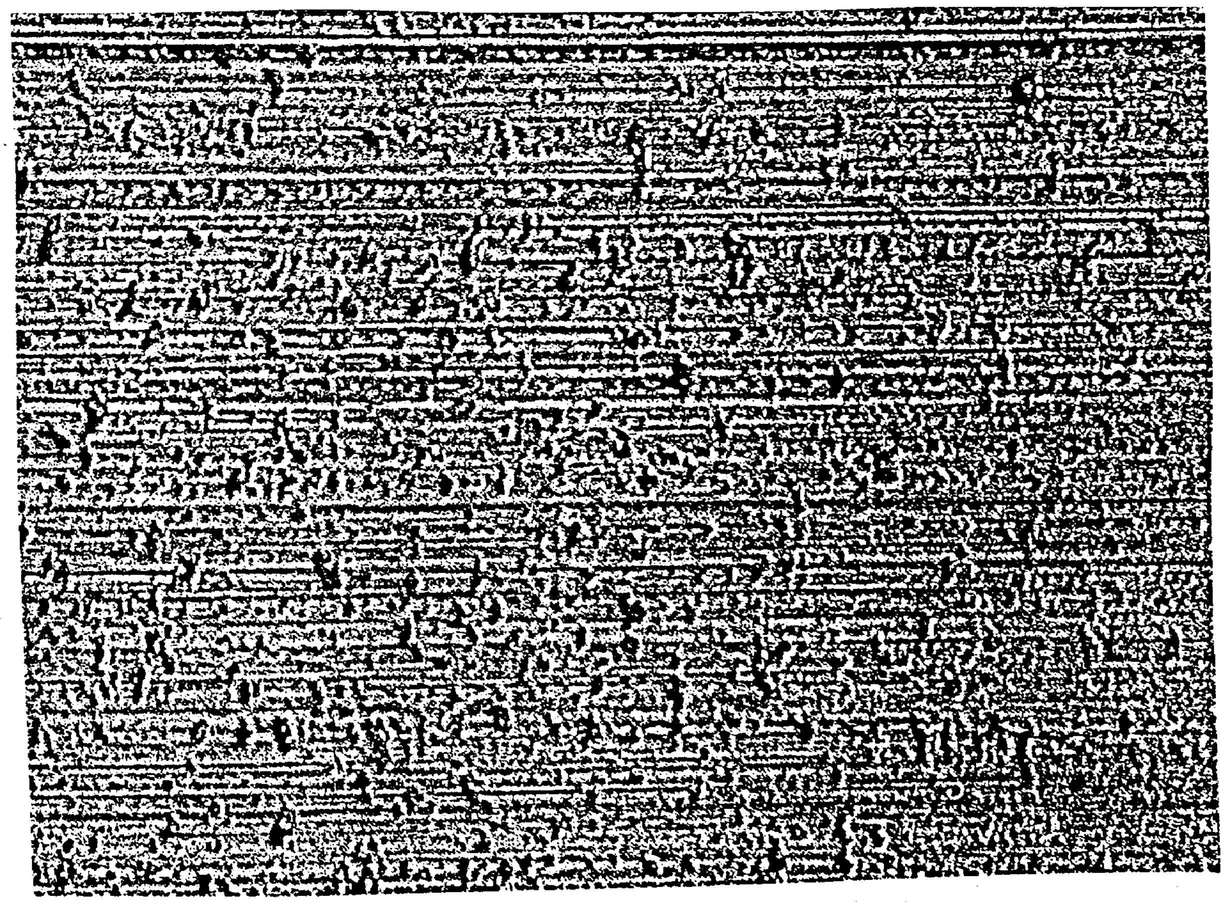

Figure 6.1. 'Normal' foil surface (x75)

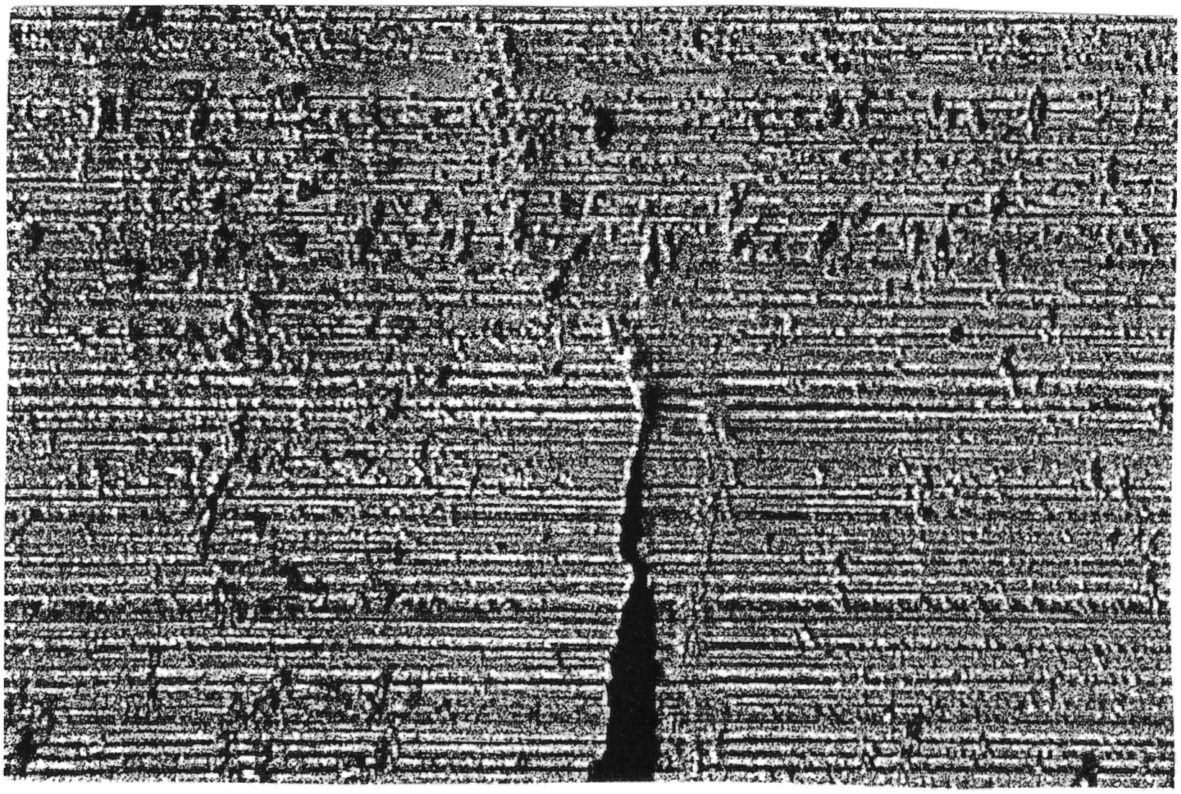

Figure 6.2. **Ladder defect (x75)**

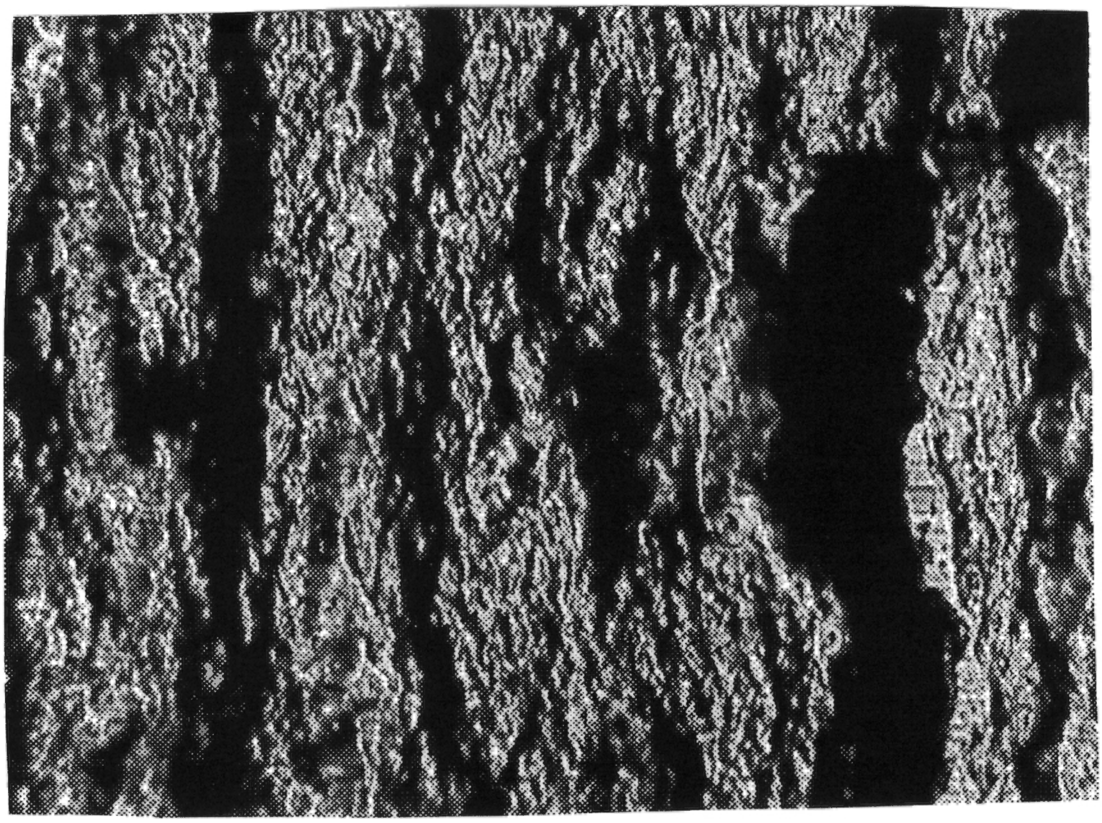

Figure 6.3. **Ladder defect (x200)**

6.2.1.2. Discussion - Development of the Mansell Curve

Oskar, Rasp and Draese discussed the influence of roll speed and oil viscosity on the surface gloss and structure of rolled sheets. They found that by increasing speed and viscosity elongated lubricant pockets transverse to the rolling direction formed on the surface, Figures 6.4 and 6.5.

With faster rolling speeds, higher oil viscosities and softer materials, the hydrodynamic effect is stronger resulting in larger, more numerous lubricant pockets. The hydrodynamic pockets resulted in more holes at penetration depths greater than the final sheet thickness. Increasing the amount of lubricant in the work zone means that large parts of the web are no longer deformed through direct contact with the roll surface but in free deformation through a pressure cushion built by the oil film.

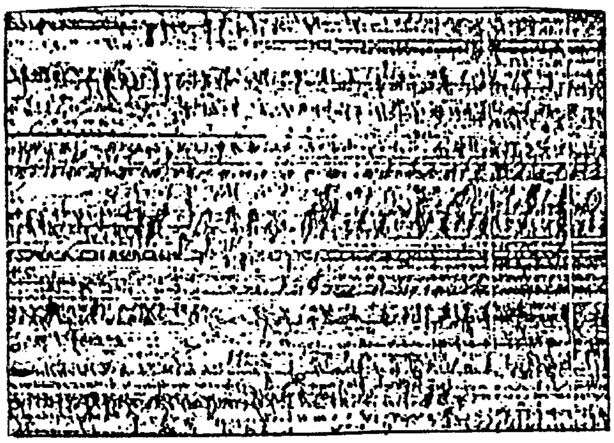

→ rolling direction $v = 10$ m/min $h_1 = 0.234$ mm

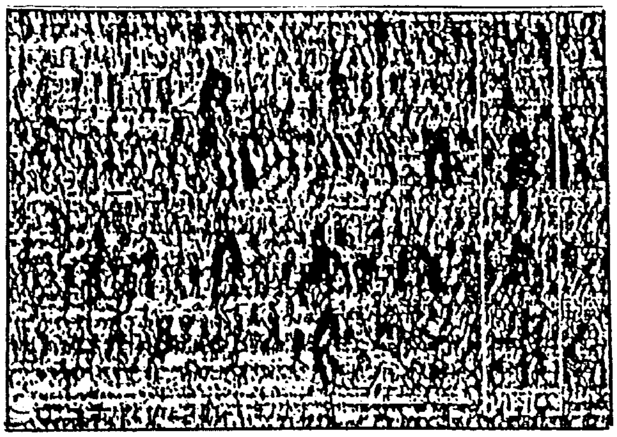

→ rolling direction $v = 200$ m/min $h_1 = 0.184$ mm

Figure 6.4. Surface specimens at different rolling speeds

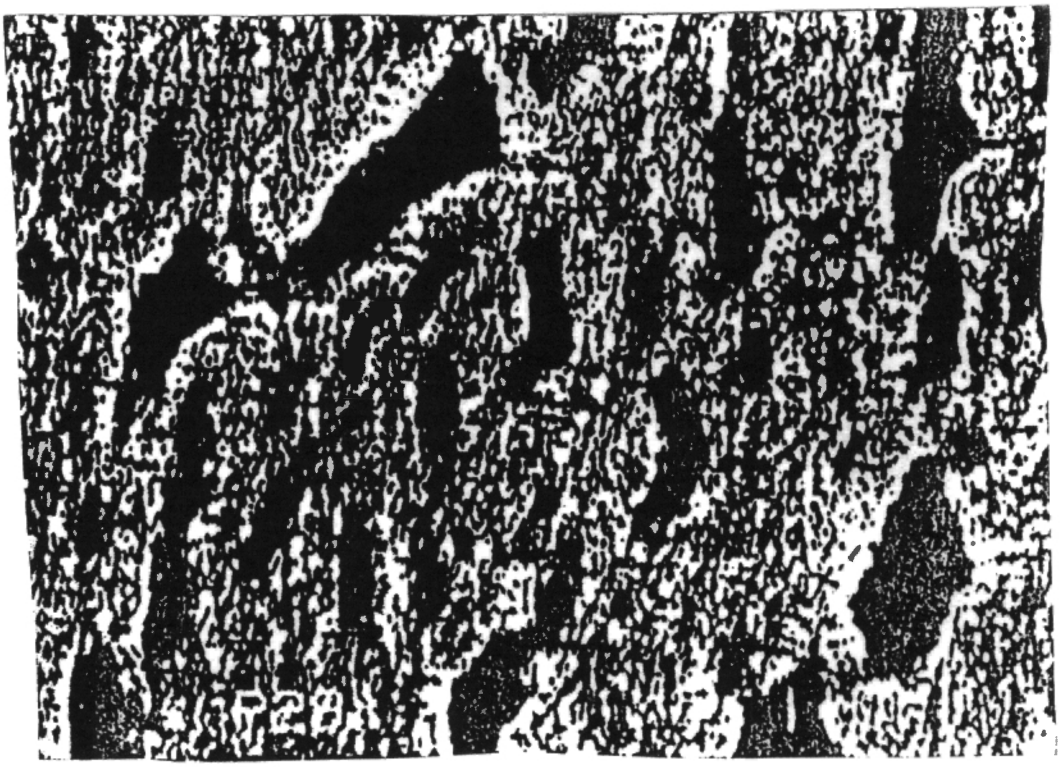

Figure 6.5. **Specimen surface with penetrating lubricant pockets (200x)**

Higher rolling lubrication temperatures promote less viscous rolling oil, allowing a brief dialogue on herringbone mechanisms relating to roll bite lubrication to be discussed. Decreasing the film thickness due to less viscous rolling lubricants can lead to "Herringbone", Figure 6.6, where lubrication breaks down at the mill bite resulting in metal-to-roll contact.

The lubrication breakdown can either be a result of insufficient film strength or film thickness. Traditionally, modifications to the additive level have been used to control film strength and hence the incidence of herringbone. However this can have negative effects on coil unwind-ability post annealing.

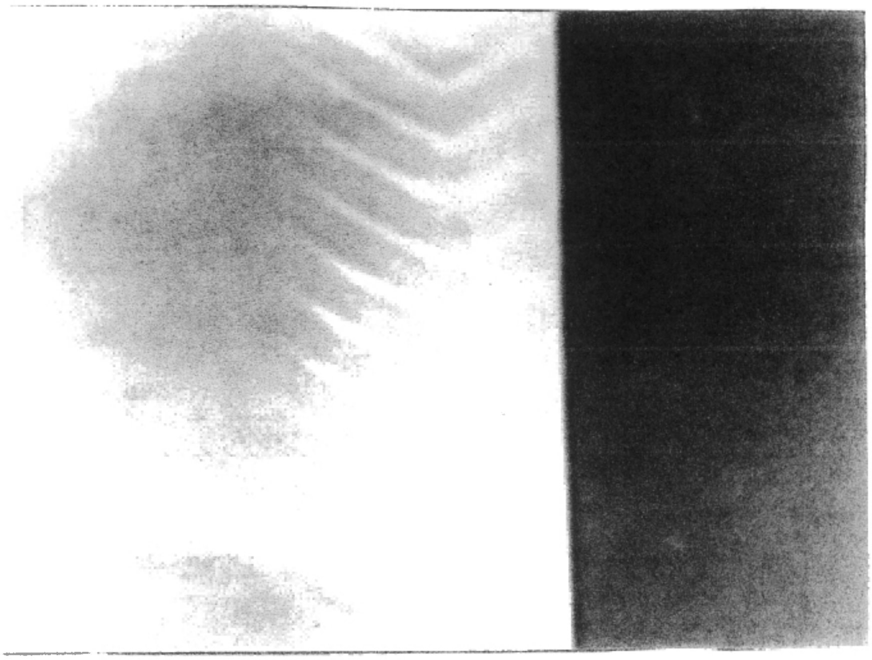

Figure 6.6. **Herringbone Defect**

As film strength and thickness increases, herringbone is less likely to occur. At a critical point at which lubrication pocket pressure exceeds the burst strength of the metal, the web fractures result in "ladder" defect. Film strength is believed to have a more linear effect on ladder as is it proportional to the additive concentration.

One way of representing the relationship between 'ladder' and herringbone formation using film strength and film thickness is proposed for light gauge foil, Figure 6.7. Fissure penetration and density are reduced by decreasing the lubricant viscosity. This involves increasing the re-circulation lubricant temperature by reducing the number of nucleation sites for web failure. This has the added benefit of increasing rolling speed but can result in visual surface defects.

Other ways to manipulate the film strength and viscosity include controlled dosages of additives such as acid and alcohol, as well as increasing the viscosity of the base oil as discussed in Chapter 4; For example, a C-10 acid addition in place of a C-12 acid should create favourable conditions as C10 acid is less viscous. Other approaches include decreasing rolling speeds, increasing metal hardness, and examining roll finish.

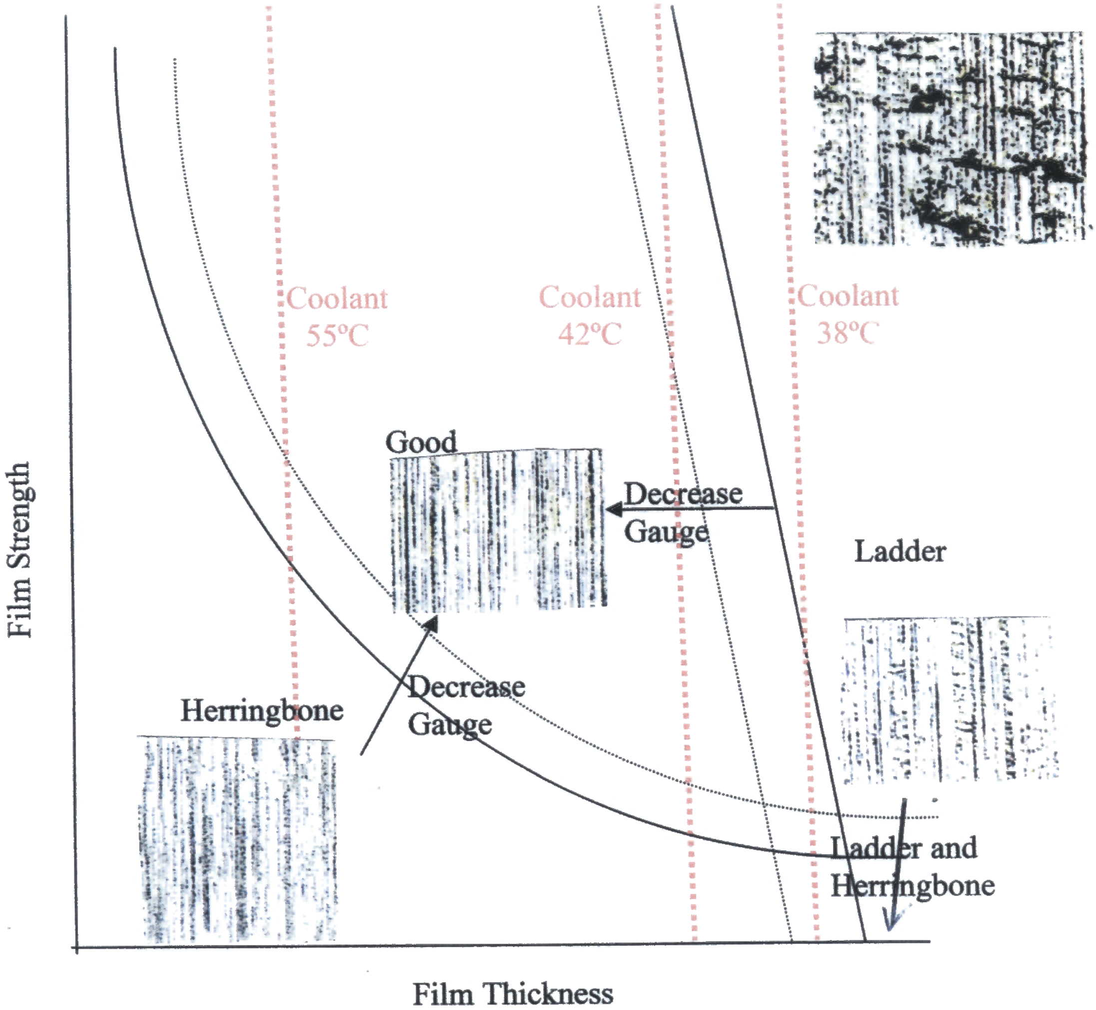

Figure 6.7. **Mansell curve – film thickness versus film strength for 6.5µm 1145 foil.**

Increasing the coolant temperature from 38°C to 42°C resolved the ladder defect but some mild herringbone became evident (as frayed course dull parallel lines on the macrograph). The film strength was increased using alcohol additions, eliminating the herringbone marks. The coolant temperature was further increased to maximise rolling speeds, and a good compromised between rolling speed and excessive fume generation was reached at 55°C.

6.2.1.3. Conclusion

Figure 6.7 is used to explain the ladder defect and its relation between film thickness and film strength. Increased coolant temperature coupled with increased alcohol additions resulted in adequate control of surface defects resulting from coolant viscosity and strength. This was achieved while increasing rolling speed.

6.2.2. Effects of Entrained Polymers on Web Failure

The effect of rolled-in foreign metals and/or oxides (including sand) has been well examined and documented, including Chapters 6.1.1 – 6.1.2. However the effect of polymer deposits down-stream from polymer rolls such as spacers and hold-down rolls is not well understood. As polymer inclusions are expected to occur during cold rolling or offline slitting from polymer rolls or spacers.

6.2.2.1. Experimental Procedure

Several coils were processed with random, sparse unidentified fine polymer particles rolled into the metal. The high aspect ratio indicated that the defect occurred at or below 0.48mm gauge during the slitting process during the production of 6.5 micron final gauge foil.

Aluminium samples with marks were taken throughout the process and examined under light microscopy (40x). These included samples taken at:

- 480μm from the arm slitter
- 220μm final cold rolling gauge incoming to foil
- 120μm after one pass on our mill
- 6.5μm after final rolling

The surface of the stained aluminium sheets were washed with boiling toluene. The solvent was concentrated and evaporated on salt plates to recover a tiny amount of oily residue. This residue was analysed using Fourier Transform Infrared Spectroscopy (FTIR). The abraded surface of the aluminium was analysed using a Scanning Electron Microscope (SEM) equipped with EDAX to determine the inorganic elements present on the surface.

6.2.2.2. Results of the Investigation

In the final gauge product, the defect appeared as a long stain/mark between the doubled layers. The length varied from a few millimetres to a couple of metres, occurring in several positions across the strip (usually in 50 or 100mm increments) at random intervals throughout the coil.

The centre of the stains appeared as abrasion marks along the length of the foil, with the outer edges of the abraded areas discoloured but not abraded. A close up of the surface reveals parallel marks, indentations and tears associated with the defect, refer to Figure 6.8.

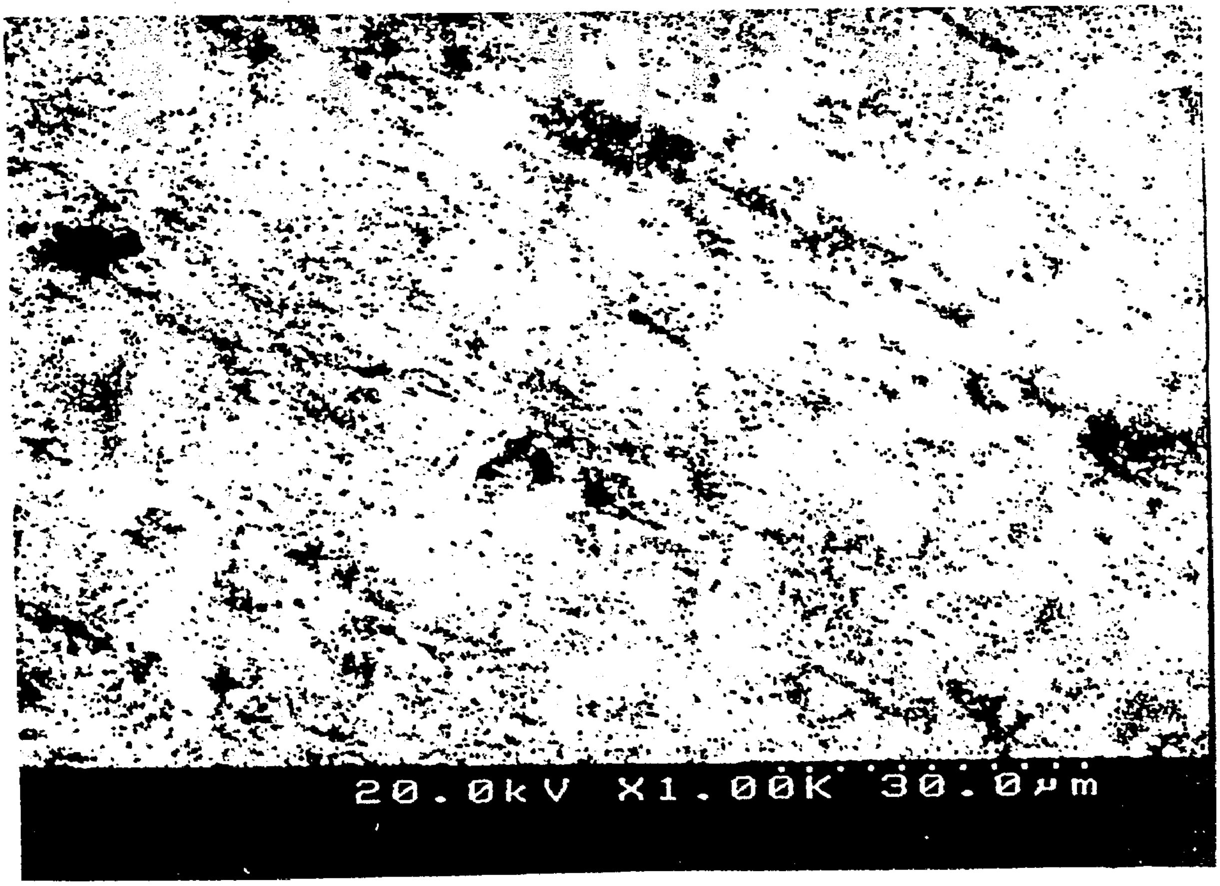

Figure 6.8. Macrophoto of defect

The result of the FTIR analysis of the black mark taken at 6.5 micron and 220 micron gauges is given in Figure 6.9. Note that the black mark occurred at other gauges in-between and varied in width, length and intensity. Due to the lower concentration of residue taken from the 6.5 micron sample, the peaks are less intense:

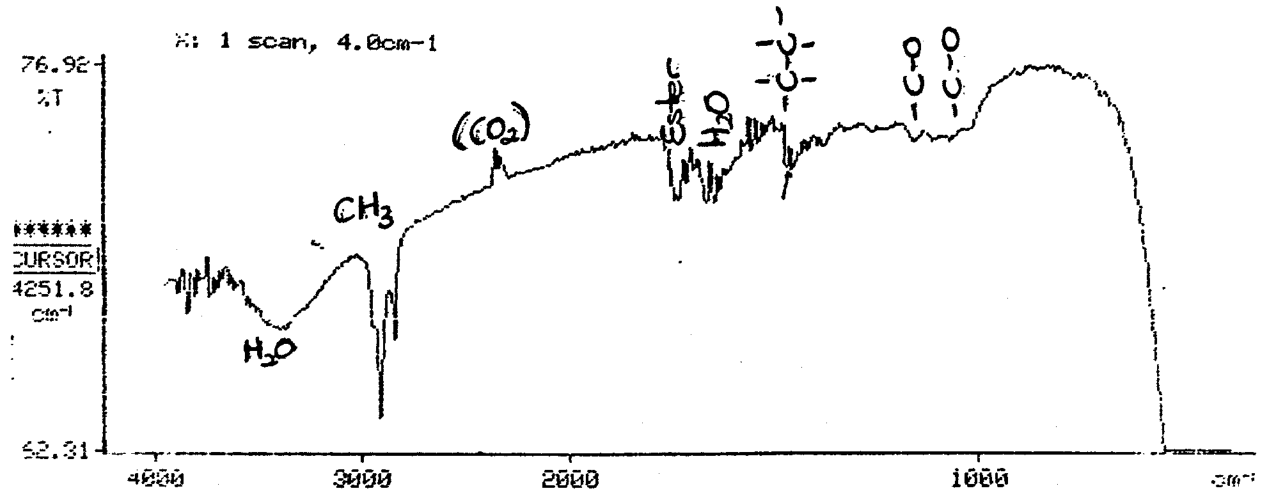

(a)

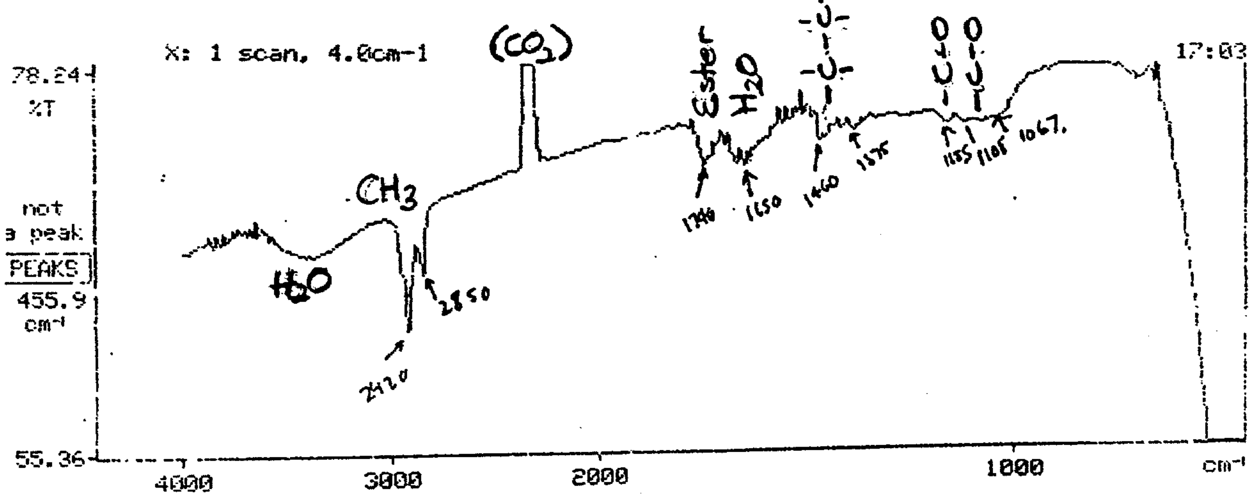

(b)

Figure 6.9. **FTIR finger print for black stain for samples (a) 6.5 micron and (b) 220 micron**

An examination of the graph indicated the presence of an ester type substance on the surface. EDAX analysis of the inorganic particles (which are fluorescing), yielded the presence of calcium, silicon and titanium compounds, Figure 6.10:

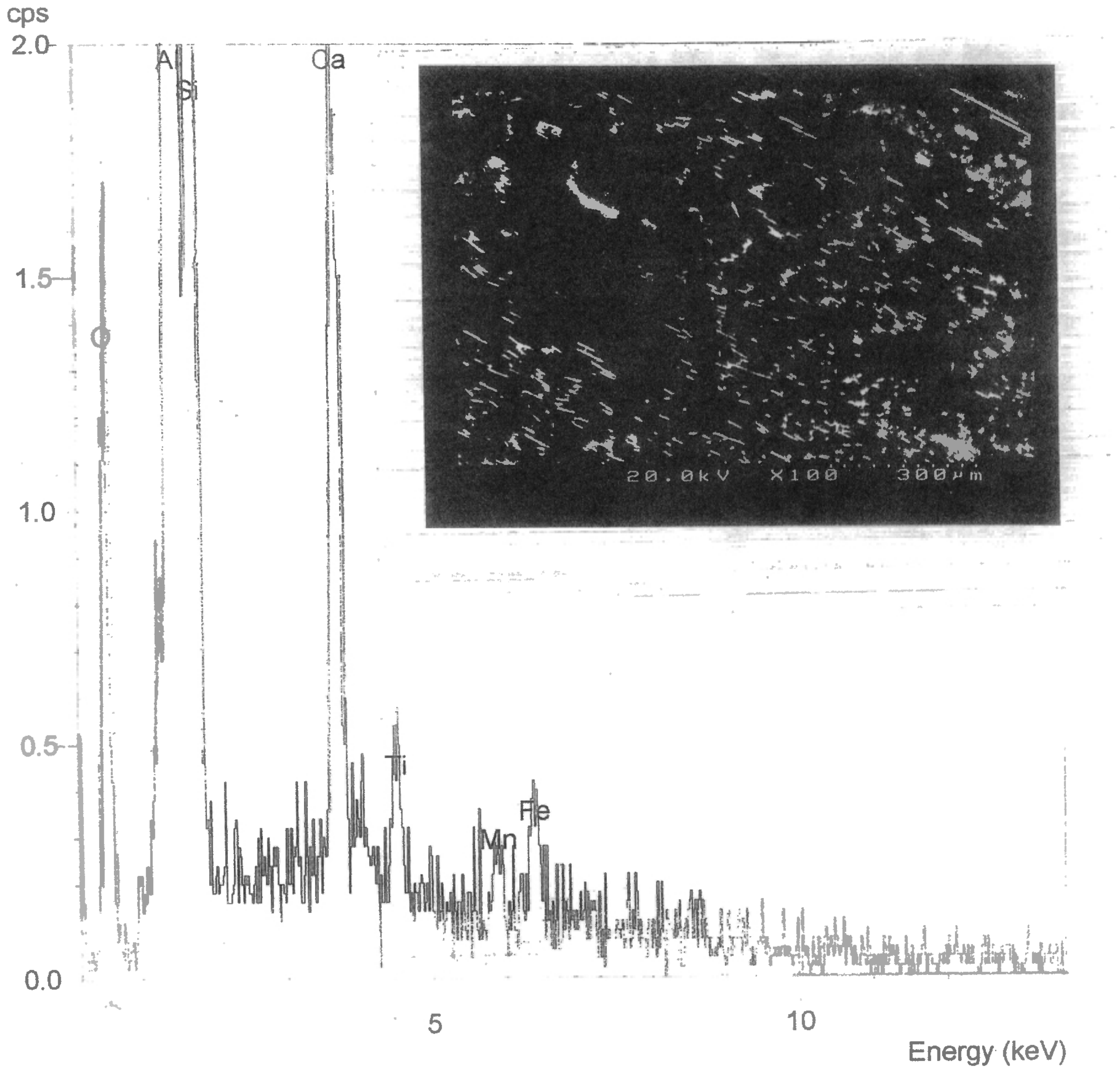

Figure 6.10. **EDAX analysis for the black stain on the 220 micron sample**

6.2.2.3. Discussion and Conclusion

The marks on the surface consisted of indentations and minute tears within a parallel abrasion structure. EDAX analysis of inorganic contaminants indicated traces of calcium, silica and titanium. These are all typical substances found in most semi-exposed industrial environments.

Minute traces of oily residue extracted from the polymer particles were found to be ester based, becoming sticky under the influence of pressure and heat (such as rolling). The ester compound appears to have been contaminated with dirt, grit and paint during normal processing, with these particles scoring the surface.

With this information, all known sources of ester-based compounds including coolant additions, rolls and spacers, and plastic sheeting were investigated using FTIR fingerprints to determine the structure. Several samples were analysised with the only match being several fraying polyester spacer rolls used to regulate the trim width during slitting. This is the first recorded instance of the effect of surface polymer contaminate on final product runnability.

6.2.3. Filtration Methods for Foil - Web Failure

As discussed in Chapter 2.3, an important attribute of aluminium foil is its high-barrier property. This prevents the transmission of light, water vapour, oxygen and other gasses that constitute aromas and odours through the foils laminates[180].

As final gauges get thinner, this attribute becomes dependent upon the number and size of voids or "pinholes" in the web, Table 6.1. Pinholes are defined as randomly distributed voids in foil under 20 microns gauge with a round or oval shape and a maximum dimension of 0.20mm. They are generally not visible to the naked eye and are measured by means of a light table in a dark room[181], Figure 6.11 .

Foil Thickness (μm)	Average Pinholes (m^{-2})
6.02	508
6.65	390
7.16	270
8.25	160

Table 6.1. Typical pinhole variation with decreasing gauge

There have been a number of investigations into the major causes of pinholes formation, which include[182,183]:

- Non-metallic inclusions (eg Si, K, Ca), titanium diborides[184], large constituent size (eg $Al_6(Fe,Mn)$ in 8xxx alloys formed during casting);
- Metallic and non-intermetallic debris in the rolling lubricant or generated in the roll bite at various stages of the process[185,186];
- Roll-in or rolled over scratches or marks from prior rolling passes;
- Presence of bright spots of matte size, excessive corrugation of matte side;

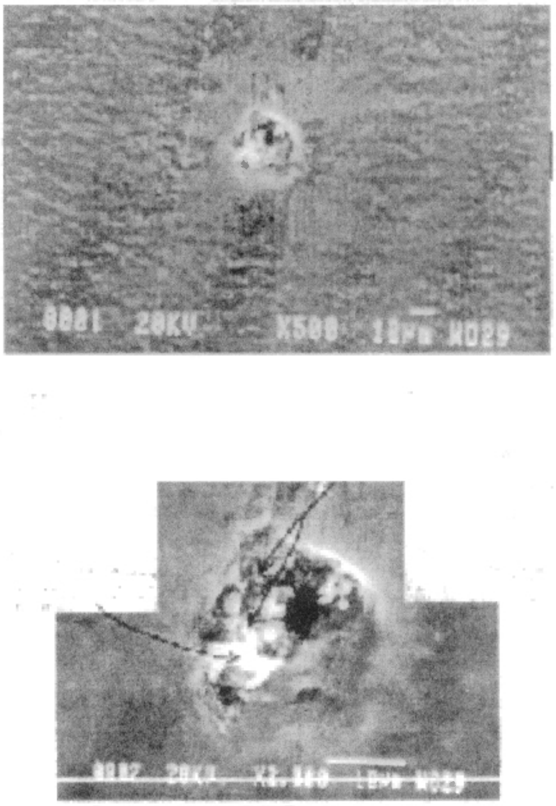

Figure 6.11. **Pinholes in light gauge foil**

Other causes of pinholes include[187]:

- Roll grind
- Amount of final cold work
- Accumulation of dust and debris in metal surface from environment or transport damage
- Lack or non-uniformity of ingot scalping (cracking of oxide film), centre line segregation, hotmill pickup
- Metal flatness, profile

As discussed, casting inclusions are a major cause of pinholes in thin film foil. Currently, all thin foil products cast using standard cake filtration as the principal method to remove inclusions. The objective of this trial is to quantify the impact of deep bed filtration (DBF) when it is compared to cake filtered metal or ceramic foam filtration (CFF).

Work by Guillaume Clement[188] provides a useful summary of the expectations of DBF. Although principally aimed in Canstock, the conclusions can be applied to foil:

- A DBF filter stops on average 10 times as many inclusions as a 30 ppi CFF (ppi = pores per cubic inch)
- The DBF filter remained more efficient than CFF, even after 4000 cast tonnes.
- There was a 10% drop in filter efficiency after 4000 cast tonnes.
- There was a 60+% drop in global defects at rolling plants (300+ casts monitored).
- There was a 40% drop in casthouse defects, decreasing to 30% after 60 casts.
- To evaluate DBF 1145 alloy in relation to the light gauge foil rolling practice, particularly with respect to 6.35 micron.

6.2.3.1. Experimental Procedure

Several blocks of DBF 1145 feed are to be rolled to thin-film foil. Most of the coils will be rolled to 6.5 microns following a normal production route which includes cake filtration over a period of three months, with the remaining blocks rolled to 6.35 microns as per experimental procedure attached, Table 6.2. Particular attention to web failure rate, pinhole/roll mark count, stickiness and wettability, and burst strength are examined. It is believed that the introduction of DBF will aid in down-gauging from our current 6.5 micron specification to 6.35 micron and potentially 6.00 micron. The theory behind Cake and Deep Bed Filtration is given in Chapter 2.3.2.2.

Pass	**6.5um Final Product**	**6.35um Final Product**
FM1 pass 1	0.22 – 0.116 (47.3% red.)	
FM1 pass 2	0.116 – 0.058 (50% red.)	
FM1 pass 3	0.058 – 0.029 (50% red.)	0.058 – 0.027 (53.4% red.)
FM2 pass 4	0.029 - 0.014 (51.7% red.)	0.027 - 0.013 (51.9% red.)
FM2 Pack pass	0.028D - 0.013 (53.6% red.)	0.026D - 0.0127 (51.2% red.)

Table 6.2. Process flow path

Web failures, or break rates as they are internally referred as, are a measure of the number of web failures against the volume of metal processed. The volumetric measure is referred to as a mevil and is calculated based on the strip width multiplied by the constant which is dependant on the wall build-up, Appendix 5.

Roll marks, as defined in Chapter 6.1.2, result in uniform holes in the metal which have a pitch equal to that of the work roll or ironing roll circumference. If present, they can compromise the barrier properties of the foil film. They are detected using a strobe-light that has a frequency proportional to the speed of the web.

Pinholes are random holes as describe in Chapter 6.1.2. They are measured by cutting a sample $0.167m^2$ from the parent coil, separating the two strips, and placing on a light box in an enclosed dark area, Figure 6.12. The number of lights or 'pinholes' in the sheet are counted and multiplied by six to give a result in m^2.

(a)

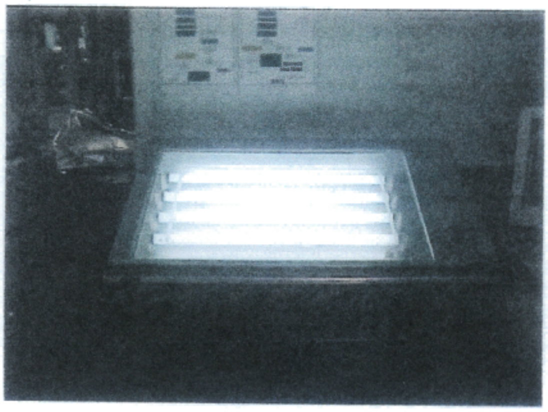

(b)

Figure 6.12. **Light box used to calculated pinholes, (a) general (b) in use**

6.2.3.2. Results and Discussion

a. Reduction in roll changes #2 Foil Mill due to roll marks.

The most significant system shift was observed in relation to roll changes per number of passes. Figure 6.13 shows the effect of using DBF in comparison with CFF over a 5 month period on roll changes. A set of rolls is expected to remain in the mill for at least 4 days (32 - 50 passes). Each unplanned roll change incurs 1 hour downtime. Examining each point in detail:

Passes per Roll change: During the trial period, 36 roll changes were carried out. Of these, 90% were unplanned and due to roll marks, Figure 6.14. The average number of passes per roll change was 11. A mevil is the coil weight in kilograms divided by the width in centimetres.

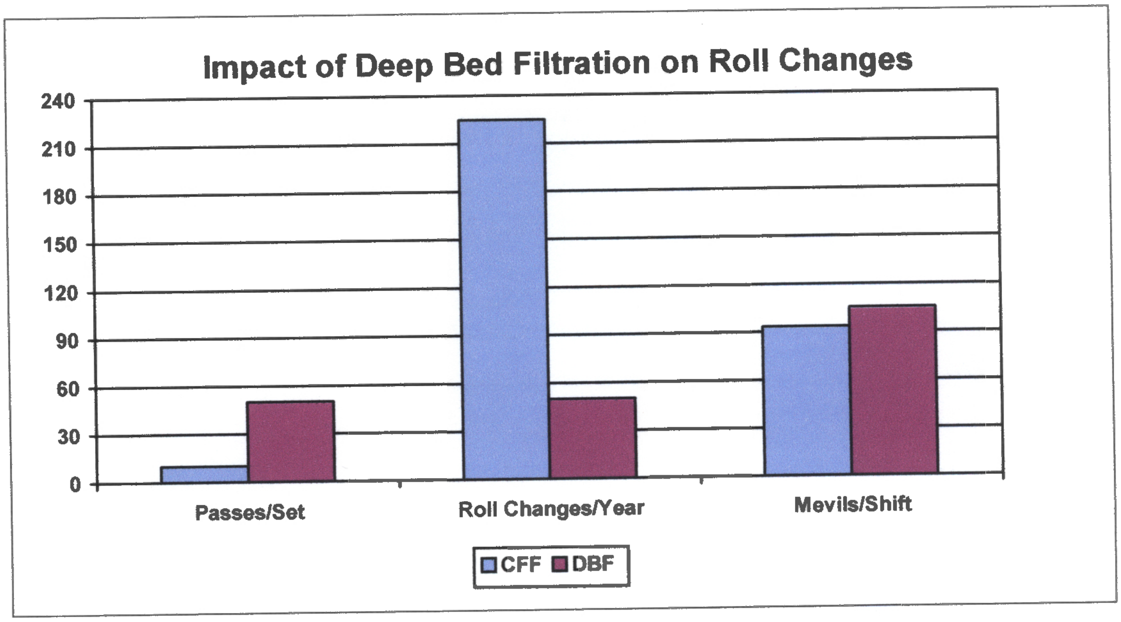

Figure 6.13. **Roll changes per year (a mevil is coil weight divided by the width in centimeters).**

DBF has fewer roll changes: DBF was run consecutively with CFF metal. The average number of passes per roll change with DBF increased by 150% from 11 to 28. Anecdotal evidence indicated that when a CFF coil was run after a DBF coil, a roll change due to roll mark would soon follow, where-as no DBF metal resulted in roll marks. The estimated improvement in passes per roll change with DBF is up to 50 passes from an average of 11. Unplanned roll changes equate to approximately 228 hours per annum (4.4 hours per week). The equates to $175000 per annum

The inferior nature of the CFF filters resulting on the formation of large particles, often exceeding half the through thickness of the foil. The particles could either mark the roll directly or cause a web failure which in turn could mark a work roll.

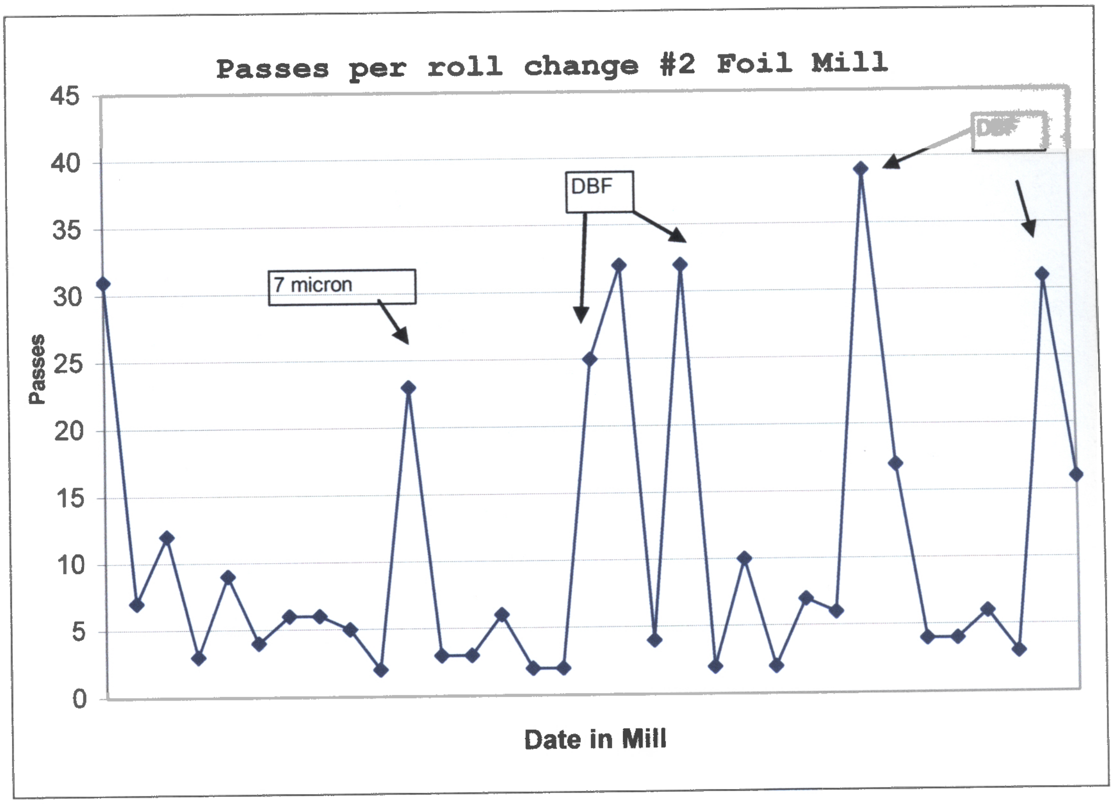

Figure 6.14. Roll Change Frequency (all values are 6.5 micron 1145 product unless stated).

Full lot scrap: When roll marks occur, the incidence of full coils scrapped is quite high. It is estimated that on an annual basis at least 12 full coils are scrapped due to roll marks. This is expected to be halved with the introduction of DBF metal, resulting in a saving of $107000. An additional benefit is the removal of the requirement to split a coil, contributing $350000 in extra productivity. The 7μm product is excluded from the trial as the increased thickness will reduce web failure as more tension leading to greater localised stresses are required to cause foil web failure.

Web Integrity

A further benefit experienced with DBF is an improvement in web integrity. Using web failure rate expressed in breaks per 100 kilograms of product as an indicator of a web defect, an increase in strip breaks are a good indicator of the susceptibility of the web to fail at the customer's plant. During the trial, DBF metal had a breakrate in excess of 50% lower than the CFF product, equivalent to a $100000 saving per annum. The trial coils were randomly rolled over a period of 10 weeks to allow for processing variation.

This implies that a majority of web failures are a result of casting defects, in-line with observations by Clement[188]. Figure 6.15 illustrates the difference in break rate between DBF and CFF. The DBF product demonstrates a lower break-rate than CFF product run over the same time period..

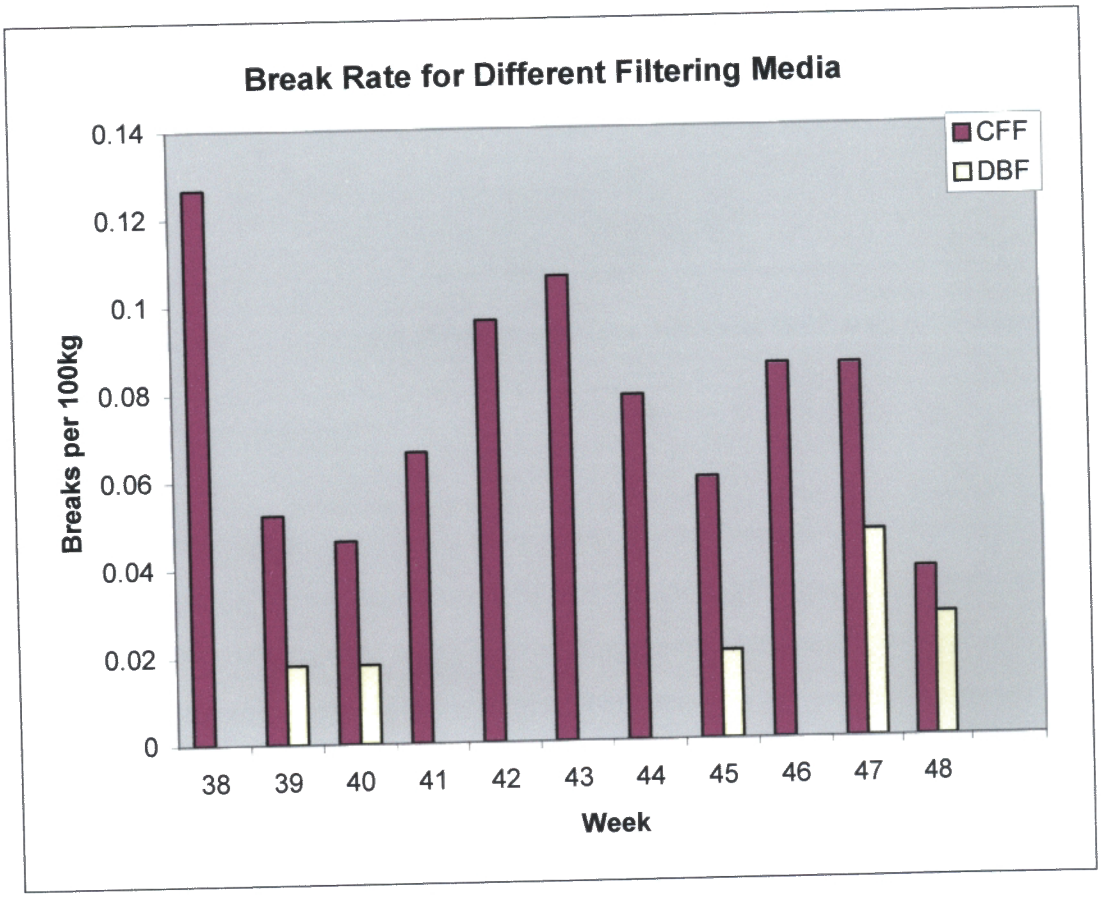

Figure 6.15. **Break Rate Trials for 6.5μm 1145 foil**

c. **Pinhole count**

A further aspect to web integrity is pinhole count, which is a measure of lamination permeability. Increased pinhole count reduces the foil's ability to insulate against moisture. There was a noticeable decrease in pinhole count with DBF averaging 50-60/m^2 compared with CFF with 170/m^2. While still in an acceptable range this is significantly higher, contained in the attached CD.

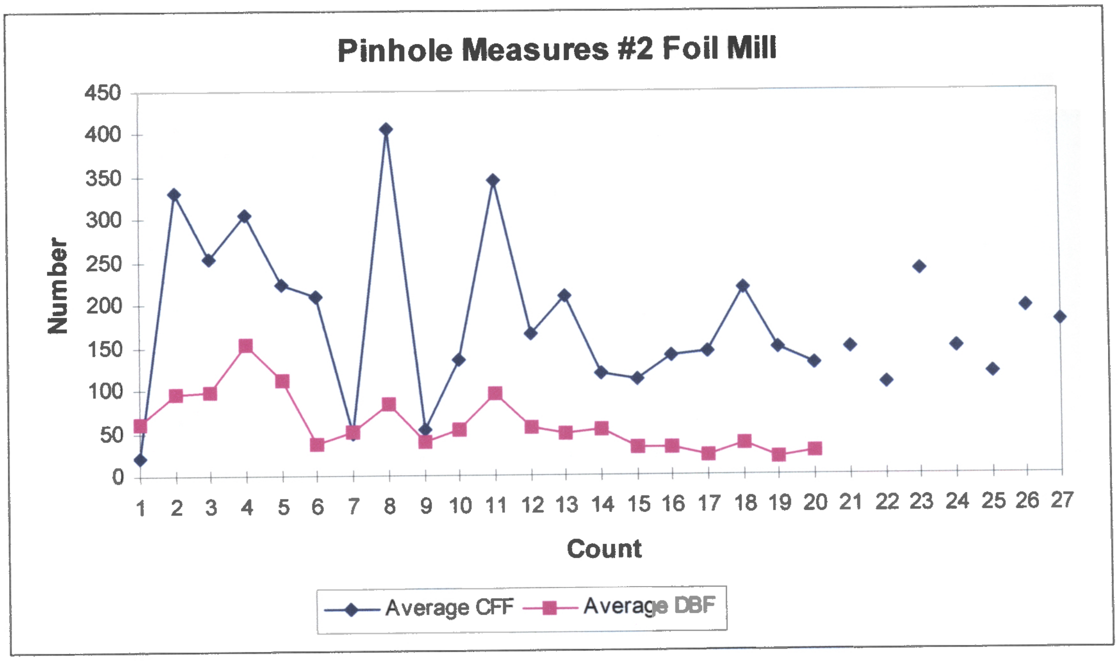

Figure 6.16. **Pinhole Comparison between DBF and CCF Product.**

6.2.3.3. Conclusion

The benefits of utilising deep bed filtration in the foil process were investigated. From the data obtained, it was found that deep bed filtration techniques reduced the incidence of roll marks (and hence the number of roll changes) and reduced the occurrence of strip breaks. The combination of these effects will result in an increase in throughput of approximately 12% due to less unplanned downtime, less planned downtime, a reduction in full coil losses and a reduced pinhole count.

The benefits are summarised in Table 6.3 and highlight the tangible benefits as well as predicting a cost benefit.

BENEFITS FROM DBF

1	80% REDUCTION IN ROLL CHANGES DUE TO ROLL MARKS
2	80% REDUCTION OF FULL COIL LOSS DUE TO ROLL MARKS
3	CAPABILITY TO ROLL FULL COILS AND DOUBLE RESULTING IN A 12% LINEAR INCREASE IN THROUGHPUT
4	50% REDUCTION IN STRIP BREAK RATE
5	PREVENT 20% LOSS IN MARKET SHARE (NEED FOR 6.35)
6	A 50-80% REDUCTION IN PINHOLE THROUGH THE LIFE OF THE ROLLS

RETURN FROM DBF

1	DOWNTIME DUE TO UNSCHEDULED ROLL CHANGES (including Lost revenue)	$176 031
2	SCRAP COST FROM ROLL MARKS (including Lost revenue)	$107 100
3	DOWNTIME COST DUE TO BREAKS (including Lost revenue)	$100 195
4	DOWNTIME COST ON SPLIT COILS (including Increased throughput)	$350 000
5	CAST SAVINGS PER TONNE (filter - $8/ton)	$24 000
6	LOSS OF MARKET SHARE (20%)	
	TOTAL ANNUALISED BENEFIT	**$757 326**

Table 6.3. Predicted tangible and financial benefits of using DBF metal

CHAPTER 7 STEADY-STATE VELOCITY VARIABLES

7.1. Introduction

A coil rolling sequence comprises a set-up period, acceleration to steady-state rolling conditions, deceleration to rest followed by a reset period for the next coil. The acceleration duration of the strip is defined as the time to reach a zero gauge deviation i.e. when the gauge target is achieved. Ideally, the acceleration time is used to set the ironing roll pressures, check the shape of the metal and set the correct steering arrangement.

The sequence is often interrupted by web breaks, due largely to metal defects or equipment failure. During this period, the rolling process is stopped with a short deceleration period, the mill cleaned and reset, followed by acceleration to steady-state rolling. The doubling or pack pass often takes in excess of 2 hours to complete with steady-state conditions encompassing over 90% of coil rolling time (acceleration, deceleration and web failures comprise the remainder).

Once a process is deemed to be in-control and capable from a mill specification and metal quality perspective, an assessment of mill productivity focusing on steady-state mill velocity and strip break frequency is mandatory. A major factor that affects mill productivity with regards to tonnage is the exit gauge. Decreasing the final gauge results in a corresponding increase in linear web length, assuming negligible transverse spread occurs.

The current rolling mode employs TEN-SPD (tension - speed) control to achieve a desired gauge. In this instance the entry tension is set high and initial target gauge is heavy. To allow time to set the ironing roll pressures and steering without compromising rolling speed, a standard low stress target and heavier initial gauge target is required. Once the tasks have been completed, the tension is increased which inturn decreases the gauge. This is demonstrated in Figure 7.1, where running at lower tensions results in an increased speed.

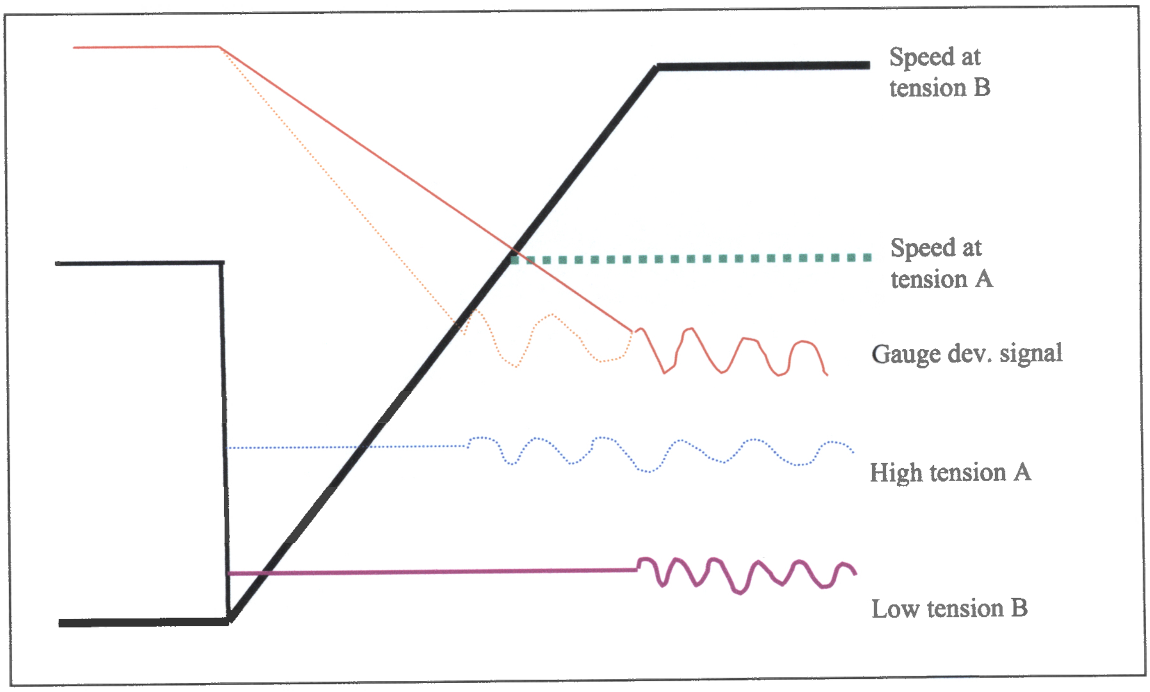

Figure 7.1. **Variation in speed with tension**

Velocity is measured at the roll bite and is dependant primarily on the amount of reduction. Orowan mechanics dictate that load is primarily used to control reductions and hence speed, with de-coil and re-coil tensions playing a secondary role. However in thin-foil rolling, traditional theory predicts a second order dependence on the friction hill parameter, introducing the concept of a limiting reduction. Hence there must be several other factors in addition to reduction percentage that determine strip velocity during thin-foil rolling. A brief list of factors is given in Table 7.1.

Major Effect	Minor / Unknown Effect
Rewind tension	Work Roll diameter
Coolant viscosity / viscosity	Ironing roll pressure and size
Reduction	Back up roll camber
Unwind tension	Work roll camber
Alloy Hardness / inter-anneal	Two spindles versus one spindle
Work roll finish	Strip width
Work rolls - chromed versus unchromed	Matting solvent viscosity
Roll load	

Table 7.1. **Mill speed variables**

As no significant change to the pass schedule and hence reduction percentage is proposed in decreasing the exit gauge, rolling velocities are expected to remain constant unless other variables are manipulated. Hence a decrease from 6.5um to 6.0um will increase the steady state rolling time by 7.5%, reducing mill productivity by a similar amount. With a light gauge foil production targets of 250 tonnes per month for 6.0 micron foil, the average pass velocities require increases to nominal targets.

Breakdown:	From 400 m/min to 490 m/min	(22.5%)
Final Single:	From 498 m/min to 600 m/min	(20.5%)
Double Pass:	From 466 m/min to 530 m/min	(13.7%)

Process modelling to achieve a target mill velocity recommended optimising process settings for unwind tension/stress, lubricant viscosity, load and rewind tension/stress. The factors were chosen based on ease of adjustment and monitoring over a short time period and are known not to significantly influence the slitting and annealing characteristics. While the mill production settings are not directly transferable, they do give an insight into the effect of these key variables on other foil mills.

Each crew was evaluated with regards to speed, load and unwind / rewind tensions, with the optimal process settings chosen from data analysis taken over several weeks for three passes. The three passes are 59 to 29 micron, 29 to 14 micron and 28 to 13-doubled micron (6.5 micron separated). Also included are minimum / maximum settings based on previous experiences in rolling foil. Variation in entry and exit tensions with strip width to give a constant stress is also included.

7.2. Initial Settings

In establishing target rolling parameters, benchmarks need to be determined across all crews based on exiting rolling speeds. The data was collected from all four crews over a period of 6 weeks. The data was analysed according to pass (breakdown, final single and double), with each pass further explored according to width. The widths chosen varied slightly in response to customer requirements.

The data was obtained from the Toshiba OIS5000 data acquisition system using a Toshiba translator v1.03 program. A summary of the data is given below:

7.2.1. Exit Tension / Stress

In determining the existing exit tension setting, each of the four crews were consulted and observed. Stress is a function of tension over the cross-sectional area, with exit being the rewind settings, and entry the unwind settings. In the absence of standard operating procedures, the following guidelines were established:

- Breakdown Single 59 to 29 micron — No standard
- Final Single Pass 29 to 14 micron — 5.0 kg/mm^2
- Doubling Pass 28 to 13 micron — 3.5 kg/mm^2
- To calculate the exit stress from the exit tension, the load is divided by the area (width x gauge). The legend gives the product width.

Single 59 to 29 micron pass:

As this pass was only recently moved to Foil Mill 2 for flow reasons, little correlation between crews is expected. The exit tension data varied from 3.5 to 5.1 kg/mm^2 with a broad increase with increased width, Figure 7.2 – 7.3. Due to the infrequency of the product, no data was collected for C crew.

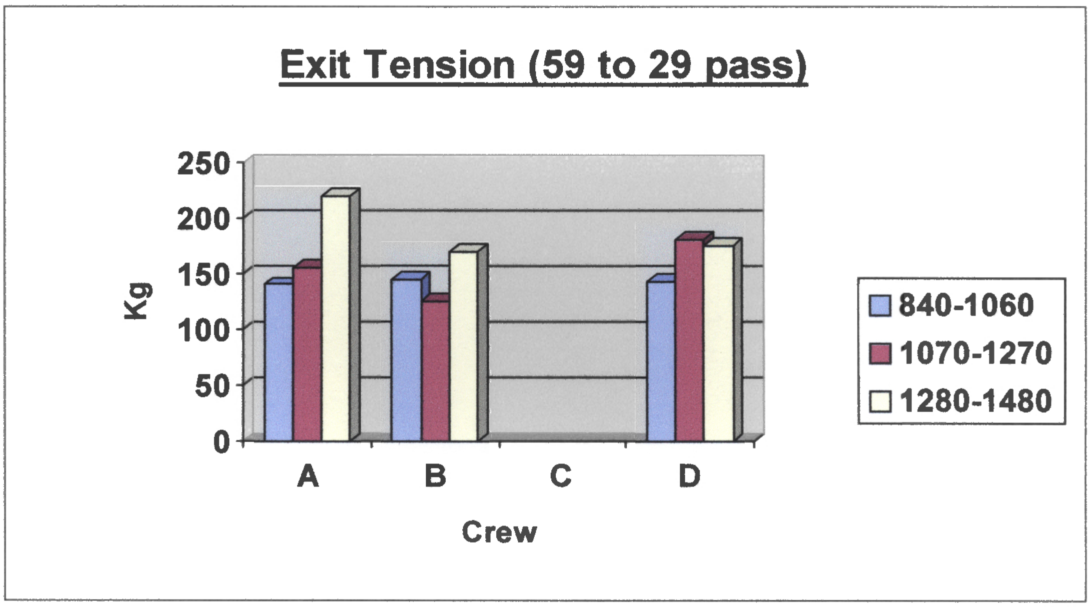

Figure 7.2. Exit tension – breakdown pass

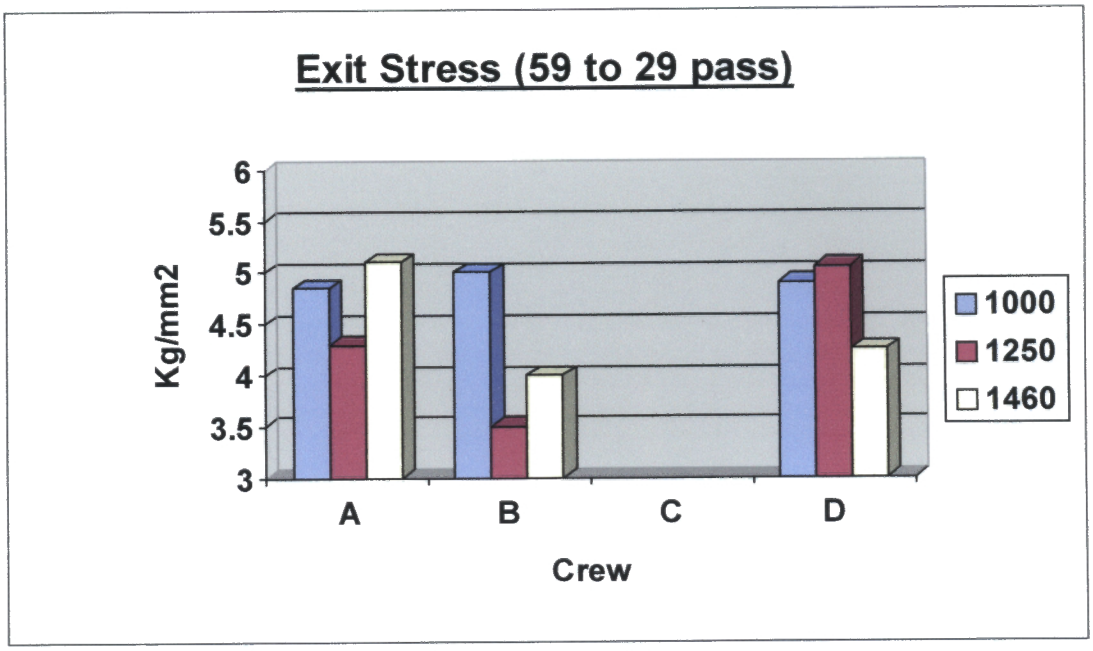

Figure 7.3. Exit stress – breakdown pass

Single 29 to 14 micron pass:

The penultimate pass exit tension settings are well entrenched resulting in little variation between crews for all widths, with the standard exit tension range between 4.5 to 5.1 kg/mm^2, Figure 7.4 – 7.5.

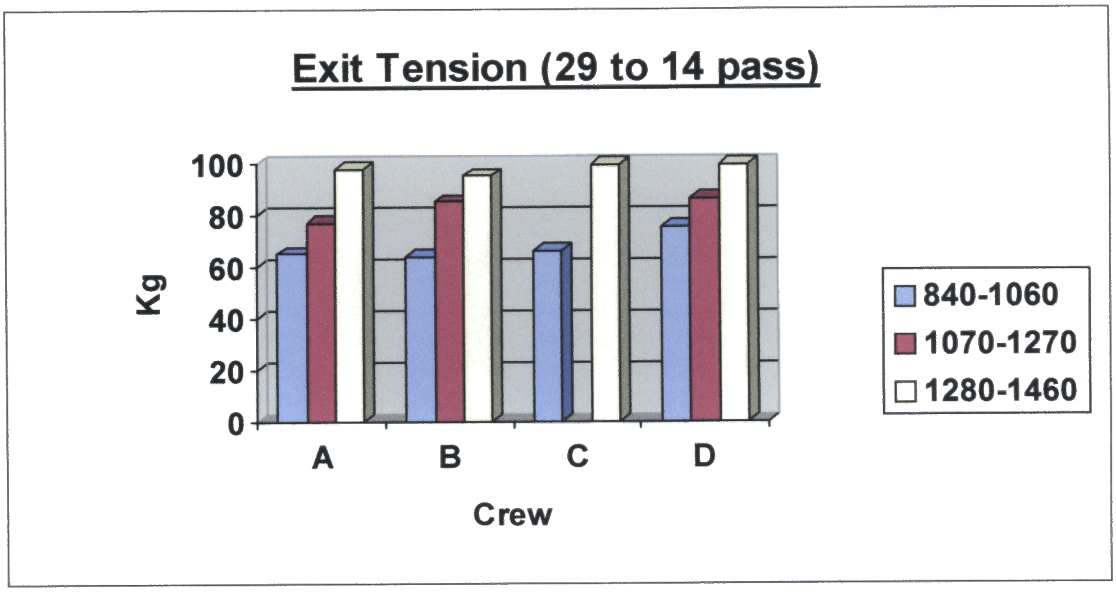

Figure 7.4. Exit tension – final single

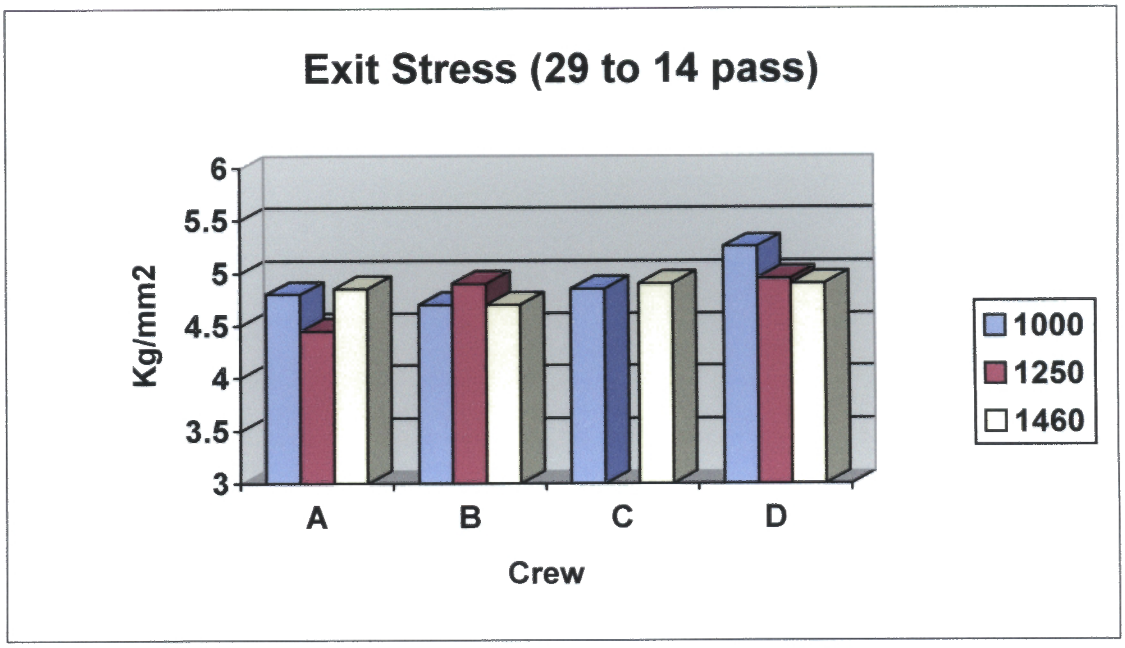

Figure 7.5. Exit stress – final single

Double 28 to 13 micron pass:

The doubling or pack pass exit tension settings are well entrenched resulting in little variation between crews for all widths, with the standard exit tension range between 3.5 – 4.0 kg/mm^2. Due to quality issues relating to ironing roll pressure and bounce, the settings are valid up to speeds of 500 m/min only, Figure 7.6 – 7.7.

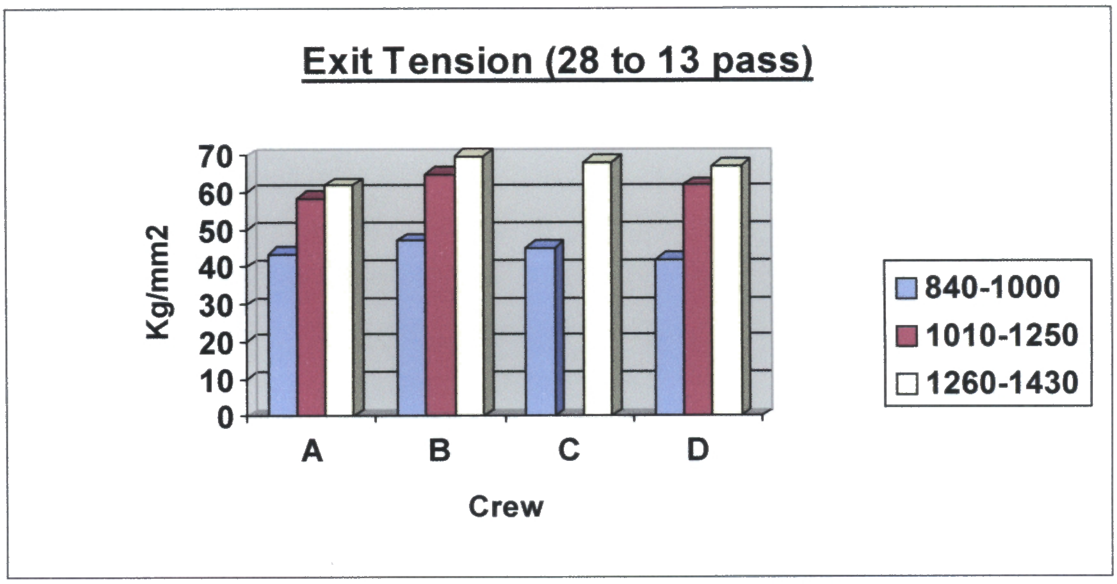

Figure 7.6. Exit tension – double pass

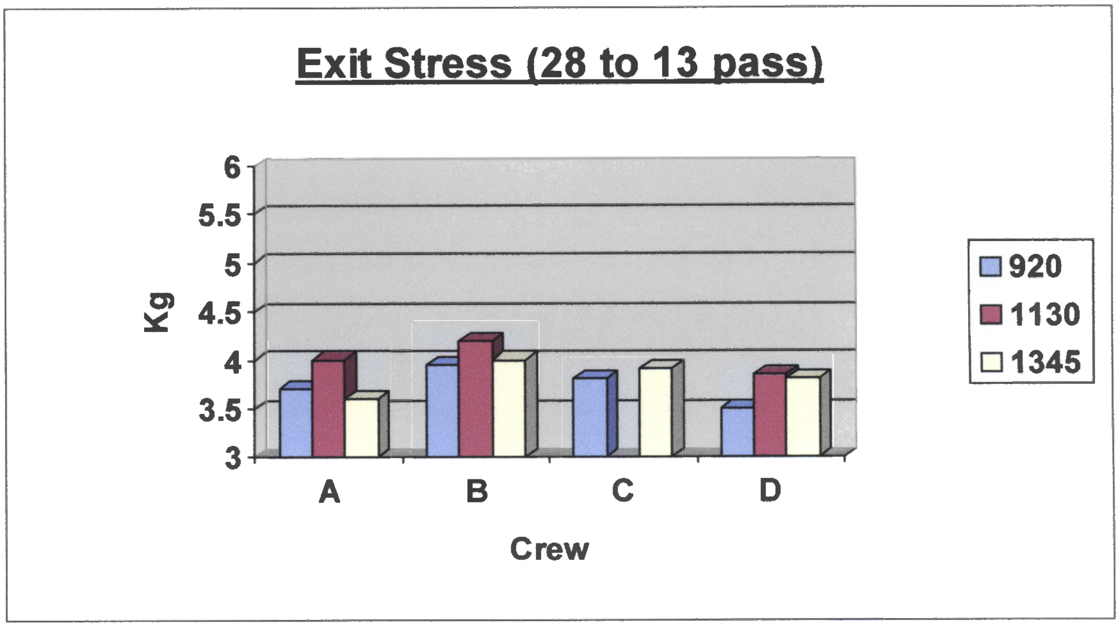

Figure 7.7. Exit stress - double pass

The infrequent nature of 59 to 29 micron pass is shown in the high variation in exit stress with width across the four crews. The values varied by nearly 50% with the general trend to run at high tensions demonstrating no standard rolling practice. The following two passes had much more even stress across products and between crews.

7.2.2. Entry Tension / Stress

The value of the entry tension (stress) is one of the most important parameter settings with regards to both quality and speed as it indicates the tension across the strip. The existing control system uses tension as the primary control variable for gauge control, termed Gauge Control Mode TEN-SPD. Once an optimal stress value is determined, it is recommended to change the Gauge Control Mode to SPD-TEN, where speed is the primary control variable.

Single 59 to 29 micron pass:

The entry stress target for the 59 to 29 micron pass exceeds 5kg/mm^2, which is higher than the stress target of 4.6 kg/mm^2 at the No1 Foil Mill. This can be explained in part by the different mill characteristics and control systems between the mills, Figure 7.8 – 7.9.

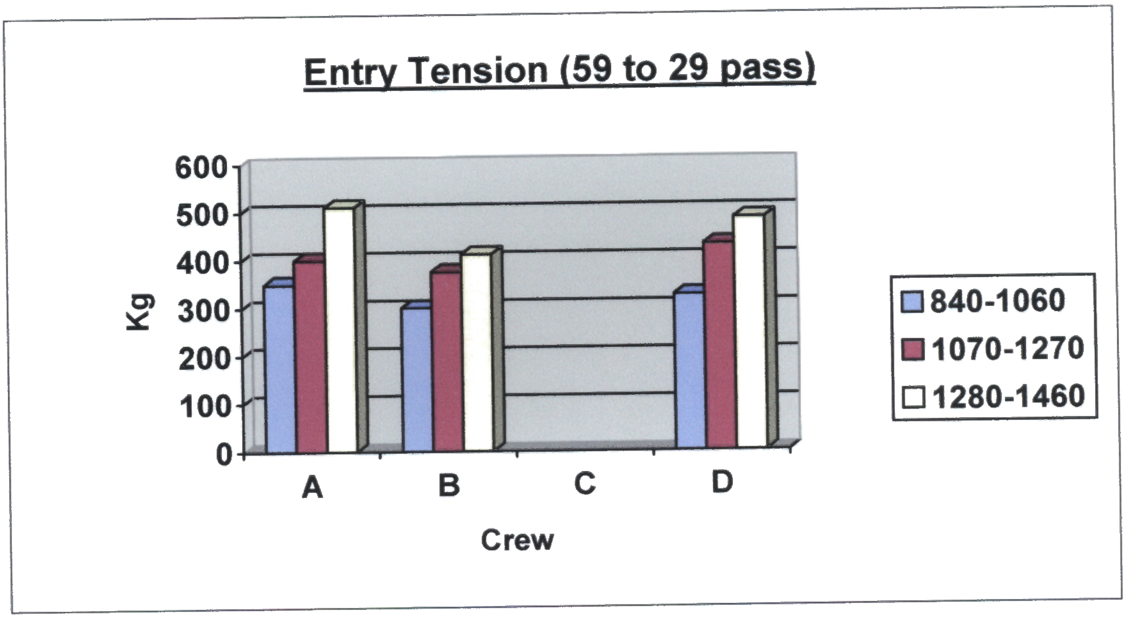

Figure 7.8. **Entry tension – breakdown pass**

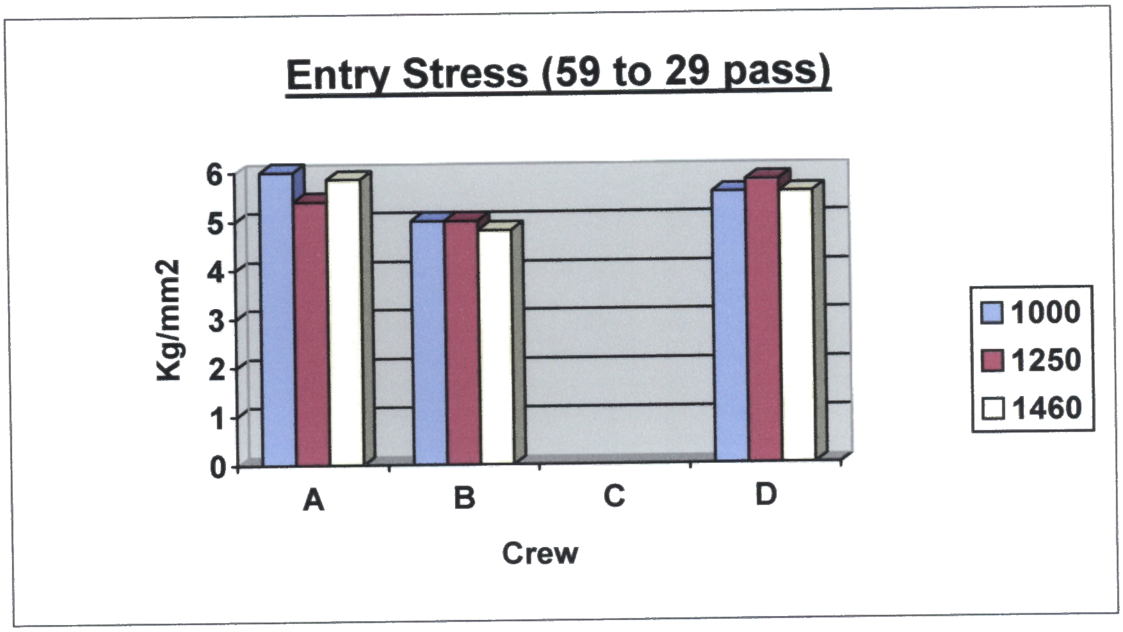

Figure 7.9. **Entry stress – breakdown pass**

Single 29 to 14 micron pass:

The entry tension setting is rarely below 6kg/mm^2 across all crews. Entry tension is the principal lever to control mill speeds, Figure 7.10 - 11. There is a belief that increased rolling speed results in a corresponding increase in breakrate, especially at lower gauges. A common mill practice to reduce speed is to increase tension[189].

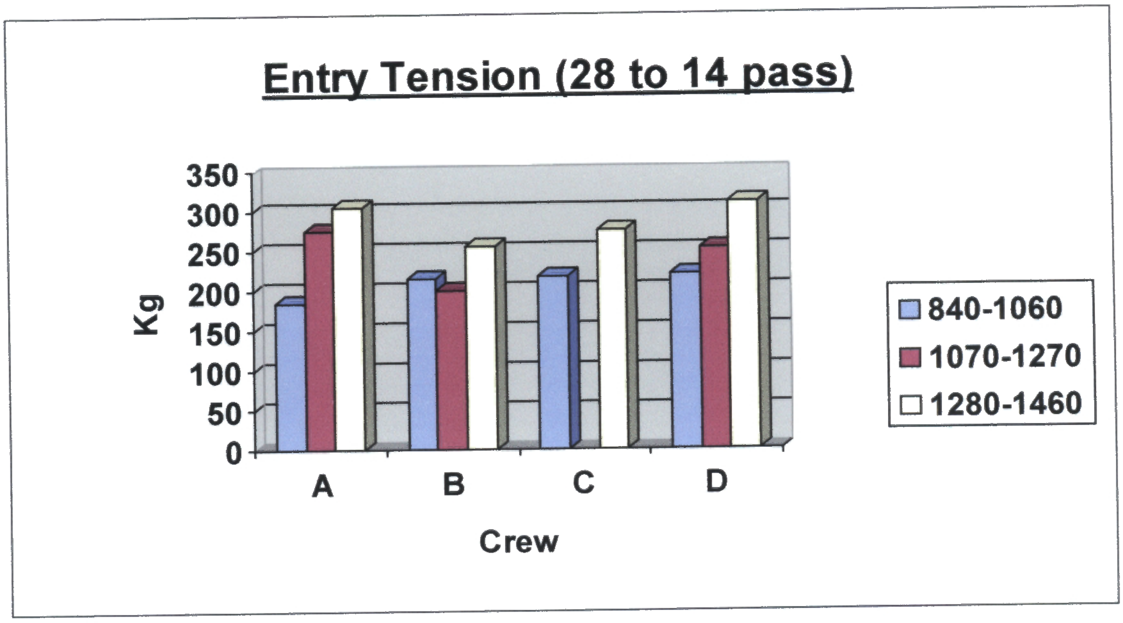

Figure 7.10. **Entry tension – final single**

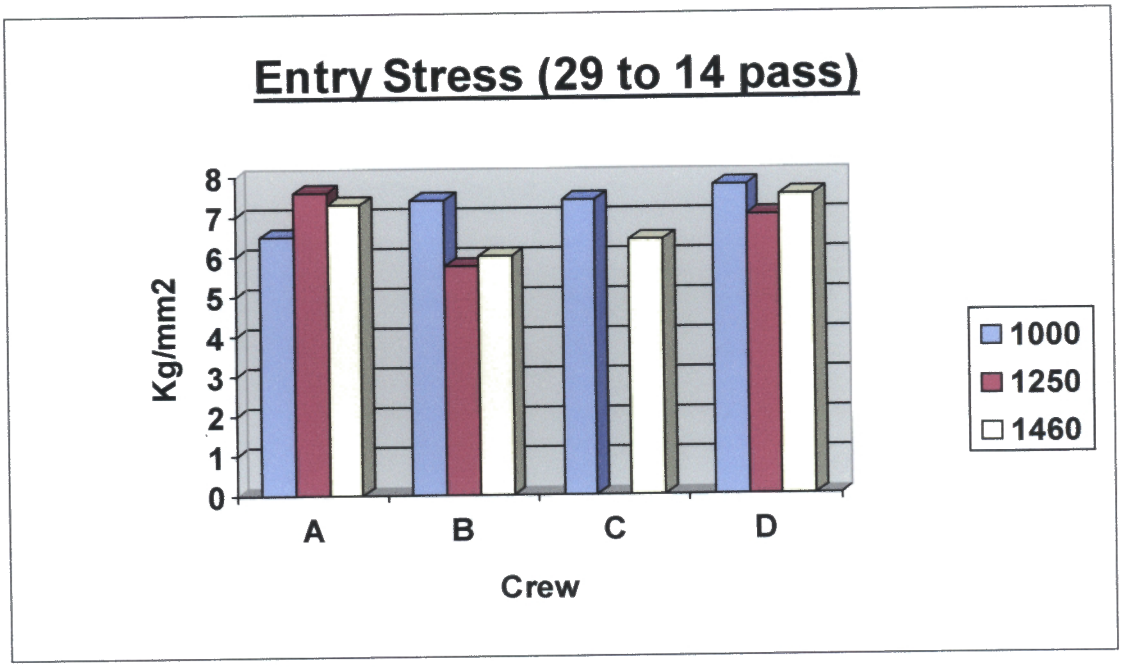

Figure 7.11. **Entry stress – final single**

Double 28 to 13 micron pass:

The entry tension was found to vary between crews and for different widths. However the significance of the coil width was reduced once stresses were considered as stress is a function of width, Figure 7.12 – 7.13.

- For narrow coils, the settings varied between 3.8 to 5.1 kg/mm^2.
- For medium width coils, the settings varied between 4.5 to 5.1 kg/mm^2.
- For wide coils, the settings varied between 4.9 to 5.3 kg/mm^2.
- The narrower coils had a lower stress, indicating a greater confidence in the metal with regards to strip breaks.

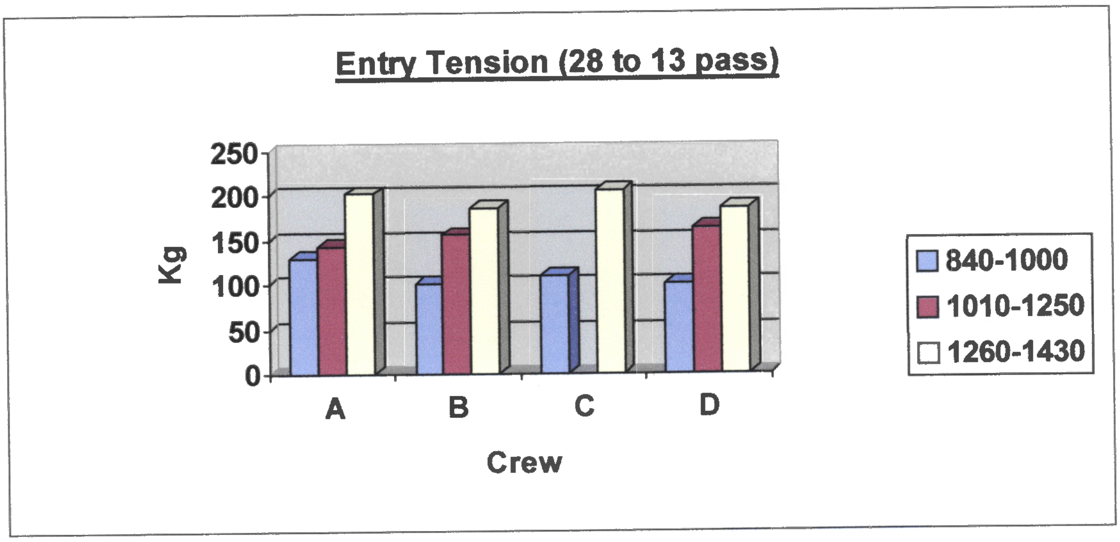

Figure 7.12. Entry tension – doubling pass

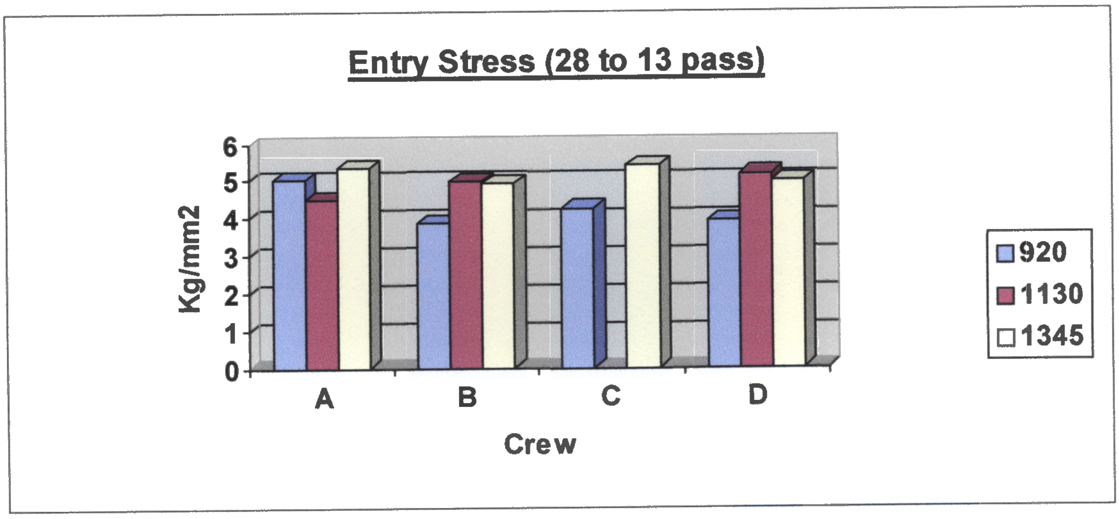

Figure 7.13. Entry tension – doubling pass

The results illustrate that entry stress during the 59 to 29 micron pass is better controlled across product widths; however there is still significant variation between crews. The variation in entry stress at lower gauges is greater than that recorded for the exit stress.

7.2.3. Load

While the effect of load is secondary to exit and entry stress on final speed, it does significantly affect gauge variation and backup bearing life, hence its inclusion. The set load required is largely dependent on mill and chock geometry and can differ by close to 100% for different mill designs. As an example, Alcoa mills in Spain run with rolling loads of less than 300 tonnes, while Yennora Mills run with loads in excess of 500 tonnes.

Single 59 to 29 micron pass:

This pass has recently been transferred for the No1 Foil Mill to the No2 Foil Mill due to process constraints upstream. Baseline data, shown in Figure 7.14, indicated that the load target should be set at less than 400 tonnes, independent of width.

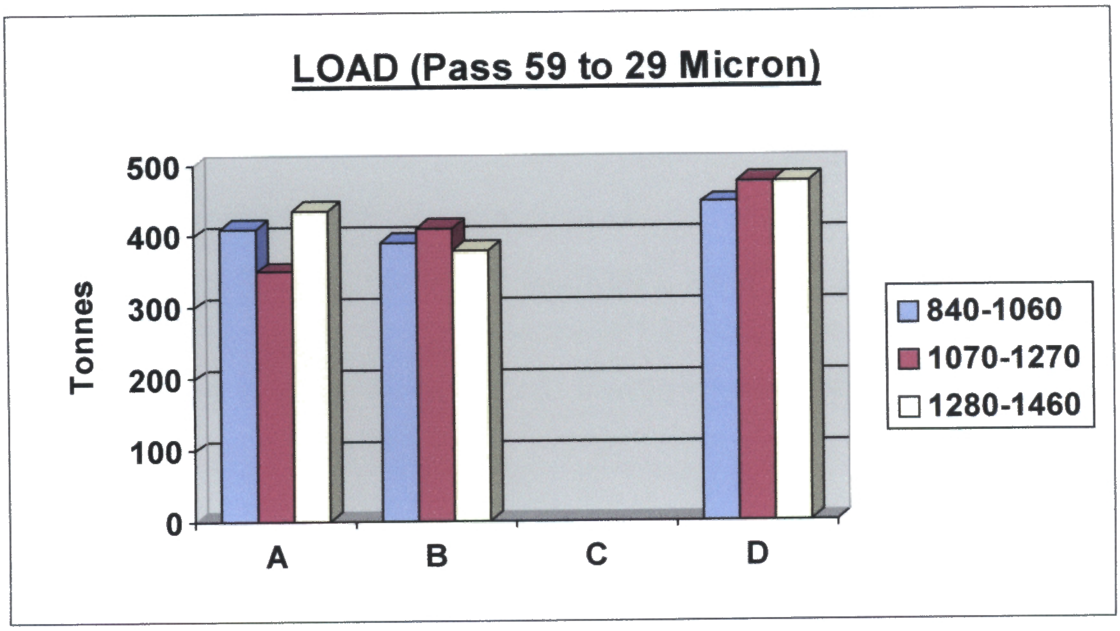

Figure 7.14. Load – breakdown pass

Single 29 to 14 micron pass:

When examining the variation between crews it was found that crews A, B and D use a similar load of around 470 tonnes, with C crew averaging 505 tonnes. A confusing practice of rolling with higher loads for narrower coils was observed on crews A, B and C; with D the only crew to roll with lower roll loads, Figure 7.15.

Force is a measure of load over area. As strip width decreases, the load required to maintain a set force will also decrease. No reason was given for this practice.

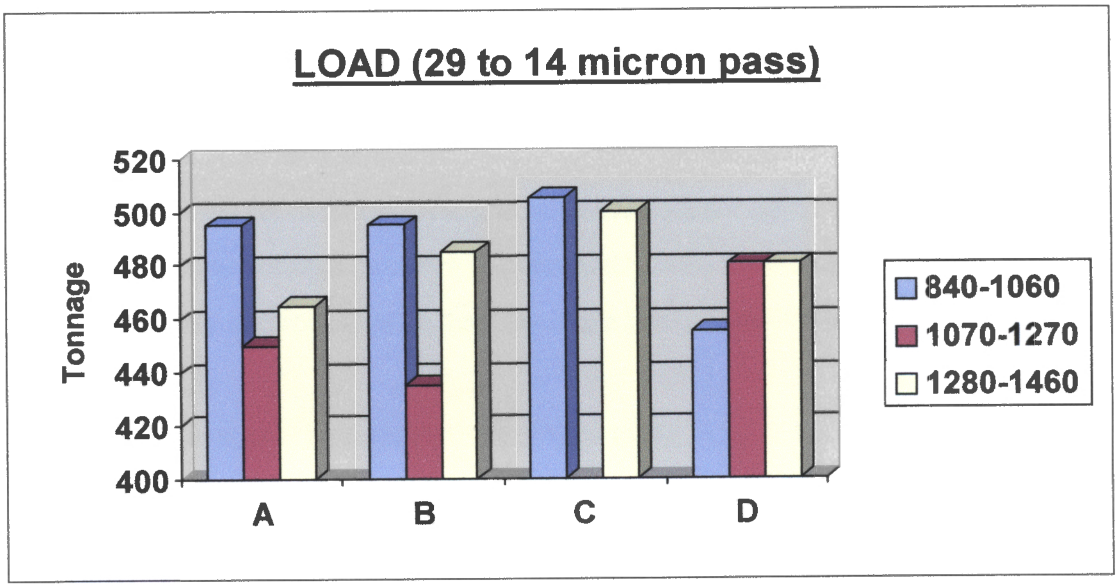

Figure 7.15. Load – final single

Double 28 to 13 micron pass:

During doubling, crew variation was significantly lower than previous passes with loads around 500 tonnes. Previous experience has shown that loads less than 460 tonnes can result in creases on the mill and annealing issues, Figure 7.16.

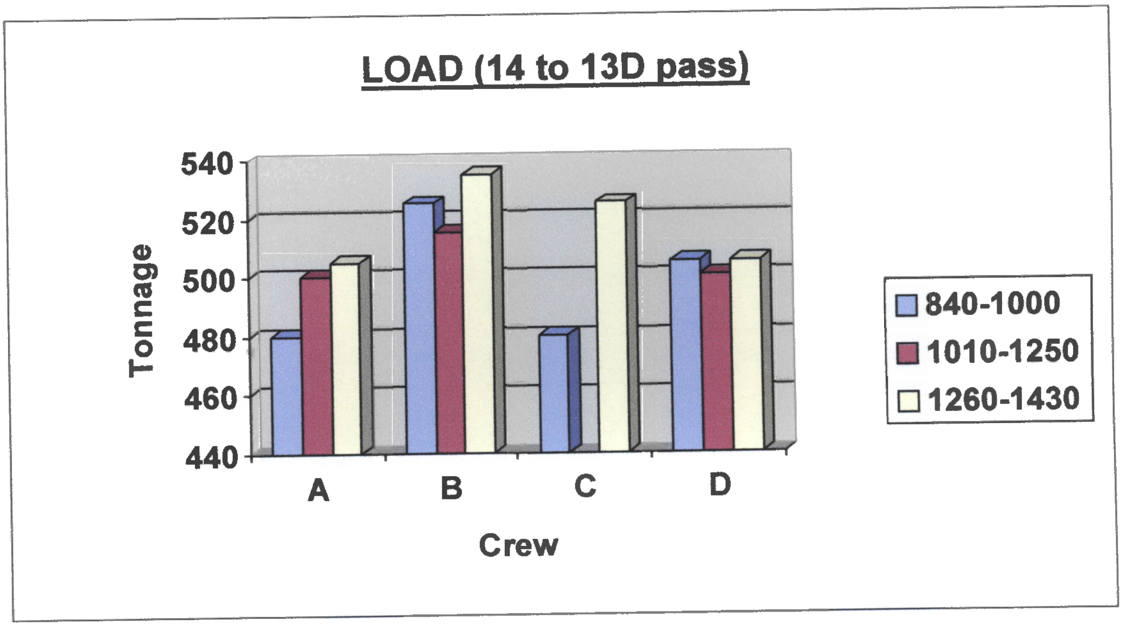

Figure 7.16. **Load - double pass**

The effect of load on thin-foil rolling is not well understood by the foil rolling crews. Variation in load settings between widths and across crews for all passes does not demonstrate any methodology in determining a load parameter setting.

7.2.4. Coolant Temperature / Viscosity

Coolant temperature is limited to between 38°C - 42°C due to web surface defects (refer to Ladder/Herringbone defect). At temperatures below 38°C, the roll lubricant collects in locally on the roll surface, effectively punchering the metal resulting in strip breaks[190]. At temperatures greater than 42°C, a surface mark, sometimes termed herringbone, occurs on the bright side of the foil web[191]. The relationship is schematically described using the Mansell curve – Figure 6.7. While this defect has no metallurgical significance, it creates a surface blemish that is unacceptable to the customer.

7.3. Final Speed Settings

As discussed in the introduction, to target in excess of 250 tonnes per month of light gauge foil, the average pass velocities require increases to nominal targets outlined:

Breakdown (59 to 29μm): From 400 m/min to 490 m/min (22.5%)

Final Single (29 to 14μm): From 498 m/min to 600 m/min (20.5%)

Final Pass (28 to 13-doubled μm): From 466 m/min to 530 m/min (13.7%)

The rolling parameters for each crew for the breakdown, intermediate and final passes for 6.5μm foil were collected and analysed. The large variation in stresses between crews and due to different widths was identified as a major variable that required a reduction in variability.

Optimal settings based on current rolling practices were determined for unwind tension/stress, lubricant viscosity, load and rewind tension/stress to achieve the desired mill speed.

Exit Gauge	**AGC Mode**	**Load**	**Exit Stress**	**Entry Stress**	**Speed Target**	**Speed Actual**
μm		Tonnes	Kg/mm^2	Kg/mm^2	m/min	m/min
29	TEN-SPD	360	4.6	4.6	700	≈ 490
14	TEN-SPD	460	5.0	5.0-5.5	700	≈ 600
13D	TEN-SPD				700	≈ 530
Coolant Temperature:						>45°C

Table 7.2. Suggested rolling parameters – Foil Mill 2 Yennora

These rolling parameters were introduced in Week 10 as shown in Figures 7.17 - 19. Optimising the critical rolling parameters resulted in an increased rolling speed in the vicinity of 15-20%, exceeding target velocities once the rolling parameters were set .

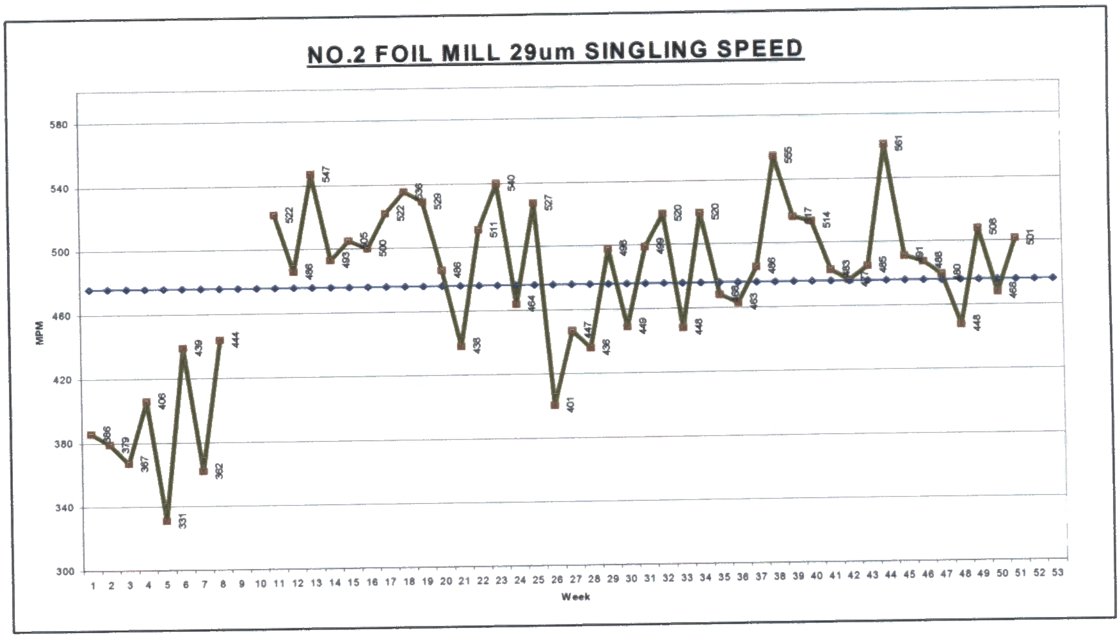

Figure 7.17. Speed increase with modified rolling parameters - 29μm

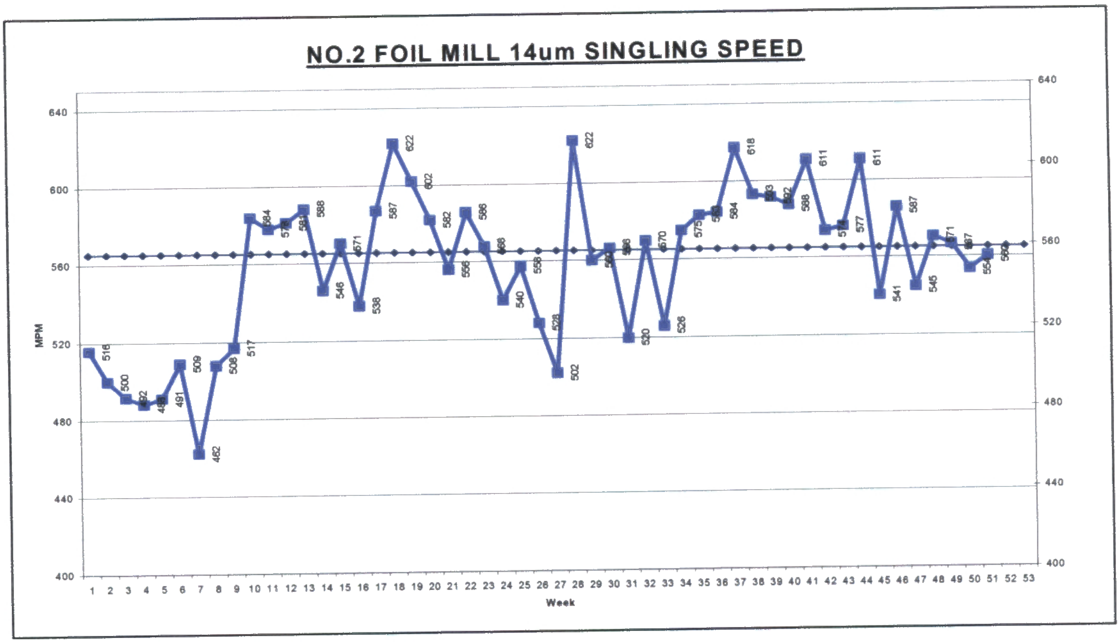

Figure 7.18. Speed increase with modified rolling parameters - 14μm

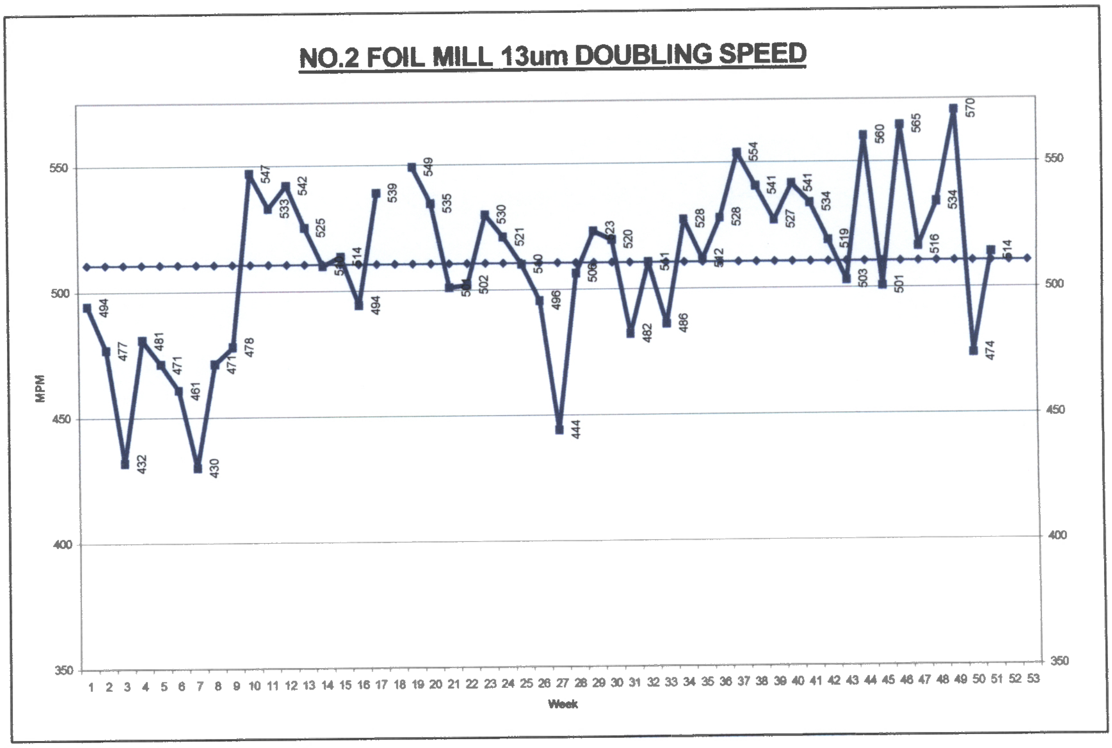

Figure 7.19. **Speed increase with modified rolling parameters – 13Dμm**

7.4. Break Rate

A common perception in light gauge rolling is that increasing rolling speeds will increase the break-rate frequency. A comprehensive review into with web defects and increasing speeds was completed. When break-rate data, expressed as breaks per mevil, was compared to speed, it can be seen that break-rate decreases with increasing speed demonstrating that break-rate has a second-order or lower dependence on speed. While the time between breaks will decrease with increasing speed for similar break-rates, no direct correlation between web failure and speed has been established.

Other factors, such as the introduction of Deep Bed Filtered (DBF) metal, water ingress prevention techniques and increased upstream vigilance had a significant influence for these changes.

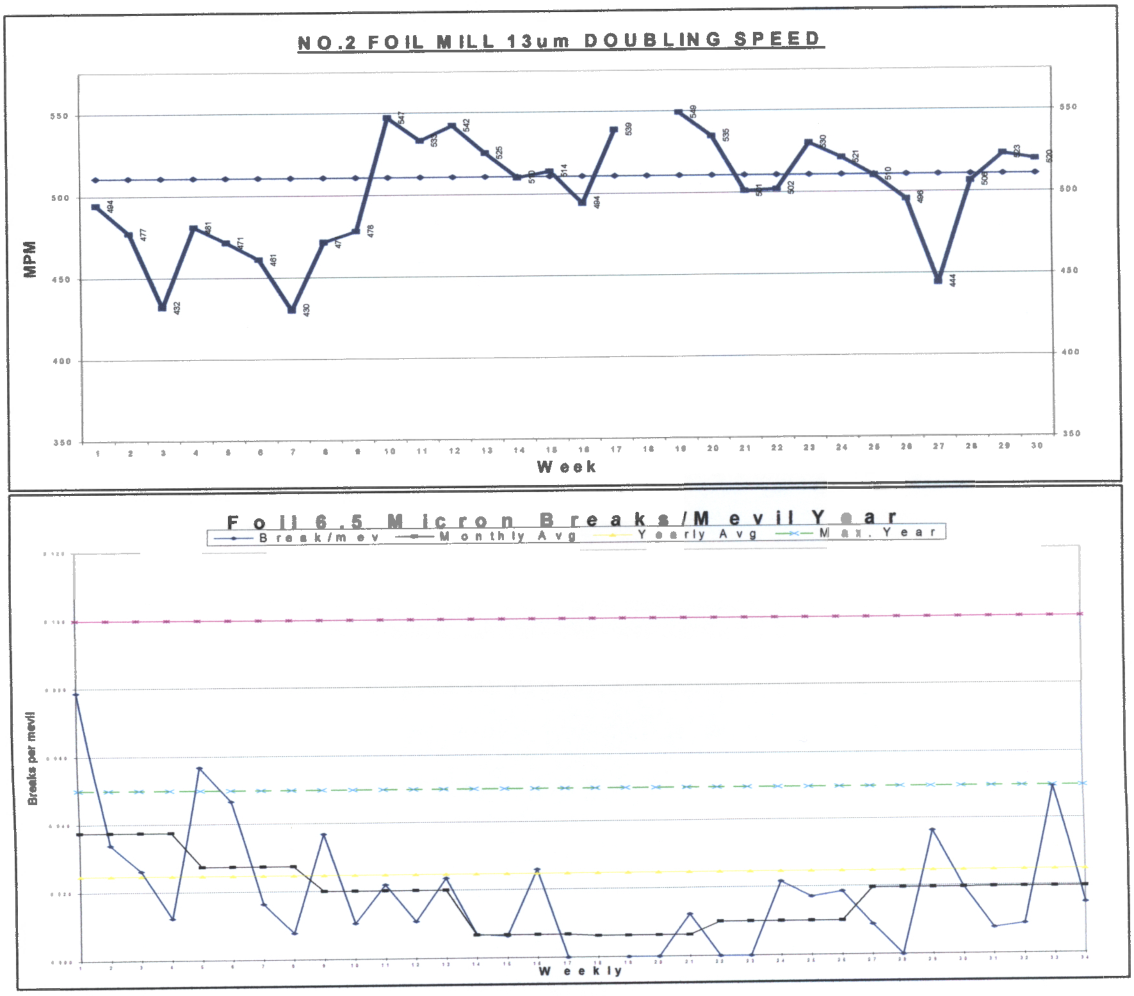

Figure 7.20. Speed versus breakrate relations – 13μm doubled product

7.5. A Comparison between Chromed and Steel Work Rolls

Roll changes contribute greatly to the financial cost and productivity of rolling. Most ALCOA aluminium foil mills employ the use of steel work-rolls to achieve a desired end product. It has been observed that mill efficiency can drop by up-to 30% with 8-12 hours of continuous rolling after a roll change. This results in a roll change is required every 8-12 hours (2-3 per day on a continuous shift basis) as a result of a loss of rolling speed. The steel industry, under much harsher rolling conditions operates with a similar roll change frequency. Frequent roll changes reduce mill availability, tie-up roll grinding and operational resources and require a larger roll inventory.

During close-gap rolling, the contact between the rolling lubricant in combination with the aluminium strip on the roll surface effectively buffs the steel roll surface. This reduces the roll roughness (Ra) to levels that are less able to entrain the metal web, which is observed as a speed drop. To reduce the severity of the speed drop, the surface hardness of the work roll is increased by either nitriding the surface or electro-plating the surface with a harder metal such as chromium. In addition to abating roll roughness losses, the harder surface also reduces the incidence of roll marks due to damage to the roll surface from a rolled over particle on the web surface. A secondary benefit of chrome rolling is the ability to change coil widths several times without inducing shape issues or surface marks on the sheet caused by the web edge marking the roll surface.

Historically, roll change frequencies at Yennora for chromed work rolls have been steady at two and a half changes per week, primarily for roll marks. Speed drops have been observed to stabilise at around 10% after 36 hours. With improved control concentrating on strip cleanliness, the roll change frequency has been reduced to approximately one and a half changes per week.

7.5.1. Chroming Process

The roll grinding–chroming process involves grinding a roll set to a work roll finish slightly greater than the final desired specification. The rolls are then electro-coated with a 40-50μm chrome layer via immersions of the roll in a chromate solution. The chrome deposits onto the surface in the form of chrome nodules, Figure 7.21.:

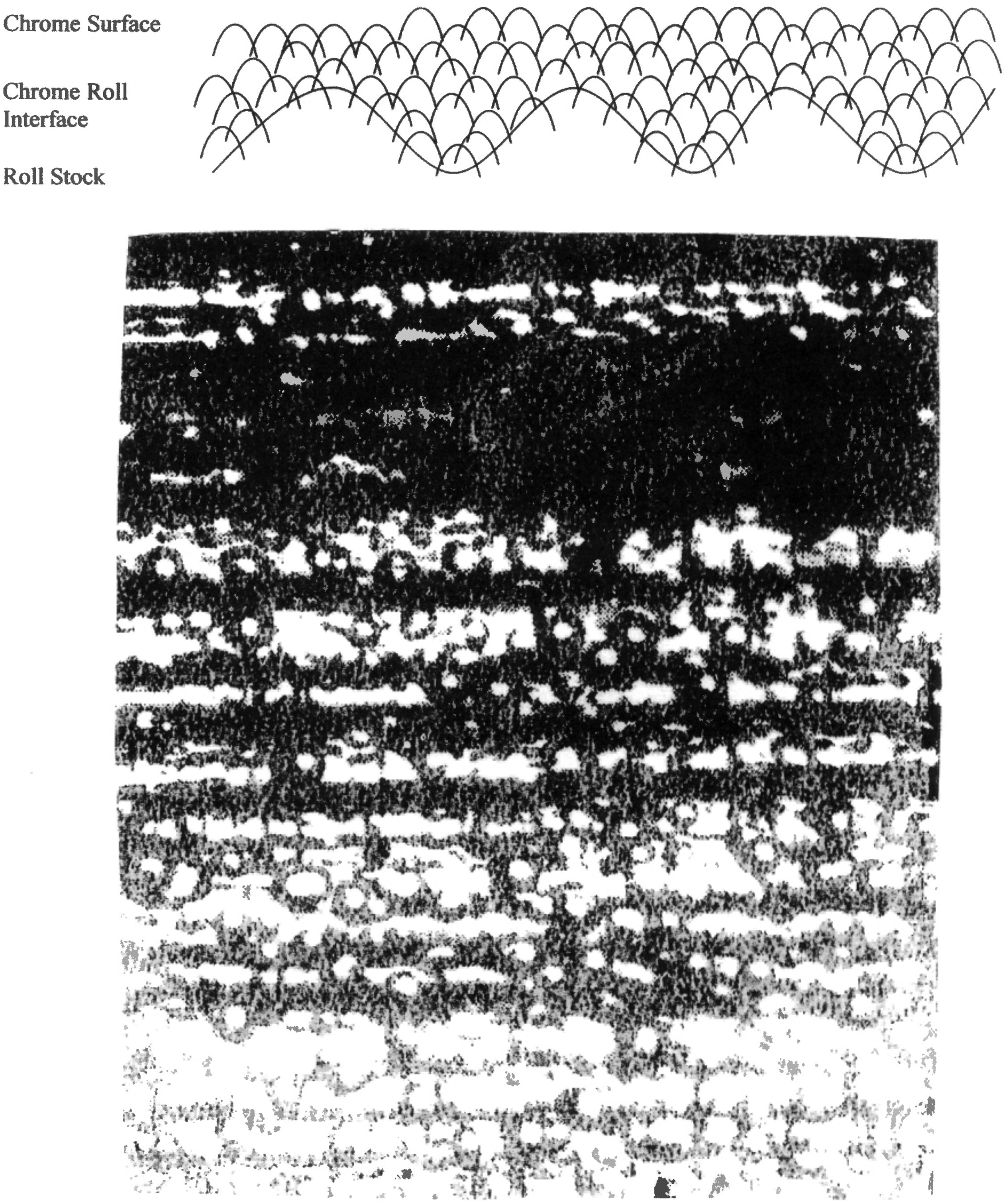

Figure 7.21. Schematic of chrome nodules at work roll surface (80x)

The surface is then microfinished to remove the nodules, producing a smooth surface, Figure 7.22. Microfinishing involves the mechanical removal of surface material using a rotating grinding tape that transverses across the surface of the roll.

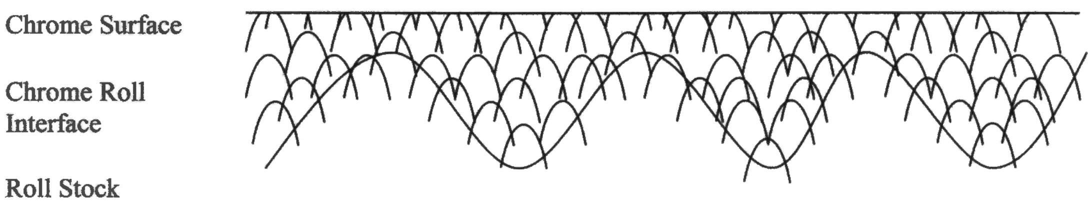

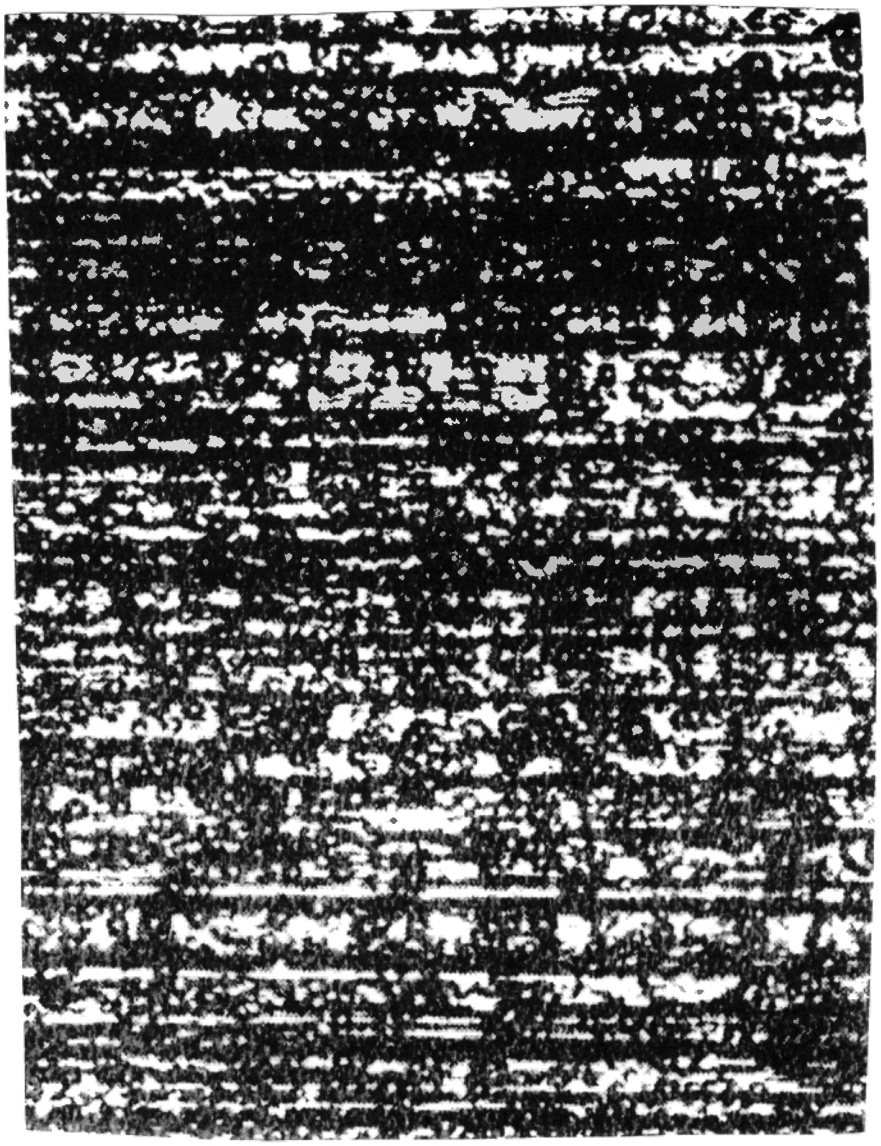

Figure 7.22. Micro-finished surface of work roll (40x)

The final process is to grind the surface to designated specification suitable to the finish required, generally 5-7 Ra. An additional benefit of chroming is that the chrome layer thickness allows the rolls to be re-ground without the need to microfinish and chrome if they are not damaged in the rolling process.

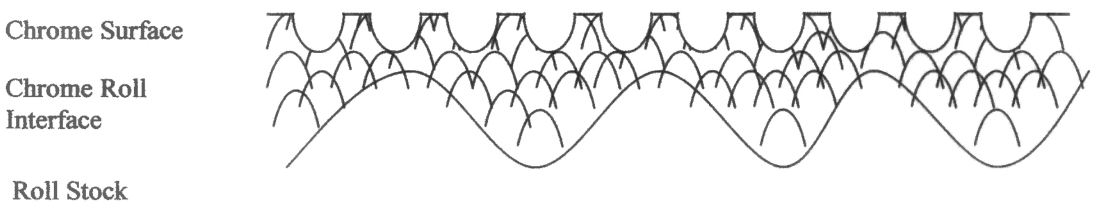

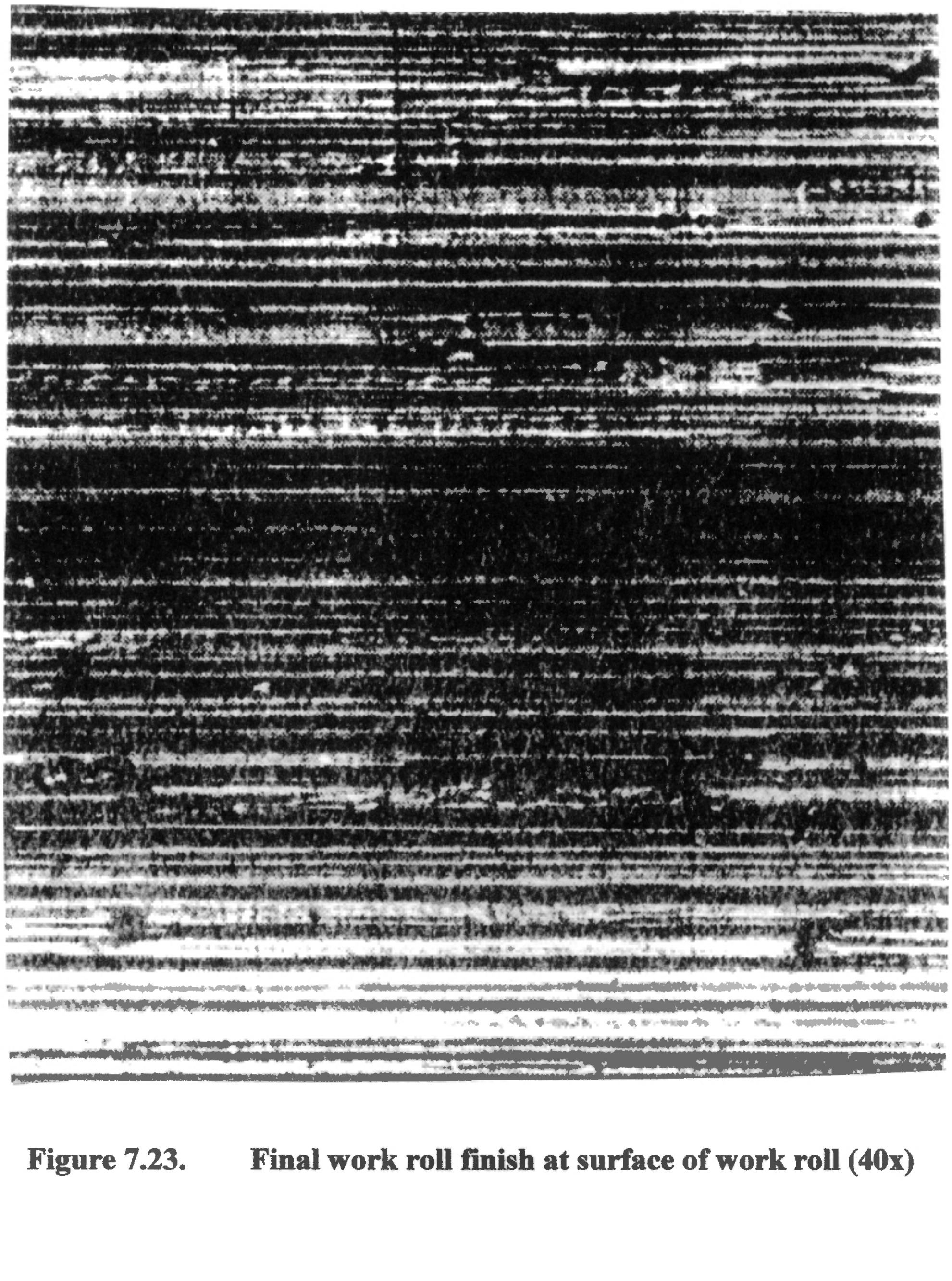

Figure 7.23. Final work roll finish at surface of work roll (40x)

7.5.2. Speed changes

The drop in rolling velocity with roll time on steel rolls is a well understood phenomena. With increased metal-roll contact time, the Ra decreases reducing the "grabbing power" by decreasing the surface coolant entrapment of the rolls and hence the speed. A harder roll surface reduces the surface wear, maintaining the Ra close to its original value, maintaining mill efficiency for longer periods.

Table 7.3 contains plant data based on steel versus chrome-plated roll trials. The chrome-plated rolls maintain higher speeds for longer periods with the gaps for the steel rolls indicating a roll change for speed. No conclusions on the effect of chroming on initial speeds were made.

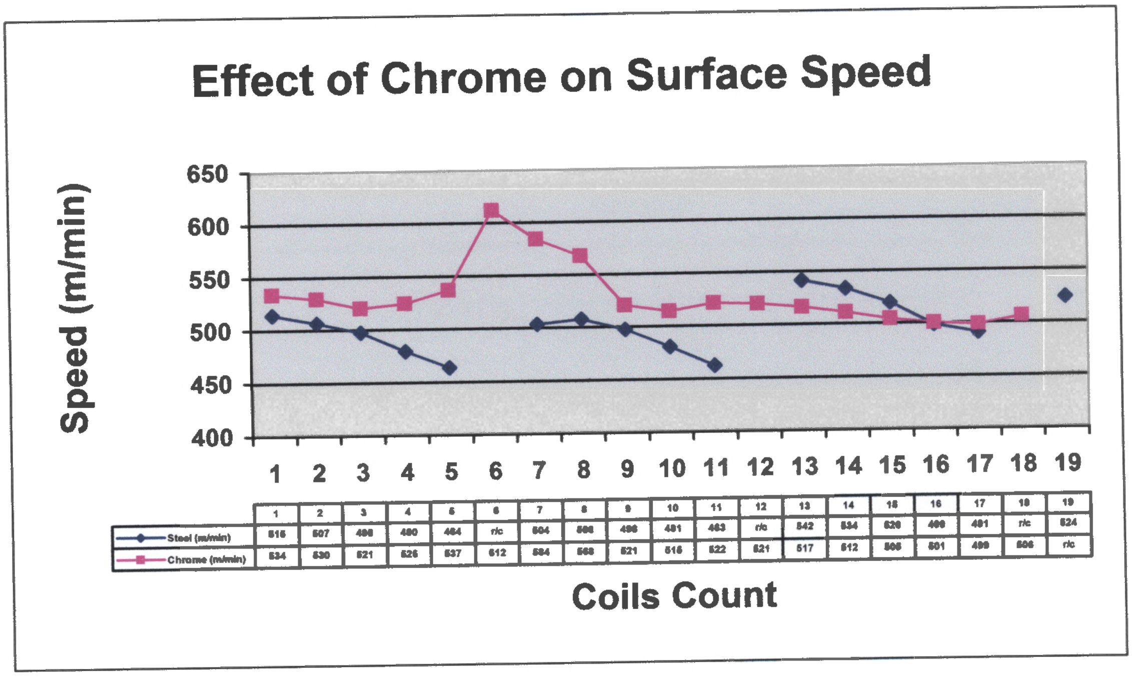

Table 7.3. Effect of surface on rolling speed

7.5.3. Pinholes

A trial to examine the effect of roll surface material on web surface quality as a function of pinholes was performed. Samples were collected at the end of each rolling schedule from the centre of the strip width for each coil. On both sets of rolls, the same rolling schedule was used on metal processed using the same input metal.

The gauge was checked for each sample to eliminate the influence of gauge on pinhole count, with all samples at 6.50um ± 1%. The samples were carefully transferred to a light box that had a surface area of 0.167m^2. The room was darkened and a count made. The results were multiplied by 6 to convert the measure to m^2 and are shown in Figure 7.24.:

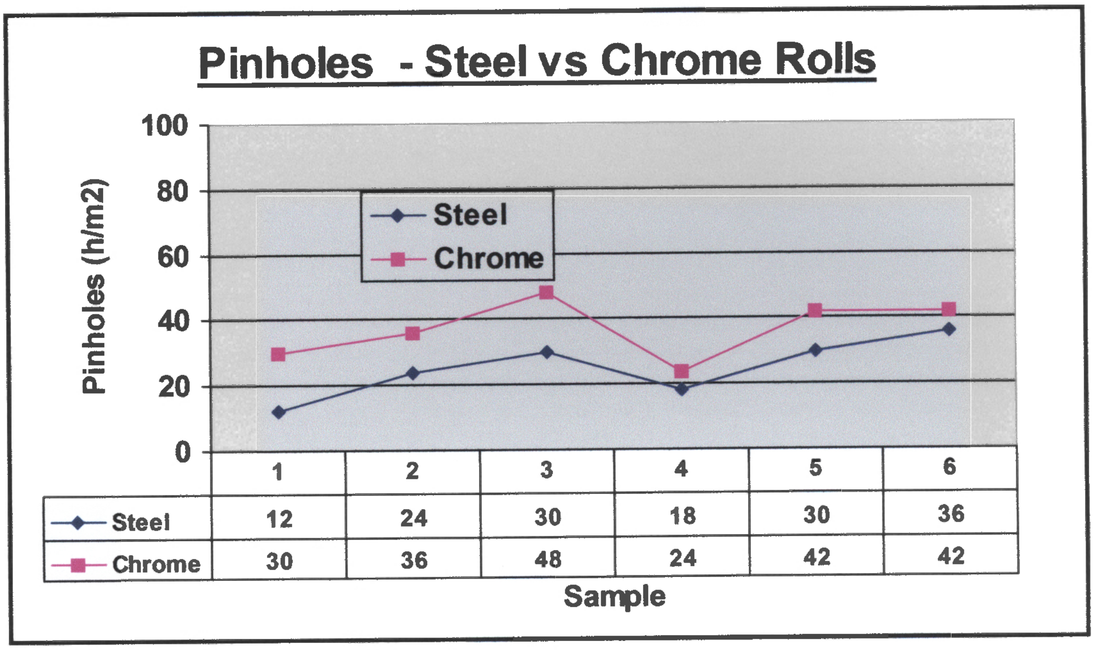

	1	2	3	4	5	6
Steel	12	24	30	18	30	36
Chrome	30	36	48	24	42	42

Figure 7.24. Pinhole count for steel and chrome rolls

The number of the pinholes over a 24 hour period for both roll surface materials was recorded. As the typical pinhole count for 6.5 micron is in the order of several hundred, there was no significant difference between the two rolling surfaces. After this time, speeds drop to levels that make the use of steel rolls uneconomical and hence data collection is extraneous. The pinhole from the steel rolls were consistently lower than that for chrome, possibly due to the electroplating process which results in the formation of chrome nodules on the surface. If not correctly ground to the final roll finish, these may induce pinholes.

While the benefits of chroming are significant, it must be stressed that tight control over the chroming process combined with a satisfactory grinding technique must be developed and adhered to, or chrome flecking and strip surface finish issues may arise.

7.5.4. Conclusion

Roll changes are generally a result of a reduction in rolling speed or a quality defect. DBF metal has been shown to reduce roll changes from roll marks by up to 80%. To maintain higher mill rolling speeds, chromed steel rolls have shown to delay speed drop associated with 8 – 12 hours of continuous rolling without an increase in pinhole count.

REFERENCES

[1] Conversations with Milt Milner, ALCOA Technical Centre, ALCOA

[2] Hall, A.; "The European Foil Industry" Light Metal Age (USA), vol. 54, no. 11-12, pp. 20-33, Dec. 1996

[3] "Aluminium Foil: Even more and even thinner", Verpack.-Berat. (Yugoslavia), no. 12, pp. 32, Dec. 1991

[4] "Aluminium: Technology, applications, and environment – A profile of a modern metal; 6th edition", Dietrich G. Altenpohl.

[5] Zwick, S.; "Aluminium foil production climbs [in Europe]" American Metal Market (USA), vol. 106, no. 74, pp. 6, 20 Apr. 1998

[6] "Germany's aluminium foil production in health condition again" Aluminium, 71, (2), 133, Mar – Apr. 1995

[7] "Satisfactory turnover and quality growth for aluminium foil [in Germany]" Aluminium (Germany), vol. 74, no. 4, pp.195, 198, Apr. 1998

[8] EAFA – www.alufoil .org/eng/alufoil_95.html

[9] Itoh, M.; "A survey of foil manufacturing plants in China", Light Met. Age, vol. 52, no. 11-12, pp. 47-52, Dec. 1994

[10] "China's aluminium foil industry", Nalk Report (Japan), vol. 87, pp. 8, Jan. 1998

[11] Aluminium Association Inc.

[12] Buch, E et. Al.; "Technological advances in Aluminium Rolling". 6th Arab International Aluminium Conference (ARABAL 93), Cairo, Egypt, 11-14 Dec. 1993

[13] Nussbaum, Al.; "Flat Rolled Process Technology for the 1990's: From Molten Aluminium to Finished Sheet". Light Metal Age, 49, (3-4), 8-83, Apr. 1991

[14] Ruttinger, U.; "Technologies for the Enhancement of Aluminium Rolling Mills". Aluminium, 70, (11-12), 666-669, Nov-Dec. 1994

[15] Formisano, V.; "Aluminium Foil: Innovation and Outlooks", Alluminio e Leghe (Italy), 8, (84), 63-67, Dec. 1996

[16] King, F,; "Aluminium Alloys and its Alloys", 1987

[17] "Continuous Caster threat to Conventional Mills Grows". Aluminium Today (UK), vol. 9, no.1, pp. 3, Feb-Mar, 1997

[18] Perrone, A.; "New Rolling Technologies", Alluminio Magazine (Italy), vol. 7-8, pp. 19-22, July-Aug. 1995

[19] "Development of a thin gauge/high-speed roll casting technology for foil production". Aluminium (Germany), vol. 74, no. 10, pp. 750-753, Oct. 1998

[20] "Four High Caster is World's First". Thirty-Three (33) Metal Producing (USA), vol. 34, no.4, pp.55, Apr. 1996

[21] "Latest Technical Developments in Continuous Casting", Aluminium, 73, Jan 1997, pp 685 – 689.

[22] Charlier, P and Ekstrom, H; "Strip Cast Aluminium Foil", Aluminium Alloys for Packaging 2

[23] Atack, PA; Robinson, IS.; "An investigation into the control of thermal camber by spray cooling when hot rolling Aluminium", J. Mater. Process. Technol. (Netherlands), 45, (1-4), 125-130, 1 Sept. 1994

[24] Kaseda, Y.; "Control of flatness defects and warping in processing plant", Curr. Adv. Mater. Process., 5, (5), 1463-1466, 1992

[25] Nikolaeva, EG, et. al.; "Fine filtration of Rolling Oil in a Foil Rolling Mill", Light Met. Age, 40, (7-8), 25-26, Aug. 1982.

[26] Strohmeier, BR.; "Testing and Improving the Wettability of Aluminium Foil", Aluminium (Germany), 68, (11), 983-988, Nov. 1992

[27] Zoeller, LR.; "Web scanning experiences in Aluminium Products", The Rolling Technology Sessions at Alumitech '94: Sheet and Plate, Ingot Casting, Foil, Aluminium Association, The, 275-286, 1994

[28] Barten, A.E., "Aluminium Foil Rolling", Metallurgical Plant and Technology International (Germany), 20, (6), 68-70, 72, 75-77, Dec. 1997.

[29] Barnes, HR.; "Advances in Aluminium Rolling – Hot Mills", Advances in Aluminium Rolling, 17-30, 1993

[30] Internal KAAL memo, 1998

[31] Internal AARP memo (formally KAAL), 2003

[32] "Aluminium Foil: Even more and even thinner", Verpack.-Berat. (Yugoslavia), no. 12, pp. 32, Dec. 1991

[33] Dietrich G. Altenpohl; "Aluminium: Technology, Applications, and Environment", 6th Edition, 1998.

[34] I.J. Polymer, "Wrought Aluminium Alloys", Materials Forum, pp 1-26, vol. 21, 1997

[35] *Registration Board of International Alloy Designations and Chemical Composition Limits for Wrought Aluminium and Wrought Aluminium Alloy Products*, Aluminium Association, New York 1985

[36] Metals Handbook, 10^{th} Edition, Volume 2: Introduction to Aluminium and Aluminium Alloys. American Society for Metals, Metals Park, OH

[37] Ekstrom, H.E. and Charlier, P.; Minerals, Metals and Materials Society/AIME, 1996

[38] Monteiro, S.N.; "New Aluminium Alloys", Metal ABM, vol 44, no 369, pp. 774 – 778, Aug 1988

[39] Mondolfo, L.F., *Aluminium Alloys: Structure and Properties*, Butterworths, London 1976.

[40] Furrer, P; "Aluminium Foils – Alloy Development Trends and Recyclability", Aluminium Alloys for Packaging, Chicago, Illinois, Nov 1-5, 1992.

[41] Szekely, A.G., "An Alternative to Chlorine Fluxing of Aluminium: The SNIF Process", Union Carbide Corporation, pp. 35-41, AIME, 1976

[42] Nilmani, M., Thay, P.K. and Simensen, C.J., " A comparative Study of Impeller Performance", pp. 939-946, Light Metals, 1992

[43] Internal Presentation, 1999 Ingot Casting training notes; Mike Scherbak, Knoxville, TN

[44] Miller, H.E.; Aluminium (1972), pp. 368 – 371.

[45] Farber, J.J., Rupp, F.M.; Light Metals, Vol. 2 (1979), pp. 733 – 740.

[46] Scherbak, M and DeYoung, D; 1999 Ingot Casting Training, ALCOA

[47] F.A. Acosta G., A.H. Castillejos E., E. Ruiz A., M. Mendez N., J.C. Escobedo B. "A study of the role of fluid velocity and particle size on deep bed filtration behaviour". Light Metal 1996 pp. 823 – 829.

[48] Guthrie, R., "General Principles of Melt Treatment", Aluminium Melt Refining and Alloying – Theory and Practice, Melbourne, July 10 – 12, 1989.

[49] Eckert, C.E., and Miller, R.E., "Molten Aluminium Filtration: Fundamentals and Models"

[50] Westengen, H., (1982). Aluminium, 58, 398 – 401

[51] Crea, R., Newell, J.M., "Effect of Homogenisation Time and Temperature on the Primary Particle Size in Foil Alloy 1145", 21/12/1992, CRC/TR/92/279.

[52] Nock, J.A.., Jr. (1947). Division Technical Report, Alcoa Laboratories.

[53] Mould, P.R. and Cotterill, P. (1967), J. Materials Science, 2, 241-255.

[54] Humphreys, F.J. (1980). In Recrystallisation and Grain Growth of Multi-Phase and Particle-Containing Materials, 1st Riso International Symposium on Metallurgy and Materials Science, Riso National Laboratory Roskilde, Denmark, pp. 31-44.

[55] Nes, E. (1976). Acta Met,. 24, 391-398

[56] Bay, B., and Hansen, N. (1979). Met. Trans. A, 10A, 279-288.

[57] Bay, B., and Hansen, N. (1983). In The Metallurgy of Light Alloys. Institution of Metallurgists, London, pp. 231-235.

[58] Chan, H.M., and Humphreys, F.J. (1984), Acta Met., 32, 235-243

[59] Anderson, W.A. (1947). Division Technical Report, Alcoa Laboratories.

[60] Ekstrom, H et. al; "Influence of the Microstructure on the Mechanical Properties of Aluminium Foil", (4th International Conference on Aluminium Alloys, Atlanta, Georgia, USA, Sept. 11-16, 1994) Vol. I, 297 – 304.

[61] R.W.K. Honeycombe, *The Plastic Deformation of Metals*, Arnold, 1985

[62] Aluminium Alloys – Their Physical and Mechanical Properties, Vol 3, Non-Heat-Treatable Aluminium Alloys edited by E.A. Starke, and T.H. Sanders, Engineering Materials Advisory Services, Warley, U.K. 1986.

[63] Stumpf, H.C. (1969) Progress Report, Alcoa Laboratories

[64] Stumpf, H.C. (1970) Progress Report, Alcoa Laboratories

[65] Comalco Technical Memorandum, 87272, (not published).

[66] *Aluminium*, Volume 1, Edited by K. Van Horn, American Society for Metals, Cleveland, Ohio, 1967.

[67] Smith, W.F., *Principles of Material Science and Engineering*, McGraw-Hill, 1986

[68] Texture and Microstructure of Warm Rolled Aluminium Alloys, Thesis by G.O. Schumann, May 1989

[69] Porter D.A., and Easterling, K.E.; Phase Transformation in Metals and Alloys, V.N.R. International, 1988.

[70] Smallman,R.E.; Modern Physical Metallurgy, 4th Ed., Butterworths, London.

[71] Csanady, A., Barna, A., and Barna, P.B.; "The Direct Observation and Investigation of the Oxidation of Aluminium in the Transmission Electron Microscope", Oxid. Metals, 13, 3, 245-254, 1979.

[72] Lea, C., and Ball, J.; "The Oxidation of Rolled and Heat Treated Al-Mg Alloys", Appli. Surf. Science., 17, 344-362, 1984

[73] H.J. Van Beek and E.J. Mittemeijer., "Amorphous and Crystalline Oxides on Aluminium", Thin Solid Films, 122, 131-151, 1984.

[74] K. Shinohara, T. Seo and H. Kyogoku, "Transmission Electron Microscopy Studies on the Oxidation of Aluminium", Z. Metallkde, 73, 12, 774-780, 1982.

[75] A.F. Beck, M.A. Heine, E.J. Caule and M.J. Pryor, "The Kinetics of the Oxidation of Al in Oxygen at High Temperature", Corros. Sci., 7, 1-22, 1967.

[76] T. Ronnhult, U. Rilby and I. Olefjord, "The Surface State and Weldability of Aluminium Alloys", Mater. Sci. Eng., 42, 329-336, 1980.

[77] Aluminium Association Inc.

[78] T. L. Williams, "Some Studies of the Annealing Behaviour of Coiled Light Gauge Aluminium Foil", Thesis, UNSW, June 1992

[79] H.J. Van Beek and E.J. Mittemeijer., "Amorphous and Crystalline Oxides on Aluminium", Thin Solid Films, 122, 131-151, 1984.

[80] I. Olefjord and A. Karlsson, "Surface Analysis of Aluminium Foil", Conf. Proc. Aluminium Technol., London, 77-78, March, 1986.

[81] M. Textor, "The Chemical Composition of Oxide Films on Aluminium and Its Influence on Surface Properties Studied by SIMS, XPS, and AES"., Secondary Ion Mass Spectroscopy. SIMS III, Springer-Verlag, 372-376, 1982

[82] E. Janssen, "Chemical Characterisation of Industrial Steel and Aluminium Sheet Surfaces by Secondary Ion Mass Spectrometry, Glow Discharge Optical Spectroscopy and other Surface-Sensitive"., Mater. Sci. Eng., 42, 309-320, Jan-Feb. 1980.

[83] M. Textor and R. Grauer, "A Photoelectron and Secondary Ion Mass Spectrometric Study of the Chemical Composition of Thermal 'Oxide' Layers on Technically Pure Aluminium"., Corros. Sci. (1983), 23 (1), 41-53

[84] Csanady, A.; "The Relationship Between the Corrosion Resistance and Impurity Content of Aluminium Oxide Layers"., Corros. Sci., 24, (3), 237-248, 1984.

[85] T. Ronnhult, U. Rilby and I. Olefjord, "The Surface State and Weldability of Aluminium Alloys", Mater.Sci. Eng., 42, 329-336, 1980

[86] R.E. Sanders Jr, S.F. Baumann and H.C. Stumpf., "Wrought Non-Heat-Treatable Aluminum Alloys", Treatise on Materials Science and Technology, Vol 31, 1989

[87] Tsuchida, S., and Baba, Y; "Development of Aluminium Alloys for Packaging in Japan", Aluminium Alloys for Packaging, Chicago, Illinois, Nov 1-5, 1992.

[88] Alcan Patent – 69048 / 74

[89] Domanti, S.A and McElwain, D.L.S; "Cold Rolling of Flat Metal Products: Contribution of Mathematical Modelling", Proc Instn Mech Engrs, 1998, 212B, 73 – 86, Proc Instn Mech Engrs

[90] Zygmunt Wusatowski, "Fundamentals of Rolling", Pergamon Press, 1969.

[91] Orowan, E; "The calculation of roll pressure in hot and cold flat rolling", Proc Instn Mech Engrs, 1943, 150, 140 – 167.

[92] Hitchcock, J; "Roll neck bearing. Report of ASME Special Research Committee on Heavy-Duty Anti-friction Bearings, 1935, Appendix 1.

[93] Smet, R.P. and Johnson, R.E., "An Asymptotic Analysis of Cold Sheet Rolling", Trans. ASME, J. Appl. Mech., 1989, 56, 33 – 39.

[94] Johnson, R.E., "Shape Forming and Lateral Spread in Sheet Rolling", Int. j. Mech. Sci., 1991, 33, 449 – 469.

[95] Zienkiewicz, O.C., Jain, P.C. and Onate, E.G., "Flow of Solids during Forming and Extrusion: Some Aspects of Numerical Solutions", Int. J. Solids Structs, 1978, 14, 15 – 38.

[96] Li, G. and Kobayashi, S., "Rigid-Plastic Finite-Element Analysis of Plane Strain Rolling", Trans. ASME, J. Eng. Industry, 1982, 104, 55 – 64.

[97] Mori, K., Osakada, K. and Oda, T., "Simulation of Plane-Strain Rolling by the Rigid-Plastic Finite Element Method", Int. J. Mech. Sci., 1982, 24, 519 – 527.

[98] Yarita, I., Mallett, R.L. and Lee, E.H., "Stress and Deformation Analysis of Metal Rolling Processes", In Proceedings of the 1st International Conference on Technology of Plasticity, Toyko, 1984, pp. 1132 – 1137.

[99] David, C., Bertrand, C. and Chenot, J.L., " A Transient Three Dimensional Analysis of Hot Rolling of Thick Slabs", In Proceeding of Numiform'86 Conference, Gothenburg, 1986, pp. 219-224

[100] Mori, K., Osakada, K., Nikaido, H., Naoi, T. and Aburatani, Y., " Finite Element Simulation of Non-Steady State Deformation in Rolling of Slab and Plate", In Proceedings of the 4th International Steel Rolling Conference, Deauville, 1987, pp. F6.1 – F6.8.

[101] Hwu, Y and Lenard, J.G., "A Finite Element Study of Flat Rolling", Trans. ASME, J. Eng. Mater Technol. 1988, 100, 22 – 27.

[102] Santino A. Domanti, W. John Edwards and Peter J. Thomas; "A Model for Foil and Thin Strip Rolling", Presented at the 1994 AISE Annual Convention Cleveland, Ohio.

[103] Orowan, E; "The Calculation of Roll Pressure in Hot and Cold Flat Rolling", Proc. Instn. Mech. Engrs., Vol. 150, 1943, pp. 140-167.

[104] Huggins, P.J.W., "Roll Indentation: It's Relation to Limiting Reduction and Limiting Thickness in Cold Rolling", J. Inst. Metals., Vol.11 1966, pp. 238 – 244.

[105] Stone, M. D., "Rolling of Thin Strip", Iron and Steel Engineer, Feb 1953, pp. 61 – 74.

[106] Johnson, K. L. and Bentall, R. H., "The Onset of Yield in the Cold Rolling of Thin Strip", J. Mech. Phys. Solids, Vol. 17, 1969, pp. 253 – 264.

[107] Fleck, N. A. and Johnson, K. L., "Towards a New Theory of Cold Rolling Thin Foil", Int. J. Mech Sci. 1987, 29, pp. 507 – 524.

[108] Fleck, N. A., Johnson, K. L., Mear, M. E., and Zhang, L. C., "Cold Rolling of Foil", Proc. Instn. Engrs, Part B, Journal of Engineering Manufacture, 1992, 2069B2), pp. 119 – 131.

[109] Gratacos, P., Montmitonnet, P., Fromholz, C., and Chennot, J.L., "A Plane-Strain Elastoplastic Finite-Element Models for Cold Rolling of Thin Strip", Int. J. Mech. Sci., 1992, 34, pp. 195 – 210.

[110] Jortner, D., Osterle, J. F. and Zorowski, C. F., "An Analysis of Cold Strip Rolling", Int. J. Mech. Sci., Vol 2., 1960, pp. 179 – 194.

[111] Grimble, M. J., Fuller M. A. and Bryant G. F., "A Non-Circular Arc Force Model for Cold Rolling", Int. J. Num. Methods Eng., Vol. 12, 1978, pp. 643 – 663

[112] Yuen, W. Y. D., "On the Heat Transfer of a Moving Composite Strip Suppressed by Two Rotating Cylinders", J. of Heat Transfer, Vol. 107, 1985, pp. 541 – 548.

[113] J.W. Martin, Micromechanisms in Particle-Hardened Alloys, Cambridge University Press, Sydney, 1980, pp. 151 – 164.

[114] F.J. Humphreys, "The Nucleation of Recrystallisation at Second phase Particles in Deformed Aluminium", Acta Met, 25 (1977), 1323.

[115] N. Hensen and B. Bay, "Initial Stages in Aluminium Containing both Large and Small Particles", Acta Met., 29, (1981), 65

[116] R.D. Doherty and J.W. Martin, "The effect of Dispersed Second Phase on the Recrystallisation of Al-Cu Alloys", Journal Inst. Met., 91, 332, (1962).

[117] E. Koken, et. Al., "The Role of Particle Distribution in Recrystallisation in Two-Phase Alloys", Mat. Science and Engineering., A104, 1988, pp.163.

[118] F.J. Humphreys, "Recrystallisation Mechanisms in Two Phase Alloys", Metal Science, 13, 136, 1979.

[119] F.J. Humphreys, "The Nucleation of Recrystallisation at Second Phase Particles in Deformed Aluminium", *Acta Met.* 25 (1977), 1323

[120] M.F. Ashby, "The Deformation of Plastically Non-Homogeneous Materials", Phil. Mag. 1970, 21, pp. 399 – 424.

[121] R.D. Doherty and J.W. Martin, "The Effect of a Dispersed Second Phase on the Recrystallisation of Al-Cu Alloys", *Journal Inst Met.*, 91, 332, (1962)

[122] F.J. Humphreys and P.N. Kalu, "Dislocation-Particle Interactions During High Temperature Deformation of Two-Phase Aluminium Alloys", Acta Metall. 35, 1987, pp. 2815

[123] E. Koken, et al. "The Role of Particle Distribution in Recrystallisation in Two-Phase Alloys", *Mat. Science. and Engineering.*, A104, 1988, pp. 163.

[124] E. Nes, et al, "On the Zener Drag", Acta Metall. 33, 11 (1985).

[125] A.S. Jayatilake and K. Trustrum, "Statical Approach to Brittle Fracture", J. Material Science, pp. 1426 – 1430, 1977

[126] K. Wallin, et al. "Fracture of Brittle Particles in a Ductile Matrix", Int. J. Fracture, 32, pp. 201 – 209, 1987.

[127] B. Ren, "Primary Particle Size Distribution in CAC Canstock Al During Fabrication", CRC:TN:92:920

[128] B. Ren, "Evolution of Second Phase Particle Distribution in CRP Canstock Al During Fabrication", CRC:TN:92:921

[129] J.E. Tibbles, "A model for the Effect of Rolling on the Size Distribution of Second-Phase Particles", Internal Memo

[130] J.E. Tibbles, "Conversion of Image Analysis Data on Particles with Complex Shapes to Equivalent Elliptical Sections". CRC/TN/ 92:810

[131] J.E. Tibballs, "A Model for the Effect of Rolling on the Size Distribution of Second-Phase Particles", Comalco Research Centre, 1994

[132] A.S. Jayatilake and K. Trustrum, "Statistical Approach to Brittle Fracture", *J. Material Science,* pp. 1426-1430, 1977.

[133] H.J. McQueen, "Controversies in the Theory of Dynamic Recrystallisation", Recrystallisation, 92, pp. 429 – 434.

[134] Personal communication with John Tibbles, Comalco Research Centre, 1993

[135] O. Johannsen, Geschichte des Eisens, Verlag Stahleisen, Dusseldorf, 1953

[136] C.S. Smith, "Metallurgy", Encyclopaedia Britannica. Vol. 15, 1967, p. 237

[137] William A. Glaeser, "Friction", Lubrication Engineer, February 1992, pp 129-132.

[138] Discussions with Mike Ringle – ALCOA Rolling Principle

[139] J.A. Schey, "Metal Forming Plasticity", H. Lippmann (ed.), Springer, Berlin 1979, pp. 336-348.

[140] S. Marcilla, A. Marcilla, "Lubricating systems for Aluminium foil rolling I", Aluminium (Germany), 69, (3), 163-166, Feb. 1993

[141] S. Marcilla, A. Marcilla, "Lubricating systems for Aluminium foil rolling II", Aluminium (Germany), 69, (3), 259-262, Mar. 1993

[142] K. Matsui, T. Matsushita, K. Takatsuka, Y. Yamaguchi, "Evaluation of Lubricants for Rolling of Aluminium Sheet and Foil", Advanced Technology of Plasticity, Vol. 1, Japan Society for Technology of Plasticity, 247 – 252, 1984

[143] R.D. Guminski and Willis; "Development of Cold Rolling Lubricants for Aluminium Alloys," J. Inst. Metals, 88, 481-492, Aug, 1960.

[144] Meisel, H; "Influence of the Oil Composition on the Surface Quality of Aluminium Semi-finished Products during Cold Rolling", Z. Metallkde., 61, 5, 323-325, 1970

[145] Meisel, H; "Influence of the Oil Composition on the Surface Quality of Aluminium Semi-finished Products during Cold Rolling", Z. Metallkde., 61, 5, 323-325, 1970

[146] Tsuchida, S., and Baba, Y., Sumitomo Light Metals Tech. Rep., 1983, vol. 24, pp. 27 – 30.

[147] Kobayashi, Y., Proc. Of 18th Symp. "Recrystallisation and Grain Size of Aluminium Alloys, pp. 60 – 64, Japan Inst. Light Metals, Tokyo, 1981.

[148] Moriyama, T., Yoshida, H., and Tsuchida, S; J. Japan Inst. Light Metals, 1989, vol 39, pp. 184 – 189.

[149] Minami, I. and Fukuoka, K; Sumitomo L.M., Nagoya, unpublished research, 1990

[150] Yamamoto, S., Mizuno, M., and Kirihata, A; J. Japan Inst. Metals., 1992, vol 56, pp. 142 – 147.

[151] Mahmudi, R., et al.; Aluminium, 1987, vol. 63, pp. 62 – 66.

[152] W.C. Wake, "Adhesion and Formulation of Adhesives", Applied Science, London, 1976.

[153] Kerth, Amann, Raber and Weber, "Aluminium Foil Production", Int. Metall. Rev., 20, 185-207, Dec 1975.

[154] Hofling and Baur, "Some Chemical Reactions Involved in the Annealing of Aluminium Foil", Lubr. Eng., 42, 620-624, Oct. 1986.

155 B.R. Strohmeier, "Surface Characterisation of Aluminium Foil Annealed in the Presence of Ammonium Fluoborate", Appl. Surf. Sci., vol. 40, no. 3, pp. 249-263, Dec. (I) 1989.

156 R.J, Dean and W. Hauser, "Production of High Quality Aluminium Foil", BNF 6th International Conference Proceedings, Sept, 1986.

157 N. Cabrera, N.F. Mott, "Theory of the Oxidation of Metals" Rep. Prog. Phys. 12, 163 – 184, 1948 – 1949.

158 D.T. Clark and K.C. Tripathi, "ESCA Studies of Surfaces of Aluminium Foil", Nature Phys. Sci., 244, 135, 77-78, July 1973

159 T. Ronnhult, U. Rilby and I. Olefjord, "The Surface State and Weldability of Aluminium Alloys", Mater. Sci. Eng., 42, 329 – 336, 1980

160 W.W. Smeltzer, J. Electrochem. Soc. 103, 209, 1956

161 H.J. Van Beek and E.J. Mittemeijer, "Amorphous and Crystalline Oxides on Aluminium", Thin Solid Films, 122, 131-151, 1984

162 Styner, A.R.; "Creasing of Thin Aluminium Foil", BE Thesis, 1993

163 Conversations with Jim Rushing

164 Pfeiffer, J.D.; "Web Guidance Concepts and Application", TAPPI Journal, Vol. 60, No. 12, pp. 53 – 58, Dec 1977

165 Pfeiffer, J.D.; "Mechanics and Dynamics of Web Motion Between Spans", Journal of Dynamic Systems, Measurement and Control, pp.180 – 186, Sept. 1971

166 Friedrich, C.R., Good, J.K.; "Stability Sensitivity of Web Ripples on Rollers", TAPPI Journal, pp. 161 – 165, Feb. 1989

167 Wistreich, J.G.; "Control of Strip Shape During Cold Rolling", Journal of Iron and Steel Institute, pp. 1203 – 1206, December 1968.

168 Blodgett, O.W.; "Design of Welded Structures", The James F. Lincoln Arc Welding Foundation

169 Yoshida, K., Komorida, H., Usuda, M., Hayashi, H., Oikawa, H., Ohwue, T., Amaike, T.; "The Effects of Mechanical Properties of Sheet Metals on the Growth and Removing of Buckles due to Mon-uniform Stretching", Scient. Papers Inst. Phy. Chem. Res., Vol. 68, pp. 88 – 93, 1974.

170 Aoki, I., Matoba, T., Ataka, M.; "Effect of Mechanical Properties on the Growth of Wrinkles in Sheet Metal Forming", 12th Biennial Congress, IDDRG, Ligure, Italy, pp. 221 – 229, 1982.

171 Wang, X., Lee, L. H.; "Wrinkling of an Unevenly Stretched Sheet Metal", Journal of Engineering Materials and Technology, Vol. 111, pp. 235 – 242, July 1989.

[172] Segedin, R.H., Collins, I.F., Segedin, C.M.; "The Elastic Wrinkling of Rectangular Sheets", International Journal of Mechanical Sciences, Vol. 30, pp. 719 – 732, 1988.

[173] Leissa, A.W., Ayoub, E.F.; "Tension Buckling of Rectangular Sheets Due to Concentrated Forces", Journal of Engineering Mechanics, Vol. 115, No. 12, pp. 2749 – 2762, 12 Dec. 1989

[174] Amirbayat, J.; "The Buckling of Flexible Sheets Under Tension Part 1: Theoretical Analysis", J. Text. Inst., Vol 82, No1, pp. 66 – 70, 1991

[175] Friedrich, C.R., Good, J.K.; "Stability Sensitivity of Web Ripples on Rollers", TAPPI Journal, pp. 161 – 165, Feb. 1989

[176] Metallurgical Handbook – ALCOA Web page via intranet

[177] G.D. Gray and W.G. Fricke, "Inclusions and Unwanted Particles in Aluminum", Internal Report – Alcoa, 1970.

[178] Pawelski, O., Rasp, W., Draese, S., "Investigation of the influence of rolling speed on the tribological phenomena in cold rolling", pp 407 – 413.

[179] Conversations with Gerry Biddle. RMIT Lecturer and former Alcoa employee

[180] "Barrier Properties of Aluminium Foil", British Aluminium Foil Rollers Association., 20 Portland Place, London, W1N 4AU. 1974, 26 p (Pamphlet)

[181] European Standard EN 546 - 4

[182] Matsui, K., "Mechanism of Pinhole Formation in Aluminium Foil Rolling", Kobelco Technology review No12. Oct. 1991

[183] Anderson, A.N., "Typical Causes of Pinholes in Pack Rolled Foil", Lubrication Engineering, 622 – 625, vol 44, 7, 1988.

[184] Rachlitz, R., Streckenback, E., "Behaviour of Titanium Diboride in the Manufacture of Aluminium Foil", Aluminium, vol. 67, no.1, pp. 75-80, Jan. 1991.

[185] Reich, R.A., Epp, J.M., Gantzer, D.E., "A mechanism for generating Aluminium Debris in the Roll Bite and its Partitioning between the Surface of the Work roll and the Surface of the Sheet as Smudge", Tribology Transactions (USA), 39, (1), 23-32, Jan 1996.

[186] Januszkiewicz, K.R., Stratford, G., Ward, T., "Roll Bite Conditions Controlling Formation of Wear Debris during Cold Rolling of Aluminium", J. Mater. Process. Technol. (Netherlands), 45, (1-4), 117-124, 1 Sept. 1994

[187] Vicente Martin, Internal Memo, not published, 2000

[188] Clement, G., "The Pechiney Deep Bed Filter", Light Metals 1995 pp.1253 – 1262

[189] Conversations with Foil light gauge rollers, Yennora AARP.

[190] Pawelski, O., Rasp, W., Draese, S., "Investigation of the Influence of Rolling Speed on the Tribological Phenomena in Cold Rolling", IAS

[191] Komori. K,. "Analysis of Herringbone Mechanism in Sheet Rolling", Journal of Materials Processing Technology, 60 (1996) 377-380